Porosity in Configured Structures

Effect of Ply Drops and Caul Sheets in the Processing of Composite Parts

by

Martin Roy

B.Eng., McGill University, 2013

A THESIS SUBMITTED IN PARTIAL FULFILLMENT OF

THE REQUIREMENTS FOR THE DEGREE OF

MASTER OF APPLIED SCIENCE

in

THE FACULTY OF GRADUATE AND POSTDOCTORAL STUDIES

(Materials Engineering)

THE UNIVERSITY OF BRITISH COLUMBIA

(Vancouver)

December 2015

Abstract

Fiber reinforced polymer composites offer a variety of processing advantages in the manufacturing of high performance structures. However, due to a variety of potential quality defects, there is a great deal of risk associated with composite processing. Amongst these numerous defects, porosity has always been one of critical concern. Although there exists a great deal of literature on the subject, the bulk of existing research to date is restricted to the processing of flat uniform parts. As such, there exists a discrepancy between the current academic understanding and the practical knowledge needed in current practice.

The objective of this thesis is to advance our knowledge of porosity to processing scenarios commonly seen in current practice. This has been done by conducting a comprehensive examination of the relationship between the mechanisms driving void evolution and the use of two commonly used structural configurations. These are ply drops and caul sheets. In this study, a series of configured composite parts were manufactured to parametrically assess the effect of ply drops and caul sheets both separately and in combination. The porosity content and final thickness profile of the parts were evaluated through optical microscopy and thickness measurements. The results from this parametric study show that resin pressure shielding due to lack of compliance between the laminate and the caul sheet can be a primary cause of porosity. It has also been found that lack of compliance caused resin migration which carries with it adverse effects on final part quality.

The resin pressure distribution of ply-drop laminates processed with and without caul sheets was tracked in-situ through the use of instrumented tooling. The results from these experiments support the findings of the parametric study and provide a comprehensive understanding of the dominant mechanisms. These mechanisms where simulated with state of the art finite element software. These simulations demonstrate that commercially available software packages can be used to enhance our understanding of void evolution in complex processing scenarios. As such, the findings presented in this thesis are of great engineering value to current practices since they can be applied to a wide variety of applications.

Preface

The research presented in this thesis was performed and interpreted by Martin Roy (author). The author received valuable input and supervision by Dr. Anoush Poursartip as well as input and technical assistance by Malcolm Lane, Alastair McKee and Alireza Forghani of Convergent Manufacturing Technologies [1].

The experiments in chapter 3 and 4 were conceived, designed, performed and interpreted by the author. Critical equipment used for the experiments in chapter 3 were provided by Convergent Manufacturing Technologies and Malcolm Lane provided guidance in the design and installation of the equipment. All of the simulations presented in chapter 5 where executed by the author with the use of COMPRO V2 [2] plug-in in ABAQUS V6-14 [3]. Assistance with setting up the model input parameters and the interpretation of the data was provided by Alireza Forghani. The material characterization experiments presented in chapter 5 were conducted by Alastair McKee. Raw data was provided for reduction and interpretation by the author.

Table of Contents

List of Tables

List of Figures

Acknowledgements

Thank you to my supervisor Dr. Anoush Poursartip for guiding me during the course of my studies and for inspiring in me a desire to push the expectations of my work and myself.

I would also like to thank the current and past members of the Composite Research Network and UBC Composites group to whom I owe a great deal of gratitude for their dependability and support. It has been a privilege to work amongst such talented and intelligent individuals.

For their technical assistance, I would like to thank Malcom Lane, Alireza Forghani and Alastair Mckee of Convergent Manufacturing Technologies. Without their collaboration, much of the work presented in this thesis would not have been possible. Thanks to Mr. Mike Thompson and Dr. Karl Nelson of the Boeing Company for engaging me in constructive discussions throughout my time here.

Last but not least, I would like to thank my family without whom this would not have been possible. Pour votre soutien et amour inconditionnelle, merci Marc, Lorraine et Michelle.

Je dédicace cette thèse à mon grand-père.

André Séguin

1929-2015

A un père entièrement dévoué à sa famille et une vie bien réussie à tous points de vues.

Chapter 1: Introduction

Composite materials offer a variety of processing advantages of considerable importance in the manufacturing of high performance structures. In particular, the utilization of carbon fiber epoxy materials can allow for the manufacturing of light weight structures all the while delivering mechanical performance equivalent to structures made of conventional materials. With respect to the transportation industry, weight reduction is financially beneficial to the end user by reducing fuel consumption or enabling the use of alternative energy sources. Furthermore, composite processing also works to benefit product manufacturers by allowing for the production of large complex monolithic parts. This a processing advantage of particular importance because it allows manufacturers to reduce costs associated with the assembly process.

However, a variety of quality defects can occur during composite processing and must be properly managed in order to avoid costs associated with the production of defective parts. Amongst these numerous defects, the accumulation of void spaces within the material, referred to here as porosity, is one of the most important ones. As such, a great deal of academic research concerned with porosity in composite processing exists. Although it can be said that a fairly good understanding of the relationship between porosity and its driving state variables has been established, our current state of understanding is such that this is only true in the processing of flat uniform parts. Therefore, there exists a discrepancy between our current academic understanding and the practical knowledge needed in industry. To address this problem, relationships between configured structures common in practice and their influence on the driving state variables of porosity must also be established.

The research presented in this thesis focuses on porosity in configured structures. Here the term configured structures refers to non-uniformities inherent in the composite part or in the tooling used to manufacture the part. Essentially anything that is more complex than the processing of flat uniform parts. Specifically for this thesis, the effect of ply drops and caul sheets on final part porosity will be studied. The relationship between numerous parameters of these structural configurations and the flow and compaction phenomenon which effect porosity are presented and discussed. It should be noted that the findings presented in this work are not exclusive to the implementation of ply drops and caul sheets solely. The research presented in this thesis aims to provide a thorough examination of the fundamental mechanics involved, and can therefore be applied to a variety of other structural configurations.

The current chapter positions the work within the industry. As such, an overview of the composite materials, processing techniques, porosity and configured structures relevant to the scope of this thesis is presented. A summary of the research motivations, thesis objectives and structure is also included.

1.1 Current Applications of Composites

In its most generic form, composites refer to materials whose constituents are made up from more than one distinct material. Amongst the numerous types of composites, fiber reinforced polymer (FRP) composites are one of the most important and widely used materials. FRPs refer to a composition of fiber reinforcements which are encapsulated and bound together by a polymer matrix. The matrix is typically comprised of thermoset polymers such as epoxies or polyesters, however, thermoplastics may also be used. The most typical materials used for the reinforcements are glass, aramid and carbon fibers. Amongst these common combinations in FRPs, carbon fiber epoxy composites offer the highest specific strength and stiffness and low weight. As such, this material is primarily used for high performance applications and is heavily used in aerospace industries[4]. Due to its importance, this material has been selected to be the focus of this study and the remainder of the discussion will therefore focus on this class of material.

In addition to high specific strength and stiffness and low weight, composites offer a variety of other advantages as well. Their anisotropic mechanical properties offer for application specific tailoring. This also means that further weight savings can be achieved by controlling the fiber orientation such that the load paths of the part are optimized.

One of the most important advantages in composite processing is in the ability to manufacture large complex monolithic parts. This capability allows for significant cost savings by eliminating the need for the assembly and/or joining process. This is a processing advantage which is typically not accessible when conventional materials such as aluminum are used in

manufacturing. When using conventional materials, complex structures often need to be manufactured through an assembly of many sub-structures because the mechanical properties of these materials are set prior to part fabrication. Since both the final mechanical properties and geometry of the part are achieved simultaneously in composite processing, complex structures can be manufactured within a single part. These complexities constitute features such as, multiple planes of curvature, non-uniform thickness profiles and inserts to name a few. Due to the advantages that composite processing offers, composite parts typically manufactured in practice are seldom flat in geometry or uniform in layup constituents. Figure 1.1 illustrates the complexity of composite structures typically manufactured in industry.

Figure 1.1 – Lockheed Martin composite cargo aircraft fuselage [5].

1.2 Composite Processing

There are many different techniques used to process composite parts, such as; manual lay-up and spray-up, resin transfer molding (RTM), vacuum infusion and prepreg processing techniques[6]. Although procedures and tooling vary from one technique to the other, composite processing can be reduced to a sequence of three general steps. These are; material deposition, debulking/consolidation and curing.

In aerospace, the prepreg processing technique is used extensively since higher fiber to resin volume fractions can be achieved with better process control resulting in high performance parts. In addition, it also offers relatively simpler handling and manufacturing in contrast to other processing techniques. Due to its prominent use, prepreg processing is the manufacturing technique that will be studied in this thesis. As such a brief overview of this technique is provided in the following section.

1.2.1 Prepreg Processing

Prepreg stands for pre-impregnated fibers. Thermoset prepregs are made by partially impregnating collimated fibers (tapes) or a fiber weave (fabrics) with resin. The partially resin impregnated fiber bed is then subject to a succession of controlled heating stages which advances the cure of the resin to what is referred to as a stage-B cure [7]. At this cure stage, the resin is said to be at the middle stage of the thermosetting reaction and comprises of a gel like tacky solid at room temperature. This allows for easier handling during the layup process. The prepreg is then rolled with a release film onto a take up roll, bag sealed, and stored in a freezer. These rolls are typically referred to as the “raw” incoming materials.

In prepreg processing, the material deposition phase is referred to as layup. In general, during the layup process, the raw material is defrosted to room temperature within the bag. Following thawing, plies are then cut from the roll to the required dimensions and laid onto a tool according to specified fiber orientations. The resulting assembly of prepreg plies is referred to as a laminate. The laminate is then sealed with a bagging assembly which typically consists of a vacuum bag, release film and breather cloth. The bag is then vacuumed to consolidate the laminate and extract any gases that may remain in the system. This part of the process is referred to as the debulking stage. The consolidation pressure results from the differential pressure between the internals of the bag and the ambient pressure outside of the bag. The ambient pressure can simply be the surrounding atmospheric pressure or it can be amplified by inserting the assembly into an autoclave (which is essentially a pressurized oven).

While maintaining the consolidation pressure, the vacuumed bagged assembly is subject to a cure cycle. Ovens, autoclave or heated tools can be used for this step. The cure cycle consists of a succession of temperature ramps and holds. Ideally, as the temperature of the resin increases, its viscosity will subsequently drop due to increased mobility of the short polymer chains. This will allow the resin to flow into the un-impregnated regions of the prepreg thereby eliminating void spaces. This temperature rise will also cause crosslinking reactions between the polymer chains of the thermoset. This ongoing reaction results in the buildup of a tightly bound polymer network which causes the resin viscosity to increase by several orders of magnitude. As the cure advances and crosslinking continues, the glass transition temperature increases until the final cure condition is reached. At this stage the resin exhibits a glassy behavior (i.e. high stiffness and high strength) and the mechanical properties of the final part have been set.

Note that the overview provided here is only intended to give a general understanding of prepreg processing. A more detailed overview will be provided in Chapter 2.

1.2.2 Quality Defects

Regardless of the processing technique implemented, the main objective in the processing of composite materials is the production of a *defect* free part. There are many different kinds of defects which can arise during the various stages of processing (e.g. material deposition, curing and part removal). Within the realm of quality management, defects refer to physical processing outcomes which are deemed unacceptable when measured against specifications. The most common quality defects are:

- Voids & porosity. (e.g. surface and bulk porosity)
- Thickness variations. (e.g. thinning and thickening)
- Dimensional distortion. (e.g. warping)
- Fiber misalignment. (e.g. out of plane and in-plane wrinkling)
- Fiber/resin ratio content discrepancies. (e.g. resin depletion and pooling)

These quality defects can have negative impacts on part performance ranging from minor tribulations (such as unaesthetic surface finish) to more severe downstream processing failures (such as degradations in mechanical properties).

1.2.3 Porosity in Composite Processing

Amongst the quality defects listed in the previous section, porosity is one of great importance. Porosity is a type of quality defect in composite processing which refers to the accumulation of void spaces in a part (see Figure 1.2). Porosity is generally undesirable and can cause degradation of the matrix dominated mechanical properties (i.e. transverse and shear modulus) [8], [9], [10], [11]. In practice, specifications are implemented which dictate the acceptable amount of porosity content in a final part. Parts which exceed this porosity content are discarded. For example, in aerospace applications, primary structures (i.e. critical load bearing structures) made of composites are deemed unsatisfactory if their porosity content exceeds roughly 1-2% following inspection [12].

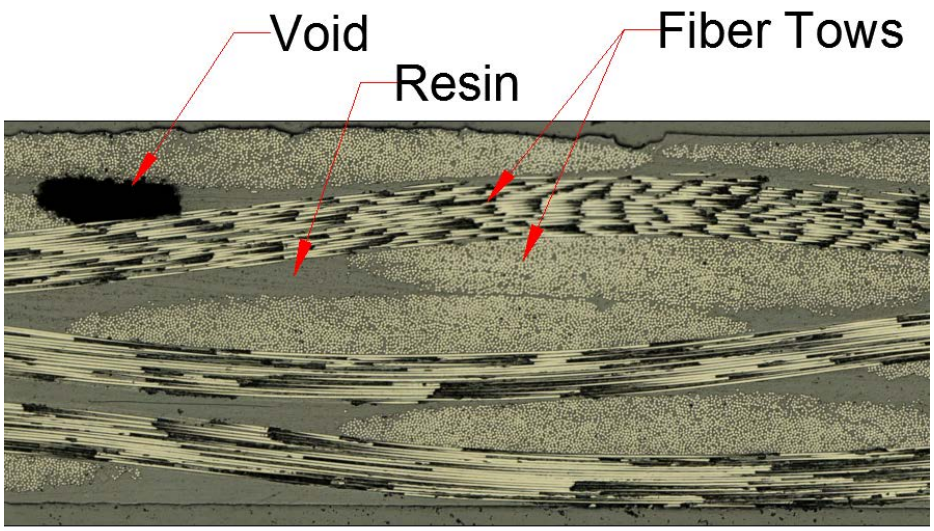

Figure 1.2 – Cross-sectional image of composite material illustrating void, resin and fiber tows.

Porosity occurs when the initial void spaces of the raw material are not infiltrated by the resin during the low viscosity phase of the cure cycle. In general, this occurs when the hydrostatic pressure of the resin does not exceed the internal pressure of the voids in addition to the surface

tension forces at equilibrium. Gas entrapment during material deposition, off-gassing from imbedded moisture or other volatiles and bag leaks can enable this phenomenon to occur and are commonly referred to as void sources.

Some of these sources are often inevitable in composite processing. As such, the presence of void sources must be balanced by mechanisms which act to suppress void growth, commonly referred to as void sinks. These are gas extraction and resin pressurization. Gas extraction is achieved by pulling vacuum on the part. This thereby reduces the internal gas pressure of the void and promotes their collapse. In contrast, void collapse can also be achieved by increasing the hydrostatic pressure applied to the resin. With regards to the void sinks, it should be noted that only resin pressurization can work exclusively to eliminate voids. That is to say, in the absence of gas extraction it is possible to drive the internal gas content into solution and eliminate porosity providing the resin is sufficiently pressurized. However, it is not possible to eliminate porosity through gas extraction alone since there is no driving force to enable the resin to infiltrate the void spaces. This highlights the importance of resin pressure.

1.2.4 Autoclave versus Out-of-Autoclave Prepreg Processing

Currently, the bulk of aerospace composite structures are manufactured with the use of an autoclave. Higher quality parts can be achieved in autoclave processing by the application of positive pressures (typically between 5-7atm). Since consolidation pressure is shared between both the fiber bed and the resin [13], an increase in consolidation pressure will subsequently increase the hydrostatic pressure of the resin. As previously mentioned, high resin pressure is

desirable since it deters the stabilization and growth of entrapped gases and promotes their collapse.

However, autoclave processing requires high capital investments due to initial, operating and maintenance costs of the autoclave itself. The cost of an autoclave also increases exponentially with size which further limits the affordability of manufacturing large parts. For this reason there has been a growing interest in the use of Vacuum-Bag-Only (VBO) prepreg processing techniques. The promise here is to reduce the cost of composite processing by eliminating the need for an autoclave altogether and using low cost curing methods instead (e.g. ovens and heated tools).

Although financially beneficial, VBO processing also presents a greater risk of producing parts with porosity. Since the consolidation pressure is limited to atmospheric pressures, the mechanism of void collapse through resin pressurization is highly restricted. This can result in parts with higher porosity content. For this reason, material manufactures have specifically tailored certain prepreg systems for VBO processing[14]. These special prepreg materials are called Out-of-Autoclave (OoA) prepregs. They have been optimized by incorporating interconnected gas pathways into the prepreg commonly referred to as engineered vacuum channels (EVACs). These EVACs allow for a greater extraction of air during the debulking stage. A more in depth discussion regarding the difference between autoclave and OoA prepregs will be presented in Chapter 2. However, it should be noted that the compaction and flow behavior involved in the processing of both these materials are essentially the same.

Regardless of the differences between autoclave and OoA prepregs, the issue of porosity in the processing of both these materials continues to be of major concern. However, it can be said that OoA materials demonstrate greater sensitivity to the processing parameters which influence porosity. For this reason, an OoA material and process was used for this study. It should be noted that this does not imply that the findings presented in this thesis are restricted to OoA applications. Since the flow and compaction behaviors of these materials are the same, the findings presented in this document can be extended to autoclave practices.

1.3 Configured Structures

A great deal of research concerned with the fundamental flow and compaction phenomenon which influences porosity exists and will be discussed in greater detail in the next chapter. Although the bulk of this existing work primarily deals with flat uniform parts, it can be said that a fairly good understanding of the relationship between porosity and its driving state variables has been established. However, as will be discussed in this section, the physics and mechanisms involved in composite processing become much more complex when dealing with configured structures. As previously mentioned in section 1.1, due the advantages that composite processing offers, composite parts manufactured in practice are seldom flat in geometry or uniform in constituents. As such, there exists a discrepancy between our current academic understandings and the practical knowledge needed in industry. To address this problem, relationships between configured structures common in practice and there influence on the state variables driving porosity must be established.

The focus of this study is on the processing of composite parts which have been termed as being configured structures. For the purpose of clarity, the use of this term with respect to this thesis is elaborated here. Configured structures refers to the non-uniform geometries of the composite part (e.g. corners, multiple planes of curvatures etc.) and also refers to its constituents. Parts may be structurally configured at the constituent level in the sense that the layup of the laminate is non-uniform. Ply gaps, ply drops, ply overlaps, inserts and cores are examples of such structural configurations. As an example, Figure 1.3 illustrates a cross section of a composite hat stiffener which contains a variety of structural configurations at the geometrical and constituent level.

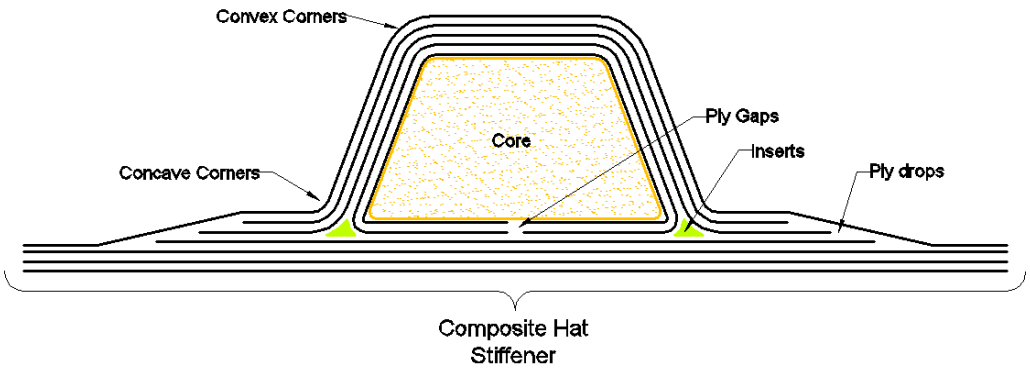

Figure 1.3 – Composite hat stiffener comprising of various geometrical and constituent structural configurations.

Permutations at the tooling level or in the methods used to consolidate a composite part also exist in current practice. These may also be non-uniform in their nature. For this reason, these are considered to be within the realm of configured structures. Matched die tooling, pressure intensifiers or the use of caul sheets are examples of configured structures at the tooling level. Figure 1.4 illustrates various tooling methods that could be used to consolidate the composite hat

stiffener shown in Figure 1.3. A conventional tooling arrangement is shown in the upper rows of the figure whereas the lower rows are illustrations of configured tooling.

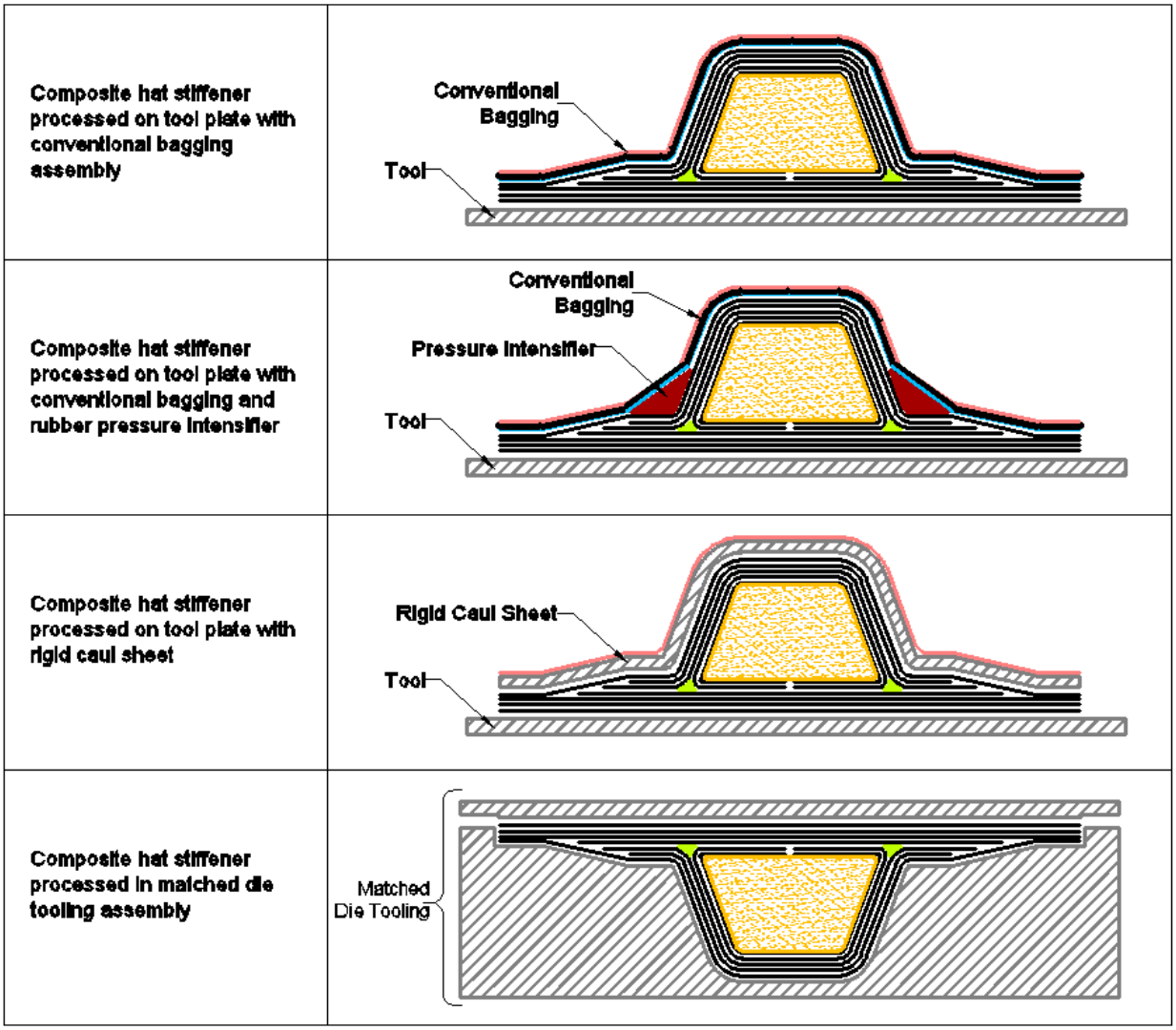

Figure 1.4 – Illustration of various tooling arrangements for processing composite hat stiffener (conventional tooling in upper row and configured tooling in bottom three rows).

The incorporation of structural configurations complicate the physical mechanisms (e.g. consolidation, gas extraction, heat transfer etc.) involved in the processing of composite parts. As these phenomenon become increasingly complex, so does the management of quality defects.

Consider, as an example, the processing of the composite hat stiffener with the use of a conventional bagging arrangement (shown in Figure 1.5).

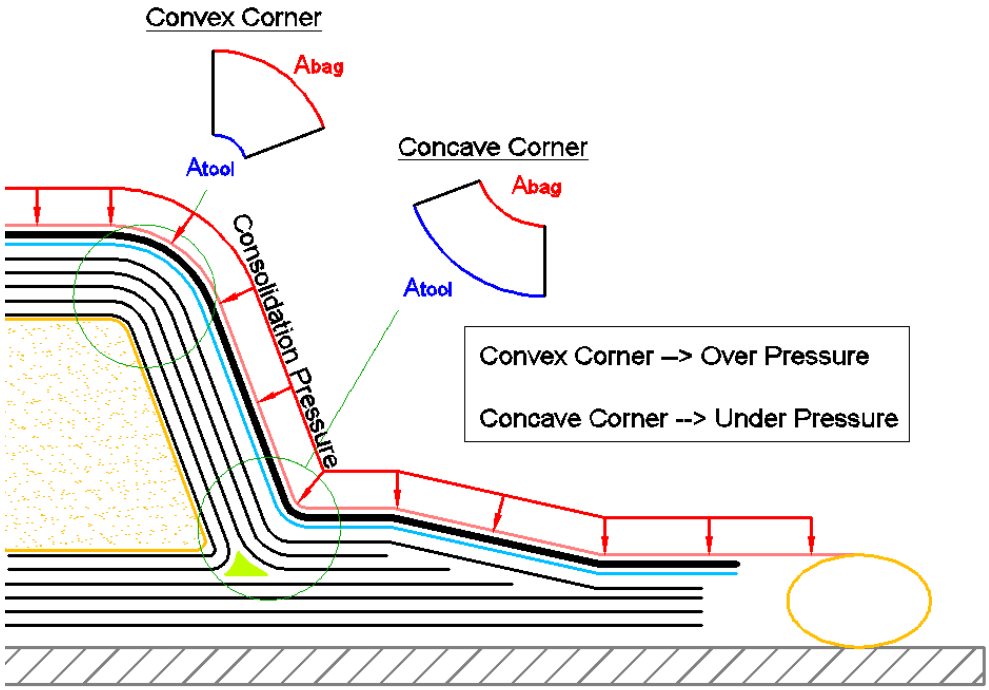

Figure 1.5 – Illustration of corner consolidation pressure distortion for composite hat stiffener processed with conventional tooling and bagging.

As vacuum is applied to the bagging arrangement, a consolidation pressure will be applied to the part. Ideally, this pressure will be uniform throughout the entirety of the structure. However, due the curvatures of part, this will not be the case. In the case of the convex corner, since the bag side surface area (i.e. the surface exposed to the compaction pressure) is greater than the tool side surface area (i.e. the surface facing the tool), this region will be subject to over pressurization. The opposite is true in the case of the concave corner. These variations in consolidation pressure will have a downstream effect on the flow and compaction phenomenon inherent in the process.

In turn, this can result in numerous quality defects such as; wrinkling, thickness variations, resin pooling/depletion and voids.

To compensate for quality defects incurred by structural configurations at the geometrical and constituent level, practitioners commonly turn to the use of structurally configured tooling (i.e. pressure intensifiers, caul sheets and matched die tooling). However, configured tooling can also result in quality defects. In this case, undesirable effects on process phenomenon can be incurred if the surface of the tooling does not comply perfectly with the surface of the part. Gaps between the tool and the part can occur unintentionally during material deposition or through improper tooling design. For example, consider the scenario of ply misalignments for the composite hat stiffener processed in a matched die tooling assembly (shown in Figure 1.6).

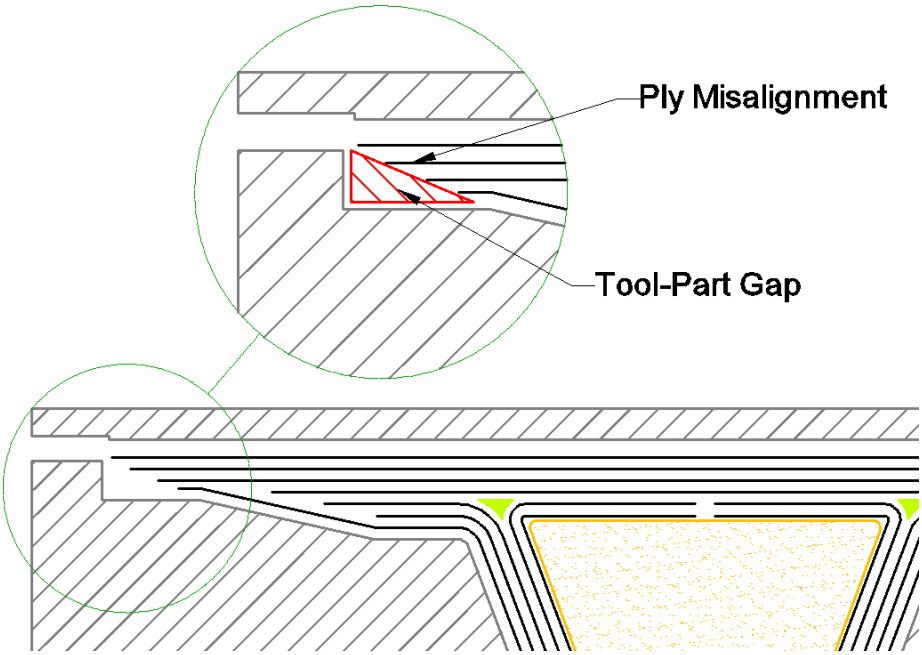

Figure 1.6 – Illustrations of tool-part mismatches (gaps) for composite hat stiffener processed with matched die tooling.

Furthermore, it should be noted that practitioners will sometimes introduce gaps deliberately in order to achieve a desired distortion. An example of such a scenario is the use of flat caul sheets on tapered laminates which is the particular focus of this thesis. As such, a brief overview of this processing scenario will be provided in the following section and discussed in greater detail in Chapter 2.

1.3.1 Ply Drops and Caul Sheets

The two configured structures that will be studied in this research are ply drops and caul sheets. These two configured structures were selected due to their simplicity and common utilization in practice. Their purpose, mode of implementation and potential effect on final part quality will be discussed in greater detail in the next chapter. Here, only a general description of these configured structures is presented.

The bagging assembly which holds the laminate is shown in Figure 1.7. The laminate consists of two types of prepreg plies, terminated plies and the plies which encapsulate them. These types of plies are commonly referred to as partial plies and base plies respectively. A ply drop is the collection of partial and terminated plies as shown in Figure 1.7. The inclusion of ply drops results in non-uniform laminate constituents and part geometry.

Caul sheets are essentially a secondary tooling interface inserted between the laminate and the bagging assembly. Caul sheets can be made of the same material that the tool is made of (i.e. typically aluminum, steel, invar or composite). Although the caul sheet shown in Figure 1.7 is flat and uniform in thickness, it should be noted they can also range in overall structure. Caul

sheets can have curvatures and non-uniform thickness profiles. These are designed at the discretion of the practitioner to suit the processing requirements of the part. Caul sheets result in non-uniform pressure distribution on the laminate. Note that this is true even in the cases where both the laminate and caul sheet are flat and uniform. This is due to the fact that the caul acts as a rigid membrane inserted within the load path of the consolidation pressure (i.e. the differential pressure between the internals of the bag and the ambient pressure outside of the bag).

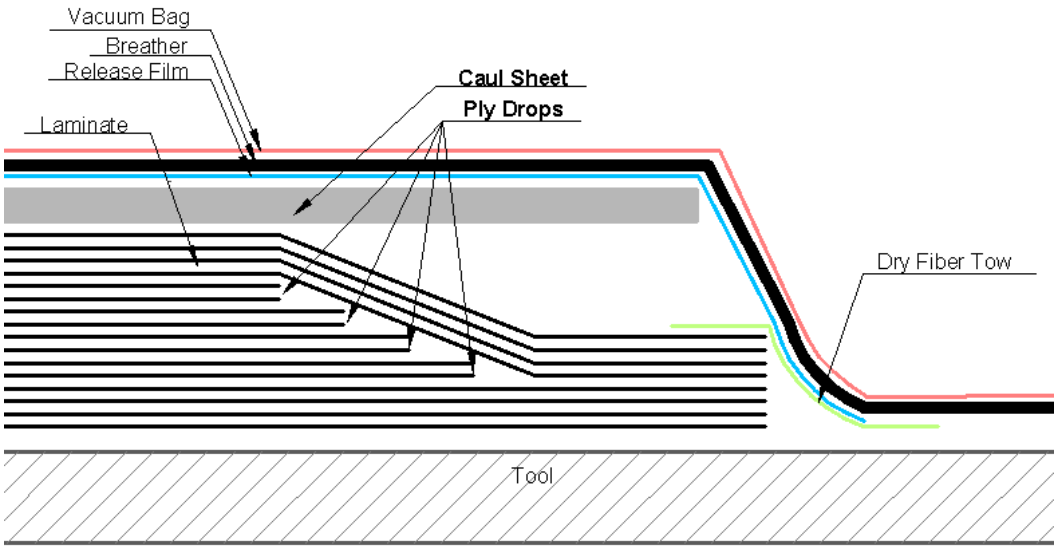

Figure 1.7 - Illustration of ply drops and caul sheets in combination.

Although Figure 1.7 illustrates the implementation of ply drops and caul sheets as a combination, it should be noted that this is not necessarily true in all cases. These structural configurations can be implemented both separately and in combination.

1.4 Research Scope and Objectives

1.4.1 Problem Statement

A great deal of academic research which attempts to develop a fundamental understanding of the interconnected driving mechanisms of porosity for prepreg processing exists. Centea [15] synthesized a summary of the bulk of the publications related to this topic with respect to OoA prepreg processing. However, the bulk of the works published to date have restricted their research scopes to dealing with flat uniform parts. These simplified scopes are necessary to produce an unimpaired evaluation of the fundamentals of the problem. As such, there exists a gap between what is researched in academia and what is practiced in industry.

Although parametric and demonstrator studies relating to porosity in configured structures do exist [15], little emphasis is placed on explaining the effects that the configured structures have on porosity by means of the fundamental physics of the materials and processes involved.

1.4.2 Motivation and Scope of Research

The motivation of this research is to take the first step in advancing our knowledge of porosity by incorporate the inclusion of structural configurations in the processing of composite parts. Since configured structures add to the complexity of the flow and compaction phenomenon which drive porosity, this study can serve as a milestone in evaluating the state of our current understanding. Specifically, this study can help to assess how well the current knowledge serves in the dissection and understanding of porosity in practical processing scenarios. Furthermore, identifying the areas in which the current knowledge is lacking is of great importance and use.

Such findings will help to direct future research efforts in a manner which is useful to the current industrial needs.

Since there is an abundance of structural configurations in existence, the scope of this work has been refined to focus on two simple yet commonly used structural configurations. These are ply drops and caul sheets. It should be noted, however, that this does not mean that the findings presented in this study are restricted to this particular set of complexities. Provided that the findings can be explained on the basis of their fundamental physics, the knowledge developed through this study can be applied to a wider variety of applications. For this reason, the development of a thorough understanding of the problem was considered to be of crucial importance in this study.

1.4.3 Objective

The objective of this work is to evaluate the mechanisms by which porosity is incurred as a result of implementing ply drops and caul sheets in the processing of composite parts. These mechanisms will be described in the context of our current understanding of void formation in composite processing. This objective will be pursued by the following:

- Perform a small scale parametric study to evaluate the effect that caul sheets and ply drops have on the final void content of composite parts.
- Identify the key effects that these structural configurations have on the flow and consolidation mechanisms which leads to porosity and provide an in-situ analysis of the paramount mechanisms with the use of an instrumented tool.

- Simulate the flow and consolidation histories observed experimentally with existing simulation software.

1.4.3.1 Thesis Structure

The following structure is used to present the work in this thesis:

- Chapter 1 (Introduction) provides an overview of the composite materials, processing, porosity and configured structures relevant to the scope of this thesis. A summary of the thesis objectives is also included.
- Chapter 2 (Background and Literature Review) includes a literature review of the current understanding of void growth in prepreg processing. A discussion on the purpose, mode of implementation and potential effect on final part quality for ply drops and caul sheets is also presented.
- Chapter 3 (Small Scale Parametric Study) presents the experimental methods and results of a small scale parametric study conducted for laminates with ply drops and caul sheets. Here the effect of caul sheets and ply drops both separately and in combination are studied. Parameters of interest include cure cycle conditions, caul sheet bending stiffness and ply drop configuration. A discussion of the results is also included in the later part of the chapter.
- Chapter 4 (Instrumented Tool Tests) presents the experimental methods and results of an instrumented tool test for laminates with the same ply drop configuration and caul sheets of various thicknesses. Here the internal hydrostatic resin pressure is monitored during the cure.

- Chapter 5 (Simulations) presents Darcy flow-compaction simulation results from two exercises. The first exercise looks to assess the effect that the material properties have on the resin pressure and flow. The second exercise assess the models ability to mimic the pressure histories observed in the experimental trials of Chapter 4. The COMPRO V2 plug-in [2] and ABAQUS V6.14 [3] finite element software were used for both exercises.
- Chapter 6 (Conclusions) includes concluding remarks with regards to the results presented in this study. A discussion with regards to future work is also included.

Chapter 2: Background and Literature Review

In order to contextualize the work presented in this thesis, a clear understanding of the processing techniques used in this work and the mechanics of porosity must be reviewed. As such, an overview of prepreg processing as well as the fundamentals of porosity is provided in sections 2.1 and 2.2 respectively. Since an Out-of-Autoclave (OoA) prepreg was studied in this thesis, section 2.3 provides an outline of the key characteristics pertinent to this type of material. This section has been included to help distinguish the differences and commonalities between OoA processing and traditional autoclave processing. A review of the material used for this study is also included in this section. Based on a synthesis of the reviewed literature, the potential effect of ply drops and caul sheets on porosity is discussed in section 2.4. In addition, some of the existing literature dealing with porosity in configured structures is presented. This literature review is not restricted to ply drops and caul sheets. This has been done to impart upon the reader the complex nature of this field of study as well as short comings in the existing knowledge base.

2.1 Prepreg Processing

Amongst the various composite processing techniques available, prepreg processing has gathered considerable interest in the manufacturing of high performance structures and is favored by the aerospace industry. The main advantages that prepreg materials offer is in the relative ease of handling and manufacturing and the high level of control that can be exhibited over the fiber to resin ratios and fiber alignments. In general, prepreg processing consists of three steps: Layup, debulking and curing. The current section provides an overview of prepreg materials and the processing steps involved.

2.1.1 Prepregs

In general, prepregs consist of collimated fibers (tapes) or weave (fabrics) which are partially pre-impregnated with resin. This is achieved via a hot melt or solvent dip process[16]. The degree of resin impregnation varies from one material system to another but in general the fiber bed is not fully saturated. For thermoset prepregs (which is the material systems studied in this thesis) the resin is partially cured to what is referred to as a “stage-B” cure [7]. At this cure stage the resin consists of a gel-like tacky solid at room temperature. This material is then rolled onto a take up roll, sealed, frozen and shipped to the client. The purpose of sealing the material is to limit water condensation in the material when thawing it for use. Condensation would add to the moisture content of the material which, as will be discussed later, results in higher porosity by increasing moisture off-gassing during the cure.

2.1.2 Layup

At the beginning of the layup process, the material is removed from the freezer and thawed within the bag. After the material is thawed to room temperature within the bag, the roll is removed from the bag and plies of the desired geometry and fiber orientation are cut from it. These plies are then stacked onto a tool until the desired thickness is achieved. The final stack of plies is referred to as the laminate. The laminate is then vacuum bagged with the appropriate consumable arrangement. Figure 2.1 provides an illustration of typical consumable arrangement for vacuum bagged laminate.

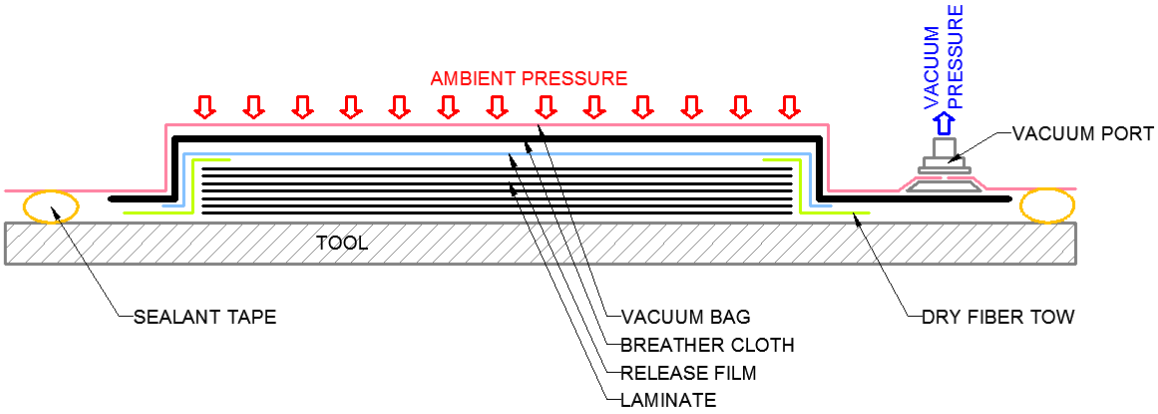

Figure 2.1 – Illustration of typical vacuum bagging assembly for flat laminate.

The tool (typically made of aluminum, invar, steel or composite) is treated with a chemical release agent which prevents adhesion between the tool and the part. A release film is placed over the laminate to prevent the breather material from adhering to the laminate. Prepreg systems which are designed to not bleed during processing (these are referred to as net systems) will utilize release films which are impermeable to resin. In contrast, prepreg systems which are designed to bleed during processing will utilize release films which are permeable to the resin. The breather serves as a breathable media and provides two functions. The first function is to provide a breathable media for the extraction of gases initially contained within the bag and laminate. The second function is to prevent the vacuum bag from sealing itself off from the vacuum source. This allows the bag to form to the part completely and provides maximum consolidation pressure. In order for gas to escape the unsaturated regions of the laminate, the permeable network of the prepreg must be connected to the breather. To do this, dry fiber tows are placed in such a fashion that they are in contact with the laminates edge and the breather. Breathable edge dams such as cork or fabric wrapped sealant tape can also be used for this purpose. Note that this is of greater importance for low pressure application (i.e. out-of-autoclave

(OoA) processes), however dry fiber tows and breathable edge dams can still be used in high pressure applications (i.e. autoclave practices). The final step in the layup process is to seal the assembly with a vacuum bag (typically nylon bagging) and sealant tape.

Note that there exist many different combinations and permutations amongst various prepreg layup techniques such as; the implementation of non-breathable dams, bleeder fabrics, the use of caul sheets, or other pressure intensifiers to name a few. These variations in bagging techniques become more numerous and common in the processing of configured structures. As such, the description given above is only intended to give a general overview of a generic layup process.

2.1.3 Debulk

Following the layup process, gas is pulled from the bag and a vacuum is created for a given period of time at room temperature prior to cure. This is done to consolidate the laminate plies and extract the gas contained within the system. With respect to gas extraction, this debulk time is generally dependent on the permeability and size of the laminate being processed [12], [17], [18], [19], [20]. A great deal of work has been done on relating the laminates permeability to air, length and thickness to the required debulk time. This body of work will be discussed in greater detail in section 2.2.1.1. In general, however, the bigger and less permeable the laminate, the more time is required for the debulk phase.

The consolidation pressure results from the differential pressure between the internal contents of the bag and the ambient pressure outside of the bag. The ambient pressure can simply be the surrounding atmospheric pressure or it can be amplified by inserting the assembly into an

autoclave. To better consolidate the laminate prior to cure, short debulking periods can be imposed intermediately during the layup process. For example, a debulk cycle can be applied for every fourth ply laid down. This can be done with the final consumable assembly shown in Figure 2.1 or with a reusable nylon bag specifically built for this purpose.

For OoA processing, a vacuum is maintained after the debulking phase and throughout the cure cycle. For autoclave processing, the vacuum bag is sometimes vented during the cure. However, the reasons and applications of this practice is beyond the scope of this thesis.

2.1.4 Curing

Following the debulking step, the part is now ready for cure. Cure cycles consist of a succession of temperature ramps and dwells. A simulation of typical cure cycle is shown in Figure 2.2. This cure simulation was generated with the use of the national center for advanced materials performance (NCAMP) data implemented in the Raven[21] simulation software. The cure kinetics model used for this simulation is that of an MTM45-1 [22] resin system.

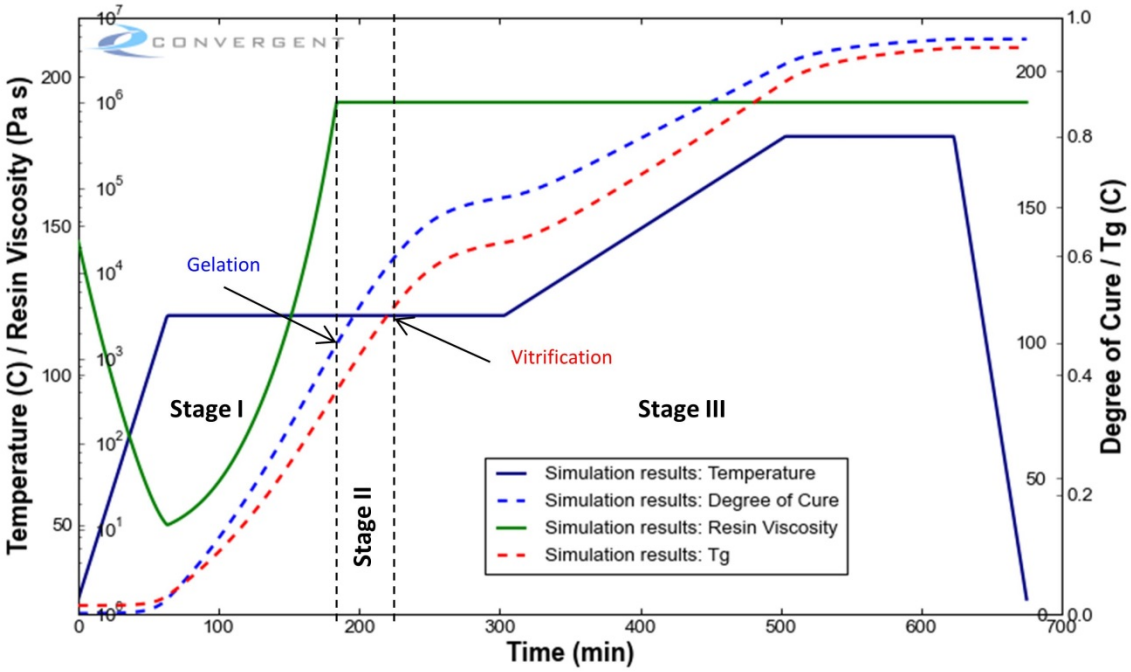

Figure 2.2 – Cure simulation of an MTM45-1 resin system [21]

A typical thermoset cure cycle can be divided into three stages. At the beginning of the first stage, the resin is in a semi-solid state (i.e. short polymer chains). As the temperature increases to the initial dwell temperature, the high level of free volume allows for high molecular mobility which causes the viscosity to decrease substantially. The viscous behavior of this first stage of cure allows for the impregnation of void spaces in the prepreg. The mechanics of void impregnation will be discussed in greater detail in section 2.2.1. During this stage of cure, the increased temperature will also cause cross-linking reactions to occur between the polymer chains. This ongoing reaction causes the buildup of a three dimensional polymer network, which subsequently causes the resin viscosity to increase by many decades. As the molecular weight of the resin approaches infinity, the point of gelation is reached, which marks the beginning of the

second stage of cure. Gelation is an irreversible process which only occurs in thermoset polymers (i.e. thermoplastics do not gel).

With respect to porosity, it should be noted that void impregnation will only occur when the resin exhibits viscous behavior (Stage I). Therefore, it is crucial that void impregnation is allowed to occur prior to gelation. Once the resin gels, the internal macro structure of the laminate is set and the morphology of the voids cannot change.

Past gelation, during the second stage of cure, the resin exhibits a rubber like behavior (i.e. low elastic modulus but relatively high viscosity). As the degree of cure increases, the polymer network becomes increasingly entangled causing a decrease of free volume and an increasing glass transition temperature. The beginning of the third stage of cure is marked by the vitrification point. By definition, vitrification is the point when the glass transition temperature of the resin surpasses the ambient temperature (i.e curing temperature). During the third stage of cure, the resin exhibits a glassy behavior (i.e. high stiffness and strength). A second dwell is sometimes used to further increase the glass transition temperature and mechanical properties of the part.

2.2 Porosity in Prepreg Processing

In this thesis, porosity refers to the accumulation of void spaces in the material. Porosity is one of the main issues when processing composite materials. The presence of porosity can cause a severe degradation of the matrix dominated mechanical properties. Harper et al. [9] found that a 5-6% void content in a 4 ply AS4/3502 unidirectional composite epoxy laminate causes

approximately a 33% and 25% reduction in the transverse and shear moduli respectively. Zhang et al. [10], [11] studied the relationship between ultrasonic attenuation, void content and various matrix dominated strengths for $[0/90]_{3s}$T700/TDE85 prepreg laminates. They found that for void contents of 3.2%, the laminates suffered an 18% reduction in inter-laminar shear strength, a 22% reduction in flexural strength and a 14% reduction in tensile strength.

Due to its severe negative impact on mechanical properties, a great body of work has been undertaken over recent years to evaluate the effects and formation of porosity in prepreg materials. In its simplest and most practical form, porosity management can be thought of as a balancing exercise between porosity sources (i.e. aspects which generate voids) and sinks (i.e. aspects which dissipate voids).

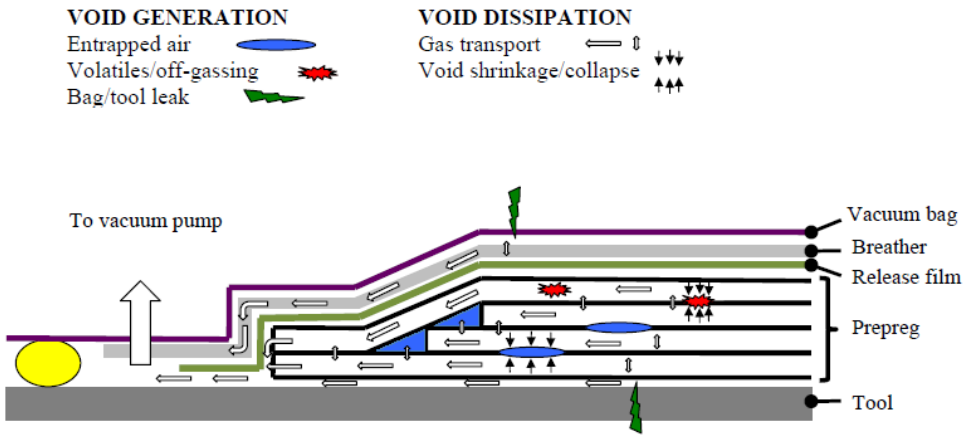

Figure 2.3 – Schematics of void sources and sinks in composite processing [23].

Voids are generated prior to cure in the form of mechanically entrapped air. Since prepregs are partially impregnated, this means that these sources of voids are inherently contained in the raw

material prior to layup. Air can also be entrapped during layup between plies or at internal ply terminations. Voids can also form during the cure via off-gassing of embedded moisture and other volatiles.

Regardless of the source, in order to exist the internal gas pressure of the void must be equal to or greater than the hydrostatic pressure of the surrounding resin in addition to the surface tension forces at equilibrium (equation 2-1) [12], [13], [24]. Failure to meet this criterion will lead to void dissolution or collapse.

$$\begin{aligned} P_g &> P_r + \frac{\gamma_{LV}}{m_{LV}} \quad \text{(Void Growth)} \\ P_g &= P_r + \frac{\gamma_{LV}}{m_{LV}} \quad \text{(Void Equilibrium)} \\ P_g &< P_r + \frac{\gamma_{LV}}{m_{LV}} \quad \text{(Void Collapse/Dissolution)} \end{aligned} \tag{2-1}$$

Where P_g is the internal gas pressure of the void, P_r is hydrostatic pressure of the resin, γ_{LV} is the liquid resin-void surface tension forces and m_{LV} is the void volume to surface area ratio.

The internal gas pressure (P_g) of the void is dependent on the type, amount and temperature of the gas. Therefore, internal gas pressure can increase with increasing temperature or if air, moisture or other volatiles diffuses into the void spaces. Likewise, decreasing the temperature or reversing the diffusion gradient will cause the internal gas pressure to decrease. Furthermore, the internal gas pressure can also be reduced by simply removing the gas content from the voids. This is achieved by creating a vacuum within the laminate such that the gasses contained within the interconnected void spaces travel by advection out to the vacuum system.

The hydrostatic pressure of the resin (P_r) is dependent on the compaction pressure imposed on the laminate. This overall compaction pressure is shared between the fiber bed and resin based on the flow and compaction behavior of the material (equation. 2-2) [13].

$$\sigma = \bar{\sigma_f} + P_r \tag{2-2}$$

Where σ is the overall compaction pressure imposed on the laminate, $\bar{\sigma_f}$ is the fiber bed effective stress and P_r is the hydrostatic pressure of the resin

As such, from a processing parameters perspective, the two mechanisms by which voids can be dissipated (i.e. void sinks) is by successfully removing the gas contents or by increasing the hydrostatic pressure of the resin.

Also included as void sources are bag and tool leaks. It is thought that leaks cause void generation both by the introduction of ambient gasses to the system and by the reduction of vacuum quality. To date, it is still unclear as to whether gasses introduced via a leak manage to travel through the laminate or if they primarily flow through the breather [25]. However, the effects of reduced vacuum quality have been studied [18], [19], [26], [27] and are known to reduce the effectiveness with which gases can be removed from the system. Furthermore, poorer vacuum quality also reduces the overall compaction pressure imposed on the laminate, thereby reducing resin pressure.

2.2.1 Void Formation and Evolution

The current section will give an overview of the formation and evolution of void spaces in prepreg processing. Since an OoA prepreg material has been used in this study, the discussion on void formation and evolution presented here is with respect to this type of prepreg system. However, it should be noted that this does not mean that the following discussion applies exclusively to OoA processing since these materials themselves are also not exclusive to OoA processing. These prepregs can still be processed with the use of an autoclave. Rather, what is being specified here is the material system rather than the process. The defining characteristics which separates OoA from traditional autoclave prepreg systems will be discussed in section 2.3.

Here, the ideal case in which porosity is fully removed from the material by the end of the cure is presented. Later in the section, the modes of failure which lead to porosity will be discussed. These topics of discussion constitute the bulk of existing work with respect to porosity in prepreg processing.

Figure 2.4 provides a schematic of the void morphology at layup, debulk and cure. The porosity in the as laid up laminate can be subcategorized into three different types of voids. These are; fiber tow voids, inter-laminar voids and resin voids.

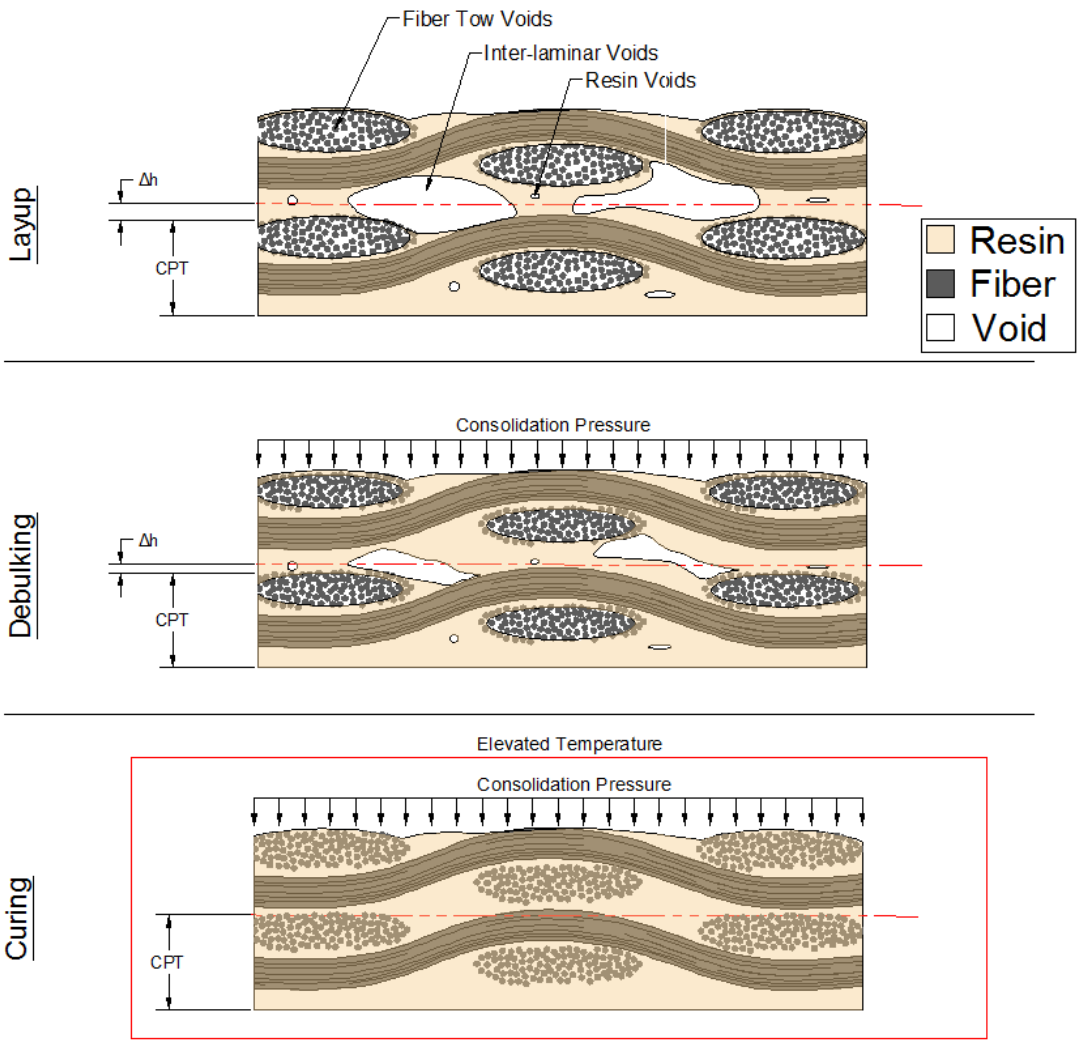

Figure 2.4 – Schematic of void evolution in prepreg processing (based on figure from T. Centea [15]**).**

Fiber tow voids are essentially the un-impregnated regions of the fiber tows. These are a result of partial impregnation and lack of fiber tow compaction [12]. Fahrang [12] and Centea [28] used micro computed tomography (Micro-CT) to evaluate the three dimensional structure of voids for MTM45-1 five harness satin weave carbon fiber prepreg. These images showed that the fiber tow voids consisted of continuous interconnected channels along the length of the part. Furthermore, Fahrang [12] correlated a decrease in in-plane air permeability to fiber tow

impregnation, demonstrating that gas transport within the part is achieved through the fiber tow voids. Therefore, the fiber tow voids act as an interconnected vascular network for gas to flow out of the laminate by advection.

Inter-laminar voids are a result of entrapped air between the interfaces of individual plies (indicated by the red line in Figure 2.4) during the layup process. Their initial shape and size is dictated by the fiber bed architecture and resin application of the prepreg [12]. Due to the mechanism by which these voids are initially formed, they are typically large and elongated in shape and are encapsulated by both resin and dry fiber tows. Resin voids are much smaller and make up the smallest share of porosity in the as laid material. These voids can be formed during resin mixing, prepreging or by off gassing during cure [12]. Unlike the inter-laminar voids, these voids are fully encapsulated by resin and are thus not connected to the vascular network.

During the debulking process, air is extracted from the un-impregnated fiber tow regions and the laminate is subject to a consolidation pressure. The fiber tow voids will decrease in volume due to the consolidation pressure and some minor resin impregnation. However, due to the high resin viscosity and fiber tow stiffness, these voids will remain un-impregnated and continue to act as an interconnected vascular network. Since the inter-laminar voids are in contact with the dry fiber tows, air can be removed from these voids as well. As a result, the volume of these voids decreases significantly during debulk. Due to the fiber bed stiffness and relatively high resin viscosity, some inter-laminar void space will remain. Resin voids are entirely surrounded by resin and are not connected to the vascular network. Therefore, these voids must either be

dissolved into solution through resin pressurization or removed through a diffusion process which is very slow at low temperatures [12].

During cure, the viscosity of the resin drops as the temperature is increased. As the resin is able to flow, it first infiltrates the inter-laminar void spaces [29], [30] leaving the fiber tow voids and resin voids. Once the inter-laminar void spaces are fully saturated, fiber tow impregnation commences. If sufficient compaction pressure is imposed on the laminate, it is possible for the resin voids to dissolve into solution. If this is not the case, it is thought that resin void contents decrease as the diffusion process accelerates with increasing temperature or by coalescence of resin void with inter-laminar voids or fiber tow voids [12], [31], [32]. The full dissipation of all void volume from the laminate causes a reduction in thickness specified by the bulk factor (Δh) and the plies should now be of a thickness representative of the designed fiber and resin content (i.e. the cured ply thickness (CPT)).

In order to produce a porosity free part, all void contents must escape the system prior to the impregnation of the vascular network (i.e. fiber tow impregnation) or be dissolved into solution through resin pressurization. Furthermore, tow impregnation must happen prior to resin gelation. If void content remains following the full impregnation of the fiber tows, and insufficient resin pressure exists to dissolve these voids into solution, these voids are in essence trapped and remain in the final part. Such a scenario can occur if high levels of gas exist inside the system or in the absence of adequate gas transport. Insufficient resin pressurization due to lack of consolidation pressure or resin starvation can also lead to this scenario. Furthermore, improper cure cycle design can influence the resin rheology such that the viscosity decreases too soon and

results in premature fiber tow impregnation. In contrast, porosity can also reside in the final part if the resin gels before full tow impregnation can occur. This can also be caused by improper cure cycle design and other parameters which influence the resin rheology.

The mechanisms by which void evolution differs from the ideal case and results in porosity in the final part has been the subject of many studies. The bulk of these works are discussed in the following two sections. These sections overview the bulk of our current understanding with regards to porosity in prepreg processing. Studies related to the systems internal gases are discussed in the *gas induced voids* section, whereas, studies related to the resin flow are discussed in the *flow induced voids* section.

2.2.1.1 Gas Induced Voids

The formation of gasses inside the prepreg has been discussed earlier in the chapter (section 2.2) and it has been noted that the existence of gas within the prepreg is an inevitable feature for the type of composite processing being discussed here. As such, these gasses need to be removed from the system and their sources need to be mitigated as best possible. A great deal of work which studies gas transport phenomenon in prepregs and other sources of gas has been undertaken and is overviewed here.

Arafath [17] derived a steady state equation to describe unidirectional gas transport in prepreg materials based on Darcy's law and the ideal gas law. The equation calculates the time required to evacuate a given mass fraction of gas. Several fundamental relationships were outlined by this

equation. The time required for gas extraction is linearly proportional to air viscosity and quadratically proportional to the path traveled by the gas.

Arafath's equation [17] also showed that extraction time decreases with increasing permeability. Permeability data from a variety of OoA prepreg materials have been generated by many authors [12], [17], [33], [34], [35], [36]. In general, several aspects of gas permeability in prepreg material are fairly well understood. These are:

- In-plane permeability is significantly greater than through thickness permeability (by 2-4 orders of magnitude).
- Both in-plane and through thickness permeability are higher in fabric prepregs than in tape prepregs.
- In-plane permeability decreases as fiber tow impregnation progresses.
- In-plane permeability remains constant with increasing laminate thickness whereas through thickness permeability decreases with increasing thickness.
- In-plane permeability is higher along the fiber tow direction.

Off-gassing from embedded moisture during cure is another source of gas which can potentially lead to void formation. Off-gassing from embedded moisture increases the internal gas pressure of the voids. Void growth occurs if the internal gas pressure exceeds the hydrostatic resin pressure of the laminate (as shown in equation 2-1). Grunenfelder et al. [37] exposed a series of MTM44-1 carbon fiber laminates to environments of controlled moisture content and cured the laminates in- and out-of-autoclave. Little to no porosity was measured for the laminates which were cured in autoclave due to the high resin pressures achieved in this process. For the

laminates cured out-of-autoclave, it was found that void content was exponentially related to the initial relative humidity of the material. Grunenfelder et al. modeled this behavior based on a diffusion based framework from Kardos [38]. The model showed good agreement with the experimental results. The effect of embedded moisture was also shown experimentally by Kay et al. [18], [19], [27]

In addition to moisture content, Kay et al. also evaluated the effect of debulk time, part length and vacuum quality on the final porosity of flat uniform parts. He found that reduced vacuum pressure, increased distance from the vacuum source, increased moisture content and short debulk times lead to increased porosity content. Furthermore, he also found that these processing parameters have an exacerbating effect when combined. Centea [26] evaluated the effect of reduced ambient pressure and vacuum quality on final void content of flat uniform parts. He found that reduced ambient pressure lead to increased inter-laminar and resin void content. This was attributed to a reduction in consolidation pressure which in turn reduced the hydrostatic resin pressure which allows the voids in the resin rich areas to stabilize and grow. Reduced consolidation pressure did not, however, increase fiber tow void content. For the case of reduced vacuum quality, an increase in fiber tow void content was also found in addition to increased inter-laminar and resin void content. This was attributed to a reduction in consolidation pressure and an increase in gas content in the laminate. Therefore, for this case, fiber tow impregnation is primarily impeded by the internal gas pressure within the fiber tow and not by hydrostatic resin pressure.

One will note here, that all of the work discussed in this section deals with flat uniform parts. Although there does exist some literature regarding gas induced voids in structural configurations, these bodies of work are scarce. Furthermore, the mechanisms by which gas induce voids formulate themselves in any given category of structural configuration is not as widely agreed upon in contrast to research dealing with uniform parts.

2.2.1.2 Flow Induced Voids

The internal gas pressure within the fiber tow is not the only mechanism which can inhibit fiber tow impregnation. Fiber tow impregnation can also be impeded by the state variables relating to the resin flow. During cure, the resin spends a finite amount of time in a viscous state such that it can flow into the dry fiber tows. This period of time as well as the minimum viscosity of the resin is dependent on the degree of cure of the resin. The degree of cure can be altered by the cure cycle or if the material has been exposed to ambient temperatures for a prolonged period of time prior to cure (i.e. out time). Grunenfelder et al. [39] found increased porosity contents in 5320 OoA prepreg system when the material exceeded its working out life (21 days for this system). Fiber tow impregnation for OoA prepregs of various resin systems and fiber architecture was modeled by Centea et al. [40]. With this model, Centea et al. performed a parametric study to evaluate the effect of various processing parameters on fiber tow impregnation. He found that increased initial degree of cure (i.e. degree of cure prior to cure) resulted in a decrease of minimum resin viscosity and time for fiber tow impregnation to occur. Furthermore, increased temperature ramp rates and lower fiber tow fiber volume fractions lead to faster impregnation. Grunenfelder et al. [41] generated experimental fiber tow void content data for 5320 5HS OoA laminates which were subject to various out times. She compared this

experimental data with the prediction generated by Centea's et al. model and found that both experiment and model produced the same trend.

By extension, it could be thought that the effects that resin rheology and cure cycle have on fiber tow impregnation could also be applicable to inter-laminar void impregnation. Temperature dependency of resin film impregnation was demonstrated by Thomas et al. [29] and Cender et al. [30]. The results presented in this research are applicable to both the manufacturing of the prepreg (prepreging) and the processing of prepreg laminates. They demonstrated that impregnation speed is positively proportional to temperature. Cender et al. [30] also showed that impregnation speed is positively proportional to compaction pressure. Furthermore, for the material studied in his research, he showed that as impregnation progresses, some of the consolidation pressure is born by the fiber bed. This in turn causes a decrease in hydrostatic resin pressure which slows down the impregnation process and increases the potential for void growth.

With regards to configured structures, there exists some works which study the influence of various structural configurations on phenomenon relating to the flow and compaction of the part during processing [42], [43], [44], [45], [46], [47]. However, since most of the scope of these works are not predominantly concerned with quality defects, it is often difficult to clearly conclude the mechanisms by which voids formulate themselves as a result of the configurations involved.

2.3 Out-of-Autoclave Prepreg Processing

In reviewing the literature on porosity in prepreg processing, it can be concluded that resin pressure is one of the most important processing parameters with respect to void evolution. Since Out-of-autoclave (OoA) prepreg processing is restricted to consolidation pressures of 1atm, it can also be said that this processing technique demonstrates greater sensitivity to the processing parameters which influence porosity. It is for this reason that an OoA material and process was used for this study. As such, the current section provides an overview of OoA prepreg materials in general and presents the material used for this study. It should be noted, however, that this does not imply that the findings presented in this thesis are restricted to OoA applications. Since the flow and compaction behaviors of OoA and autoclave prepregs are the same, the findings presented in this document can be extended to autoclave practices.

2.3.1 Out-of Autoclave Prepregs

OoA prepreg materials are an alternative to traditional autoclave prepreg material systems. As the name suggests, OoA prepregs are material systems which are specifically designed to be vacuum-bagged-only (VBO) processed. This means that they are processed without the use of an autoclave. Eliminating the need for autoclaves is advantageous because it eliminates the acquisition, operational and maintenance costs associated with this type of technology[15]. OoA prepregs have also been designed to incorporate high performance low temperature cure resin systems[14]. The ability to cure at low temperatures enables the use of low-cost tooling materials and reduces processing defects caused by thermal expansion mismatches. Furthermore, the use of low-pressure cycles allows for low cost tooling to be used and reduces high pressure induced defects such as core crush and face-sheet dimpling[15].

However, one of the main drawbacks of OoA prepregs is in the increased likelihood that porosity will remain in the final part. Traditionally, for autoclave processing, entrapped gasses and embedded volatiles would be dissolved into solution through the application of high compaction pressures (ranging from 5atm to 7atm). Since the compaction pressures in OoA processing is limited to 1atm, the production of void free parts relies more heavily on successfully removing entrapped gases and volatiles prior to cure. Consequently, material manufactures alike have developed newer generations of OoA prepreg such that they can “breath”. This design feature is what separates second generation OoA prepregs from traditional autoclave prepregs.

There are many types of OoA prepregs commercially available through a multitude of material manufactures. Due to the processing needs previously discussed, commonalities amongst all of these OoA prepregs can be identified. These common features, as outlined by Repecka and Boyd [48] and Ridgard [14], are presented below:

1. OoA prepregs have a lower degree of resin impregnation such that the fiber tows can better act as an interconnected vascular network. This network allows for the transport of gasses within the material and is commonly referred to as engineered vacuum channels (EVaCs).
2. In order for gas to escape from the prepreg, a permeable media which connects the prepreg stack to the breather and subsequently the vacuum system must be incorporated in the layup strategy. This is typically achieved with fiber tow strands or breathable edge dams (i.e. cork dams or fabric wrapped sealant tape) as discussed in section 2.1.2.

3. The resin rheology and cure cycle specifications for OoA prepregs are typically designed such that these EVaCs remain un-impregnated by the resin for longer periods of time (i.e. during the room temperature vacuum holds and early stages of cure). As such, these materials are typically cured with the use of an intermediate low temperature dwell followed by a high temperature post dwell. The intermediate dwell is designed to provide the maximum amount of time for gas extraction and is typically around 80°C-120°C. The post dwell, which ideally precedes the full impregnation of the EVaCs, and is intended to achieve the maximum mechanical properties and glass transition temperature (Tg). This post dwell is typically around 180°C temperature range.
4. OoA prepreg systems are designed to be no-bleed systems. This is due to the fact that resin bleed can lead to more of the compaction pressure being born by the fiber bed which thereby decreases the hydrostatic resin pressure (as shown by equation 2-2). Since the compaction pressures in OoA processing are inherently low, the potential for void growth due to a decrease in hydrostatic resin pressure is much greater.
5. The integrity of the vacuum is of much greater importance for OoA prepregs and must be of high quality throughout the cure. As such, material manufactures will typically emphasize the importance of maintaining a minimum vacuum gauge pressure of 94.8kPa (28 in Hg).

2.3.2 MTM45-1 Prepreg System

The material system that will be used in this study is coded as MTM45-1/CF0526A produced by Advanced Composites Group (Now CYTEC). It consists of HTS40 E13 3K carbon fiber tows woven in a plain weave (PW) fabric produced by Toho Tenax America, Inc. The MTM45-1 resin system is a high performance, toughened epoxy optimized for low pressure VBO processing [22]. This resin system was designed to offer a variety of cure temperatures and as such, a variety of manufacturer recommended cure cycles (MRCC) are provided by the manufacturer including cure cycles for autoclave processing. Table 2.1 presents the summary of the initial cure process parameters recommended by the manufacturer for OoA and autoclave processes.

Table 2.1 – Summary of MRCC (initial dwell temperatures) of MTM45-1 resin system [22]**.**

	Vacuum Bag Processing	**Autoclave Processing**
Ramp Rate	1-3°C/min (1.8-9°F/min)	1-3°C/min (1.8-9°F/min)
Pressure	N/A	89-207inHg (3-7bar)
Vacuum Pressure	>28inHg (0.95bar)	>28inHg (0.95bar)
Cure Time	20 hours @ 80°C (176°F) or 4 hours @ 120°C (248°F) or 2 hours @ 130°C (266°F)	20 hours @ 80°C (176°F) or 4 hours @ 120°C (248°F) or 2 hours @ 130°C (266°F) or 2hrs @ 180°C (356°F)

In order to achieve maximum Tg and mechanical properties, it is recommended that these materials be postcured (i.e. secondary dwell) at a temperature of 180°C.

Other properties that are provided by the manufacturer are various mechanical properties of the cured lamina (single ply of prepreg). These are the fiber areal weight (FAW) of a single ply,

resin to fiber ratio by weight (%RW), fiber to resin volume fraction (%VF) and cured ply thickness (CPT). The manufacturer does not provide this information for all available prepregs. However, these properties are listed for an MTM45-1/CF0525 prepreg which has the same fabric style of the material used in this study but consists of a different carbon fiber (AS4 by Hexcel). Since the density and filament diameter of the AS4[49] and HTS40[50] fibers are similar, one can assume that the mechanical properties discussed above and listed below (Table 2.2) are also similar.

Table 2.2 – Summary of mechanical properties for MTM45-1/CF0525 prepreg [22]

ACGM Material Specifications	ACG Nomenclature	Fibre/Style	FAW (g/m^2)	%RW	%VF	CPT (mm)
…	…	…	…	…	…	…
1001-07	MTM45-1/CF0525-36R%W	AS4/ 3K PW Fabric	193	36	54.34	0.201

It should be noted that the mechanical properties for the prepreg used for this study are not available through open source publications, such as those published by the national center for advanced materials performance (NCAMP).

This material (like most prepreg materials) undergoes a slow curing reaction at room temperature and therefore must be sealed and kept in a freezer (-18°C storage) when not in use. As such, there is a set amount of time that this material can be exposed to room temperature, otherwise referred to as working out life. The working life for this material is 21 days [22].

2.4 Configured Structures: Ply Drops and Caul Sheets

In this thesis, the effect of ply drops and caul sheets on final part quality will be studied. As such, section 2.4.1 will review the purpose of use and mode of implementation for ply drops and caul sheets. Based on a synthesis of the reviewed literature dealing with porosity in prepreg processing (overviewed in section 2.2), the potential effect of ply drops and caul sheets on porosity will also be discussed in section 2.4.2. A brief overview of some of the existing literature concerned with porosity in structural configurations will be provided in section 2.4.3. Note that this overview is not primarily restricted to literature dealing with ply drops and caul sheets. This has been done in order to identify and discuss common trends and short comings of the research in this area.

2.4.1 Physical Features of Ply Drops and Caul Sheets

Ply drop laminates contain internal ply terminations (as shown in Figure 2.5). The plies which span the entire length of the part are referred to as base plies, whereas, the plies which are terminated within the laminate are referred to as partial plies. Multiple plies can be terminated at the same time. The distance between each ply termination is referred to as the ply pitch (scatter distance is also commonly used). Ply terminations are known to have an effect on the delamination strength of the laminate [51], [52]. As such, design guidelines for ply drop configuration have been proposed [53]. However, the existing guidelines are only concerned with determining layup strategies which deliver maximum part performance. Guidelines based on part quality and processability do not exist.

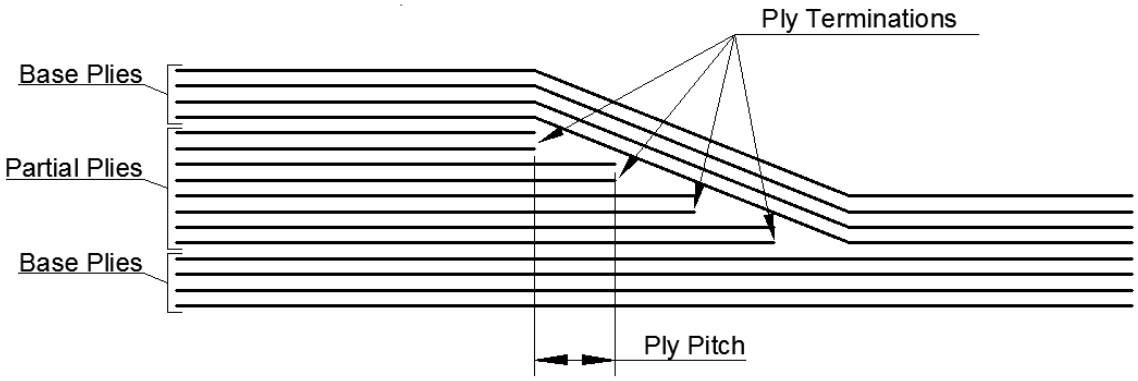

Figure 2.5 – Illustration of laminate containing ply drops.

One general reason for implementing ply drops is to process tapered laminates. However, another reason is to build up the thickness at specific location in the laminate where mechanical reinforcement is required. Typically, regions where holes are to be drilled in the cured part (for fastening purposes) will commonly be subject to this fashion of local reinforcement (commonly referred to as pad-ups).

Caul Sheets are essentially a secondary tooling interface placed between the laminate and the bagging consumables (see Figure 2.6)

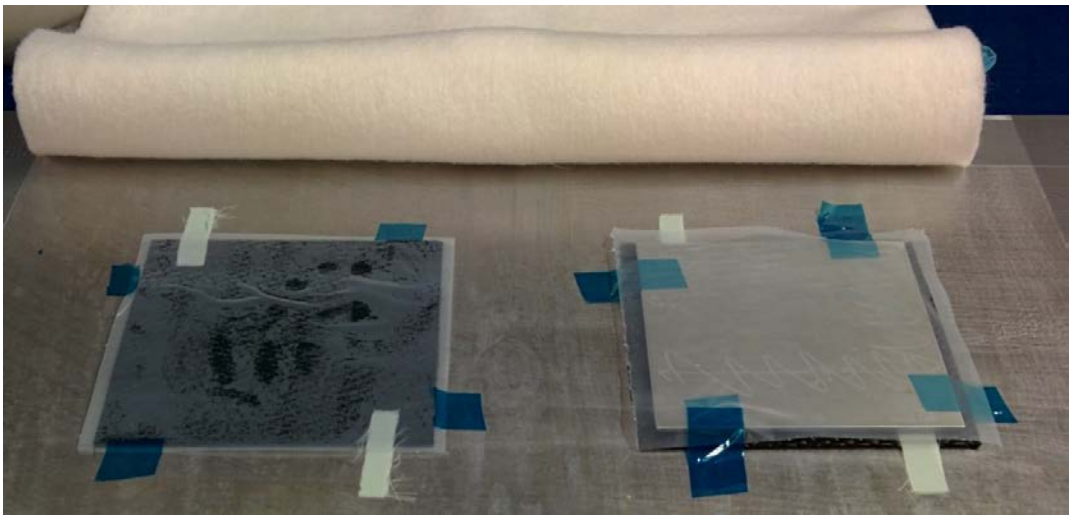

Figure 2.6 – Capture of partial prepreg layup without caul sheet (left) and with caul sheet (right).

Caul sheets can be made of any material that the tool is made of. Furthermore, like the tool, the caul sheet can be design specific, meaning that its geometry is suited to conform to the geometry of the laminate being processed. Currently, guidelines for the design of caul sheets do not exist. Caul sheets are manufactured at the discretion of the practitioner to suit the processing requirements of the part. Although individual practitioners have developed their own guidelines based on past experience, these guidelines have not been published nor have they been recognized for being based on anything other than empirical knowledge.

One general guideline that is commonly recognized is that caul sheets need to be undersized such that they do not overlap the laminates boundaries. If the caul sheet overlaps the laminates boundaries, either unintentionally or by design, a void pocket will form in the cavity surrounded by the tool, caul sheet and laminate edge (see Figure 2.7). Once air is drawn from the bag, the low pressure at this cavity will cause the bagging material to be drawn into it. As the caul sheet deforms under atmospheric pressure (or higher pressures for autoclave processing) it effectively

collapses onto the bagging material. This phenomenon is called bag pinching and can lead to the formation of leaks in the bagging assembly. Figure 2.7 below illustrates the phenomenon of bag pinching. Due to its implication and practicality, the guideline of undersized caul sheets will be respected in this thesis.

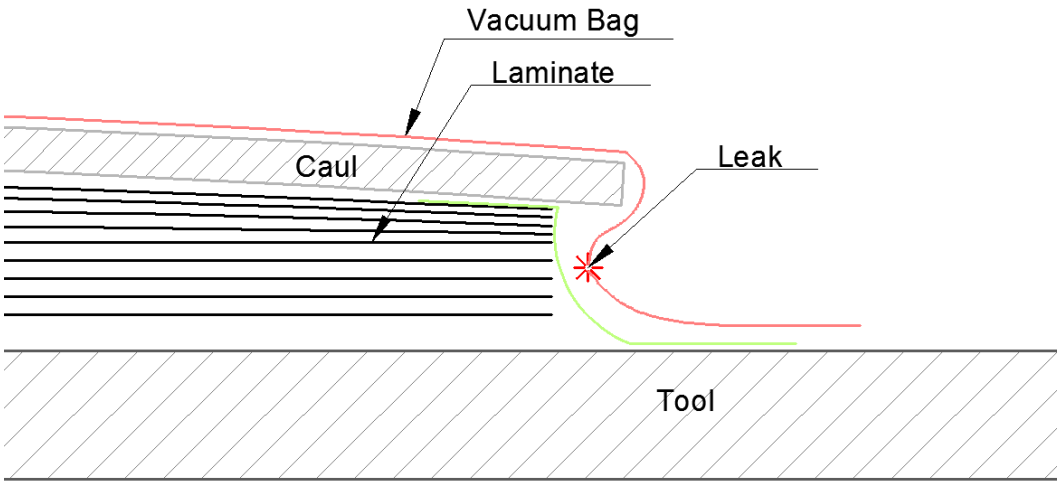

Figure 2.7 – Illustration of bag pinching phenomenon.

One general reason for using cauls is to achieve uniform surface finishes on both sides of the laminate (i.e. tool side and bag side). As seen in Figure 2.8, in the absence of a caul sheet, the bag side of the laminate is left with the impression of the breather material which results in a rough textured surface finish. When a caul sheet is used, the impression left on the bag side of the laminate is that of the caul sheet. This results in a smooth uniform surface finish which is aesthetically pleasing.

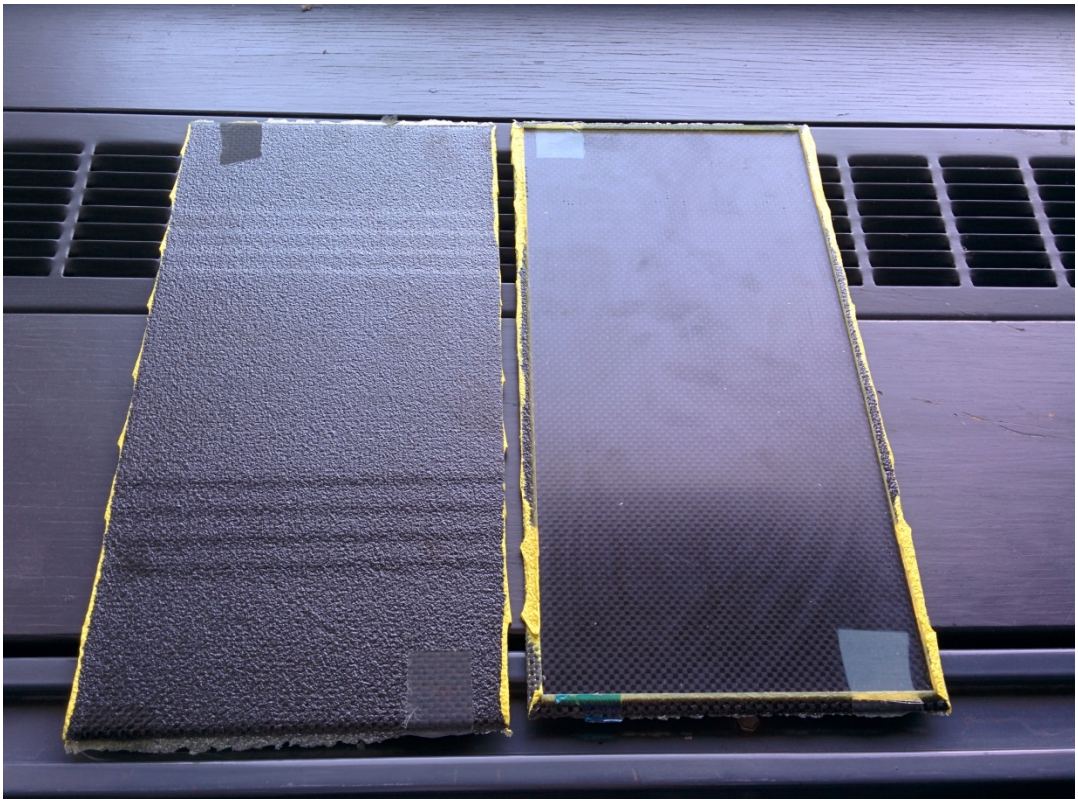

Figure 2.8 – Capture of cured ply drop laminates processed without caul sheet (left) and with caul sheet (right).

Another reason for using caul sheets is to exhibit thickness control during processing. The resin content of prepreg material used to manufacture these parts is not always consistent. As such, the thickness of the as laid laminate may also be inconsistent. Since the bagging material acts as a flexible membrane (i.e. low bending stiffness) it conforms to the laminate completely and therefore the inconsistent thicknesses are left with the final part. Since a caul sheet is rigid, it will act to correct these inconsistencies by applying more pressure on the thicker regions of the laminate. The result is a laminate with a more uniform thickness. Thickness variations which are designed into the laminate (such is the case for ply drop laminates) can also be smoothed in this manner. One can see the final results of this effect in Figure 2.8. For the ply drop laminate processed without a caul sheet, the ply terminations are clearly distinguishable. However, for the

laminate of the same ply drop configuration but processed with a caul sheet, it is very difficult to identify the location of the ply terminations because the thickness profile of the laminate has been rendered to be more uniform.

2.4.2 Potential Effect on Porosity

Based on an analysis of the reviewed literature detailed in section 2.2, the mechanisms by which ply drops and caul sheets influence void evolution during processing can be formulated. These mechanisms are discussed here.

Ply drops are thought to affect the gas transport mechanisms relevant to void evolution in two ways. Firstly, the inclusion of ply terminations elicits yet another source of entrapped gasses. This is illustrated in Figure 2.9 by the triangular channels which form between the edge of a terminated ply and the surface of the adjacent plies. Secondly, ply drops can also affect gas transport because a decrease in part thickness means a decrease in the cross-sectional area available for in-plane gas flow. This can present a bottleneck in the flow of gas between the thicker regions and the vacuum system. Louis [20] measured the in-plane gas flow for a ply drop laminate and compared it to the gas flow of uniform laminates of various thicknesses. It was found that for ply drop laminates, the maximum achievable gas flow is restricted by the thinnest region of the laminate.

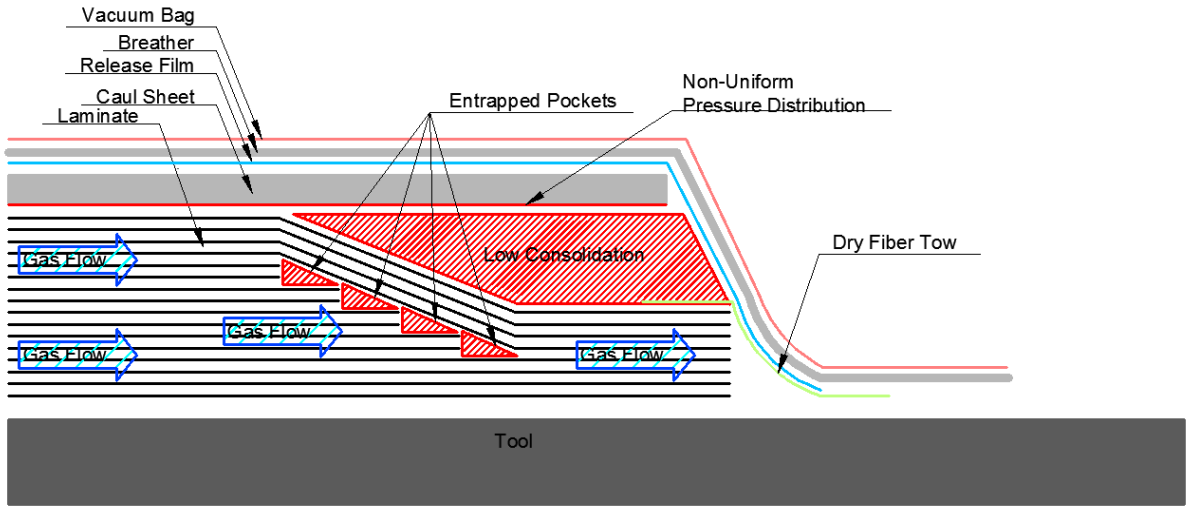

Figure 2.9 – Illustration of the effects of ply drop and caul sheet on gas transport and pressure distribution in composite processing.

A caul sheet affects the distribution of pressure in the part. As previously mentioned, the bagging material acts as a flexible membrane (i.e. negligible bending stiffness) and so it applies uniform pressure over the part by conforming to the shape of the part. A rigid caul will tend to do the opposite – to impart a more uniform surface to the part but apply a non-uniform pressure. With respect to the illustration shown if Figure 2.9, the caul will intensify pressure at the thicker regions of the laminate while reducing pressure at thinner regions. Pressure reduction in the thinner region can cause void stabilization and growth as volatiles diffuse into the void spaces if there is insufficient resin pressure to keep them in solution. Furthermore, as the resin viscosity drops, resin will flow from the high pressure regions to the low pressure regions until hydrostatic pressure equilibrates or until gelation. If a sufficient amount of resin is depleted from the thick regions, more of the consolidation pressure will be borne by the fiber bed causing a reduction in hydrostatic resin pressure.

2.4.3 Existing Literature

With respect to porosity in configured structures, some parametric and demonstrator studies do exist and a portion of them are presented here. The literature review presented here is not intended to give an overview of studies exclusively concerned with ply drops and/or caul sheets nor are these structural configurations the focus of the works discussed. Rather, this section is meant to impress upon the reader the complex nature of the problem and identify common trends and shortcomings in this field of research.

Amongst his experimental work, Hubert [42] studied the flow and compaction behavior of L-brackets processed in an autoclave. A variety of parameters were studied such as the use of concave versus a convex mold, the viscosity of the resin and the use of bleeder plies. With respect to porosity, he identified that voids were more likely to occur if the laminates were subject to bleeding or if the resin system was of lower viscosity. Furthermore, it was also observed that voids were more numerous at the corner. It was concluded that the cause for all the observed voids coincided with the loss of resin pressure. For the laminates subject to bleed, resin pressure is lost when the resin content is removed from the system. This in turn causes more of the pressure to be borne by the fiber bed rather than the resin. Resin systems of lower viscosity can flow with greater ease and are therefore more susceptible to this manner of hydrostatic pressure loss. Due to their geometry, corners are subject to over pressurization or under pressurization. At concave corners, the bag side surface area (i.e. the surface exposed to compaction pressure) is smaller than the tool side surface area. This causes a decrease in overall compaction pressure and consequently a decrease in resin pressure. For the convex corners, the opposite is true, and therefore these corners are subject to an increase in overall compaction

pressure. In the case when the convex corner is able to bleed, hydrostatic resin pressure could potentially decrease as more of the compaction pressure is born by the fiber bed. Other studies concerned with part quality of configured structures processed in-autoclave can be found here [43], [44], [45], [46], [47]. However these studies provide little to no discussion with regards to porosity.

With respect to porosity in OoA configured structures, Brillant [54] performed a parametric study on the processing of 90° angled L-shaped OoA laminates. Parts were processed on both convex and concave molds using a variety of bagging arrangements and pressure intensifiers. Elevated porosity contents were found for laminates processed on the concave mold when the breather was removed at the corner or if pressure intensifiers were utilized. Porosity was attributed to lack of connectivity between the laminate and breather arrangements. The laminate deformation was modeled using a simple finite-element model. However, this model neglected the viscous and time dependent properties of the resin and treated fiber bed deformation as linearly elastic. As such, resin flow for this problem was not modeled. Cauberghs [55] performed a parametric study on the effects of tight corners and ply drops on porosity and thickness variations. The knowledge gained from this study was used to optimize the processing of representative parts and larger complex structures. Amongst some of his conclusions was that there was no need for partial plies to be in direct contact with the breather material and that thickness deviation at corners is caused by a combination of consumable bridging, material bulk factor and shearing behavior. Grunenfelder [56] evaluated the effect of prepreg breathability (specifically the impregnation design of the prepreg) on porosity in ply drop laminate. The processability of an OoA hat stiffener (comprising of concave and convex corners) was also

evaluated in this study and compared to a hat stiffener processed in-autoclave. For the ply drop study, it was shown that porosity can be mitigated if the ply terminations are in contact with a resin poor side of the encapsulating base ply. For the hat stiffener study, it was shown that longer debulk times can mitigate porosity, however, autoclave equivalent porosity contents were not fully achievable. As an extension of Brillant's work [54], Hughes [57] evaluated the effect of consumable arrangement and material deposition strategies (ply gaps and overlaps) on the quality of OoA 90°angled L-shaped laminates processed on a concave mold. This study progressed in complexity, going from lab scale L-brackets, to demonstrator coupons and finally a full scale part. Amongst her findings, reduction in porosity was observed by incorporating gaps and overlaps near but not at the corner. It was concluded that this material deposition strategy allows for intra-ply shear at the corner which in turn reduced ply bridging at this region. She specified that gaps should not be located within the corner because the combination of entrapped air and low pressures at concave curvatures would result in porosity. Furthermore ply overlaps were also found to generate high porosity content. This was attributed to the termination of the vascular network. Other demonstrator studies concerned with porosity in configured structures can be found here [58], [59], [60], [61], [62]. However, these studies seldom provide detailed explanation for the porosity contents found in their experiments.

In reviewing the existing literature concerned with porosity in OoA configured structures, it has been noted by the author that studies often utilize explanations directly borrowed from research dealing with porosity in flat uniform parts. All the while, fundamental physics, specifically the flow and compaction behavior of composite materials, are often overlooked. These fundamental aspects serve as a link between porosity in structural configurations and the state variables which

are known to be the key drivers of void evolution. Note that flow and compaction models have been developed and published in literature concerned with in-autoclave practices [63] and are still applicable for OoA practices. Without this link, the diagnosis of porosity in OoA configured structures devolve into discussions of a more speculative nature, rather than one based on scientific finding. Furthermore, it was also found that many of the diagnostics presented are not followed up with experimental validation.

In her work, Brillant [54] attributed porosity in concave L-shaped laminates to the lack of connectivity between the laminate and breather arrangement. All the while, it was shown that the geometry of the corner and the implementation of pressure intensifiers results in pressure gradients along the laminate. This thereby elicits resin flow during the low viscosity phase of the cure. Regardless, no discussion regarding the possibility that the implicit resin flow and initial pressure variations may have influence local resin hydrostatic pressure was presented. Hughes [57] also pointed out that one of the bagging arrangements used in Brillant's [54] work caused bag bridging at the corner and could cause a reduction in hydrostatic pressure directly. Grunenfelder [56] found that porosity in the concave and convex corners of an OoA hat stiffener were not able to be removed regardless of time spent under vacuum. Yet no follow up discussion regarding how the flow phenomenon at corners could potentially lead to reduced resin pressure was presented. Cauberghs [55] claimed that air entrapped in the partial plies was able to travel to the base plies when through thickness permeability increased later in the cure cycle. If parts were too long, this entrapped air might present itself as porosity in the thin section if gelation occurred prior to the air being able to escape the laminate. This diagnostic fit well with his data however, no supporting data was presented to support this claim. Similarly, Hughes [57] attributed

porosity caused by the implementation of ply overlaps to an inability to evacuate the air from the pockets created by the overlaps, yet no supporting evidence was provided.

It should be noted that the discussion presented above is by no means intended to discredit the authors involved or their work. In fact, these authors where chosen primarily because their work were the few which provided some reasoning for the porosity data that was presented. Furthermore, the majority of the works discussed here are not solely concerned with porosity and aim to evaluate a variety of quality defects. As such, it becomes rather unfeasible to provide a fully comprehensive examination of porosity within the greater scope of the individual works. This is a common feature amongst most existing works regarding processing defects in configured structures. It is believed by the author that this feature acts as impedance in advancing our knowledge of porosity to the scale of complex structures. Therefore, some of the works that have been discussed in this section were selected in order to help identify this problem inherent within the field as a whole, rather than pointing out individual shortcomings with regards to explaining the mechanisms of porosity.

2.4.4 Relevance to Thesis Work

This thesis will evaluate the effect that ply drops and caul sheets have on porosity in OoA processing. The objectives and structure for this study have been presented in Chapter 1. With regards to everything that has been discussed in this section, it is believed that the research must be conducted and presented in a specific manner in order to generate high engineering value. It must first relate the data back to the fundamental mechanisms known to be the key drivers of void evolution. This can be done through the utilization of existing tools which have captured the

paramount fundamental mechanics. In order to achieve this in an effective manner, the research work solely focuses on porosity and the processing phenomenon which influences its evolution.

Chapter 3: Small Scale Parametric Study

A small scale parametric study was implemented to evaluate the effects of caul sheets and ply drops both separately and in combination. This was done by manufacturing a series of small laminates of equivalent size but with varying structural configurations. The processing parameters that were evaluated here where as follows: Caul sheet bending stiffness, ply drop pitch, cure cycle dwell temperature, and vacuum quality.

3.1 Experimental Method

As an initial baseline, the initial trial (Trial 0) consisted of a laminate which contained ply drops and was processed without a caul sheet and flat laminates which were processed with caul sheets of various bending stiffness. The following trial (Trial 1) consisted of laminates that contained ply drops and were processed with caul sheets of various bending stiffness. The purpose of these trials was to capture the effect ply drops and of caul sheets both separately (Trial 0) and in combination (Trial 1). To capture the effects of caul sheet bending stiffness, several laminates were manufactured with aluminum cauls of various thicknesses. In addition, the trial that consisted of laminates containing ply drops which were also processed with caul sheets (Trial 1) was repeated with altered processing conditions to capture effect of a leak (Trial 2) and curing temperature (Trial 3). Finally, the last trial (Trial 4) consisted of laminates that contained ply drops of various ply drop pitch and were processed with caul sheets of the same thickness. These were cured using the same processing conditions as Trial 0 and Trial 1. Table 3.1 below provides a summary of the experimental trials.

Table 3.1 – Summary of experimental trials for small scale parametric study.

Trial ID	Description
Trial 0	A laminate containing ply drops and three flat laminates were cured. The laminate containing the ply drops was cured without the use of a caul sheet, whereas the flat laminates were cured with caul sheets of various thicknesses.
Trial 1	Laminates containing ply drops were cured with cauls of various thicknesses.
Trial 2	Laminates containing ply drops were cured with cauls of various thicknesses and a vacuum hose known to contain a leak.
Trial 3	Laminates containing ply drops were cured with cauls of various thicknesses at a curing temperature lower than all other trials.
Trial 4	Laminates containing ply drops of various ply pitch lengths were cured with caul sheets of equal thickness.

After curing, the final thickness profiles and bulk porosity contents of all laminates were measured by the same methods and at equivalent locations. The measurement methods used will be discussed in greater detail in Section 3.1.3.

3.1.1 Tooling, laminate geometries and processing

All the laminates manufactured in this study were made MTM45-1/CF0526A. These laminates are square with dimensions of 152.4 mm by 152.4 mm (6”x6”). The layup configuration of the laminates are discussed in detail in Section 3.1.2 and summarized in Table 3.2.

The tool used in this study consisted of a 9.525mm thick aluminum 6061-T6 plate. The tools dimensions were 609.6 mm by 609.6 mm (24”x24”) which allowed for multiple laminates to be processed simultaneously for each trial. The surface of the tool was sanded with 600 grit paper and cleaned. For each trial, prior to laying the laminates onto the tool, the tools surface was cleaned and covered with three layers of FREKOTE® 700-NC spray-on mold release agent.

The caul sheets used in these trials were square and 139.7 mm by 139.7 mm (5.5”x5.5”) in dimensions. These were placed in a centered fashion over the laminates (when needed). The various thicknesses of the cauls used were 1mm, 2mm and 4mm. Caul sheets were made of Aluminum 6061-T6. The contact faces of the cauls were sanded with 600 grit paper, cleaned, and covered with three layers of FREKOTE® 700-NC spray-on mold release agent.

Regardless of the layup configuration of the individual laminates or the use of caul sheets, all of the laminates where vacuum bagged using the same bagging arrangement and subject to the same debulk strategy. During the layup, a 7.5 minute debulk was implemented at every fourth ply laid down. This was done using a Torr® vacuum bag. Following the layup and initial debulk periods, the laminates where placed on the 9.525mm thick aluminum tool. All laminates were sealed on the two edges perpendicular to the edges of the ply terminations. This was done to ensure that in-plane gas transport occurred perpendicularly across the ply terminations. When applicable, the caul sheets were placed on top of the laminates in a centered fashion. Each laminate was then covered with a release film and breather cloth. Peel ply strips extending out from under the release film were placed over the laminates to ensure good edge breathing. Figure 3.1 illustrates the general layout of the layup and bagging arrangement. The laminates where then bag sealed with vacuum bag and sealant tape and the vacuum was connected to the bagging arrangement for a short period of time (approximately 30 seconds).

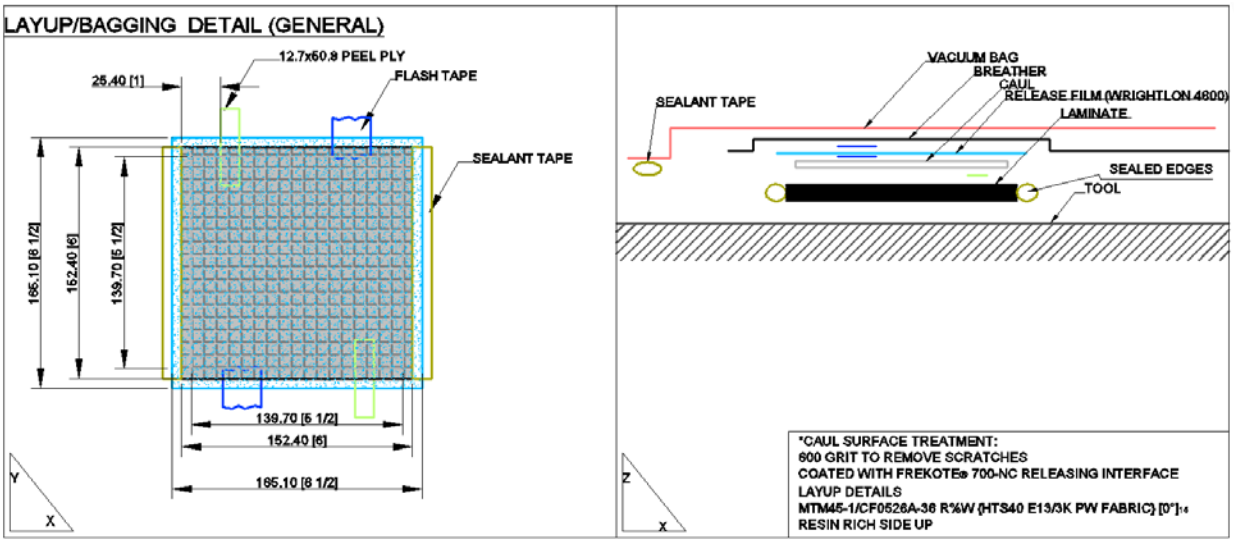

Figure 3.1 – General layup & bagging arrangement for small scale parametric study. The left of the figure provides a top perspective and the right hand of the figure provides a side perspective.

Once the vacuum bagging assembly conformed to the laminate and caul sheet (if applicable), the vacuum pump was disconnected from the bag. This was done in order to ensure that the laminates, caul sheets and consumables did not move while being transported to the oven. The assembly was inserted in a convection oven (Thermotron, Holland, Michigan, USA), the vacuum pump was reconnected the bagged assembly and the laminates were subject to an additional 30 minute debulk prior to the initiation of the cure cycle. Note that the vacuum hose used during the layup is not the same vacuum hose used while the assembly was in the oven. The ovens controller thermocouple was wrapped in sealant tape and placed on the surface of the tool. The cure cycle specifications for each trials are discussed in Section 3.1.2 and summarized in Table 3.2. For all trials, the bagging assembly remained connected to vacuum pump throughout the entirety of cure cycle.

3.1.2 Experimental Trial Description

3.1.2.1 Trial 0: Laminates with Ply Drops or Caul Sheets

This trial consisted of four laminates. The first laminate contained ply drops. For consistency, this laminate will be referred to as the ply-drop laminate (P-D) from here on. The ply-drop laminate consisted of 8 partial plies and 8 base plies. Partial plies were terminated two at a time with a ply drop pitch length of 6.35mm (1/4”). The 16 ply region was located at the center of the laminate, the 8 ply count region was located at the edges, and the ply drop region was centered between the center of the laminate and the edge. This ply drop configuration is illustrated in Figure 3.2 below. Note that the ply arrangement is uniform along the x axis. This ply-drop laminate was cured without the use of a caul sheet.

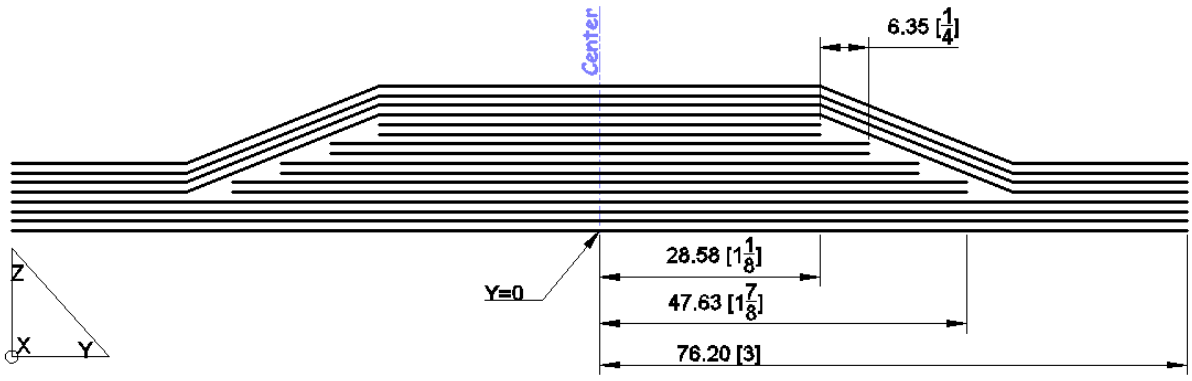

Figure 3.2 – Cross sectional illustration of ply drop configuration for small scale parametric study.

The other three laminates consisted of flat and uniform 16 ply laminates. These laminates were cured using 1mm, 2mm and 4mm thick cauls. These laminates will be referred to as the caul-sheet laminates (C-S).

The cure cycle used for this trial consisted of a 1.5 °C/min ramp to 120°C followed by 4 hour hold. The program was then terminated and laminates were then left to cool back down to room temperature.

3.1.2.2 Trial 1 to 4: Laminates with Ply Drops and Caul Sheets

All laminates in Trials 1 through 4 contained ply drops and were processed with a caul. For the remainder of this document, these laminates will be referred to as the ply-drop/caul-sheet laminates (P-D/C-S).

Trial 1 comprised of three ply-drop/caul-sheet laminates which were cured using the same debulking strategy and cure cycle as Trial 0. These laminates were cured using 1mm, 2mm and 4mm thick cauls

Both Trial 2 and Trial 3 consisted of three laminates (i.e. six in total). The laminates in the Trial 2 and Trial 3 had the same ply drop and caul sheet specifications as the laminates processed in Trial 1. The cure cycle for the second trial was unchanged but was processed with a vacuum hose which contained a leak. The leaky vacuum hose in question was used for the 30 minute debulk prior to cure initiation as well as during the cure. This leak resulted in pressures on the order of 2 kPa poorer than full vacuum (approximately 101 kPa), with occasional excursions as far as 6 kPa as the hose underwent slight movement caused by the air circulation in the oven. Note that this leak is small enough that it is not audible, and so it can potentially occur without being noticed. Trial 3 utilized a vacuum hose which was not known to contain a leak, however the cure cycle specifications were altered. The cure cycle used for Trial 3 consisted of a 1.5 °C/min ramp to

110°C followed by 8 hour hold. The program was then terminated and laminates were then left to cool back down to room temperature.

Finally, Trial 4 comprised of three ply-drop/caul-sheet laminates processed with the same debulking strategy and cure cycle as Trial 0 and Trial 1. The aluminum caul sheets used for these laminate were all 2mm in thickness. Again, these ply-drop/caul-sheet laminates consisted of 8 partial plies and 8 base plies but with varying ply drop pitch among each laminate. Partial plies were terminated two at a time with ply drop pitch lengths of 3.125mm (1/8”), 6.35mm (1/4”) and 12.7mm (1/2”). Table 3.2 below gives a detailed summary of the laminates structural configurations in accordance to their abbreviated identifications. Note that the debulk strategy (as discussed in Section 3.1.1) for all trials remained unchanged.

Table 3.2– Summary of laminate configuration and curing specifications for small scale parametric study.

Trial ID	Laminate ID	Cure Cycle	Ply Drops	Ply Drop Pitch	Caul Sheet	Caul Sheet Thickness
Trial 0	T0_1mm C-S	4 hrs 120°C	No	N/A	Yes	1mm
	T0_2mm C-S		No	N/A	Yes	2mm
	T0_4mm C-S		No	N/A	Yes	4mm
	T0_P-D		Yes	6.35mm	No	N/A
Trial 1	T1_1mm P-D/C-S	4 hrs 120°C	Yes	6.35mm	Yes	1mm
	T1_2mm P-D/C-S		Yes	6.35mm	Yes	2mm
	T1_4mm P-D/C-S		Yes	6.35mm	Yes	4mm
Trial 2	T2_1mm P-D/C-S	4 hrs 120°C +Leak	Yes	6.35mm	Yes	1mm
	T2_2mm P-D/C-S		Yes	6.35mm	Yes	2mm
	T2_4mm P-D/C-S		Yes	6.35mm	Yes	4mm
Trial 3	T3_1mm P-D/C-S	8 hrs 110°C	Yes	6.35mm	Yes	1mm
	T3_2mm P-D/C-S		Yes	6.35mm	Yes	2mm
	T3_4mm P-D/C-S		Yes	6.35mm	Yes	4mm
Trial 4	T4_3.125mm P-D/C-S	4 hrs 120°C	Yes	3.175mm	Yes	2mm
	T4_6.35mm P-D/C-S		Yes	6.35mm	Yes	2mm
	T4_12.7mm P-D/C-S		Yes	12.7mm	Yes	2mm

3.1.3 Measurements

At the end of each cure cycle, the final thickness profile of each laminate was measured. This was done simply by using a micrometer to take measurements at various locations along the y-axis starting from the center of the laminate to the near edge. These profiles were measured three times for each laminate at different x-axis locations.

Three optical microscopy samples, 76.2mm (3”) in length, were collected from each laminate. These samples were mounted in an EpoKwick® epoxy system which was allowed to cure at room temperature. After mounting, the samples were polished using 240 and 320 grit paper and 1 μm and 6 μm diamond suspension in succession. Mosaic images of the samples were taken using a Nikon EPIPHOT 300 optical microscope. These images were converted to 8-bit greyscale images. A MATLAB script was written to discretize the images into smaller sub-images so as to isolate and quantify the void content at various spatial locations along the samples. In general, regions of the images were designated as void space if their greyscale pixel value was lower than 17. Figure 3.3 below provides an illustration of this process.

Care was taken to ensure that all measurements were taken at equivalent locations for all samples. Figure 3.4 below illustrates the spatial locations of the measurements.

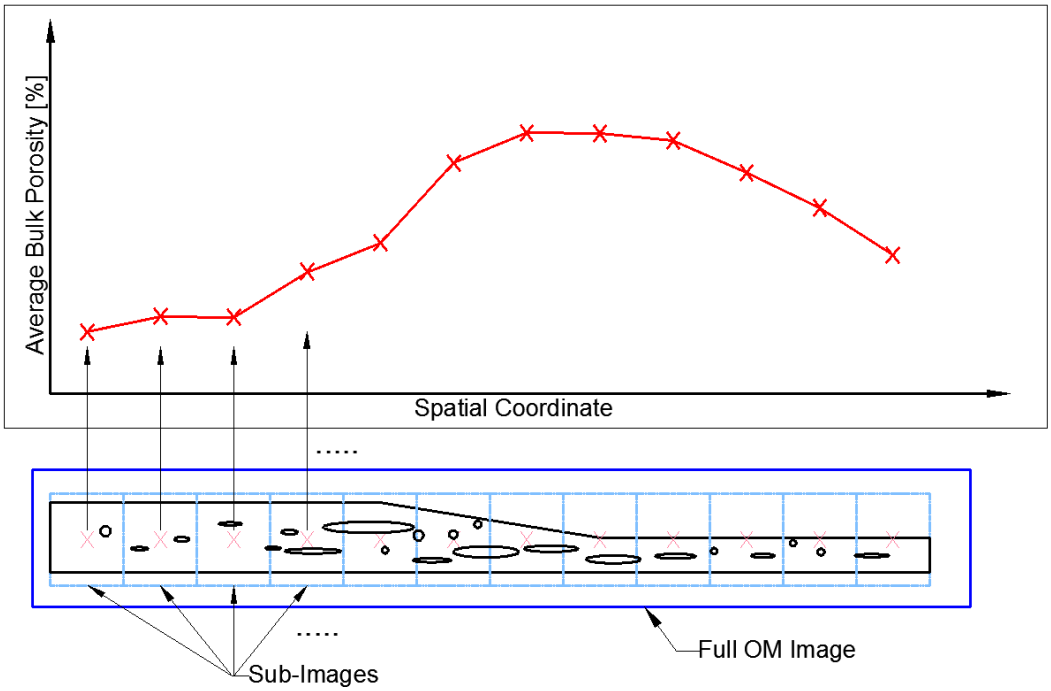

Figure 3.3 – Illustration of MATLAB script functionality. The figure illustrates how the full optical microscopy image (Bottom) is subdivided into smaller images to produce bulk porosity data with respect to the spatial coordinate of the sample (Top).

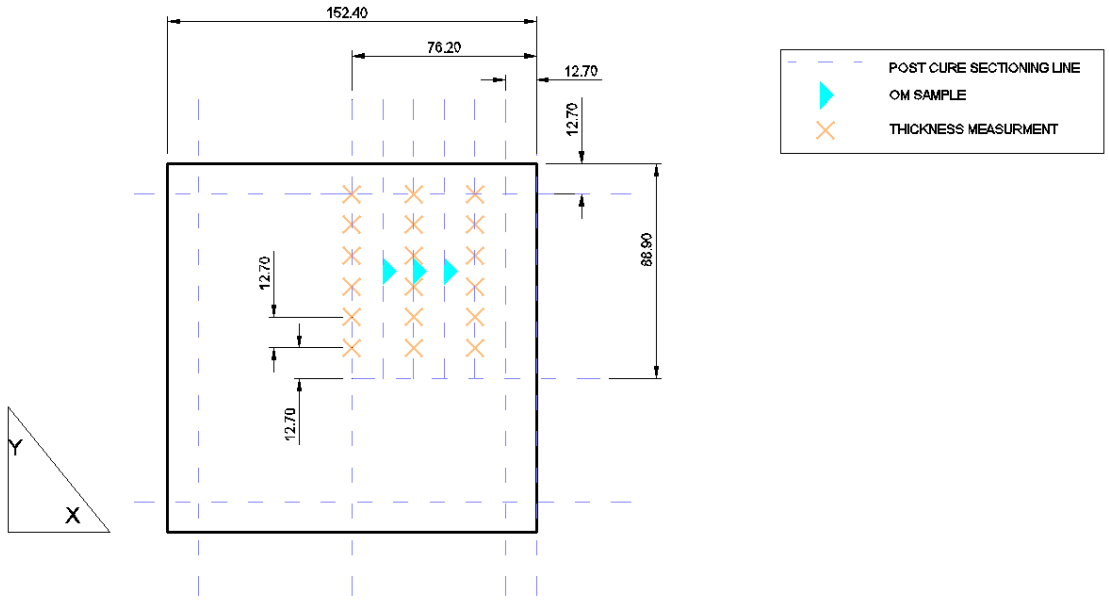

Figure 3.4– Spatial coordinates of measurements for small scale parametric study. Figure illustrates where the laminates were cut (dashed lines), the positions of the thickness measurements ('X' markers) and cross-section locations of the optical microscopy images (triangular markers)

3.2 Results

3.2.1 Effect of Caul Sheet Thickness on Porosity

Figure 3.5 below shows the average bulk porosity for flat laminates processed with caul sheets of varying thicknesses (caul-sheet laminates) at a curing temperature of 120°C. The data is presented with respect to the distance from the center of the laminate

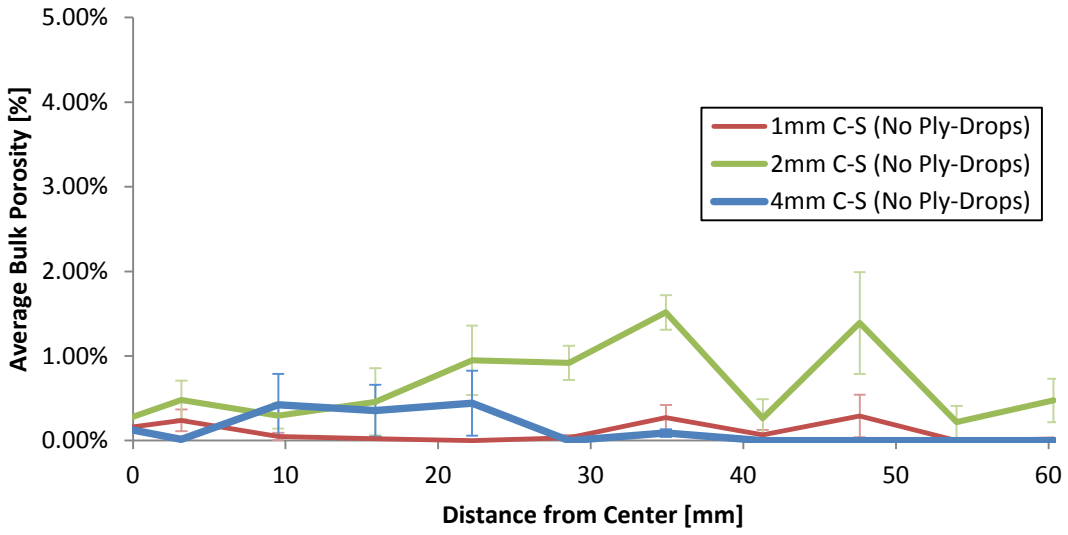

Figure 3.5 – Average bulk porosity profile for flat laminates processed with caul sheets of varying thickness S (caul-sheet laminates) cured with equivalent processing conditions at 120°C.

For the caul sheet laminates, only minor porosity was detected (≤2%). Furthermore, no discernable pattern was found between void content and caul sheet thickness or the distance from the center of the laminate.

Figure 3.6 below shows the average bulk porosity for the laminate containing ply drops and cured without the use of a caul sheet (ply-drop laminate) and the laminates containing ply drops and cured with caul sheets of varying thicknesses (ply-drop/caul-sheet laminates). All the laminates shown in this figure were cured with the same processing parameters at 120°C.

.

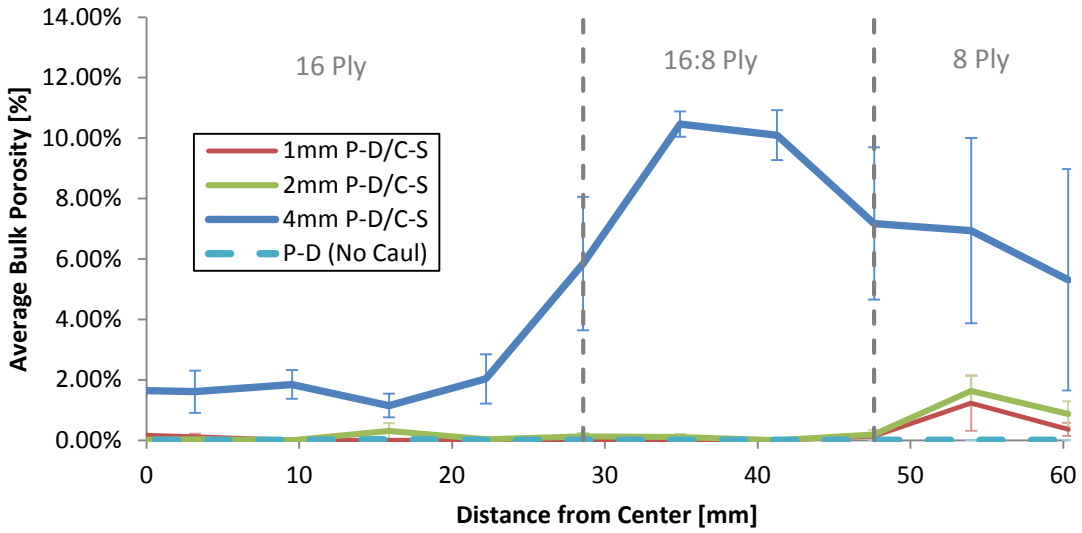

Figure 3.6 – Average bulk porosity profile of laminate containing ply drops and processed without a caul sheet (P-D) and laminates containing ply drops and processed with caul sheets of varying thicknesses (P-D/C-S) cured with equivalent processing conditions at 120°C.

For the ply-drop laminate processed without caul, no voids were found from the mosaic images. Little to no porosity was found from the images of the laminates processed with a 1mm and 2mm caul. A significant amount of porosity was detected for the laminate processed with the 4mm caul. The highest porosity content is concentrated in the ply drop region (maximum of 10.5%). It was also noted that porosity values ranging between 1-2% were found to occur near the center of the laminate processed with the 4mm caul.

With respect to the laminates which contained only ply drops or only a caul sheet (i.e. ply-drop and caul-sheet laminates), it can be concluded that -- at this scale of experimentation -- porosity is not a major source of concern. Whereas, for the laminates which contained both ply drops and

caul sheets (i.e. ply-drop/caul-sheet laminates) significant void growth is possible and seems to be related to the thickness of the caul.

3.2.2 Effect of Caul Sheet Thickness on Laminate Thickness

Figure 3.7 below shows the final cured ply thickness (CPT) profile with respect to the distance from the center of the laminate for the flat laminates processed with caul sheets of various thicknesses. The nominal thickness, calculated from the CPT value found in the data sheet, is also plotted. For this material, the CPT value is 0.201mm per ply [22]. All of the caul-sheet laminates shown in this figure were processed with the same processing parameters at 120°C.

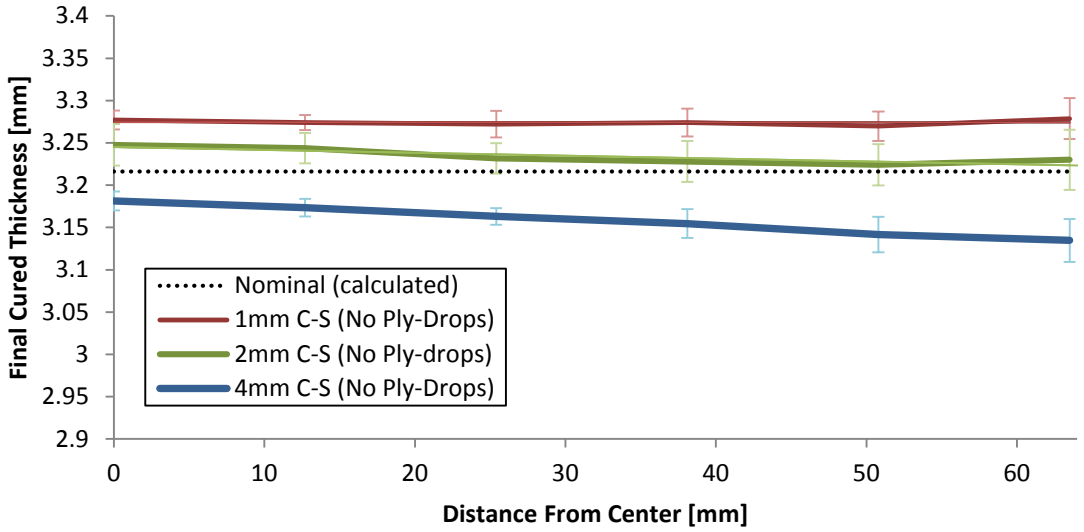

Figure 3.7 – Cured ply thickness (CPT) profile for the laminates cured with caul sheets of various thicknesses (C-S) cured with equivalent processing conditions at 120°C.

It can be seen that as caul sheet thickness increases, the thickness of the laminate decreases. Also note that caul thickness seems to influence the slope of the CPT profile. By applying a linear fit to the data for each laminate, one measures a slope of -0.06 µm/mm, -0.3 µm/mm and -0.8 µm/mm for the 1mm, 2mm and 4mm caul-sheet laminate respectively.

The CPT profile value of the ply-drop/caul-sheet laminates, the ply-drop laminate as well as the nominal CPT value calculated from the data sheet is shown in Figure 3.8. Again, all of the laminates used for this figure were cured with equivalent processing conditions at 120°C

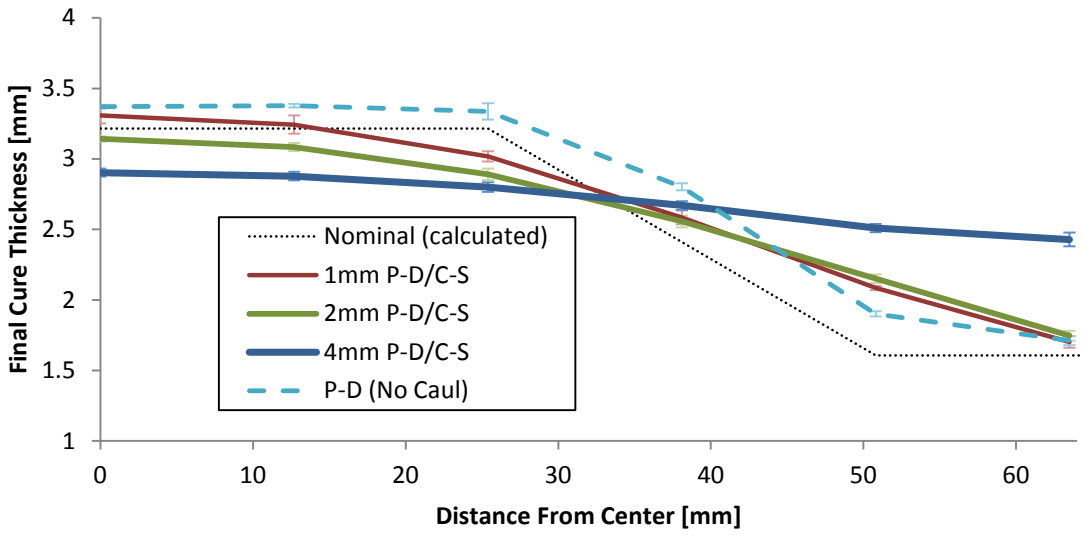

Figure 3.8 – Cured ply thickness (CPT) profile of laminate containing ply drops and processed without a caul sheet (P-D) and laminates containing ply drops and processed with caul sheets of varying thicknesses (P-D/C-S) cured with equivalent processing conditions at 120°C.

For the ply-drop laminate, one can see that the CPT of the laminate tracks the value of the nominal calculations fairly well. However, it has been observed that all thickness values are slightly higher than that of the nominal calculations. This could possibly be due to variability in the resin content of the prepreg.

For the ply-drop/caul-sheets laminates, it can be seen that as the thickness of the caul sheet increases, the CPT profile of the laminate progresses from that of a tapered laminate to that of a flat laminate. This seems to suggest that the use of caul sheets in combination with laminates that have a non-uniform thickness profile causes resin to migrate from thicker regions to thinner regions. This hypothesis is consistent with what is seen in the optical microscopy images (see Figure 3.9). Furthermore, this effect seems to be in some way proportional to the bending stiffness of the caul.

Figure 3.9 below shows some optical microscopy images taken of the 8 ply region and 16 ply region for the laminate containing ply drops and processed without a caul (i.e. ply-drop laminate) and a laminate containing ply drops which was processed with 4mm caul (i.e. 4mm ply-drop/caul-sheet laminate). For the ply drop laminate, no obvious change in fiber to resin volume fraction is observable between the 16 ply region and 8 ply region. However, for the 4mm ply-drop/caul-sheet laminate, it is clear that the fiber to resin volume fraction is much greater at the 16 ply region than at the 8 ply region. In contrast to the ply-drop laminate, it appears that the 4mm ply-drop/caul-sheet laminate has lost resin content at the 16 ply region whereas the 8 ply region increased in resin content.

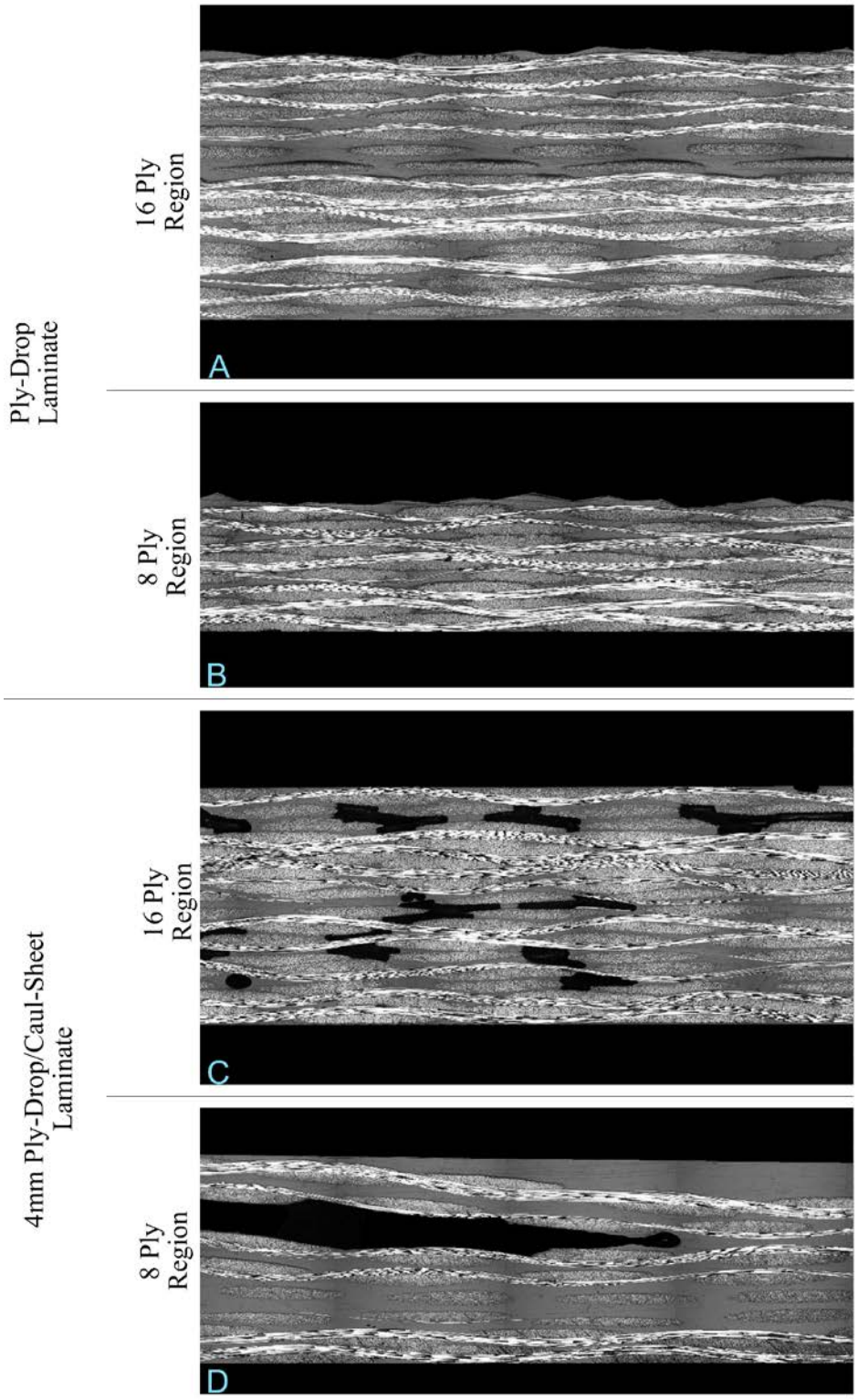

Figure 3.9 – Optical microscopy images of ply-drop laminate at 16 ply region (A) and 8 ply region (B) and 4mm-ply-drop/caul-sheet laminate at 16 ply region (C) and 8 ply region (D).

3.2.3 Effect of Leaks on Porosity in Ply-Drop/Caul-Sheet Laminates

It was previously noted in section 3.1.2.2 that the vacuum hose used for the second trial was worn and contained a small leak. The leak resulted in pressures on the order of 2 kPa poorer than full vacuum, with occasional excursions as far as 6 kPa as the hose underwent slight movement caused by the air circulation in the oven. Figure 3.10 shows the effect that this roughly 2% to 6% drop in vacuum pressure can cause on the final porosity of ply-drop/caul-sheet laminates. In this figure, the average bulk porosity of the ply-drop/caul-sheet laminates processed with a leak are plotted (solid lines) as well as the average bulk porosity of the ply-drop/caul-sheet laminates processed without a leak (dotted lines). Apart from the leak, all other processing parameters for these laminates were the same.

Note the increases in porosity for the ply-drop/caul-sheet laminates processed with a leak compared to the trial results where no leak was present. For the laminate with a 1mm caul we see a slight increase in porosity but still below 2% with no increasing trend at and beyond the ply drop region. For the laminate with the 2mm caul, at the 16 ply region we see porosity values higher than that of the laminate with the 1mm caul yet still around 2%. However, a significant and constant increase in porosity is seen at the ply drop region and beyond to a maximum of about 9%.

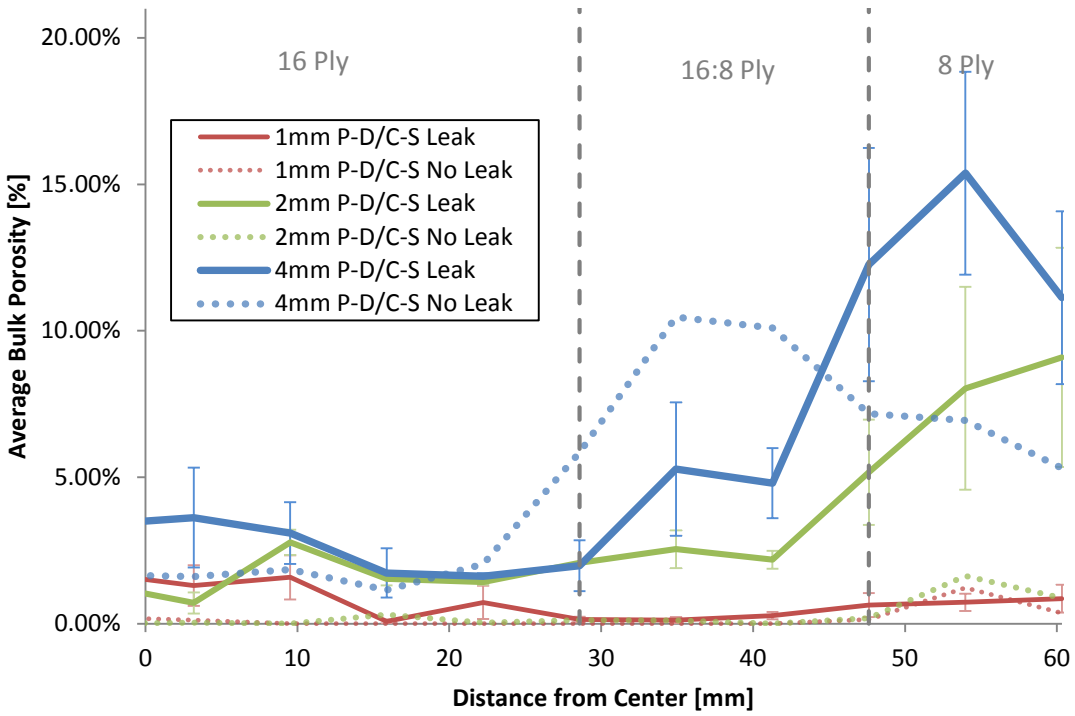

Figure 3.10 – Average bulk porosity profile of laminates containing ply drops and processed with caul sheets of varying thicknesses (P-D/C-S) cured with leak (solid lines) and without leak (dotted lines) at a curing temperature of 120°C.

For the laminate with the 4mm caul, an increase in void content is seen near the center of the laminate. At the ply drop region, a porosity decrease is seen, however, this is followed by dramatic increase at the 8 ply region to maximum of 15%. Although there are some differences in trend between the 4mm ply-drop/caul-sheet laminate processed with and without a leak, the overall pattern is the same. Specifically, minor to moderate porosity contents is seen at the 16 ply region followed by a sharp increase in void content at and beyond the ply drop region.

Overall, these results seem to indicate that the presence of gas within the system and lack of caul compliance exacerbate the risk of void growth when combined.

3.2.4 Effect of Cure Cycle on Porosity in Ply-Drop/Caul-Sheet Laminates

Figure 3.11 shows the average bulk porosity content for the ply-drop/caul-sheet laminates which were cured at 110°C for 8 hours (solid lines) as well as those cured at 120°C for 4 hours (dotted lines).

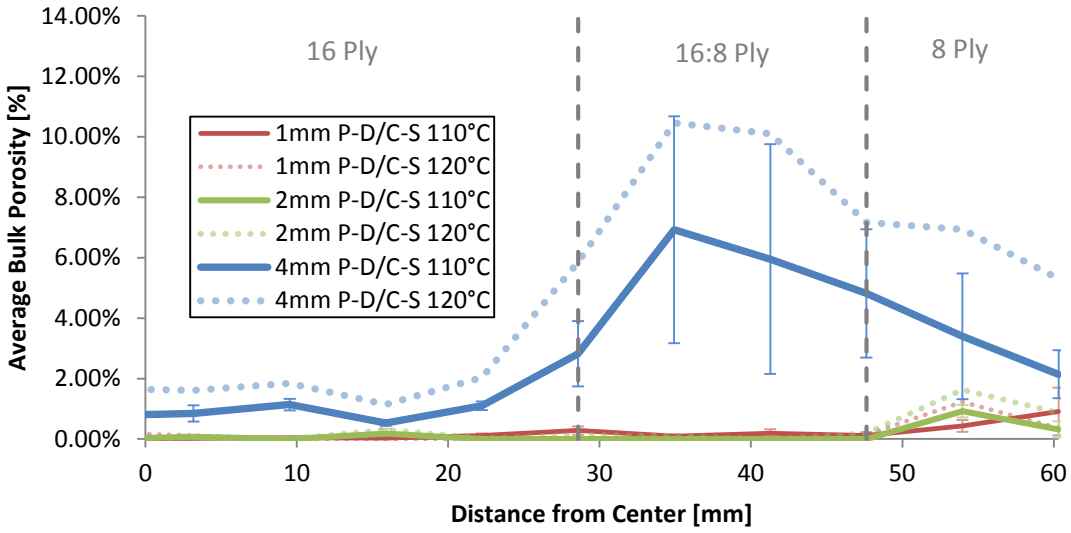

Figure 3.11 – Average bulk porosity profile of laminates containing ply drops and processed with caul sheets of varying thicknesses (P-D/C-S) cured at 110°C for 8 Hours (solid lines) and 120°C for 4 Hours (dotted lines).

For the laminates which were processed with caul sheets of the same thickness, similar trends were observed for both cure cycle conditions. However, ply-drop/caul-sheet laminates which were processed at a lower curing temperature for a longer period of time exhibited lower porosity contented than their counterparts processed at the higher curing temperature. This is true for almost all equivalent data points (with exception to one). These results seem to suggest that cure cycle specification may play some role in mitigating the effects that lack of caul compliance has on porosity.

3.2.5 Effect of Ply Drop Pitch on Porosity in Ply-Drop/Caul-Sheets Laminates

Figure 3.12 below shows the average bulk porosity profile for laminates containing ply drops with different ply pitch cured with a 2mm caul sheet at 120°C.

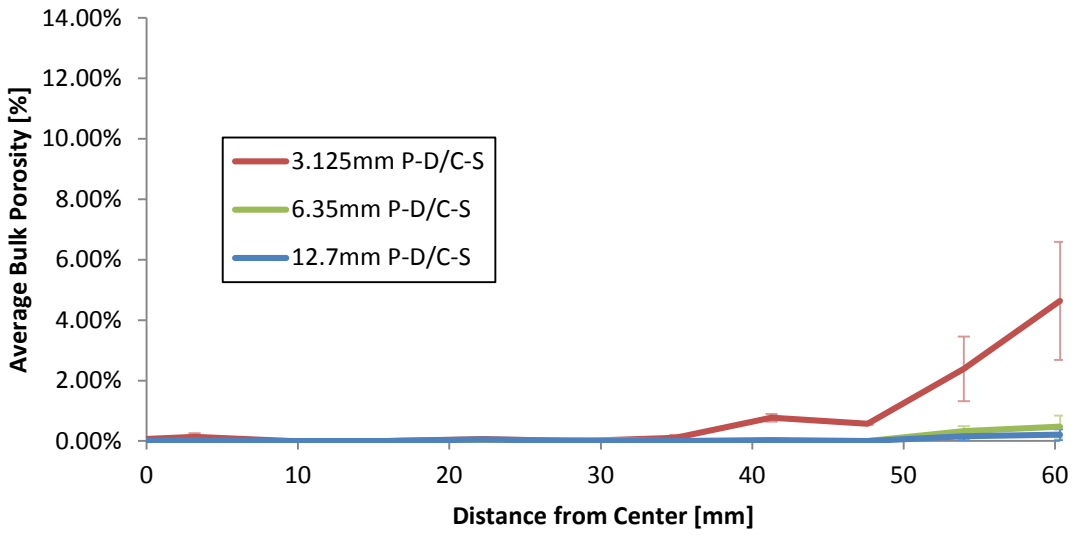

Figure 3.12 – Average bulk porosity profile of laminates containing ply drops with different ply pitch (3.125mm, 6.35mm and 12.7mm) and processed with 2mm caul sheets at a 120°C.

For the ply-drop/caul-sheet laminates with 6.35mm and 12.7mm ply drop pitch, one sees insignificant void content (less than 1%) whereas, for laminates with 3.175mm ply drop pitch, some significant void content exists at the thin region (maximum of 4.6%). The results show that ply-drop/caul-sheet laminates with longer ply pitch are less likely to contain voids because the thickness variations are gradually distributed along their lengths. As such better compliance can be achieved between the caul sheet and the part.

3.3 Discussion

3.3.1 Effect of Caul Sheet Thickness on Flat Laminates

It was shown that an increase in caul thickness causes a decrease in laminate thickness for the caul-sheet laminates (Figure 3.7). It is believed by the author that bag bridging maybe one of the main contributors to this effect. In all the laminates processed in this study, the caul sheets used where undersized in relation to the dimensions of the laminate in order to avoid bag pinching. In doing so, however, a void pocket is created as the bag bridges the region between the edge of the laminate and the caul. Figure 3.13 provides an illustration of this bag bridging phenomenon.

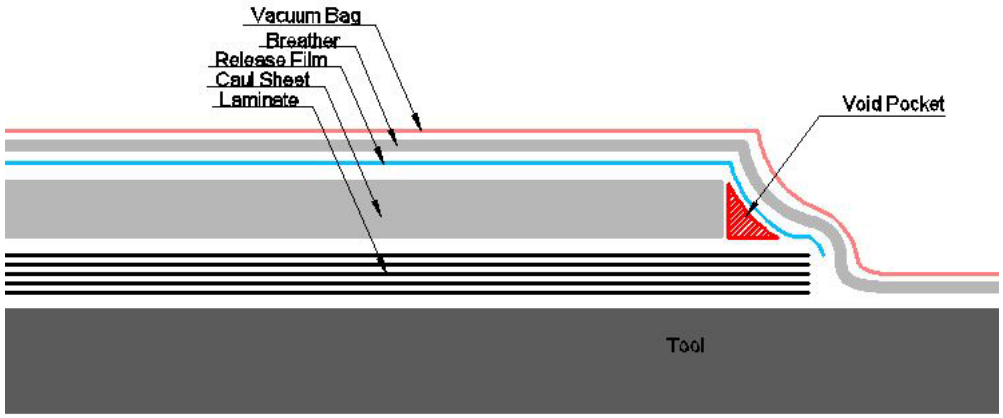

Figure 3.13 – Illustration of bag bridging for flat laminates manufactured with caul sheets.

Since resin flows from high pressure regions to low pressure regions, some of the resin initially contained within the laminate will eventually flow into these pockets once the resin viscosity has sufficiently decreased. This edge defect is formally referred to as “resin flashing”. Figure 3.14 shows a picture of this resin flash along the caul edge.

Figure 3.14 – Capture of resin flashing along caul edge for 4mm caul-sheet laminate.

Logically, as one increases the thickness of the caul, the volume of the void pocket at the edge of the caul will also increase. More resin will therefore be needed to fill the pocket which will subsequently remove more resin from the laminate and thereby cause a slight decrease in thickness.

The caul sheet pinching of the laminate was also quantified (Figure 3.7) whereby the thickness profile of the laminate is non-uniform as the caul sheets edge digs into the laminate. Also note that this effect seems to be more pronounced as the thickness of the caul is increased. It is possible that this phenomenon is due to the fact that resin migration from the laminate to the void pocket is not uniform with respect to distance from the void pocket. Instead, more resin from the perimeter of the laminate bleeds into this pocket than from the central regions.

3.3.2 Effect of Caul Sheet Bending Stiffness on Ply Drop Laminates

The results have shown that the final porosity content of the ply-drop/caul-sheet laminates is sensitive to the caul sheets bending stiffness. This seems to imply that the caul sheets ability to comply with the geometry of the ply drop laminates is one of the critical mechanisms for void formation. When processing the ply-drop/caul-sheet laminates, if the caul sheet used is too stiff, it effectively shields the thinner regions from the compaction pressure that would otherwise be achieved by the use of a flexible membrane (i.e. the bagging assembly). This shielding mechanism is a first order effect.

3.3.2.1 First Order Effect: Pressure shielding

In order to demonstrate this first order effect, simple bending cantilever beam calculations were implemented as an approximation to determine how well the caul sheets can comply with the geometry of the ply drop laminate.

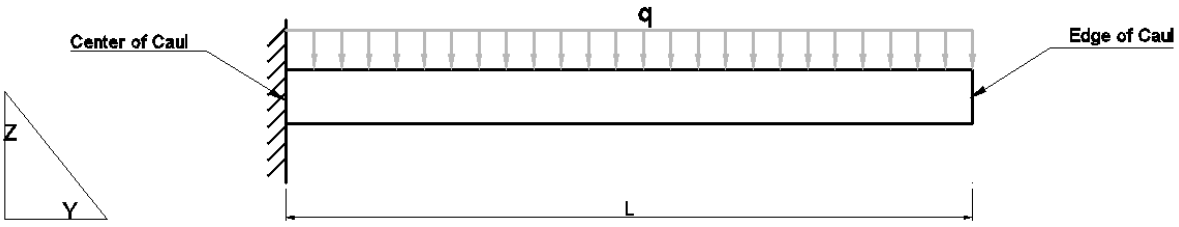

Figure 3.15 – Cantilever beam model used to calculate caul sheet deflection.

The deflection along the length of the caul can thus be calculated as:

$$\delta_{caul}(y) = \frac{qy^2}{24EI} * (6L^2 - 4Ly + y^2) \tag{3-1}$$

Where $\delta_{caul}(y)$ is the deflection of the caul along y, q is the uniform load on the caul (force per unit length), L is the total length of beam E is the elastic modulus and I is the area moment of inertia. The elastic modulus for aluminum 6061-T6 is approximately 68.9 GPa [64].

If we superimpose the downward deflection profiles for each caul onto the downward deflection requires for the ply drop configuration, we get the plot shown in Figure 3.16.

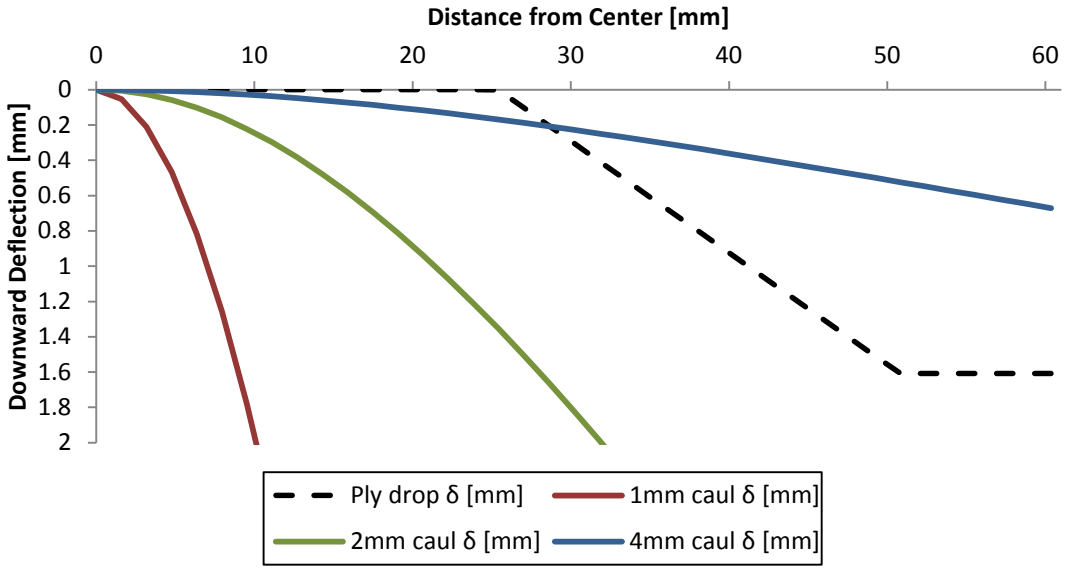

Figure 3.16 – Downward deflection of caul sheets of various thicknesses under atmospheric pressure and downward deflection required by ply drop configuration.

Taking the difference between the downward deflection of the and that required by the ply drops, we obtain a value that can give some indication as to whether or not there is a high risk of void growth.

$$\Delta(y) = \delta_{caul}(y) - \delta_{ply\ drop}(y) \tag{3-2}$$

When the difference shown in equation (3-2) is greater than zero (i.e.$\Delta(y) > 0$), the caul complies with the laminate and the risk of void growth is limited. Whereas when this difference is less than zero (i.e.$\Delta(y) < 0$), the caul sheet does not comply with the laminate, pressure shielding is occurring, and thus the risk of void growth is high.

Figure 3.17, Figure 3.18 and Figure 3.19 show the superimposed bulk porosity and $\Delta(y)$ profile for all ply drop laminates processed with a caul sheet (i.e. ply-drop/caul-sheet laminates) of the first, second and third trial.

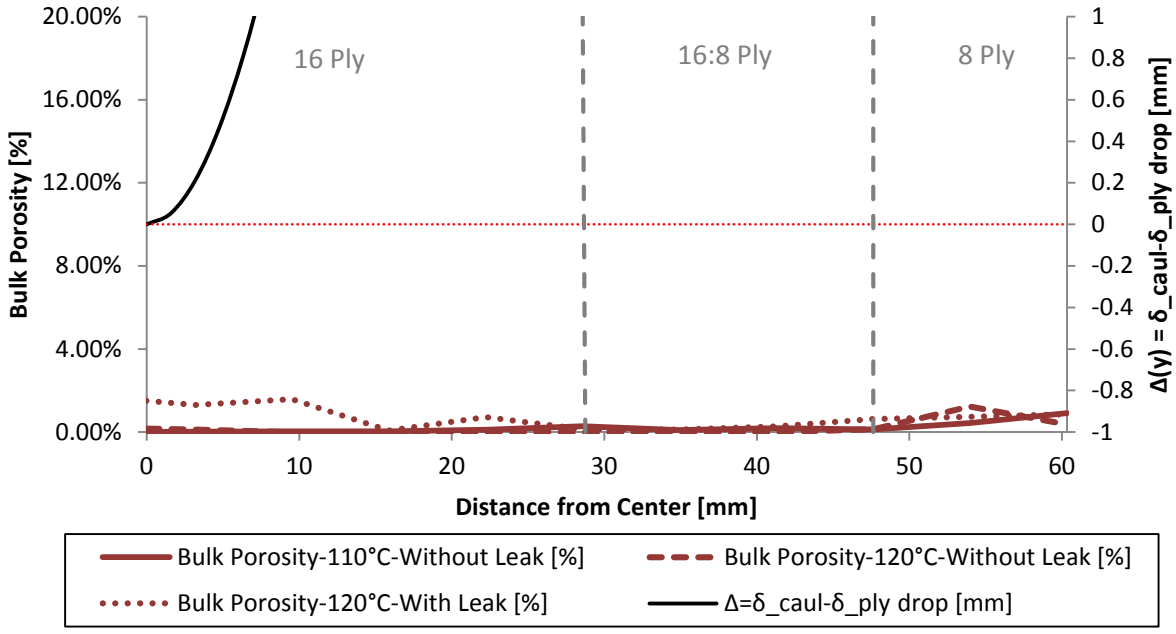

Figure 3.17 – Superimposed Δ(y) (solid black line) and bulk porosity profiles for 1mm ply-drop/caul-sheet laminate processed at 110°C without a leak (solid red line), 120°C without a leak (dashed red line) and 120°C with a leak (dotted red line).

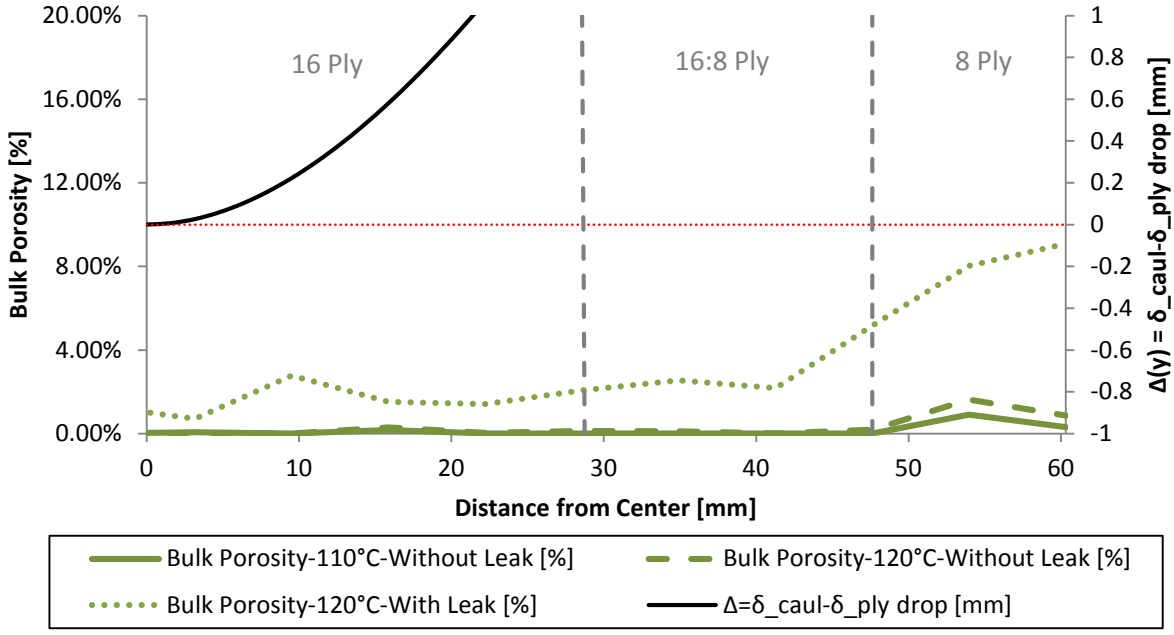

Figure 3.18 – Superimposed Δ(y) (solid black line) and bulk porosity profiles for 1mm ply-drop/caul-sheet laminate processed at 110°C without a leak (solid green line), 120°C without a leak (dashed green line) and 120°C with a leak (dotted green line).

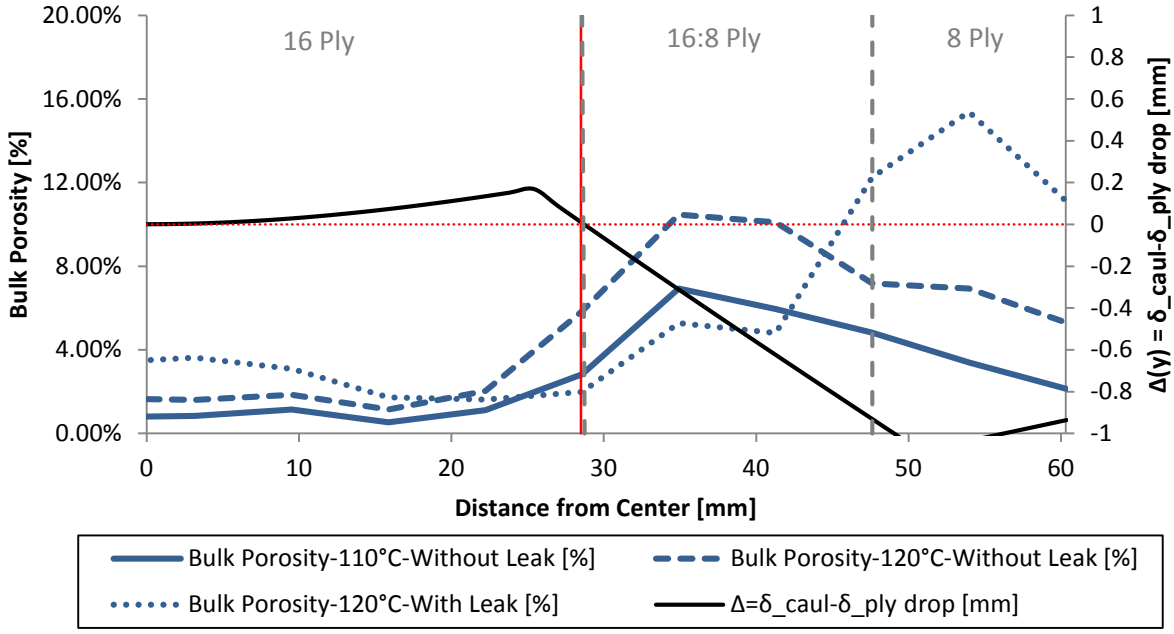

Figure 3.19 – Superimposed Δ(y) (solid black line) and bulk porosity profiles for 1mm ply-drop/caul-sheet laminate processed at 110°C without a leak (solid blue line), 120°C without a leak (dashed blue line) and 120°C with a leak (dotted blue line).

As shown in Figure 3.17, nowhere along the length of the 1mm ply-drop/caul-sheet laminate does the $\Delta(y)$ profile fall below zero. This implies that the caul sheet is able to fully comply with the geometry of the ply drop laminate and the potential for void growth is limited. Consequently, none of the laminates processed with a 1mm caul sheet contained significant porosity content regardless of the processing conditions considered in this chapter.

In the case of the 2mm caul sheet (Figure 3.18), it can again be seen that the caul sheet is able to fully comply with the ply drop laminate according to our calculations. Although no significant porosity content is found in the laminates processed without a leak, this is not the case for the laminate that was processed with a leak. As such, the presence of a leak acts as an exacerbating effect which results in significant void content for laminate processed with a 2mm caul sheet but not for the laminate processed with 1mm caul sheet. The reasons for this will be discussed in greater detail in section 3.3.3.

For the 4mm ply-drop/caul-sheet laminates (Figure 3.19), there is a significant loss in compliance at the ply drop region and beyond. Consequently, all the ply drop laminates processed with a 4mm caul sheet contain high porosity content regardless of the processing conditions considered in this chapter. Moreover, one can also observe that the location where porosity content increases rapidly coincides with the location where compliance is lost. Since compliance is not achieved at the ply drop and thin regions, the compaction pressure is shielded by the caul sheet and voids can stabilize and grow regardless of vacuum quality or curing temperature. Furthermore, in all cases, minor porosity content can be seen at the thick region

regardless of there being no loss in compliance. This porosity is due to a second order effect which is discussed in the next section.

3.3.2.2 Second Order Effect: Resin Migration

It has been shown that the CPT profile of the ply-drop/caul-sheet laminates will change from a tapered profile to a uniform one as caul sheets of higher bending stiffness are used (Figure 3.8). Since the material used for this study is a fabric prepreg, it can be assumed that the contribution to thickness variation from the change in local fiber volume content is negligible. Consequently, a change in thickness must be positively proportional to a local change in the volume of resin and/or the volume of voids. Therefore, for the regions which have undergone a thickness increase, this change can be attributed to an increase in the volume of voids and/or resin. However, for the regions which have decreased in thickness, since there cannot be a negative contribution from the volume of voids (i.e. it is not possible to have negative voids), this must mean that the volume of resin at this region has decreased. This implies that the non-uniform pressure distribution induced by the use of a caul sheet causes an internal hydrostatic pressure gradient within the resin. As a result, during the low viscosity phase of the cycle, resin will migrate from high pressure regions (in this case the thick regions) to low pressure region (in this case the thin regions). Since the consolidation pressure is shared between both the fiber and resin [13], depleting resin from any section of the laminate will inherently decrease the hydrostatic resin pressure. In doing so, the mechanisms by which voids collapse under the hydrostatic pressure of the resin is thereby compromised.

3.3.3 Effect of Curing Conditions

Three variations of cure cycle were studied for the processing of the ply-drop/caul-sheet laminates: a 120°C 4 hour hold cycle (trial 1), 120°C 4 hour hold cycle with a leak (trial 2) and 110°C 8 hour hold cycle (trial 3). Figure 3.20 below shows the average overall bulk porosity content for each of the laminates.

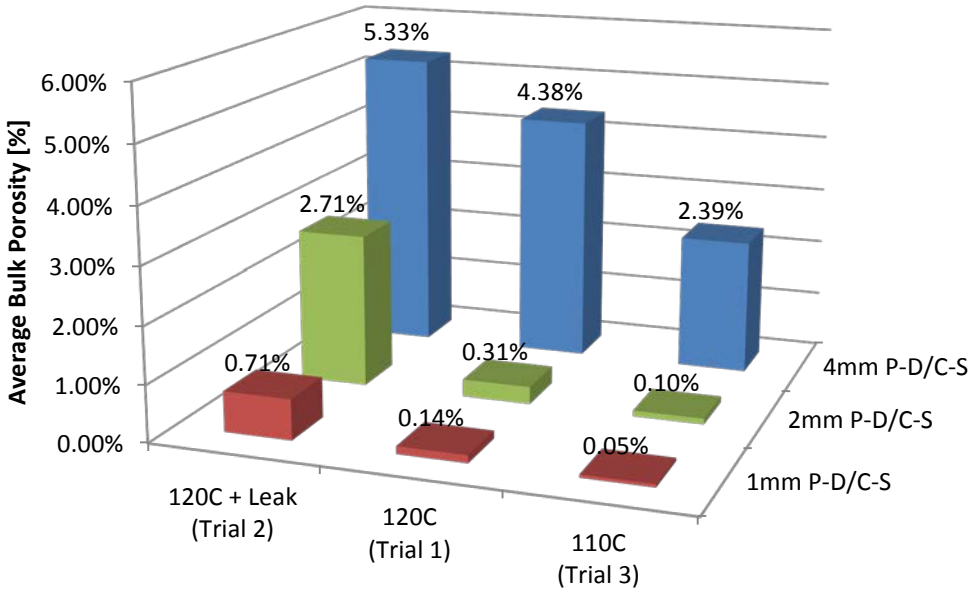

Figure 3.20 – Total bulk porosity content for ply-drop/caul-sheet laminates at various curing conditions (i.e. Trial 1, 2 and 3).

One can see from the figure above that for the ply-drop/caul-sheet laminate with the 4 mm caul, significant porosity is present in the final part regardless of the vacuum level or cure cycle. This is due to the severe lack in caul compliance to the part which, as discussed in the previous section, results in un-collapsed voids in the thin region and resin depletion in the thick region.

Note that an increase in porosity was observed for all the ply-drop/caul-sheet laminates that were processed with a leaky vacuum hose. For the ply-drop/caul-sheet laminates with the thinner cauls,

if all the gas can be removed from the void spaces in the laminate before the cure cycle begins then the result is nearly always a void-free part. This is because when the viscosity of the resin drops during the initial part of the cure cycle, the resin can flow into the void spaces with little to no resistance from gas pressure within the void spaces. As such, the voids are infiltrated by the resin with ease. However, if full vacuum is not achieved, then some gas will remain in the void spaces. In this case the gas pressure in the voids will rise as resin flows into them until it is equal to the pressure of the surrounding resin, and so the voids will remain. By extension, this should imply that the porosity content of the laminates processed with a leaky vacuum hose should be a reflection of the hydrostatic resin pressure losses for those laminates. As such, greater void content implies lower hydrostatic pressure. Consequently, the results presented here suggest that the hydrostatic resin pressure losses increase proportionally to the thickness of the caul sheet used. Therefore a greater loss in compliance results in a greater loss in hydrostatic resin pressure due to the second order effect as discussed in section 3.3.2.2.

Significant decreases in porosity content were observed for the 4mm ply-drop/caul-sheet laminate when the curing temperature was lowered to 110°C (trial 3). The underlining difference between the cure cycle of the first trial and that of the third trial is in the amount of time that the resin is in the low viscosity phase (e.g. <3000 Pa s) and is able to flow. Figure 3.21 below shows a viscosity vs. time plot of an MTM45-1 resin system for the first and third trial. These plots were simulated using the Raven software (version3) [21]. As one can see, the resin viscosity is below 3000 Pa s (equivalent to lard [65]) for 138 minutes and 196 minutes for the first and third trial respectively (i.e. a difference of 58 minutes). Consequently, the 4mm ply-drop/caul-sheet laminate experiences significant porosity reduction of 2% when the resin flow occurs over a longer period of time. These

results seem to suggest that resin migration for the 4mm ply-drop/caul-sheet laminate was not complete prior to gelation for the processing conditions of the first trial. The additional time allotted for flow in the third trial allowed for more resin to flow into the shielded region thereby reducing lack in compliance and increasing hydrostatic resin pressure at that location. This in turn allowed for more void space impregnation prior to gelation. Therefore larger pressure gradients caused by greater lack of compliance will require more time for the resin to flow and achieve a hydrostatic equilibrium. However, increasing the flow time alone will not be sufficient to eliminate the void spaces completely. Even though longer flow times allow for better resin pressure equilibrium to be achieved, the applied compaction pressure is still gradually being absorbed by the fiber bed as resin flow progresses. This inevitably leads to a decreased resin pressure at all locations which increases the risk of void stabilization and growth. This mechanism was previously referred to as the second order effect and will be studied more extensively in the Chapter 4.

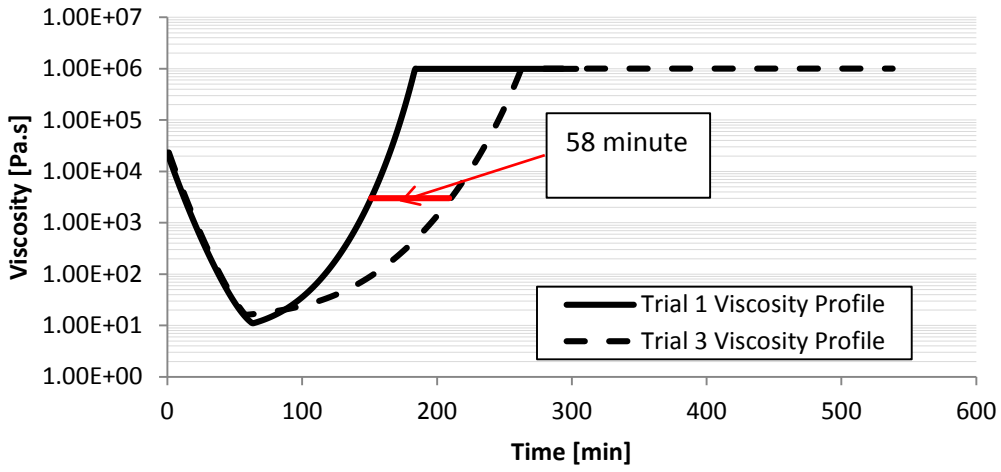

Figure 3.21 – Viscosity vs. time plots for Trial 1 and Trial 3 curing conditions (simulated with Raven [21]**) . Figure shows that the curing conditions of Trial 3 is below 3000 Pa s for 58 minutes longer than the curing conditions of Trial 1.**

3.3.4 Effect of Ply Drop Configuration

Significant void content was found for the laminate in the fourth trial which had the smallest ply drop pitch (3.175mm). This result shows that distributing the material in a more gradual way (such as the ply-drop/caul-sheet laminates with 12.7mm and 6.35mm ply pitch) can work to mitigate the lack of compliance since the geometry of the laminate is more streamlined with the deflection of the caul. When ply terminations are designed in a more instantaneous manner (such as the ply-drop/caul-sheet with 3.175mm ply pitch), pressure shielding will be in effect for a longer period of time and more resin displacement will be needed to achieve a new equilibrium.

It is noteworthy to point out here that regardless of whether the ply drop pitch or caul sheet thickness is being varied, the fundamental mechanisms and causes for void generation are the same. Therefore, the only underlining difference between the first and fourth trial is simply that the loss of compliance was achieved by a different method. By extension, it could be said that, as far as the compaction and flow mechanisms are concerned, the first and second order effects are the principle mechanisms to understand the issue of porosity for parts of any variety of structural configuration.

Chapter 4: Instrumented Tool Tests

In Chapter 3, it was concluded that resin pressure shielding due to a lack of compliance between the laminate and the caul sheet can be a primary cause of porosity. Lack of compliance is born when the caul sheets bending rigidity hinders the consolidation of the ply drop laminate. This is the first order effect by which lack of compliance reduces resin pressure. Moreover, it was also noted that lack of compliance results in internal pressure gradients which in turn causes resin depletion at regions which are initially in contact with the caul sheet (i.e. pressure overfill regions). As resin is depleted from these regions, more of the applied compaction pressure is absorbed by the fiber bed which in turn reduces the hydrostatic resin pressure of the laminate. This is the second order effect by which lack of compliance reduces resin pressure.

In order to directly support the conclusions outlined in Chapter 3, the hydrostatic resin pressure distribution of the configured structures of interest to this thesis were monitored during processing. This was done through the use of an instrumented tool. This tool was instrumented with hydrostatic MEMS pressure sensors provided by Convergent Manufacturing Technologies [1]. Three laminates of identical ply drop configuration were manufactured. Note that the ply drop configuration used in this study is similar to that seen in Chapter 3, however, the laminates in this study were of greater size. One of these laminates was cured without the use of a caul sheet while the other two were cured with a 4mm and 8mm caul sheet. This was done to demonstrate how the presence of a rigid caul sheet in lieu of a flexible bag effects the resin pressure history of the part and to show how this effect scales with the bending stiffness of the caul sheet. In addition, the final thickness profile of all the laminates manufactured in this study were captured through the use of a laser coordinate-measuring machine (CMM).

4.1 Experimental Methods: Instrumented Tool Tests

4.1.1 Tooling, Laminate Geometries and Processing

The instrumented tool used in this study consisted of a 9.94mm (.39”) thick aluminum 6061-T6 plate. The tools surface was sanded with 600 grit paper, polished with Aqua-Buff 1000 Fast-Cut polishing compound and coated with three layers of FREKOTE® 700-NC spray-on mold release agent prior to layup. This plate was instrumented to house seven 1207kPa (175psi) MEMS pressure sensors provided by Convergent Manufacturing Technologies [1]. The sensors spanned a straight line along the center of the tool and were spaced 25.4mm (1”) apart from each other. Figure 4.1 shows a capture of the instrumented tool.

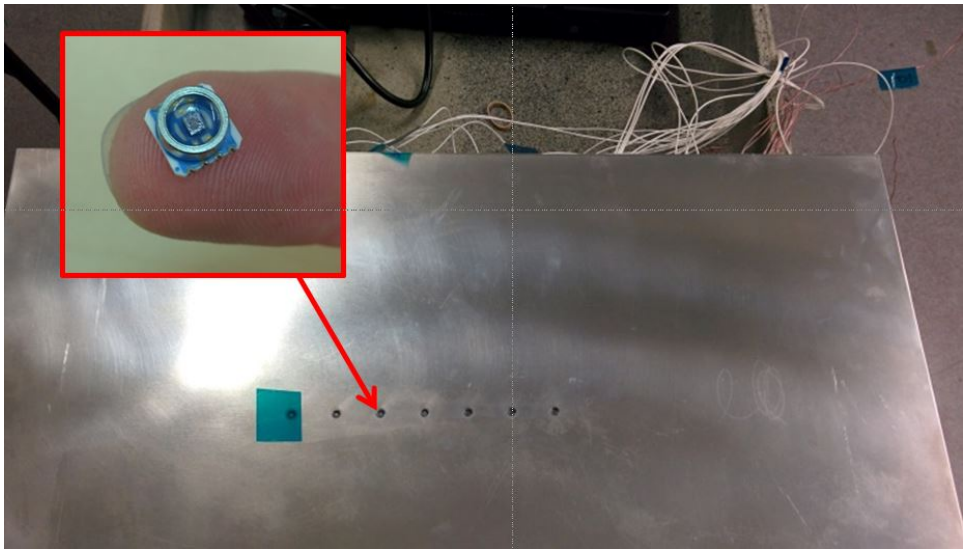

Figure 4.1 – Capture of tool instrumented with hydrostatic MEMS pressure sensors

Prior to layup, the cavities of the sensors were filled with MTM45-1 resin (see Figure 4.2 below). The resin was acquired from a roll of unsupported MTM45-1 resin film. This was done in order to reduce the time required for filling the cavities of the sensors during the low viscosity phase.

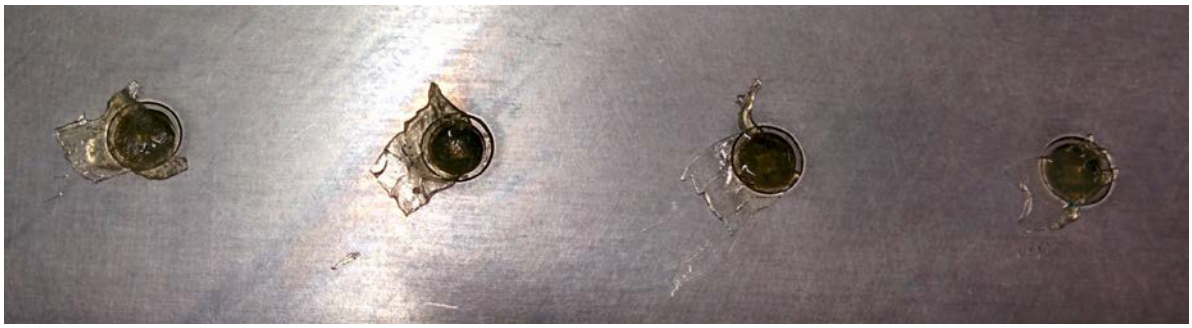

Figure 4.2 – Capture MEMS pressure sensor cavities filled with unsupported MTM45-1 resin prior to test.

Care was taken to ensure that the cavities were not overfilled with resin. Overfilling would cause an overpressure within the cavity itself and lead to a pressure response which is not representative of the hydrostatic pressure being experienced by the laminate. For this reason, the cavities were under-filled. Furthermore, care was also taken to ensure that the resin in the cavity of the sensor did not rise beyond the surface of the tool.

Three ply drop laminates were studied in this section. These laminates were made of MTM45-1/CF0526A 3K plain weave prepreg and were 317.5mm (12.5”) in length and 165.1mm (6.5”) in width. All of the laminates consisted of identical ply drop configurations. This consisted of 8 partial plies and 8 base plies laid resin rich side up. The configuration was uniform along the width of the laminate. Partial plies were terminated two at a time with a ply drop pitch length of 12.7mm (1/2”). A .254mm thick MTM45-1 unsupported resin film was also placed on the tool

side of the laminate. The purpose of this resin film was to reduce the time required for filling the cavities of the sensors. The ply drop configuration is illustrated in Figure 4.3 below. Similar to samples in Chapter 3, all laminates were sealed on the two edges perpendicular to the edges of the ply terminations. This was done to ensure that in-plane gas transport occurred perpendicularly across the ply terminations. In other words, with respect to Figure 4.3, in-plane gas transport is restricted to only occur along the y-axis.

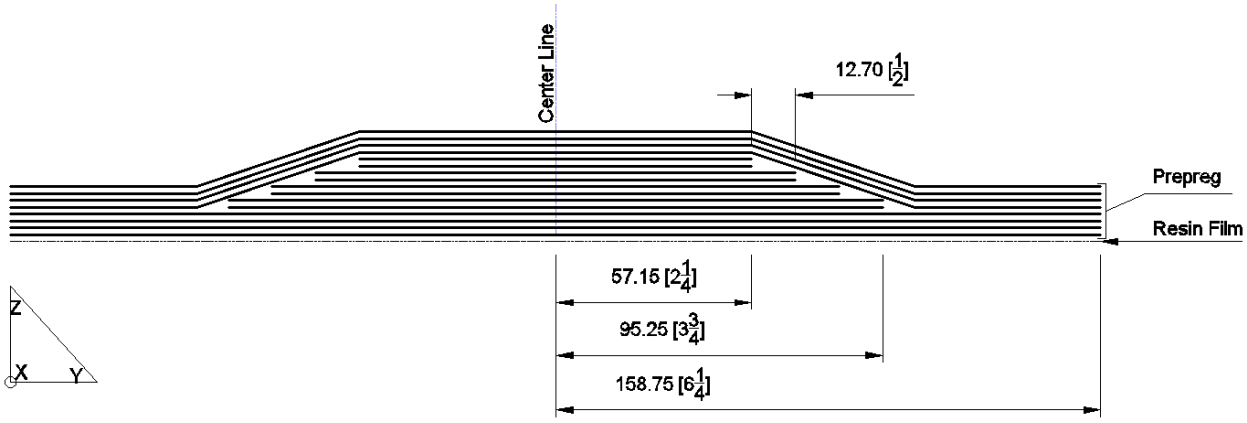

Figure 4.3 – Cross sectional illustration of ply drop configuration for all laminates in instrumented tool tests.

The first laminate was processed without the use of a caul sheet whereas the second and third laminates were processed with a 4mm and 8mm thick aluminum 6061-T6 caul sheet respectively. Like the tool, the surface of the caul sheets were sanded with 600 grit sand paper, polished with Aqua-Buff 1000 Fast-Cut polishing compound and coated with three layers of FREKOTE® 700-NC spray-on mold release agent prior to layup. Caul sheets were 304.8mm (12”) in length and 152.4mm (6”) in width. These were placed in a centered fashion over the laminates when needed.

All laminates were subject to the same debulking strategy and cure cycle. The debulking strategy consisted of a 7.5 minute debulk at every fourth ply during layup. This was done using a Torr® vacuum bag only (i.e. without the use of caul sheets). Following the layup and initial debulk periods, the laminates were then placed on the instrumented tool such that they were correctly positioned over the sensors. When applicable, the caul sheets were placed on top of the laminates in a centered fashion. Each laminate was then covered with a release film, breather cloth and vacuum bagged. In addition, peel ply strips extending out from under the release film were placed over the laminates to ensure good edge breathing. Vacuum was applied to the bagging arrangement. Once the vacuum bagging assembly conformed to the laminate and caul sheet (if applicable), the vacuum pump was disconnected from the bag. This was done in order to ensure that the internal assembly (laminate, caul sheet and consumables) did not move while being transported to the oven. The assembly was then transported and inserted in a convection oven (Thermotron, Holland, Michigan, USA), the vacuum pump was reconnected to the bagging assembly and the laminates were subject to an additional 120 minute debulk prior to the initiation of the cure cycle. For simplicity, this debulk period will be referred to as the in-oven debulk from here on. The ovens controller thermocouple was wrapped in sealant tape and placed on the surface of the tool. The cure cycle used consisted of a 1.5 °C/min ramp to 120°C followed by a 4 hour hold. The program was then terminated and laminates were then left to cool back down to room temperature. Note that the transport time (i.e. the time elapsed between the initial application of vacuum to the bag to the initiation of the 120 minute in-oven debulk) varied slightly from one trial to the other. The transport time was between 45 and 55 minutes.

Table 4.1 provides a summary of the laminate configurations and processing parameters for the instrumented tool tests.

Table 4.1 – Summary of laminate configurations and processing parameters for instrumented tool tests.

Laminate ID	Ply Drop Configuration	Caul Sheet	Caul Sheet Thickness	Debulking Strategy	Transport Time	Cure Cycle
ply drop (no caul)	16:8 ply laminate: 2 ply terminations per drop at ply pitch of 12.7 mm	No	N/A	7.5min/4th ply +120min prior to Cure	45 min	Ramp from 25°C to 120°C at 1.5°C/min hold for 4 hours
4mm ply drop/ caul-sheet		Yes	4mm		50 min	
8mm ply drop/ caul-sheet		Yes	8mm		55 min	

4.1.2 Measurements

4.1.2.1 Hydrostatic Pressure Sensors (MEMS Sensors) and Thermocouples

The MEMS pressure sensors used in this study produce a voltage relative to their excitation voltage when subject to hydrostatic pressurization. This relative voltage is proportional to the pressure and temperature experienced by the sensors. Relative voltages were monitored with the use of LabVIEW and two 4-channel universal analog input data acquisition modules (acquired from National Instruments) operating as a full Wheatstone bridge circuit. An average excitation voltage of 2.5V was supplied by this data acquisition system.

Since the sensors are also sensitive to temperature, thermocouples were used to track the temperature near the sensors on the underside of the tool. The temperatures at various locations on the bag side of the laminate as well as the air temperature of the oven was also recorded. These temperatures were tracked with the use of LabVIEW and a 16-channel thermocouple input

data acquisition module (acquired from National Instruments). Figure 4.5 provides an illustration of the MEMS pressure sensor and thermocouple locations.

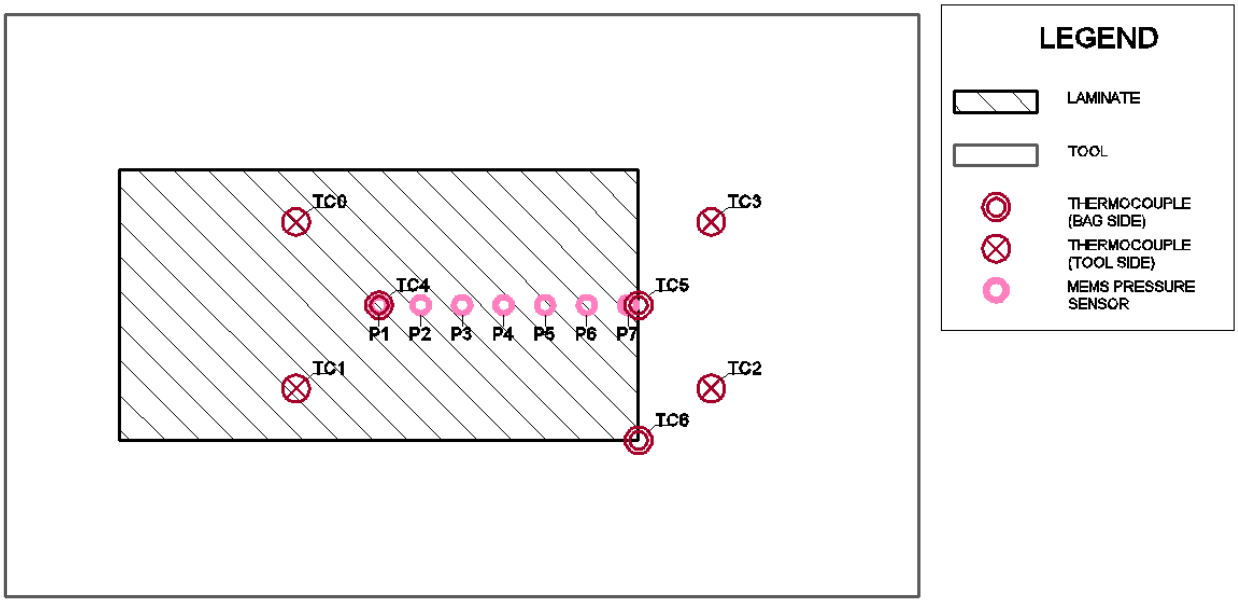

Figure 4.4 – Illustration of MEMS pressure sensors and thermocouple locations with respect to the tool and laminate position.

Both the temperature and voltage response of the MEMS pressure sensors were tracked simultaneously at frequency of 0.5Hz. Using the synchronized temperature and voltage data, the pressure seen by on the sensors can be calculated within an error bound of approximately ±13.8 kPa. Note that it is suspected that the accuracy of these sensors may be better than the error bound quoted above [66]. However, the thermal compensation and voltage response data required to determine a more representative error bound was not available at the time of this study. As such, the error bound quoted here should be considered as a conservative estimate.

The MEMS pressure sensors were strategically embedded in the tool such that the hydrostatic pressure along half the length of the laminate was tracked at every significant event. These are as follows:

- P1: Center of the laminate.
- P2: Between the center of the laminate and end of the 16 ply region.
- P3: Boarder between the 16 ply region and ply drop region.
- P4: Center of the ply drop region.
- P5: Boarder between the ply drop region and 8 ply region.
- P6: Between the end of the ply drop region and end of caul.
- P7: At the end of the caul.

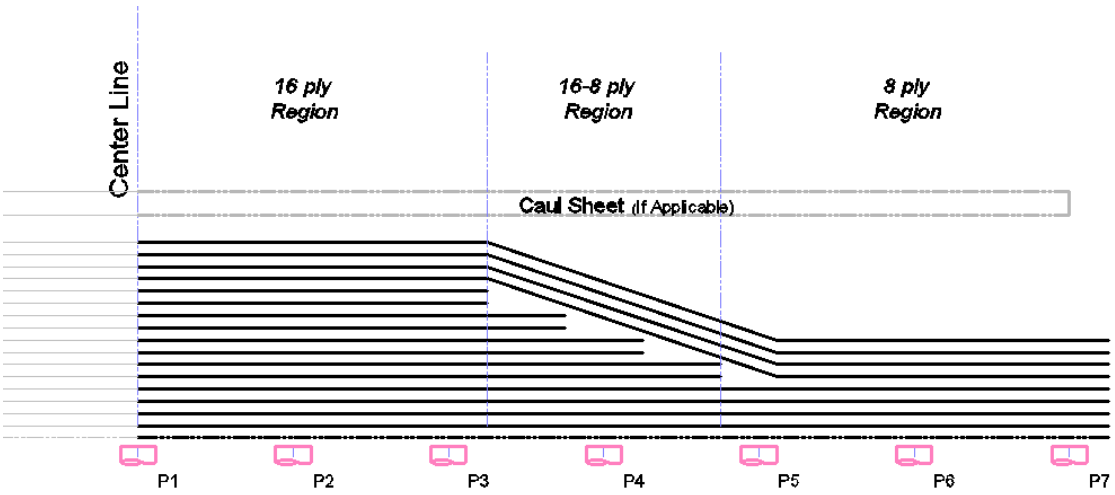

Figure 4.5 – Illustration of MEMS pressure sensor locations along ply drop configuration of laminates.

Figure 4.5 above illustrates the location of the MEMS pressure sensors along the length of the part.

Recording was initiated at the beginning of the 120 minute in-oven debulk and the response was monitored throughout the entirety of the cure cycle. In addition recordings were also taken for the ply drop laminates that where cured with 4mm and 8mm caul sheets when the vacuum was initially applied (prior to transporting the assembly to the oven).

4.1.2.2 Thickness Measurements (CMM)

The final thickness profile of all laminates were measured using a laser coordinate measuring machine (CMM) (Nikon Scanning Bridge CMM with XC65Dx(-LS) Digital Cross Scanner). This was done by scanning both the top surface (bag side) of the laminates as well as the bottom surface (tool side) of the laminate. Note that the bottom surface profile of the laminate needed to be captured in order to compensate for warpage. Once scanned, a MatLab script was used to analyze the resulting point cloud data.

Scans were performed by coating the surfaces with white fast evaporating non aqueous developer (ARDROX 9D1B). Note that the laser CMM can only detect light colored surfaces. Care was taken to ensure the surface was coated as evenly as possible. Once sufficiently coated, the laminates were placed on three supports. Three supports were used to ensure that all the supports were in contact with the laminate. In this study, 4.5mm thick cork strips were used for the supports. A white stick on label was placed over the top surface of the cork strips to ensure that the CMM could also detect the surfaces of the strips. A capture of the laminate coated with developer resting atop the cork strip supports is provided in Figure 4.6.

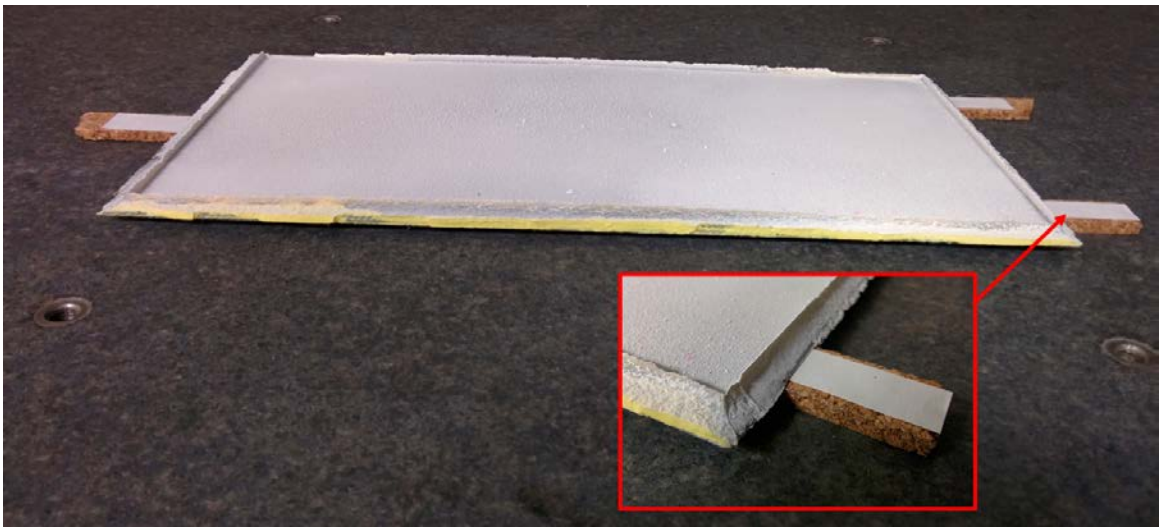

Figure 4.6 – Capture of 4mm ply drop laminate coated with fast evaporating non aqueous white developer resting atop cork strip supports covered with white stick-on labels.

Once the surfaces were scanned, the resulting point cloud data needed to be aligned in such a way that the points on top surface were properly oriented with respects to the points on the bottom surface. In the case of the top surface scan, the x-y plane (z=0) was defined by identifying three points which lay on the surface of the cork strip supports. These points were defined such that they were as near as possible to the composites point of contact with the support. In the case of the bottom surface scan, the x-y plane was defined by identifying three points on the bottom surface of the composite where the cork strip supports would have been in contact with the composite during the top surface scan. In this case, points were identified such that they were as near as possible to the perimeter of the composite edge. This was done to ensure that the x-y plane of the bottom surface scan was equivalent to that of the top surface scan. Figure 4.7 illustrates the location of the x-y plane reference points for both the top surface scan and bottom surface scan.

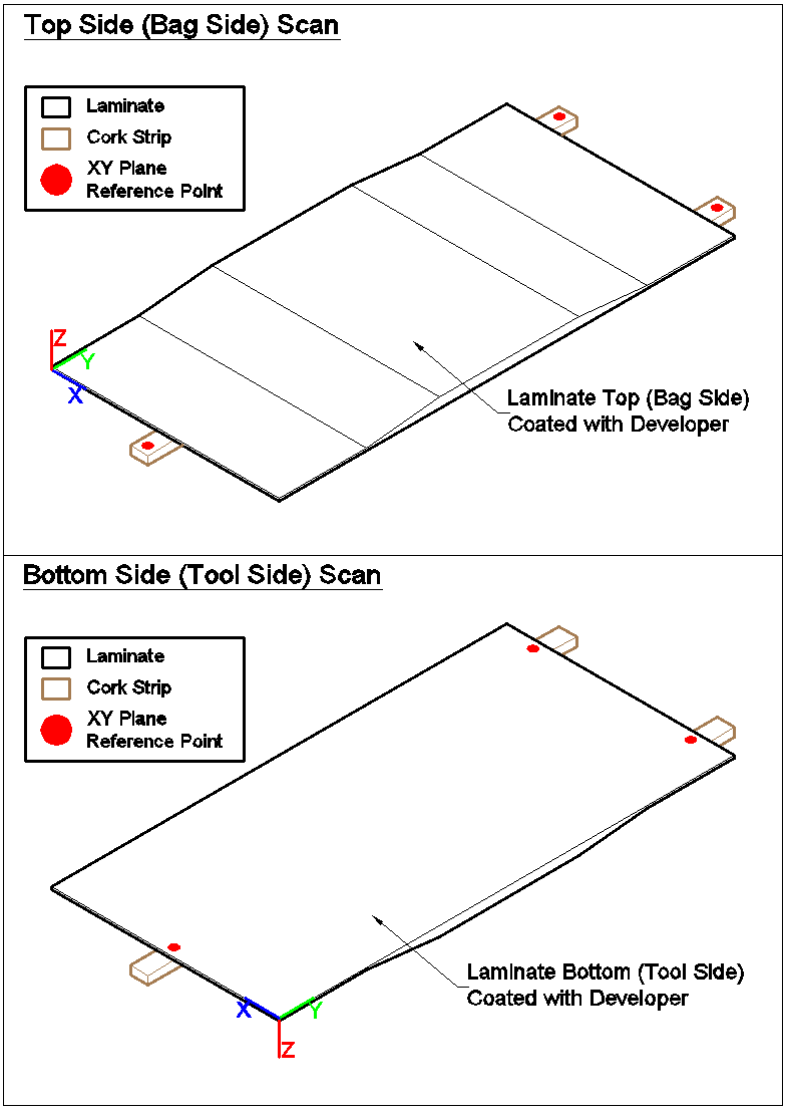

Figure 4.7 – Illustration of X-Y plane (Z=0) reference points for top side scan and bottom side scan.

Care was taken to ensure that the alignment of the Cartesian axis was equivalent for both the top and bottom surface scans. This was done by defining line segments which spanned (as best possible) the perpendicular edges of the composite. Note that the same edges were used for both the top and bottom surface scan. These line segments would then be used to define the x-axis and y-axis of the x-y plane for the top and bottom point cloud data sets (see Figure 4.7).

Once the point cloud data of the top and bottom surfaces were properly oriented with respect to each other, a Matlab script was used to calculate the thickness. The point cloud data of the top surface scan was interpolated so as to assign a mesh to the top surface and a 5^{th} order x-y plane equation was fitted to the bottom surface point cloud data. Note that an equation needed to be fitted to the bottom surface since the cavities of the sensors left resin rich extrusions on the bottom surface which were not representative of the true surface profile (see Figure 4.8)

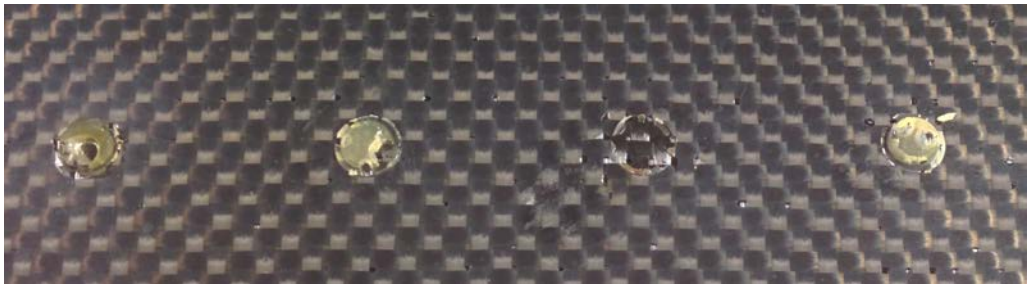

Figure 4.8 – Capture of resin rich surface extrusions on bottom surface due to sensor cavities.

Finally, the thickness was computed by subtracting the bottom surface profile from the top surface profile (see equation 4-1)

$$Thickness(x,y) = TopSurface(x,y) - BottomSurface(x,y) \qquad (4\text{-}1)$$

4.2 Results

In the interest of clarity, the results in this section will be presented in chronological order. In section 4.2.1 the initial pressure distribution for all laminates will be reviewed. Specifically, the transient pressure response during the initial vacuum application (prior to transporting to the oven) for the ply drop laminates with 4mm and 8mm caul sheets will be assessed. Furthermore, the pressure response at the very beginning of in-oven debulk (0 minutes) for all laminates will be observed. In section 4.2.2 the transient pressure response during the in-oven debulk (0 to 120 minutes) will be assessed for all laminates. Section 4.2.3 will deal with the transient pressure response during cure (120 minutes and beyond) for all laminates. Finally, the final cured ply thickness for all laminates will be observed in section 4.2.4.

4.2.1 Effect of Caul Sheet on Initial Pressure Distribution

Figure 4.9 and Figure 4.10 show the transient pressure response during the initial application of vacuum (i.e. prior to being transported to the oven) for the ply drop laminates with 4mm and 8mm caul sheets respectively. Since this is an out-of-autoclave process, the compaction pressure which is being applied to the system is roughly on the order of 101kPa. Note that a leak was formed in the bagging arrangement of the ply drop laminate with 4mm caul sheet while applying the vacuum to the bag. The effect of this leak can be seen by the pressure responses in Figure 4.9 between 0 minutes and 0.2 minutes. This leak was quickly sealed upon detection.

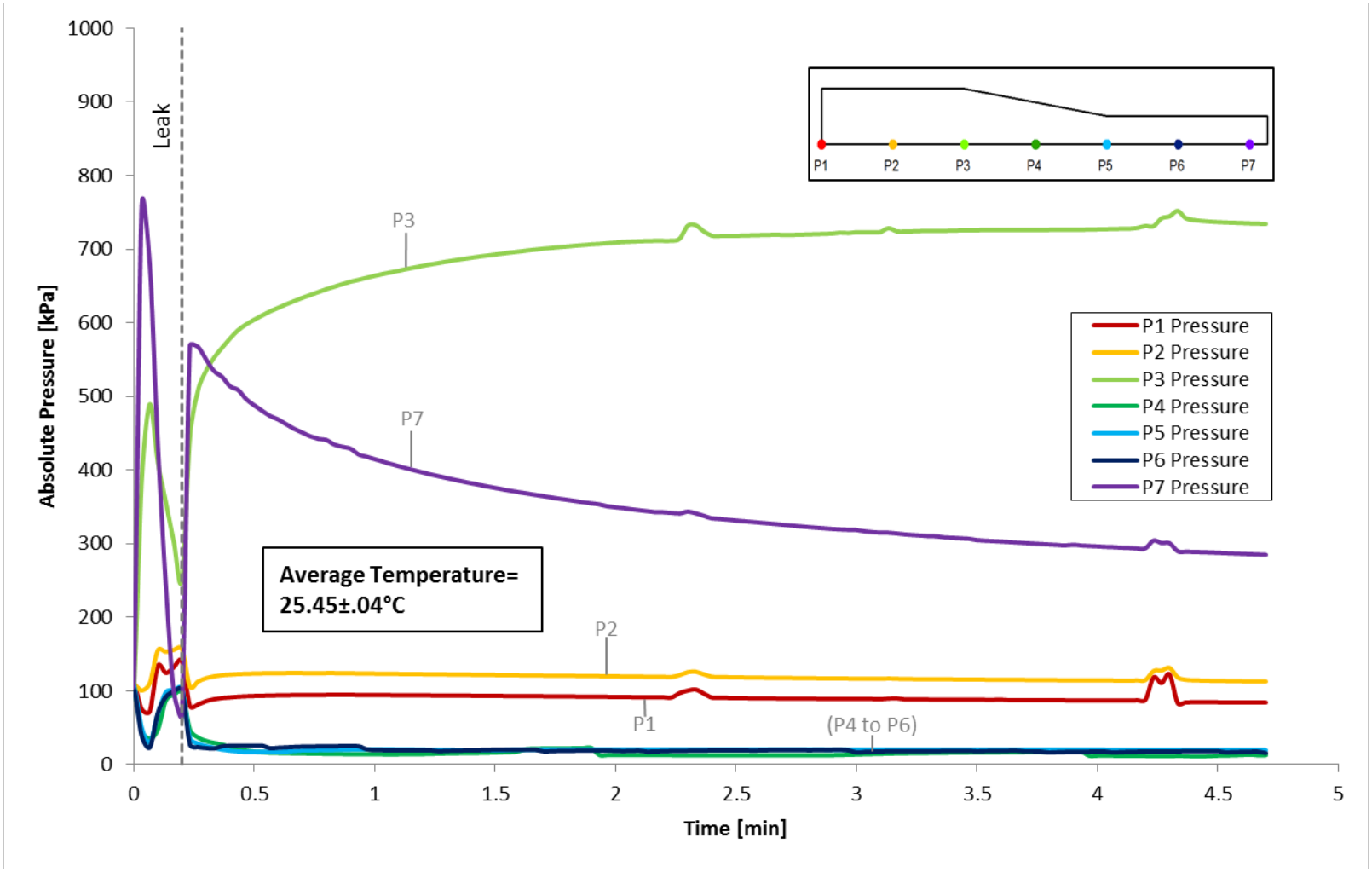

Figure 4.9– Transient pressure response of the ply drop laminate with 4mm caul sheet during the initial application of vacuum (prior to transportation to oven). Pressure histories are color coded to identify the position of the pressure response (refer to sub-figure in upper right corner).

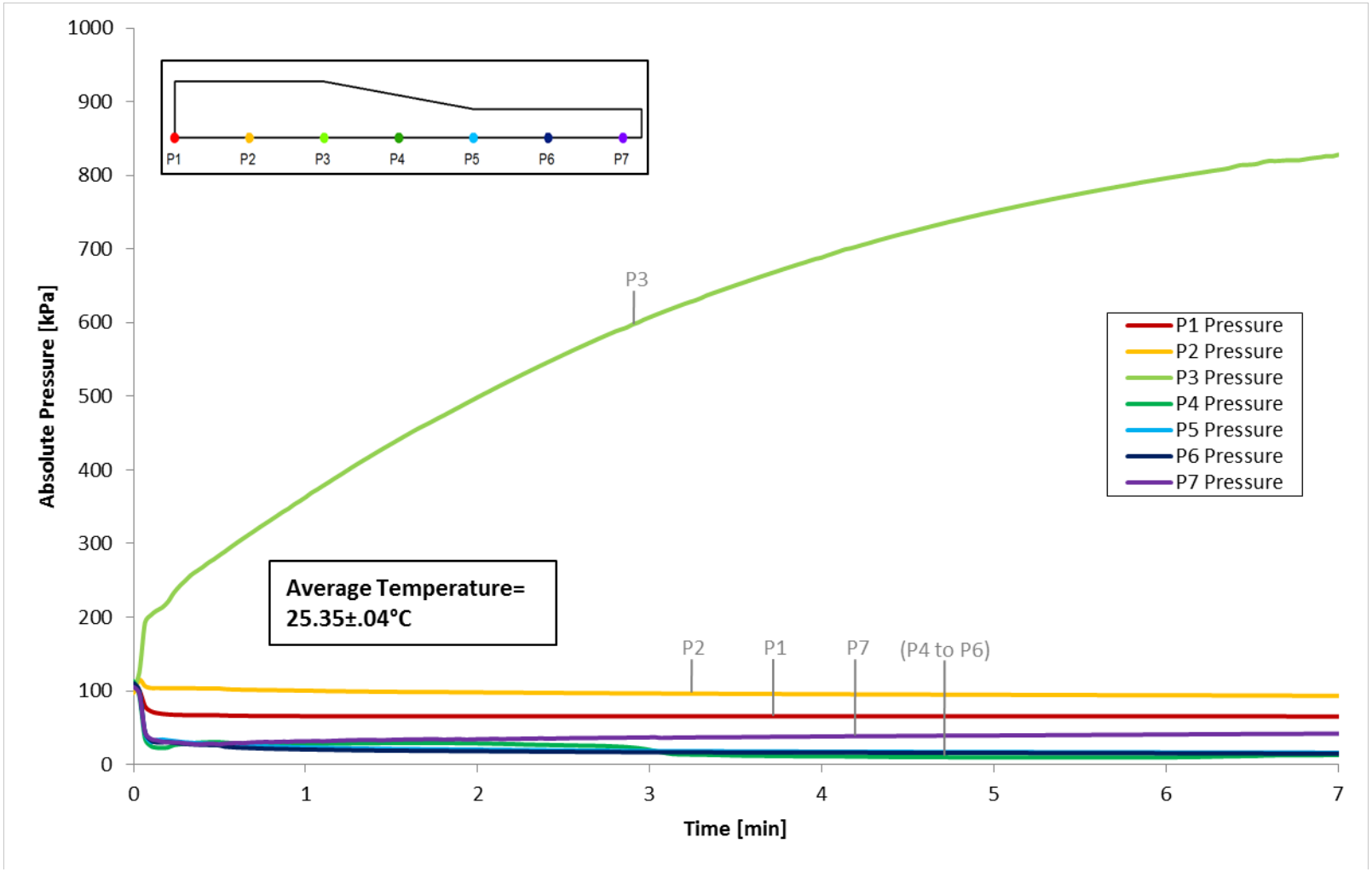

Figure 4.10 – Transient pressure response of the ply drop laminate with 4mm caul sheet during the initial application of vacuum (prior to transportation to oven). Pressure histories are color coded to identify the position of the pressure response (refer to sub-figure in upper left corner).

For the ply drop laminate with 4mm caul sheet (Figure 4.9) it is observed that the region between the center of the ply drop region and the center of 8-ply region (P4 to P6) is shielded from the consolidation pressure as soon as the vacuum is applied. In the absence of pressure at the shielded regions, it can be seen that pressure overfills exist elsewhere. Specifically, the region bordering the 16-ply region and ply drop region (P3) and the region located at the edge of the caul sheet (P7) sustain pressures which are well above the applied compaction pressure. Pressure can also be seen to exist at the center of the laminate and the region between the initiation of the ply drop region and the center of the laminate (P1 and P2) indicating that these regions are in fact in contact with the caul sheet. However, these pressures do not vary significantly as time progresses. Significant pressure variations with respect to time can be seen at the regions which bare the majority of the applied compaction pressure (P3 and P7). As time progresses, the pressure at the P7 region decays while the pressure at the P3 region increases until they both seem to stabilize at an equilibrium. This seems to suggest that while the bulk of the consolidation pressure is primarily being transferred to the laminate at the P3 and P7 regions, more of the pressure will be born at the 16-ply region as the laminate is allowed to strain and comply with the caul sheet during the debulk period.

Similar pressure responses can be seen for the ply drop laminate with 8mm caul sheet (Figure 4.10). Again, the region between the center of the ply drop region and the center of 8-ply region (P4 to P6) is shielded from the consolidation pressure as soon as the vacuum is applied. Moreover, the pressures at P1 and P2 are roughly equivalent to the applied compaction pressure but do not very significantly with time. However, in this case, it is observed that the overpressure is primarily located at the P3 region alone rather than P3 and P7. Furthermore, the P7 region

does not decrease in pressure as the P3 region increases in pressure. Rather both regions are increasing as time progresses with the P7 region showing a significantly slower rate of pressurization as compared to the P3 region. Note that it cannot be said with absolute certainty that the P7 sensor is located precisely at the edge of the caul. For this reason, it is possible that the pressure response seen at this region is partly due to the bagging material coming into contact with the portion of the laminate which is not under the caul. Overall it is difficult to conclude whether or not the edge of the 8mm caul sheet is in contact with the laminate. However, it can be seen that its contribution in transferring pressure to the laminate is much less significant as compared to the case of the ply drop laminate with 4mm caul sheet. This observation is consistent with the fact that the 8mm caul sheet is much more rigid and therefore cannot deflect as much as the 4mm caul sheet under the same applied compaction pressure. Therefore, more of the applied compaction pressure is being transferred to the 16 ply region in the case of the stiffer caul sheet.

Following the initial application of pressure, the assembly was disconnected from the vacuum system and transported to the oven. Once transported and placed in the oven, the assembly was reconnected to the vacuum system. It should be noted that in all cases, an increase in bag pressure was not detected during the transport time. Figure 4.11 shows the initial pressure distribution at the very beginning of the 120 minute in-oven debulk for the ply drop laminate without caul, ply drop laminate with 4mm caul sheet and ply drop laminate with 8mm caul sheet. An illustration of the sensor positions is provided above the legend. Furthermore, the nominal value of atmospheric pressure (101 kPa) is plotted as reference for the value of the applied compaction pressure (dotted red line). Of course, atmospheric pressure varies from day to day

(on the order of ± 2 to 3 kPa) [67], but such a variation is considered to be insignificant when compared to the pressure variations which are of interest to this study.

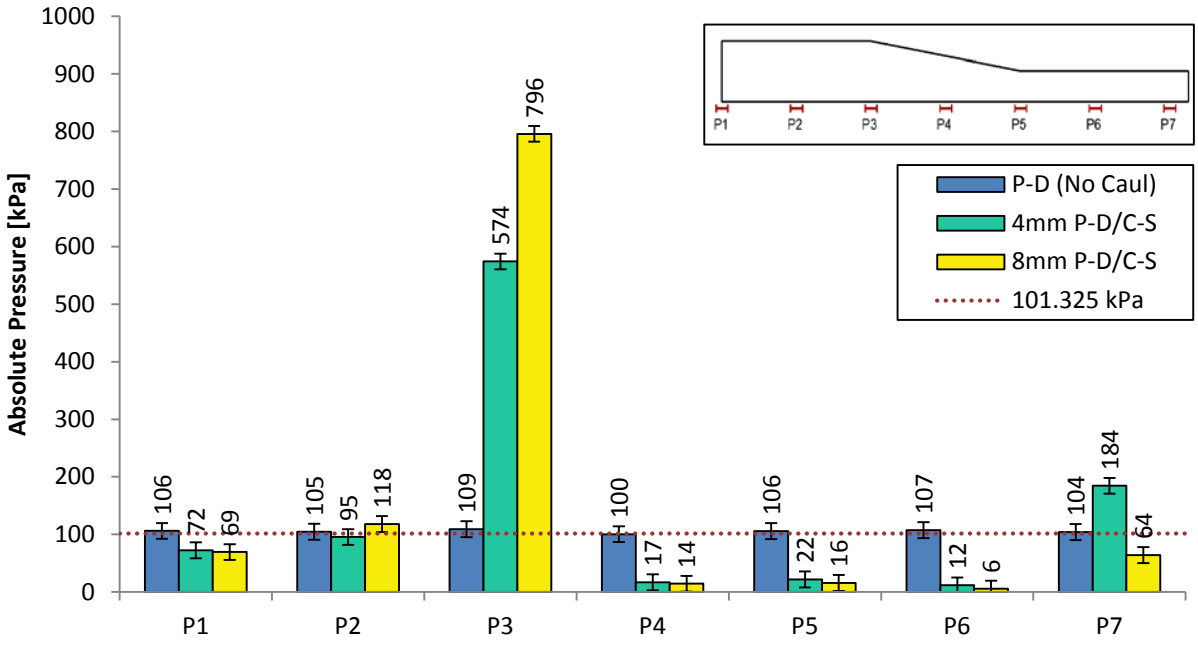

Figure 4.11 – Pressure distribution at the beginning of the in-oven 120 minute debulk for the ply drop laminate without caul (P-D), ply drop laminate with 4mm caul sheet (4mm P-D/C-S) and 8mm ply drop caul sheet laminate (8mm P-D/C-S)

As can be seen from the figure above, for the ply drop laminate without caul sheet, it can be seen that the pressure at all regions is within the range of the applied compaction pressure. Although the transient pressure response during vacuum application was not made available for this laminate, it can be concluded from the results presented here that in the absence of a caul sheet, the applied compaction pressure is distributed equally along all regions of the laminate. Of course, this is not the case when a caul sheet is used. With respect to the ply drop laminates with caul sheets, it can be seen that the pressure between the center of the ply drop region and center

of the 8 ply region (P4 to P6) is well below the applied compaction pressure. As such, no significant change has occurred during the transport to the oven and the caul sheet is still not in contact with the laminate at these regions.

Although slight variations have occurred at the pressure overfills (P3 and P7) during transport, it can be seen that the general pressure distribution remains unchanged. Moreover, the relationship with which the distribution of pressure scales with caul sheet stiffness can be seen. For the ply drop laminate with 4mm caul sheet, it can be observed that the P3 and P7 region are well above the applied compaction pressure. Therefore, for this case; there exists two pressure overfills, one at the border between the 16 ply region and ply drop region and one at the edge of the caul sheet. Whereas, for the ply drop laminate with 8mm caul sheet, it is only the P3 region that shows a pressure well above the applied compaction pressure. Note that this also coincides with lower pressure at the P7 region as compared to the case of the ply drop laminate with 4mm caul sheet laminate. As such, it can be seen that while both the 4mm and 8mm caul sheet shield the compaction pressure from the P4 to P6 region, the more compliant caul sheet (4mm) will allow for a better distribution of pressure as compared to the more rigid caul sheet (8mm).

4.2.2 Effect of Caul Sheet during In-Oven Debulk

In this section, we will be observing the transient pressure response for all laminates during the in-oven debulk (0 minutes to 120 minutes). Figure 4.12, Figure 4.13 and Figure 4.14 , show the transient pressure response of the ply drop laminate without caul, ply drop laminate with 4mm caul sheet and ply drop laminate with 8mm caul sheet respectively during the 120 minute in-oven debulk. The pressures in all figures are plotted using the same color scheme used in Figure 4.9 and Figure 4.10. The average tool side temperature, average bag side temperature and the oven air temperature is also plotted (solid black line, dashed black line and dotted black line respectively). Furthermore, viscosity is also plotted (dashed/dotted black line). Note that the value of viscosity was simulated using the NCAMP data in Raven [21] and the average bag side and tool side temperature data. Again, the nominal value of atmospheric pressure (101.325 kPa) is plotted as reference for the value of the applied compaction pressure (Grey dashed line).

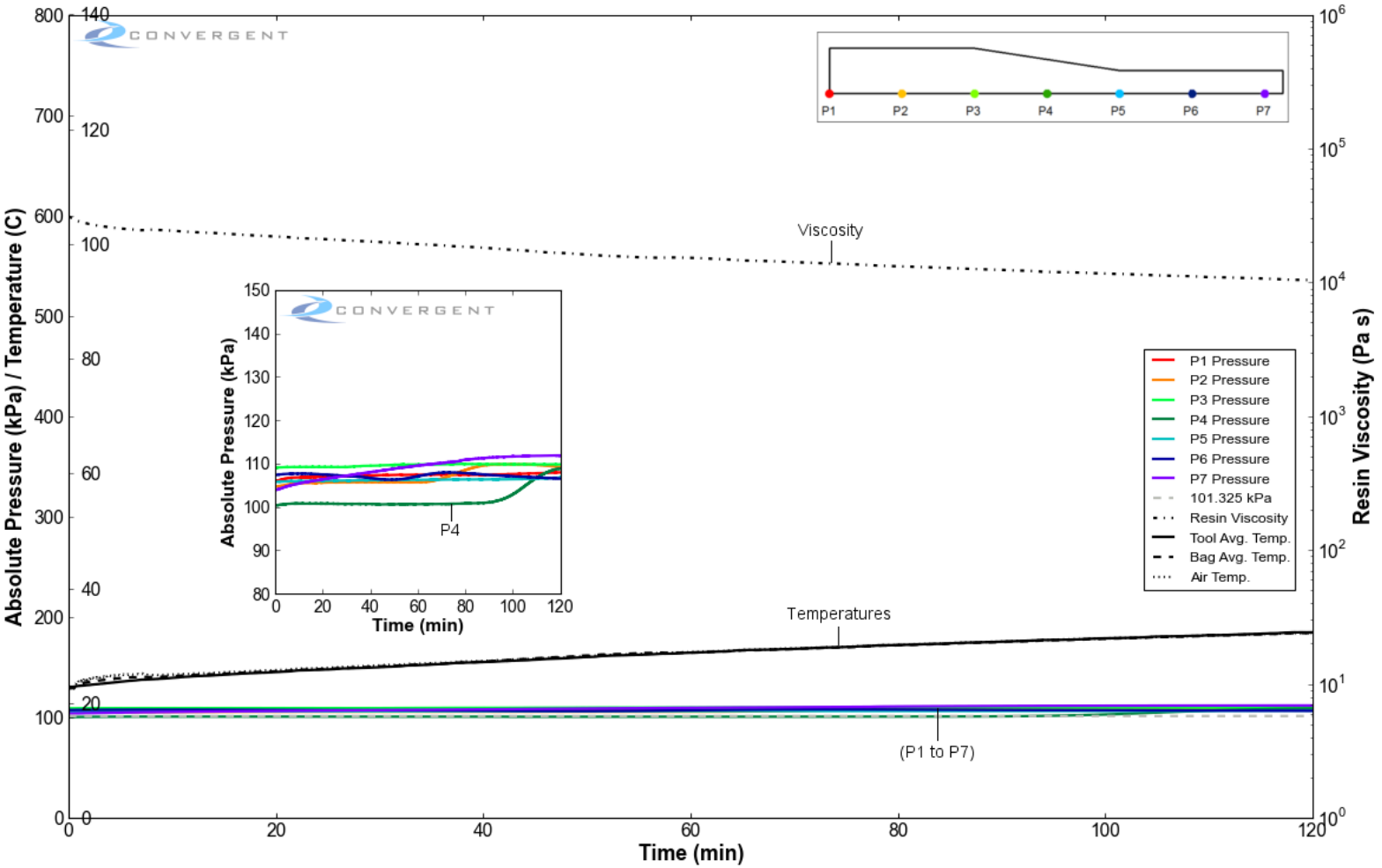

Figure 4.12 – Pressure, temperature and simulated viscosity response for ply drop laminate without caul during in-oven debulk (0-120 minutes). Pressure histories are color coded to identify the position of the pressure response (refer to sub-figure in upper right corner). Thermocouple readings (solid, dotted and dashed black line), viscosity profile (dashed/dotted black line) and atmospheric pressure (dashed grey line) also plotted. Sub-figure shows pressure variation at P4 region of note.

As can be seen in Figure 4.12, for the ply drop laminate without caul, the pressure at all regions stay relatively close to the value of the applied compaction pressure during the entirety of the in-oven debulk. The overall results suggest that the full applied compaction pressure is transferred evenly to all regions of the laminate. However, it is interesting to note the variations which occur at the region centered at the ply drops (P4). Between 0 minutes and 110 minutes it can be seen that the pressure at P4 is lower than all other regions (refer to sub-figure in Figure 4.12). Although the pressure response at P4 during this time is still within the margin of error of the applied compaction pressure, the difference between its pressure and the pressure at all other regions is very evident. Specifically, all other regions are showing pressure values of roughly l07 ± 3 kPa while the pressure at the P4 region is showing pressure values of 101 ± 3 kPa.

Although the causes for the pressure variations at the P4 region cannot be stated with certainty, the fact that these variations occur at the ply drop region seem to signify some form of causality. One hypothesis is that the additional void space elicited by the inclusion of ply drops effects the load paths within the internal structure of the laminate. As such, during the debulk, the internal structure at the ply drop region causes a redistribution of pressure which partially shields the P4 sensor from the applied pressure.

Regardless of the variations seen at the P4 region, it is clear that in the absence of a caul sheet, the applied consolidation pressure is evenly distributed to all regions of the ply drop laminate.

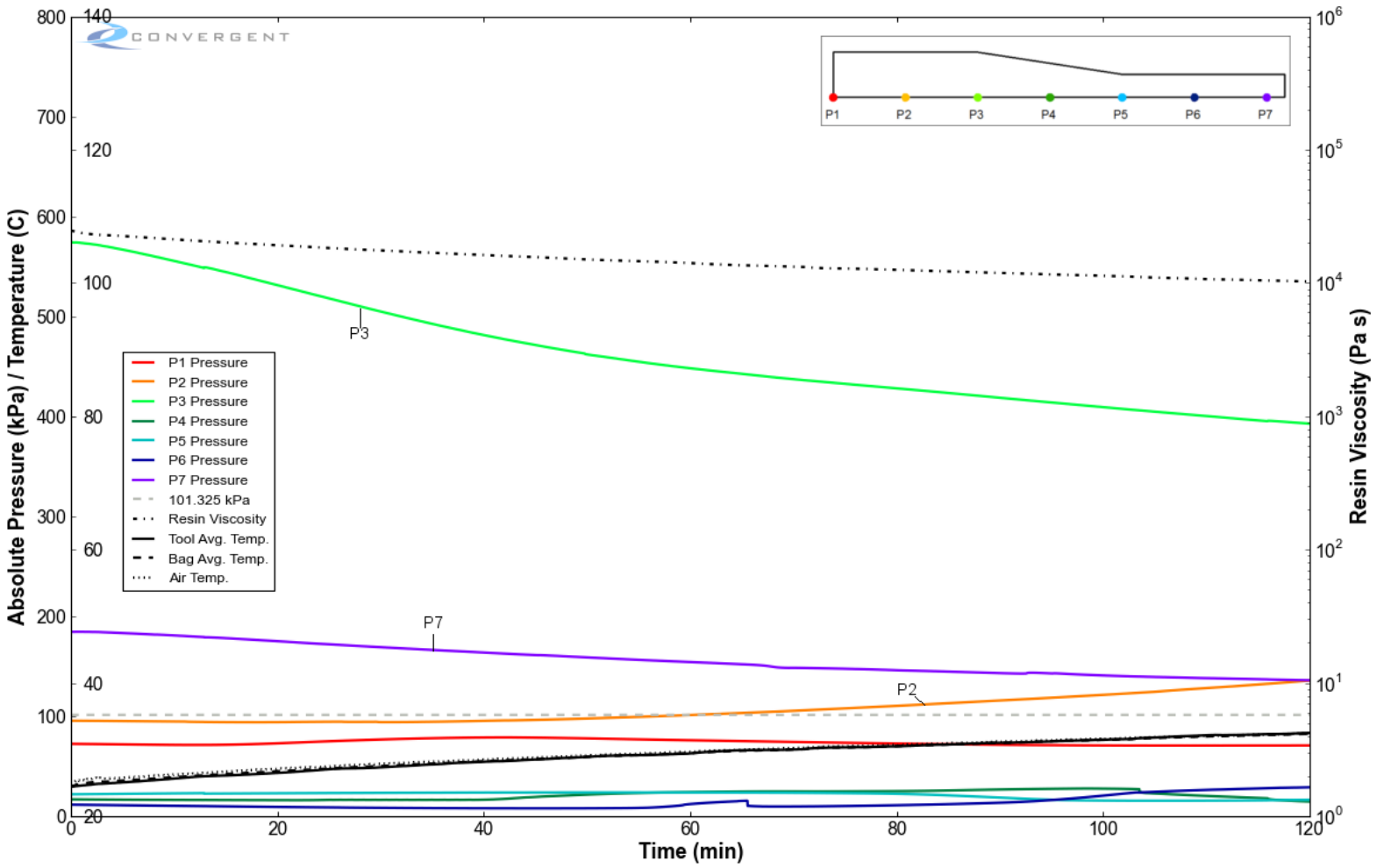

Figure 4.13 – Pressure, temperature and simulated viscosity response for ply drop laminate with 4mm caul sheet during in-oven debulk (0-120 minutes). Pressure histories are color coded to identify the position of the pressure response (refer to sub-figure in upper right corner). Thermocouple readings (solid, dotted and dashed black line), viscosity profile (dashed/dotted black line) and atmospheric pressure (dashed grey line) also plotted.

Figure 4.13 shows the transient pressure response of the ply drop laminate with 4mm caul sheet during the 120 minute in-oven debulk. From this figure, it is observed that pressure variations exist during the in-oven debulk period. Specifically, the pressure at the P3 and P7 region are in a state of decay while the pressure at region P2 is increasing. All other pressures do not undergo any significant variations during this time. Although the oven was programed to maintain a temperature of 25°C during the debulk period, the thermocouple recordings clearly show that the temperature gradually increased to approximately 34°C. Regardless, the viscosity of the resin within this range of temperature is such that it is very unlikely that the pressure variations seen here are primarily caused by a flow compaction mechanisms. Specifically, the viscosity of MTM45-1 resin within the temperature range of 25°C to 34°C is approximately 23000 Pa s to 8700 Pa s. For reference, caulking compound has viscosity range between 5000 Pa s to 8000 Pa s and window putty has a viscosity value on the order of 100000 Pa s [65]. In ruling out resin flow, it can be concluded that the pressure variations seen here are due to an ongoing stress-deformation mechanism. As the laminate is subject to debulk, the pressure overfill regions (P3 and P7) undergo compressive strain which in turn allows for more of the laminate to come into contact with the caul sheet. As more contact is established between the caul sheet and the laminate, the pressure at the P3 and P7 region will decrease. Depending on how much additional contact force has been established, the pressure at regions adjacent to the overfill regions will increase in pressure. For this case, it can be seen that as the overfill regions (P3 and P7) decrease in pressure, the pressure at the P2 region increases. This indicates that better contact has been established at the center of the 16 ply region.

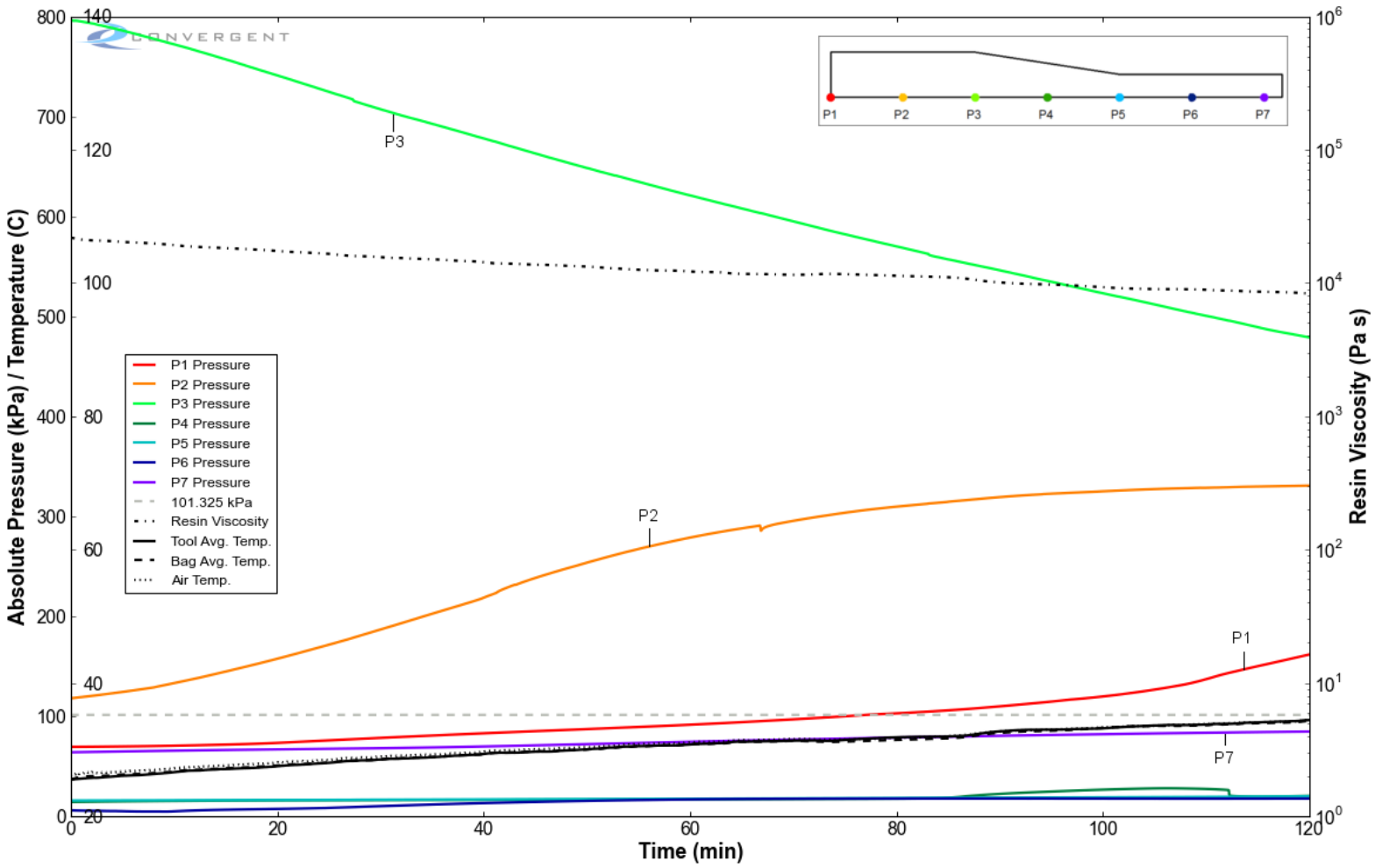

Figure 4.14 – Pressure, temperature and simulated viscosity response for ply drop laminate with 8mm caul sheet during in-oven debulk (0-120 minutes). Pressure histories are color coded to identify the position of the pressure response (refer to sub-figure in upper right corner). Thermocouple readings (solid, dotted and dashed black line), viscosity profile (dashed/dotted black line) and atmospheric pressure (dashed grey line) also plotted.

Figure 4.14 shows the transient pressure response of the ply drop laminate with 8mm caul sheet during the 120 minute in-oven debulk. Again, it can be seen that significant pressure variations exist during the in-oven debulk period. Moreover, due to the viscosity, it is again reasonable to conclude that the pressure variations seen here are caused primarily by a stress-deformation mechanism rather than one of resin flow. However, the pressure variations seen here differ from the case of the ply drop laminate with 4mm caul sheet. Here it can be seen that the P3 region is under a state of decay while the pressure at the P2 and P1 region are increasing in pressure. Note that for the ply drop laminate with 8mm caul sheet, only a minor increase in pressure is seen at the P7 region. This again coincides with the fact that the 8mm caul sheet is stiffer than the 4mm caul sheet. As such, more of the applied compaction pressure is being transferred at the 16 ply region. For the same reason, the rate of pressure decay at the P3 region and the rate of pressure increase at the P2 region are much greater than those seen in the case of the ply drop laminate with 4mm caul sheet. Moreover, one can also observe a slight increase in pressure at the P1 region, which was not seen to occur in the case of the more flexible caul sheet. This suggests that better contact is established between the laminate and the caul sheet at the 16 ply region (P1 to P3) in the case of the more rigid caul sheet.

Although significant pressure variations can be observed during the in-oven debulk for the laminates being processed with a caul sheet, the distinguishing characteristics of the pressure distributions remain unchanged. To illustrate this point, Figure 4.15 shows the pressure distribution at the very end of the 120 minute in-oven debulk for the ply drop laminate without caul, ply drop laminate with 4mm caul sheet and ply drop laminate with 8mm caul sheet.

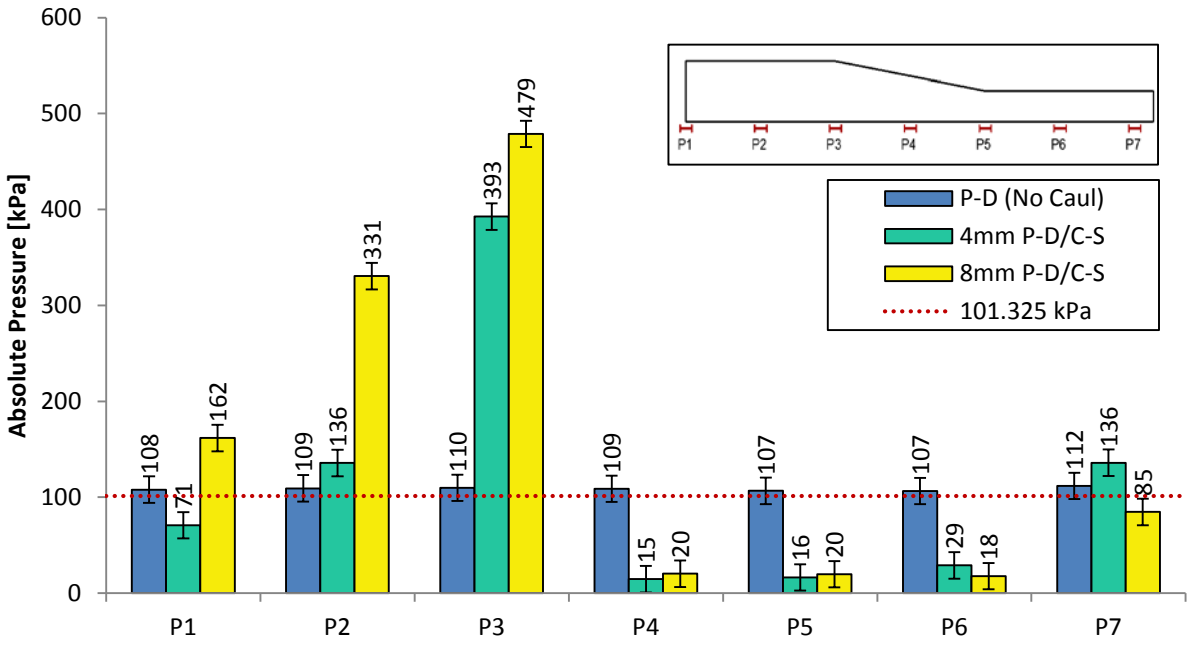

Figure 4.15 – Pressure distribution at the end of the in-oven 120 minute debulk for the ply drop laminate with no caul (P-D), ply drop laminate with 4mm caul sheet (4mm P-D/C-S) and 8mm ply drop caul sheet laminate (8mm P-D/C-S)

As can be seen from the figure above, the distinguishing characteristics for each pressure distribution observed at the initiation of the in-oven debulk (0 minutes, shown in Figure 4.11) still hold true at the end of the in-oven debulk (120 minutes). For the ply drop laminate without caul, the pressure at all regions is within the range of the applied compaction pressure. Whereas, the pressure at region P4 to P6 is shielded from the applied compaction pressure for both the ply drop laminates with caul sheets. Again for these laminates, pressure overfills are seen to exist at the 16 ply region and at the edge of the caul. Finally, the stiffer caul sheet transfers more of the compaction pressure at the 16 ply region. Therefore, regardless of the pressure variations during the in-oven debulk, the general state of pressure distribution remains unchanged in all cases.

4.2.3 Effect of Caul Sheet during Cure

In this section, we will be observing the transient pressure response for all laminates during the cure (120 minutes and beyond). Figure 4.16, Figure 4.17 and Figure 4.18 show the transient pressure response of the ply drop laminate without caul, ply drop laminate with 4mm caul sheet and ply drop laminate with 8mm caul sheet respectively during the cure. The pressures in all figures are plotted using the same color scheme used in the previous section. The average tool side temperature, average bag side temperature and the oven air temperature is also plotted (solid black line, dashed black line and dotted black line respectively). Furthermore, viscosity is also plotted (dashed/dotted black line). Note that the value of viscosity was simulated using the NCAMP data in Raven [21] and the average bag side and tool side temperature data. Again, the nominal value of atmospheric pressure (101 kPa) is plotted as a reference for the value of the applied compaction pressure (Grey dashed line).

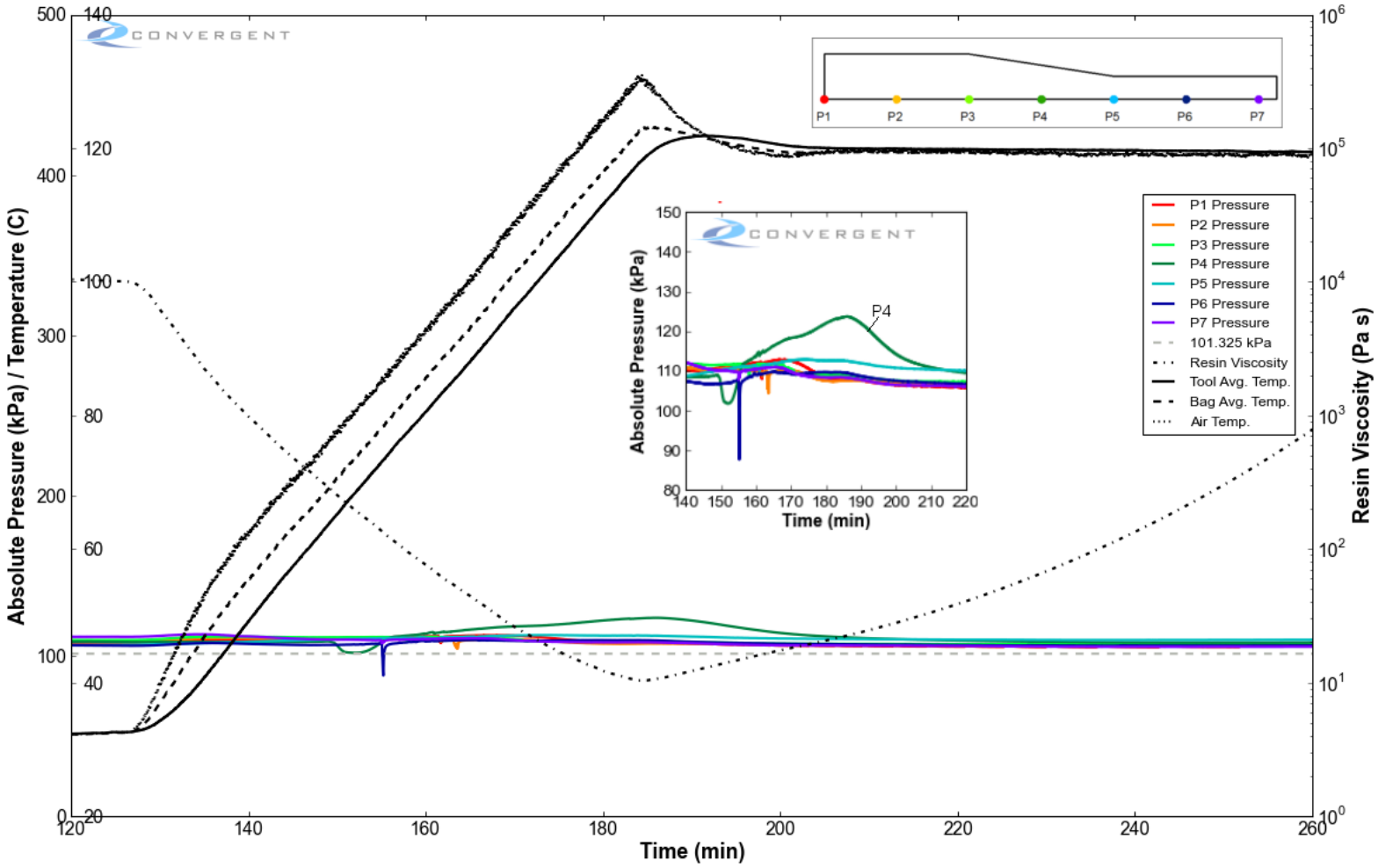

Figure 4.16 – Pressure, temperature and simulated viscosity response for ply drop laminate without caul during cure (120-260 minutes). Pressure histories are color coded to identify the position of the pressure response (refer to sub-figure in upper right corner). Thermocouple readings (solid, dotted and dashed black line), viscosity profile (dashed/dotted black line) and atmospheric pressure (dashed grey line) also plotted. Sub-figure shows pressure variation at P4 region of note.

As can be seen in Figure 4.16, for the ply drop laminate without caul, the pressure at all regions stay relatively close to the value of the applied compaction pressure during the entirety of the cure. Since little to no pressure variations existed for this laminate prior to cure, it is reasonable to conclude that resin will not flow from one region to another as the viscosity of the resin decreased. However, significant pressure variations can again be seen at the P4 region. Specifically, a significant pressure increase can be seen at region P4 between 160 minutes and 210 minutes (refer to sub-figure in Figure 4.16). This pressure increase reaches a maximum value of 124 kPa (i.e. 23 kPa above the applied compaction pressure). Note that this event takes place over significant interval of time and therefore is not likely due to noise. Although the reason for this pressure increase is unclear, it is again noteworthy to point out that this event is occurring at the ply drop region which has an internal structure significantly different from all other regions of the laminate. Specifically, it should be noted that the ply drop region contains additional void spaces due to the termination of the plies. As such, it is possible that the additional void spaces at this region resulted in a buildup of gas pressure during the temperature ramp. As the viscosity decreases, the flow of resin may have sealed the void spaces from the vascular network. As the temperature increases, the gas pressure within these void spaces increases until some phenomenon (e.g. onset of through thickness breathing) causes the void spaces to reestablish a connection with the vacuum system.

Regardless of the pressure variations seen at P4, overall it is clear that the absence of a caul sheet elicits the absence of pressure gradients. Without pressure gradients, resin flow is not possible on the macro scale and therefore the initial pressure distribution will remain unchanged during cure.

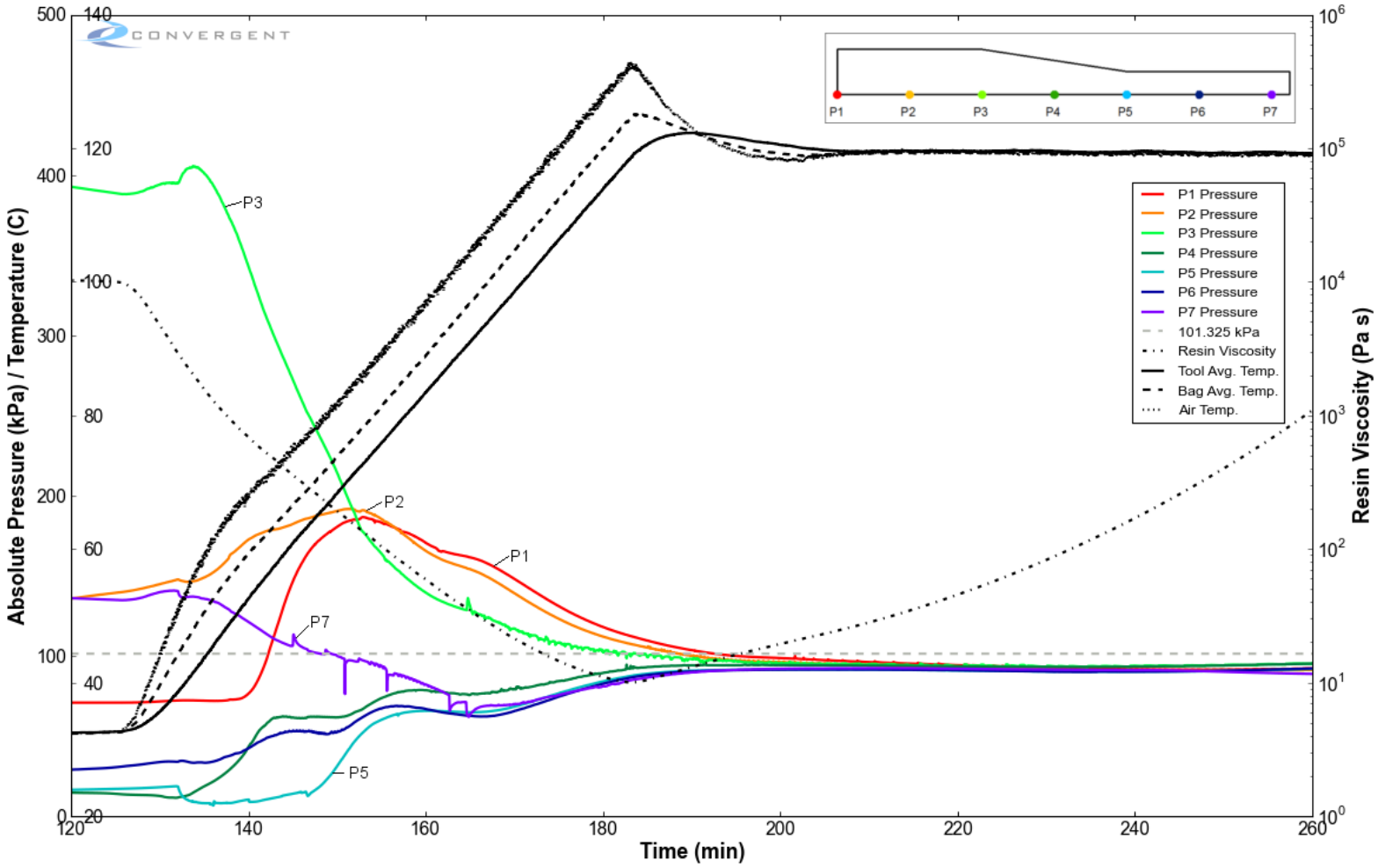

Figure 4.17 – Pressure, temperature and simulated viscosity response for ply drop laminate with 4mm caul sheet during cure (120-260 minutes). Pressure histories are color coded to identify the position of the pressure response (refer to sub-figure in upper right corner). Thermocouple readings (solid, dotted and dashed black line), viscosity profile (dashed/dotted black line) and atmospheric pressure (dashed grey line) also plotted.

Figure 4.17 shows the transient pressure response of the ply drop laminate with 4mm caul sheet during cure. From the figure above it can be seen that pressures at all regions start to change very quickly once the viscosity has decreased below a value of approximately 2000-3000 Pa s. Note that this value of viscosity is equivalent to that of lard [65]. At this point, the pressures at region P3 and P7 are decreasing very quickly. All other regions eventually undergo an increase in pressure.

At time 152 minutes, the increasing pressure at regions P1 and P2 overtake the decreasing pressure at region P3. Immediately following this event, the pressures at the P1 and P2 regions also begin to decrease. Meanwhile, as the pressure at the P7 region decreases, the pressure at the P4, P5 and P6 regions soon undergo an increase in pressure. It is interesting to note, that amongst all regions, the P5 region (border between the ply drop region and 8-ply region) is the last to experience an increase in pressure at 147 minutes. This suggests that this region was the last to come into contact with the caul sheet. This also implies that the resin flowing into the P5 region originated from both the P4 and P6 region.

At approximately 176 minutes, the values of pressure are such that the magnitudes decrease the farther away the region is from the center of the laminate (i.e. pressure decreasing as we go from P1 to P7). This implies that the resin everywhere at this point in time is flowing away from the center of the laminate towards the outer edge. As such, resin is flowing out of the thick regions (P1 to P3) and into the thinner regions (P4 to P7). As resin is depleted from the thick region, more of the applied compaction pressure is absorbed by the fiber bed. This ultimately results in a decrease in hydrostatic pressure not only at the thick region but at all other regions as can be seen

later in time. Specifically, at 220 minutes, all regions converge to an equilibrium pressure. Past this point the pressure variations have ceased since there are no significant pressure gradients to promote flow. Note that the viscosity of the resin at 220 minutes is roughly 45 Pa.s, therefore the hydrostatic pressure equilibrium was achieved well before the point of gelation. What is important to note here is the value of pressure at which all regions have converged to. The final equilibrium pressure for all regions in this system is roughly 93 kPa which coincides with an 8 kPa loss in hydrostatic pressure (i.e. 8 kPa below the nominal applied compaction pressure).

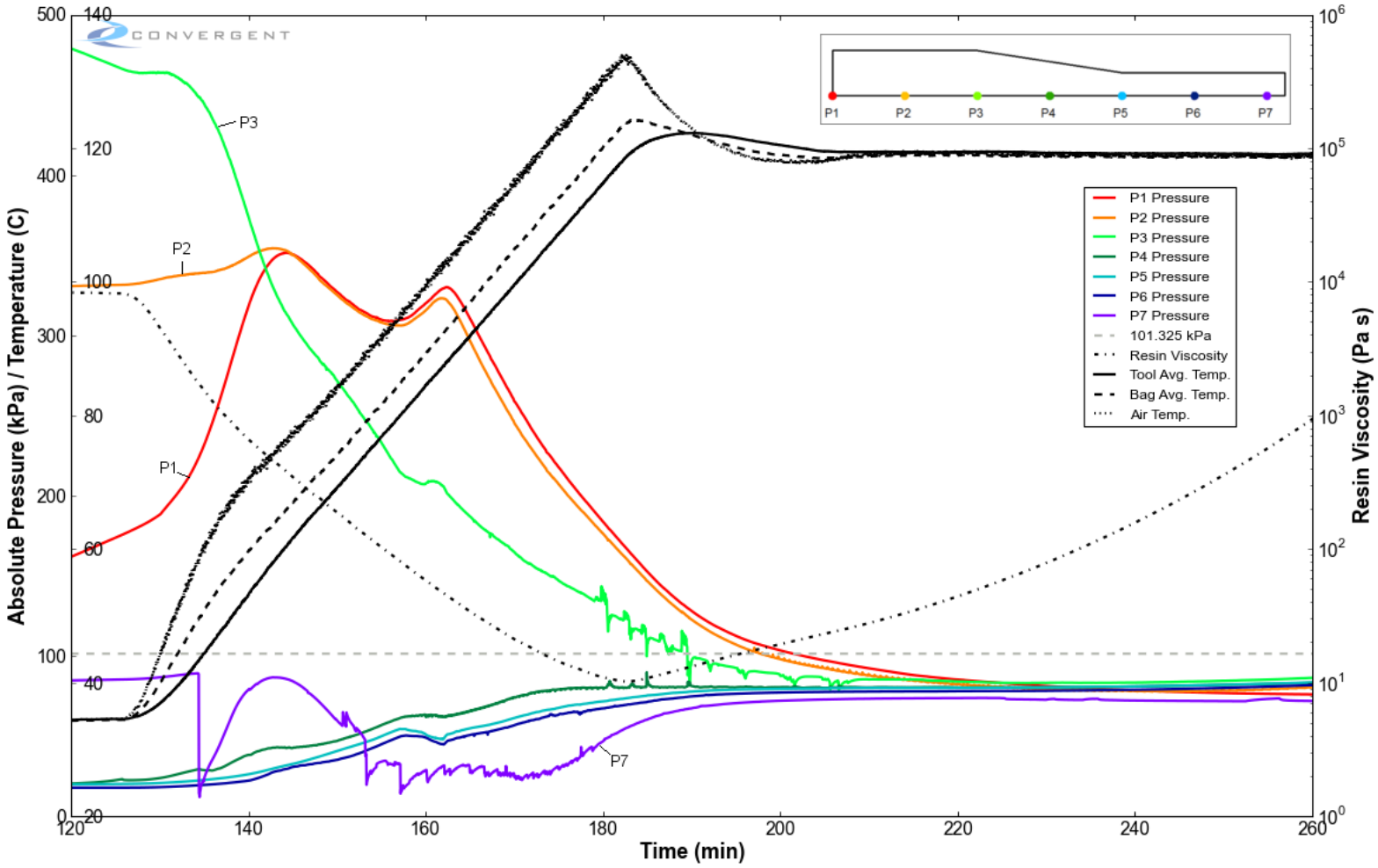

Figure 4.18 – Pressure, temperature and simulated viscosity response for ply drop laminate with 8mm caul sheet during cure (120-260 minutes). Pressure histories are color coded to identify the position of the pressure response (refer to sub-figure in upper right corner). Thermocouple readings (solid, dotted and dashed black line), viscosity profile (dashed/dotted black line) and atmospheric pressure (dashed grey line) also plotted.

Figure 4.18 shows the transient pressure response of the ply drop laminate with 8mm caul sheet during cure. From the figure above, it can be seen that the pressures change very quickly once the viscosity has decreased below a value of approximately 2000-3000 Pa s. Note that this is similar to the behavior seen in the case of the ply drop laminate with 4mm caul sheet. Again, it can be seen that the increasing pressure at regions P1 and P2 overtake the decreasing pressure at region P3. However, in this case, this event happens earlier, at approximately 140 minutes. Furthermore, unlike the ply drop laminate with 4mm caul sheet, the pressure at region P7 decreases well below the pressures at regions P4, P5 and P6 at approximately 153 minutes. This seems to imply that the resin flow has caused the caul sheet to rotate in such a way that the caul sheets edge lifts off from the laminates surface and contact pressure is lost at this region. Supporting evidence to this claim can also be seen from the pressure histories at the thick region (P1 to P3). As the caul sheets edge lifts off from the laminates surface, more of the applied compaction pressure is transferred to the 16 ply region which results in slight rise in pressure at P1, P2 and P3 regions. Overall, the results shown here support the previous claim that the contact pressure from the edge of the 8mm caul sheet at region P7 plays a less significant role as compared to the case of the ply drop laminate with 4mm caul sheet.

Note that the events recently discussed also coincide with the values of pressure decreasing the farther away the region is from the center of the laminate (at 153 minutes). Again, this implies that the resin everywhere is flowing away from the center of the laminate towards the outer edge. Note that this event was seen to occur much later in the case of ply drop laminate with 4mm caul sheet (176 minutes). This observation is consistent with the fact that the 8mm caul sheet is stiffer and therefore cannot comply with the 8-ply region as well as the 4mm caul sheet. Additional

evidence which points to this phenomenon can also be seen in the data presented here. Note that the P5 region for the case of the ply drop laminate with 8mm caul sheet is no longer the last region to undergo an increase in pressure. Rather the pressure at P5 builds up gradually following the pressurization at the P4 region and preceding the pressurization at the P6 region. This implies that these regions gradually come into contact with the caul sheet as the resin predominantly flows from the center of the laminate towards the outer edge.

Ultimately, as resin flows out of the thick regions and into the thinner regions, more of the applied compaction pressure is born by the fiber bed. At 230 minutes, all regions converge to an equilibrium pressure of 80 kPa which is 21 kPa below the nominal applied compaction pressure.

With respect to the relationship between resin pressure and caul sheet thickness, two things should be noted here. First, note that the final equilibrium pressure decreases further below the applied compaction pressure as the stiffness of the caul sheet is increases. Second, note that the stiffer caul sheet required slightly more time to achieve equilibrium. These observations will be discussed in greater detail in the discussion.

4.2.4 Effect of Caul Sheet on Final Thickness Profile

Figure 4.19 presents the cured ply thickness (CPT) profile of the ply drop laminate without caul, ply drop laminate with 4mm caul sheet and ply drop laminate with 8mm caul sheet. It can be seen that the relationship between the CPT profile and caul sheet stiffness for the laminates manufactured in this study is consistent with the relationship observed in Chapter 3. That is to say that the use of more rigid caul sheets will result in more thinning at the thick regions (16-ply region) and more thickening at the thin region (8 ply region).

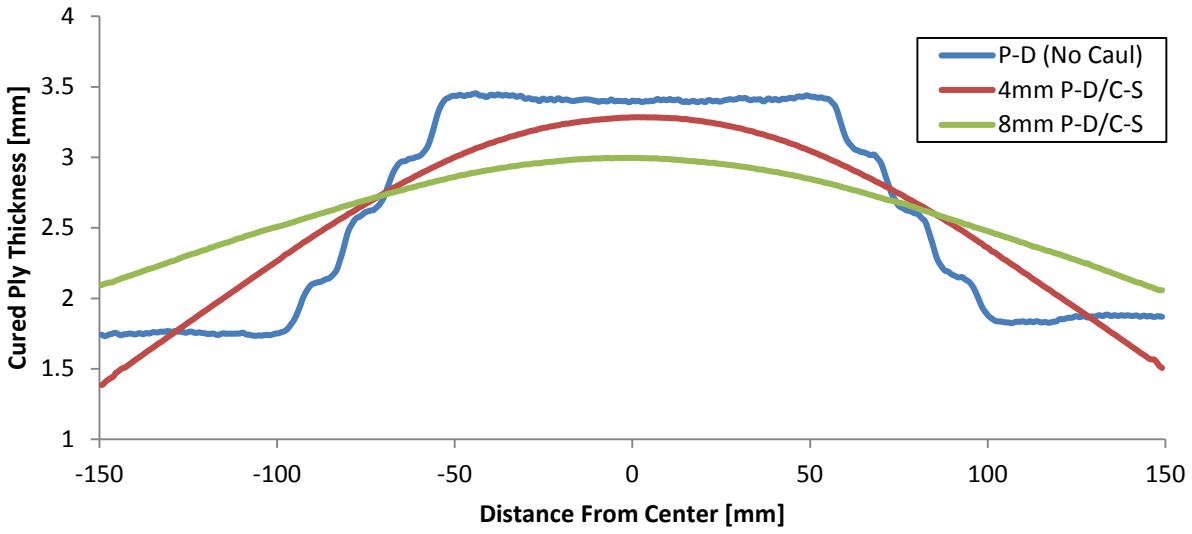

Figure 4.19 – Cured ply thickness of ply drop laminate without caul (P-D), ply drop laminate with 4mm caul sheet (4mm P-D/C-S) and ply drop laminate with 8mm caul sheet (8mm P-D/C-S).

Figure 4.20 shows the final through thickness strain for the ply drop laminates with 4mm and 8mm caul sheets. Note that the strain values were calculated by assuming that the cured ply thickness profile of the ply drop laminate without a caul sheet represented the nominal thickness profile of all laminates. In addition, the location of the sensors are also plotted.

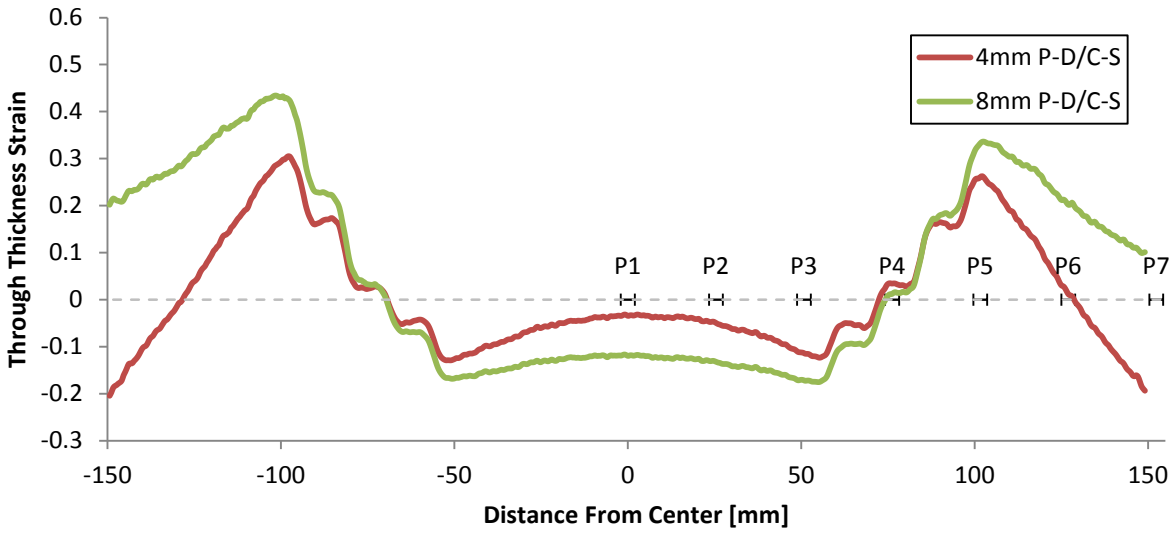

Figure 4.20 – Final through thickness strain profile of ply drop laminate (P-D), ply drop laminate with 4mm caul sheet (4mm P-D/C-S) and ply drop laminate with 8mm caul sheet (8mm P-D/C-S). The positions of the sensors have also been annotated for convenience.

From the final strain plot, it can be concluded that regions P4, P5 and P6 are all resin rich. This is true for both the ply drop laminates with caul sheets. As such, it can be said that little to none of applied compaction pressure was sustained by the fiber bed at these regions. Conversely, it is clear that the resin content at the P1, P2 and P3 regions has been depleted. Therefore, it can be concluded that some of the applied compaction pressure at these regions was born by the fiber bed.

Note that negative strain values can be seen at the P7 region for the ply drop laminate with 4mm caul sheet whereas the values of strain at this region for the ply drop laminate with 8mm caul sheet is positive. This implies that the region located at the edge of the caul is resin poor in the case of the ply drop laminate with 4mm caul sheet and resin rich in the case of the ply drop laminate with 8mm caul sheet. Since the 8mm caul sheet is stiffer, its edge will not be able to

deflect down towards the surface of the laminate as effectively as the 4mm caul sheet. Therefore more resin will be required to fill this gap in order create a pressure cell and counter act the flow of resin. In doing so, more resin must be depleted from the thick region (P1 to P3) which in turn causes more thinning at the thick region (i.e. strain values become more negative). This also suggests that the contact between the edge of the 8mm caul sheet and laminate may have been ineffective or even non-existent. This observation is consistent with the observations made in the sections dealing with the pressure results (Sections 4.2.1 and 4.2.2).

4.3 Discussion

4.3.1 First Order Effects: Pressure Shielding and Overfilling

It has been shown that the use of a caul sheet has a dramatic effect on the distribution of the applied compaction pressure to the laminates (Figure 4.11 in section 4.2.1). The inclusion of a caul sheet effectively shields the applied compaction pressure from the regions of the laminate which are not initially in contact with the caul sheet. Specifically, for the laminates studied in this chapter, the caul sheet shields the applied compaction pressure from the regions spanning between the ply drop region and the center of the 8-ply region (P4 to P6). By tracking the resin pressure at the shielded region during the debulk and cure (section 4.2.2 and 4.2.3), it has also been shown that the shielded region will remain unpressurized until sufficient resin has flown into the region such that contact can be made between the laminate and the caul sheet. As such, void spaces within the shielded region are likely to stabilize and grow.

Furthermore, since a force equilibrium must be achieved, the phenomenon of pressure shielding will inevitably result in the existence of pressure overfills. From Figure 4.11, it is obvious that the primary pressure overfill region is located at the border between the 16-ply region and ply drop region (P3). It has also been observed that a secondary pressure overfill region may also exist at the region located beneath the edge of the caul sheet (P7). Figure 4.21 illustrates the locations of the shielded region and overfill regions with respect to the laminate and sensors.

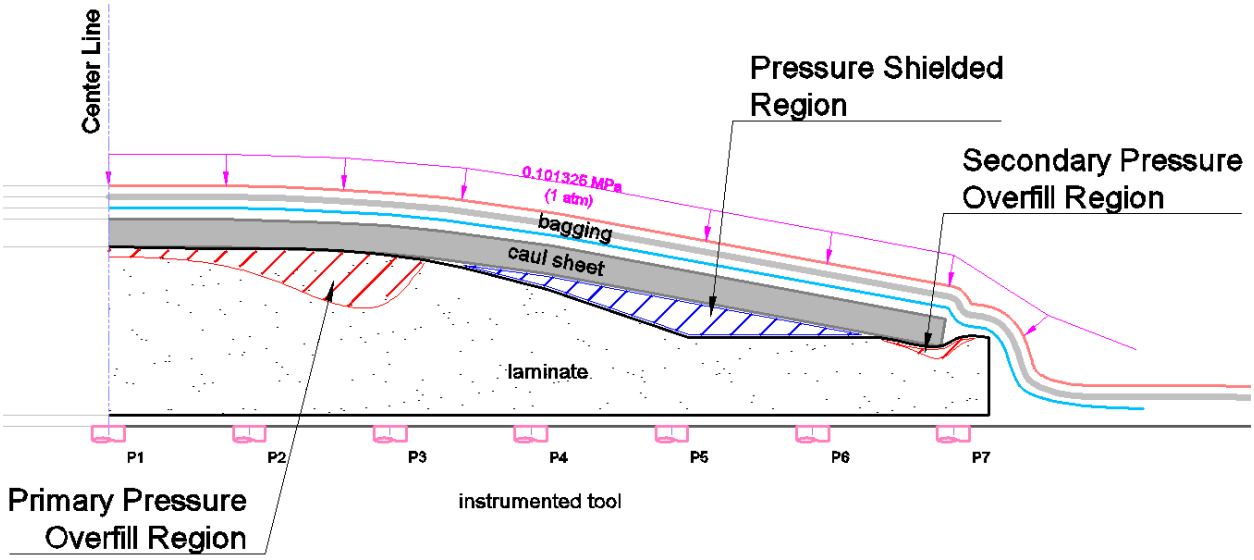

Figure 4.21 – Illustration of pressure overfill regions and shielded regions for ply drop laminates with caul sheets.

It was noted that the pressure at the primary overfill region is greater for the ply drop laminate with 8mm caul sheet than for the ply drop laminate with 4mm caul sheet. Conversely, the pressure at the secondary overfill region is greater for the ply drop laminate with 4mm caul sheet than for the ply drop laminate with 8mm caul sheet. This observation is consistent with the expected behavior of the caul sheets deflection. That is to say that as the stiffness of the caul sheet is increased, it cannot deform as easily under the same applied compaction pressure. As a

result the edge of the caul will not be able to transfer as much pressure to the laminate at the secondary overfill region. Therefore, more of the applied compaction pressure will be transferred to the primary overfill region. Of course, if the caul sheet is very stiff, the edge of the caul will not come in contact with the laminate at all and all of the applied pressure will be transferred at the primary overfill region. Therefore, it can be concluded that a caul sheet not only shields pressure from the laminate but that its stiffness also plays an important role in the distribution of pressure. With respect to porosity, the initial pressure distribution is also of great importance because it essentially sets the stage for resin migration (i.e. the second order effect). That is to say that the initial pressure gradients, which are preordained by the distribution and magnitudes of the overfill and shielded regions, will dictate the behavior of resin flow during the low viscosity period. This relationship will be discussed in greater detail in the following sections.

In conclusion, the use of caul sheets on ply dropped laminates results in a de-homogenized pressure distributions. The distinguishing characteristics of such a pressure distribution are summarized below

- Regions which are not in contact with the caul sheet are shielded from consolidation pressure
- Regions which are in contact with the caul sheet are subject to pressure overfilling
- Stiffer caul sheets result in reduced distributions of pressure. As such overfill regions are higher in magnitude and more localized.

4.3.2 Pressure Variations during In-Oven Debulk Period

It was observed that significant pressure variations occurred during the debulk period for the ply drop laminates with caul sheets. Note that an unintended increase in oven temperature during the debulk period caused a 7 minute delay for the initiation of the temperature ramp. As such, in the context of this discussion, the debulk period is considered to have taken place between times 0 minutes and 127 minutes. Figure 4.22 shows the pressure distribution of the ply drop laminates with 4mm and 8mm caul sheets at time 0 minutes and 127 minutes. In addition, Table 4.2 provides a summary of the pressure changes during the debulk period for all laminates. Note, that in the context of this discussion, variations are considered to be significant when they are greater than 10 kPa. As such, variations which meet this criterion have been highlighted in Table 4.2. Positive changes in pressure are highlighted in green and negative changes are highlighted in red.

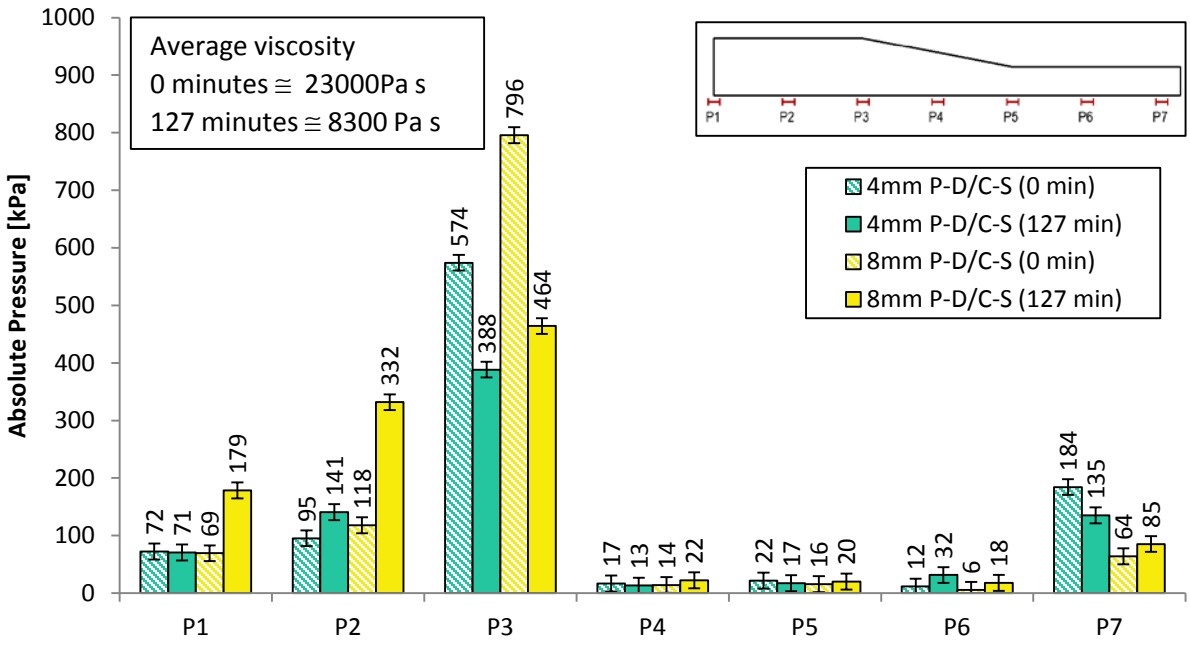

Figure 4.22 – Pressure distribution for ply drop laminate with 4mm caul sheet (4mm P-D/C-S) and ply drop laminate with 8mm caul sheet (8mm P-D/C-S) at 0 minutes (beginning of in-oven debulk) and 127 minutes (end of in-oven debulk).

Table 4.2 – Summary of pressure changes during debulk period (0 to 127 minutes) for ply drop laminate without caul (P-D), ply drop laminate with 4mm caul sheet (4mm P-D/C-S) and ply drop laminate with 8mm caul sheet (8mm P-D/C-S). Pressure changes greater Than 10 kPa are highlighted. Positive changes are highlighted in green and negative changes are highlighted in red.

	Pressure Sensor Change During Debulk (0 to 127 min) in kPa						
	P1	**P2**	**P3**	**P4**	**P5**	**P6**	**P7**
P-D (No Caul)	2	4	1	8	1	-1	8
4mm P-D/C-S	-2	45	-186	-4	-5	20	-49
8mm P-D/C-S	109	214	-332	8	4	12	22

As can be seen in Figure 4.22 and Table 4.2 significant pressure variations occur for the ply drop laminates with caul sheets during the debulk. The most significant change for both laminates is the decrease in pressure at region P3 (186 kPa and 332 kPa loss for the ply drop laminate with 4mm and 8mm caul sheets respectively). Additionally, the ply drop laminate with 8mm caul sheet experiences a pressure increase at regions P1 and P2 of 109kPa and 214kPa respectively.

Whereas, the ply drop laminate 4mm caul sheet only experiences a pressure increase of 45kPa at the P2 region. Ultimately, these pressure variations lead to a better distribution of the primary pressure overfill region (16 ply region) for both laminates (i.e. the pressure is less localize at P3 and better distributed along P1, P2 and P3).

As previously mentioned, although the oven was programed to maintain a temperature of 25°C during the debulk period, the thermocouple recordings clearly show that temperature gradually increased to approximately 34°C. Regardless, the viscosity of the resin within this range of temperature is such that it is very unlikely that the pressure variations seen here are caused by resin flow (viscosity approximately between 23000 to 8700 Pa s). As such, it is more likely that the pressure variations seen during the debulk are due a stress-deformation mechanism. As the laminate is subject to debulking, pressure overfill regions undergo compressive strain which allows the caul sheet to establish more contact with the laminate. As more contact is achieved, the pressure overfills become less localized. Although the temperature rise during the debulk is not conducive to enable flow, it can have a contributing role in the pressure variations. As the viscosity of the resin decreases with temperature, the material essentially softens (i.e. the modulus decreases) since the decreased viscosity permits for more nesting between the fiber bed plies. As a result, more compressive strain is achievable under the same loading conditions.

Although it can be seen that the pressure variations during the debulk alter the pressure distribution for the ply drop laminate with 4mm and 8mm caul sheet, the features which distinguish these pressure distributions from that of the ply drop laminate without caul (as summarized in previous section) remain unchanged. However, the observations discussed here

elicit important questions. That is: How much does the pressure distribution prior to the onset of resin flow influence the pressure history during resin flow? Moreover, can the debulk influence the distribution of pressure in such a way that final outcome is altered? For example, if one were to initiate the temperature ramp at time 0 minutes rather than 127 minutes, how much would the resulting pressure histories differ from the pressure histories which have been presented in this study? To elaborate, consider the pressure distributions shown in Figure 4.22. Note that the pressure overfills at the 16 ply region (P1 to P3) are higher in magnitude and more localized at 0 minutes as compared to 127 minutes. As such, if one were to initiate the temperature ramp (and thus resin flow) at 0 minutes, would the laminates have less time to achieve equilibrium? Would a pressure gradient get locked in at gelation? Conversely, since the pressure overfills at 0 minutes are higher in magnitude and more localized, it stands to reason that the resin flow velocity in this hypothetical scenario will be much quicker during cure. As such, does this imply that the pressure variations during the debulk are irrelevant since the proceeding flow mechanics work counter act them? The questions outlined in this discussion have been presented in order to propel future works to enhance our understanding of porosity in configured structures.

4.3.3 Second Order Effects: Resin Migration

As the temperature is increased the viscosity of the resin will decrease. This will subsequently allow resin to flow from the high pressure regions to low pressure regions. Resin migration will continue until such a point where the pressure gradients have been eliminated or until the onset of gelation increases viscosity such that resin flow is no longer possible. In the case of the ply drop laminate cured without a caul sheet, it is clear that the pressure gradients involved are very small or even non-existent during the majority of the cure and therefore the effects of resin migration for this system are negligible. However, for the ply drop laminates which were cured with a 4mm and 8mm caul sheet, it has been shown that the caul sheets cause a redistribution of pressure which elicit the existence of significant pressure gradients along the length of the laminate. As such, the ply drop laminates with caul sheets are susceptible to the effects of resin migration, the consequences of which are discussed here.

Figure 4.23 shows the pressure distribution for the ply drop laminate without caul, ply drop laminate with 4mm caul sheet and ply drop laminate with 8mm caul sheet at a 175 minutes. At this point in time, the oven temperature is just about reach 120°C and the viscosity of the resin for all trials is on the verge of reaching its minimum value of 10 Pa s. More specifically, the average viscosity amongst all three trials is roughly 15 Pa s which is equivalent to chocolate syrup [65].

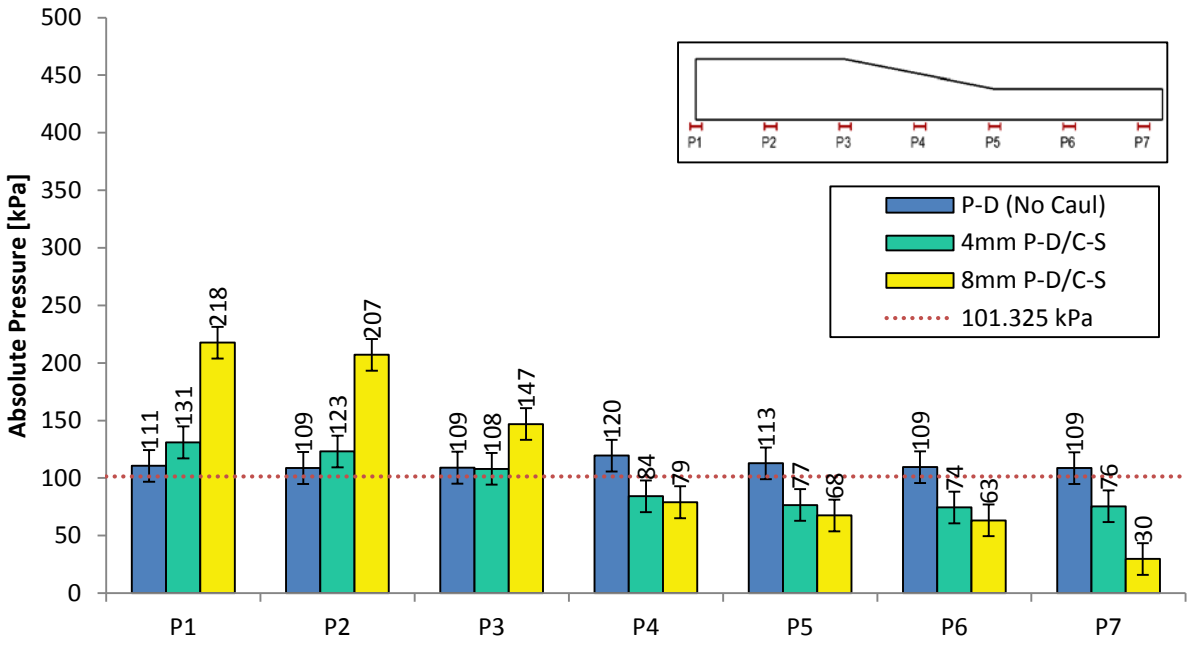

Figure 4.23 – Pressure distribution for ply drop laminate without caul (P-D), ply drop laminate with 4mm caul sheet (4mm P-D/C-S) and ply drop laminate with 8mm caul sheet (8mm P-D/C-S) at 175 minutes (close to time of minimum viscosity).

The figure above demonstrates an important effect that the caul sheet stiffness has on the pressure history of the ply drop laminates. Note that significant pressure gradients exist for the ply drop laminate with caul sheets. Since viscosity is low, this implies that resin migration is still occurring at this time. What is important to note in this figure is the difference in pressure gradients between the ply drop laminates with 4mm and 8mm caul sheets. Specifically, the pressure difference between region P1 and P7 for the ply drop laminate with 4mm caul sheet is of a magnitude of 55 kPa whereas the pressure difference between the same regions for the ply drop laminate with 8mm caul sheet is of a magnitude of 188 kPa. This implies that the stiffer caul sheet requires more time to reach equilibrium. This is due to the greater lack of compliance between the ply drop laminate and caul sheet which necessitates more resin migration. The critical implication in this instance is that stiff caul sheets may be at greater risk of not achieving

equilibrium within the low viscosity phase thereby locking in a pressure gradient at gelation. Although, this was not seen to be the case for experimental trials conducted in this chapter, this is not the only adverse consequence associated with the effects of stiff caul sheets.

As the resin disperses to reach equilibrium, more of the compaction pressure will be borne by the fiber bed at the regions which have been depleted of resin content. This ultimately hijacks the pressure from the resin which could potentially lead to void stabilization. This effect is demonstrated in Figure 4.24 below.

Figure 4.24 shows the pressure distribution for the ply drop laminate without caul, the ply drop laminate with 4mm caul sheet and the ply drop laminate with 8mm caul sheet at 270 minutes. This is the approximate point of gelation and at this time viscosity is increasing very quickly. According to the simulated viscosity profiles, the average viscosity at this point is roughly 3000 Pa s. However, since this is the point of gelation, it is difficult to attest to the accuracy of this value since viscosity is essentially increasing infinitesimally and very rapidly. Nevertheless, this point in time was selected because it can be reasonably assumed that resin will no longer flow past this point.

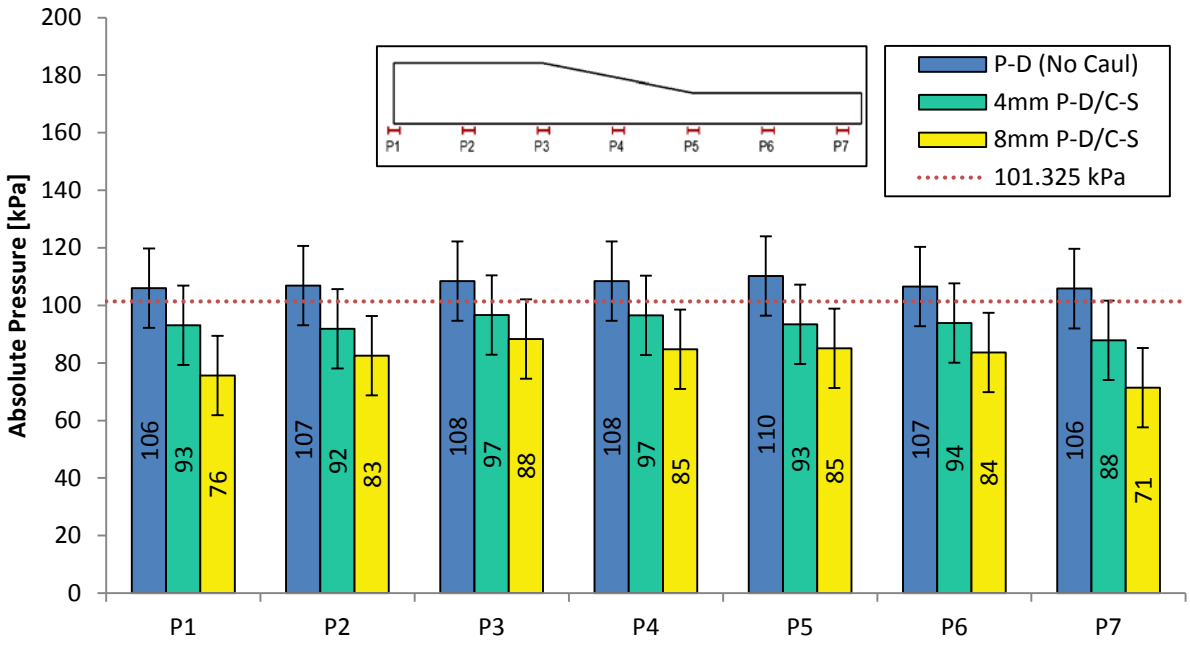

Figure 4.24 – Pressure distribution for ply drop laminate without caul (P-D), ply drop laminate with 4mm caul sheet (4mm P-D/C-S) and ply drop laminate with 8mm caul sheet (8mm P-D/C-S) at 270 minutes (approximate time of gelation).

As can be seen in the figure above, there are no concerns in the case of the laminate cured without caul since the pressures at all regions are well within the range the applied compaction pressure. However, it can be observed that the resin pressure for the ply drop laminates with 4mm and 8mm caul sheets have equilibrated to an average pressure of 93 kPa and 82 kPa respectively. In other words, the ply drop laminate with 4mm and 8mm caul sheet have sustained a 7.9% and 18.8% loss in resin pressure respectively.

The results shown here demonstrate the repercussions that come with using caul sheets to manufacture ply dropped laminates. The lack of compliance between the laminate and the caul sheet elicits resin flow which causes more of the applied compaction pressure to be borne by the fiber bed at the pressure overfill regions. Since the resin flowing into the shielded region is

driven by the hydrostatic pressure at the overfill regions, a loss in hydrostatic pressure will be incurred in both regions. Moreover, it can be seen that this effect scales proportionally to the stiffness of the caul sheet. As has been previously discussed, stiffer caul sheets elicit greater lack of compliance. Consequently, more resin migration is needed in order to achieve equilibrium. This ultimately results in more of the applied compaction pressure being absorbed by the fiber bed. As such, stiffer caul sheets result in greater losses of hydrostatic resin pressure and therefore present a greater risk of void stabilization and growth.

Chapter 5: Simulations

In the previous chapters, the relationship between porosity and resin pressure in the processing of configured structures has been addressed experimentally and explained. Specifically, in Chapter 3, it was concluded that the lack of fit between the caul sheet and the thickness profile of a ply drop laminate causes a decrease in resin pressure which in turn results in void stabilization and growth. The loss of resin pressure is caused by pressure shielding (a first order effect) and resin migration (a second order effect). This phenomenon was measured experimentally in Chapter 4 by tracking the hydrostatic pressure of various laminates through the use of an instrumented tool.

In this chapter, a Darcy flow-compaction formulation [68] as implemented in the COMPRO V2 software [2] will be used to enhance our understanding of the dominant physical mechanisms and to assess how well the model mimics the behavior observed in the experimental trials. As such, this chapter comprises two exercises.

The first exercise is a parametric study which looks to validate the use of the Darcy flow-compaction formulation for the processing scenarios of interest to this thesis. In the previous chapters, for the most part, lack of compliance was altered by using caul sheets of various bending rigidities to manufacture ply drop laminates. However, in all experimental trials the material used for the ply drop laminates was not altered. As such, what remains to be discussed is the effect that the composite material properties have on both the resin pressure history and the final shape of the part. These properties change during the cure and therefore it is inherently difficult to assess their effects experimentally. In this first exercise, the model will be used to perform a parametric study in order to address the effects of the composite material properties.

Specifically, the material properties of interest to this study are the fiber bed compaction behavior, fiber bed liquid permeability and resin viscosity.

The second exercise evaluates how well the Darcy flow-compaction formulation mimics the pressure history observed in the experimental trials (Chapter 4). In this exercise two attempts will be made to simulate the experimental pressure histories for the ply drop laminates with 4mm and 8mm caul sheets. The first attempt aims to simulate the pressure histories during the full experimental regime (i.e. the debulk and cure regimes will be simulated). The second attempt will only simulate the pressure histories during the flow dominated regime (i.e. only the cure regime will be simulated). Identifying similarities between the simulation and experiments will cast some light as to how the model can be used as a tool in making decisions in manufacturing and design. Furthermore, discussing the limitations of the model will identify physics that still need to be addressed thereby providing a direction for future works.

5.1 Darcy Flow-Compaction Model

For both exercises presented in this chapter, the flow and compaction response of the structural configurations studied in this thesis will be simulated. This will be done with the use of the Darcy flow-compaction formulation proposed by Hubert et al. [68] which is commercially available as COMPRO V2 [2]. This software is based on the soils analysis in Abaqus and implemented as an extension within Abaqus 6.14 [3] finite element software. The model formulation performs a sequential thermal, flow-compaction and stress deformation analysis in order to predict resin volume changes prior to gelation and calculate the residual stresses and deformations following gelation. Since residual stress formulations are not of interest to this

thesis, only the flow-compaction module has been used to produce the simulations in this chapter. Also, rather than solve for the thermal history, the experimental thermal history was imposed on the solution. The following is a brief explanation of the flow-compaction modeling.

The model being discussed here is commonly referred to as the Darcy flow-compaction model because it uses Darcy's law to compute resin percolation flow in and out of the laminate. In its most general form, Darcy's law is written as follows

$$q = \frac{K}{\mu}\Delta P \tag{5-1}$$

Where q is the fluid mass flux, K is the permeability of the porous medium, μ is the viscosity of the fluid and ΔP is the hydrostatic pressure gradient.

In addition to the resin flow behavior, in order to fully describe laminate consolidation during processing, the model must also compute the effective stress which is carried by the fiber bed. This is done via a stress-strain relationship. As such, the boundary stresses imposed on the laminate are distributed between the solid skeleton (fiber bed) and the fluid (resin) based on the strains resulting from resin flow.

$$\sigma = \bar{\sigma_f} + P_r \tag{5-2}$$

Where σ is the overall compaction pressure imposed on the laminate, $\bar{\sigma_f}$ is the fiber bed effective stress and P_r is the hydrostatic pressure of the resin

The three dimensional elements used to model the laminate have displacement and pressure as coupled degrees of freedom. Specifically, the laminate section for both exercises was meshed with 20-node brick elements with quadratic displacement interpolation and linear pore pressure interpolation (C3D20P). The three dimensional elements used to model the caul sheet only have displacement as a degree of freedom. The specific elements used to mesh the caul sheet section are specified in Table 5.1 and Table 5.4 for the first and second exercise respectively. Since all of the laminate and caul sheet assemblies modeled in both exercises comprised of symmetric geometries, only half of the laminate and caul sheet was modeled. The sections width (thickness in z direction as seen in Figure 5.1) is 3mm for all simulations. Figure 5.1 provides an illustration of the models boundary conditions and loads. Both the composite and caul sections were constrained such that no displacement along the x axis could occur at their left hand faces (tangential to the z-y plane). The bottom face (tangential to the x-z plane) of the composite section was constrained such that no displacement could occur along the y axis. All faces normal to the z axis were constrained such that no displacement could occur along the z axis. Furthermore, all the faces of the composite section were constrained to be impermeable.

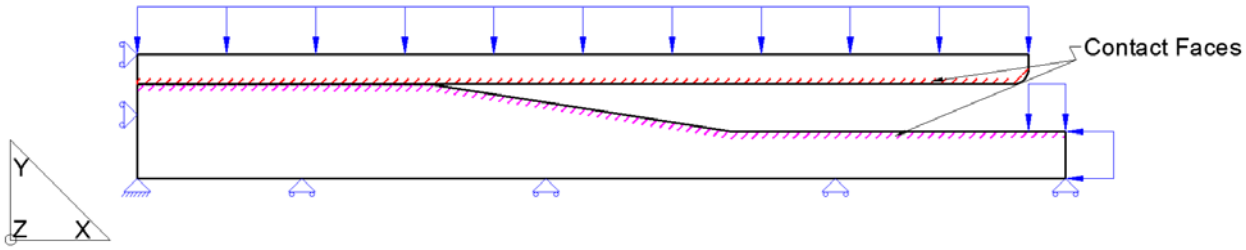

Figure 5.1 – Illustration of model boundary conditions, loads and contact face for simulation exercises.

For all simulations in this study, the interaction between the caul and composite section was specified by identifying the lower surface of the caul section and upper surface of the composite section as “hard” contact faces. The normal contact behavior was enforced with penalty method with a stiffness scale factor of 0.01. More information on the penalty method algorithm can be found in the Abaqus analysis user’s manual [69]. The tangential contact behavior was set to be frictionless. Furthermore, separation after contact was enabled.

For both exercises, a load of 101 kPa (atmospheric pressure) was applied to the top face of the composite section as well as the exposed faces at the right of the composite section. This load was applied gradually, increasing linearly from 0Pa to 1Pa within the initial 100 seconds followed by a linear increase to its final pressure state of 101kPa between 100 seconds and 500 seconds. In reality, the load application is not linear and the full load is imposed on the system within a much shorter period of time (approximately 10-20 seconds). However, attempting to simulate rapid load applications resulted in convergence issues.

For every time step, the fiber bed stiffness and permeability and the resin viscosity is updated in order to solve for resin pressure and displacement. These nodal variables are solved with the use of an implicit Euler method. Since the fiber bed permeability and fiber bed stiffness are both dependent on the nodal variables, the time integration solution is coupled with non-linear iterative techniques. More details on these techniques can be found in Hubert’s thesis [42] and Convergent Manufacturing Technologies product documentation [2]. For each time step, the resin viscosity is computed and the load vector is assembled. Through an iterative process the permeability matrix and fiber bed stiffness are updated and the model solves for resin pressure

and displacement. If convergence is achieved, the solution vector is updated and stored for the following time step.

5.2 Exercise I: Parametric Simulation Study

The purpose of this first exercise is to generate a clear understanding of the effects that the material properties bear on the resin pressure history and final shape of the part. The material properties evaluated in this exercise are of critical importance to flow and compaction. These are the fiber bed compaction behavior, fiber bed liquid permeability and resin viscosity. In evaluating the effects of these material properties, the data presented for the instrumented tool test (Chapter 4) can be better interpreted and the use of the Darcy flow-compaction formulation in the second exercise can be validated.

5.2.1 Method and Model Parameters

5.2.1.1 Model Dimensions and Mechanical Properties

The specific processing scenario considered in this parametric study was that of the 16 to 8 ply drop laminate processed with a 4mm caul sheet made of aluminum 6061-T6. The laminate dimensions of the 16 to 8 ply laminate as seen in the instrumented tool tests was adopted for this parametric study (see Table 5.1. and Figure 5.2). The width (i.e. extrusion along the z direction) of both the composite and caul sheet section was set to 3mm.

The fiber bed longitudinal modulus (E_1), transverse modulus (E_2), tensile and compressive through thickness moduli (E_{3t} and E_{3c} respectively) and shear moduli (G_{12}, G_{13} and G_{23}) are shown in Table 5.1. Note that the tough thickness compressive modulus is of critical importance

to this study while the longitudinal, transverse and shear moduli values have little to no effect on the simulation results. The layup assigned to the composite section is [0]s and the 1-direction is aligned with x-axis.

Convergence issues with regards to the normal contact behavior between the caul and composite section occurred when the elastic modulus of the caul sheet section was set to that of aluminum (~68.9GPa). To mend this issue, the elastic modulus of the caul section was set to 200 GPa and the thickness of the caul sheet section was specified such that its flexural rigidity (see equation 5-3) was equivalent to that of a 4mm aluminum 6061-T6 caul sheet. The dimensions, elastic modulus (E_c) and poisons ratio (v) for the caul sheet section are shown in Table 5.1.

$$Flexural\ Regidity_{\ caul} = E_c I = E * \frac{w h_c^3}{12} \tag{5-3}$$

Where E_c is the caul sheets elastic modulus of the, I is the second moment of inertia, w is the width and h_c is the thickness of the caul sheet.

The composite section was meshed with 20-node brick elements with quadratic displacement interpolation and linear pore pressure interpolation (C3D20P). The caul section was meshed with 8-node linear displacement brick elements with reduced integration (C3D8R). The imposed loads, boundary conditions and enforced contact behavior have been presented in Section 5.1. Table 5.1 provides a summary for the model dimensions, relevant mechanical properties and element types for the composite and caul sheet sections. Figure 5.2 provides an illustration of the

dimensions of the model sections. Note that the dimension labels shown in Figure 5.2 are in accordance to the dimensions provided in Table 5.1.

Table 5.1 – Summary of model dimensions, relevant mechanical properties and element type for parametric simulation study (exercise I)

	Caul Sheet	**Composite**
Relevant Mechanical Properties	E_c =200 GPa* v=0.3	<u>Fiber Bed Properties</u> E_1=121 GPa E_2=11 MPa E_{3t}=11 kPa E_{3c}=*As Specified by Compaction Curve (Shown in Figure 5.3)* G_{12}=3.65 Mpa G_{12}=G_{13}=G_{23}
Dimensions	h_c=0.0028m* l_c=0.1524m R=0.002m w=0.003m	l_t=0.15875m h_16=0.00347m l_16=0.0508m h_8=0.001862m l_8=0.05715m w=0.003m
Element (Type/Number)	C3D8R/1683	C3D20P/8944
* The caul sheet elastic modulus (E_c) and thickness (h_c) are specified such that the flexural rigidity is equivalent to that of a 4mm aluminum 6061-T6 caul sheet.		

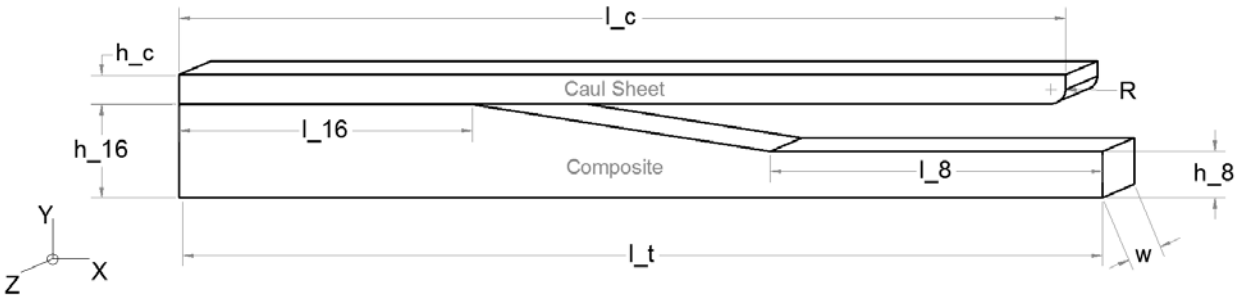

Figure 5.2 – Illustration of model dimensions for parametric simulation study (exercise I).

5.2.1.2 Input Parameters

The input parameters of interest for this parametric study are the fiber bed compaction behavior, the fiber bed liquid permeability, resin viscosity. The compaction behavior, referred from here on as the compaction curve, dictates the amount of stress which is carried by the fiber bed (i.e. the fiber bed effective stress) as a function of strain. The various compaction curves used for these simulations were computed with the use of an analytical expression proposed by Gutowski et al. [70]. This expression modeled the compaction curve by assuming the fiber bed to be a network of curved beams that obey beam bending behavior. The equation is as follows

$$\bar{\sigma_f}(V_f) = \frac{3\pi E_f}{\beta^4} * \frac{\left(1 - \sqrt{\frac{V_f}{V_{f0}}}\right)}{\left(\sqrt{\frac{V_a}{V_f} - 1}\right)^4} \tag{5-4}$$

Where $\bar{\sigma}_f$ is the fiber effective stress carried by the fiber bed, V_f is the fiber volume fraction, E_f is the elastic modulus of the fiber, β is the fiber waviness ratio (i.e. fiber span length/span height), V_{f0} is the initial fiber volume fraction and V_a is the maximum fiber volume fraction.

With the use of equation (5-4), five compaction curves were computed simply by varying the waviness factor (β) and keeping all other constants the same. The waviness factor (β) values used can be found in Table 5.2. All other constants were as follows: $E_f = 237GPa$, $V_{f0} = .5456$ and $V_a = .76$. This effectively produces compaction curves of similar shape but whose values of effective stress are different for a given value of strain. The relationship of effective stress with

respect to strain for the five computed compaction curves are presented in Figure 5.3. Note that the fiber volume fraction was converted to strain using the following relationship:

$$V_f = \frac{FAW}{\rho_{fiber} * CPT * (1 + \varepsilon)} \tag{5-5}$$

Where V_f is the fiber volume fraction, FAW is the fiber bed areal weight, ρ_{fiber} is the density of the fiber, CPT is the cured ply thickness and ε is the strain.

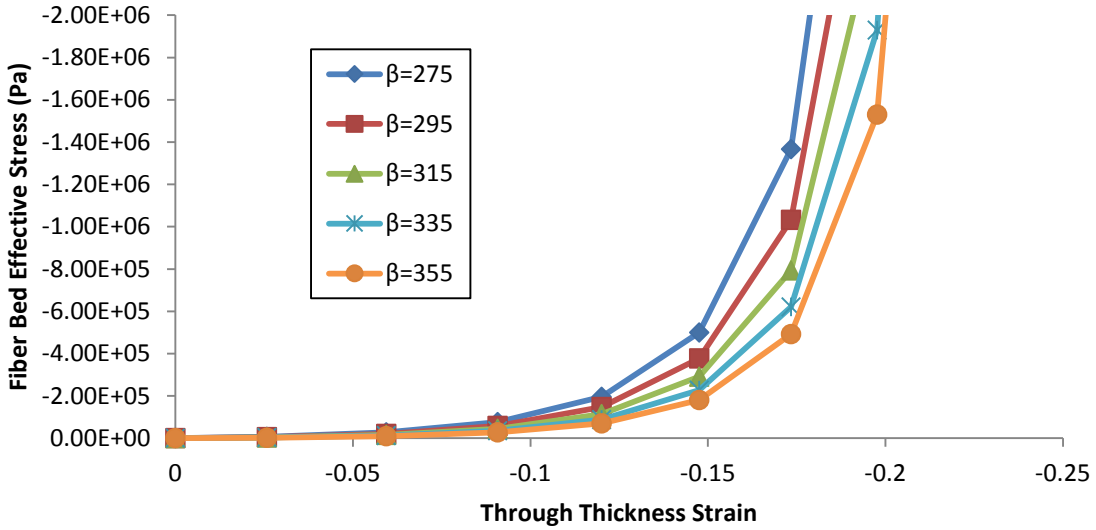

Figure 5.3 – Fiber bed effective stress with respect to through thickness strain for five compaction curves computed from Gutowski et al. [70] **model with various waviness factors (β)**

For the simulations presented in this parametric study, the viscosity and permeability models were overridden such that they remained constant throughout the simulations. This was done in order to produce an evaluation of the effect of viscosity which is constant and unchanged by the cure kinetics model and an evaluation of permeability which is decoupled from the fiber bed compaction behavior. The values of viscosity and permeability used in this study are presented in

Table 5.2. Note that the longitudinal permeability was four times greater than transverse permeability for all simulations. This ratio was maintained simply by multiplying by the baseline longitudinal and transverse permeability by the same adjustment factor (F). The values of the adjustment factor are presented in Table 5.2. Sufficient time periods were allotted for the simulations such that resin pressure equilibrium was achieved in all simulations with exception to the C.4 and P.4 simulation. These time periods are also presented in Table 5.2.

Table 5.2 - Summary of input parameters for all simulations in the simulated parametric study (exercise I).

Simulation ID	Waviness Ratio (β)	Permeability Adjustment Factor (F)	Longitudinal Permeability (K_l)	Transverse Permeability (K_t)	Viscosity (μ)	Time Period
0	315	1	F*8.32e-11 m²	F*2.08e-11 m²	10 Pa s	11800 sec
C.1	275	1	8.32e-11 m²	2.08e-11 m²	10 Pa s	11800 sec
C.2	295					
C.3	335					
C.4	355					
V.1	315	1	8.32e-11 m²	2.08e-11 m²	20 Pa s	25000 sec
V.2					50 Pa s	
V.3					100 Pa s	
V.4					500 Pa s	
P.1	315	0.5	4.16e-11 m²	1.04e-11 m²	10 Pa s	25000 sec
P.2		0.2	1.664e-11 m²	4.16e-12 m²		
P.3		0.1	8.32e-12 m²	2.08e-12 m²		
P.4		0.02	4.16e-12 m²	4.16e-13 m²		

5.2.1.3 Output Parameters

In general, the output parameters of interest for this parametric study are the resin pressure history and final thickness profile of the composite section. For each simulation, the resin pressure was tracked at seven different nodes along the base of the composite. The location of the nodes were equivalent to the locations of the sensors seen in the instrumented tool tests (see Chapter 4). For convenience, these nodes have been numbered similarly to the sensors. Figure 5.4 below provides an illustration of the node locations.

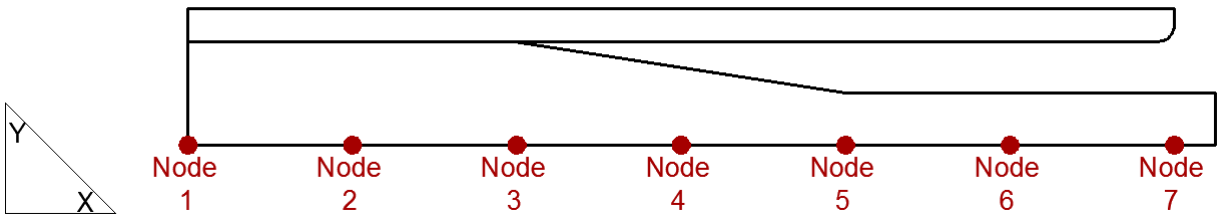

Figure 5.4 – Illustration of tracked nodes for simulated parametric study.

With respect to resin pressure history, the specific output parameters are the final resin pressure achieved at equilibrium, the time required to achieve equilibrium and the time required to achieve minimum resin pressure (i.e. resin pressure at most shielded node). The final resin pressure was reported by calculating the average pressure amongst all 7 nodes at the final time step. The time to achieve equilibrium and time to achieve minimum resin pressure was evaluated simply by plotting the resin pressure history for the nodes located at the primary overfill region and at the most shielded region (i.e. the node which lags an increase in pressure the most). From the results presented in the experimental trials (Chapter 4), it is already known that for this specific processing scenario the primary overfill region and most shielded region are located at

node 3 and 5 respectively. Finally, the final thickness of the part was evaluated by reporting the final coordinates of all nodes on the upper surface of the composite section.

Table 5.3 below provides a summary of the output parameters of interest for this study.

Table 5.3 – Summary of specific output parameters of interest for parametric simulation study (exercise I).

Output Category	Specific Output Parameter of Interest
Pressure History	Final resin pressure achieved at equilibrium (Average pressure between Node 1 to Node 7 at final time step)
	Time to achieve equilibrium (Evaluated by tracking the pressure history of nodes 3 and 5)
	Time to achieve minimum resin pressure (Evaluated by tracking the pressure history of nodes 5)
Part Shape	Final thickness profile (final coordinates of all nodes on upper surface of composite section)

5.2.2 Results

The complete resin pressure history (i.e. pressure history for all nodes) for all simulations can be found in Appendix A. Here, only the critical results will be presented in order to clearly illustrate the effects that the input parameters of interest have on the resin pressure history and final thickness of the composite section.

5.2.2.1 Effect of Different Compaction Curves on Resin Pressure

Figure 5.5 presents the average resin pressure amongst all nodes at the final step for simulations of different compaction curves (i.e. different waviness factors β).

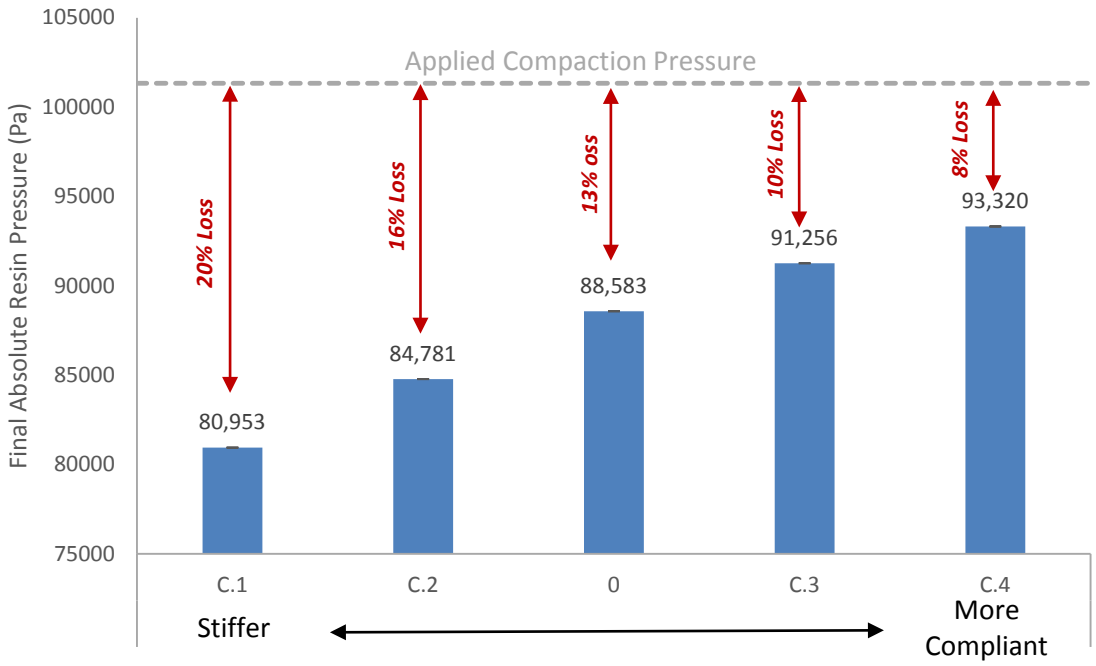

Figure 5.5 – Average resin pressure (averaged between nodes 1 to 7) at the final time step for simulations of different compaction curves (i.e. different waviness factor β). The data is arranged from stiffest compaction curve (left) to most compliant compaction curve (right). Figure shows that resin pressure decreases as fiber bed stiffness increases.

As can be seen from the figure above, as the compaction curve becomes stiffer, more of the applied compaction pressure is absorbed by the fiber bed. This thereby reduces the equilibrium pressure which all nodes converge to. From the figure above, it can be observed that the most compliant compaction curve (C.4) only losses 7% of the resin pressure to the fiber bed, whereas the stiffest compaction curve (C.1) results in 20% loss in resin pressure. As such, stiffer compaction curves present a greater risk of void stabilization due to the losses in resin pressure.

Figure 5.6 shows the pressure history of Nodes 3 and 5 for simulations of different compaction curves. Here it can be seen that more compliant compaction curves require more time to achieve equilibrium. However, Figure 5.6 also shows that more compliant compaction curves achieve higher resin pressures at the most shielded region (node 5) in less time than the stiffer compaction curves. Therefore, as far as porosity is concerned, more compliant compaction curves present less risk of void growth regardless of the time required to achieve equilibrium.

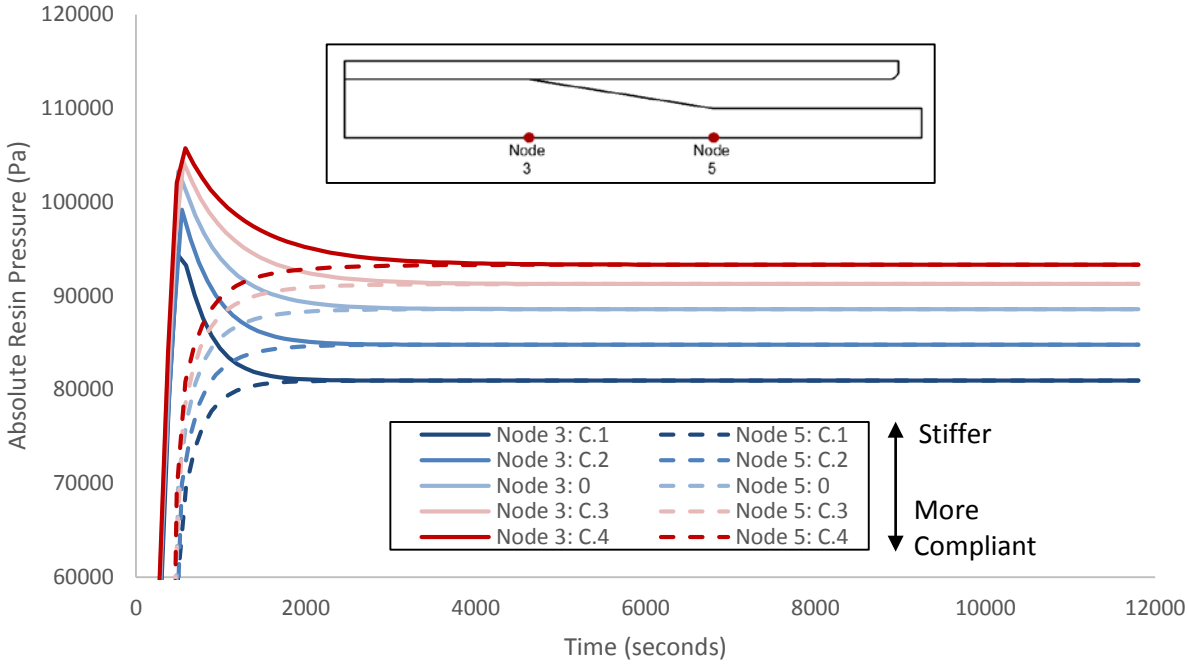

Figure 5.6 - Pressure history of node 3 (solid line) and node 5 (dashed line) for simulations of different compaction curves (i.e. different waviness factor β). The data is arranged from stiffest compaction curve (blue) to most compliant compaction curve (red).

5.2.2.2 Effect of Different Compaction Curves on Final Thickness Profile

Figure 5.7 show the final thickness profiles for simulations of different compaction curves. Note that only the region of composite section which lies beneath the caul sheet has been plotted in this figure. In addition, the initial thickness profile (gray dashed line) has also been plotted. Since the variations in final thickness profile were fairly small, additional sub-figures illustrating the same data are also provided in Figure 5.7. The sub-figure on the bottom left corner shows the final thickness profile at the 16-ply region (0 m to 0.05m from the center). The sub-figure on the upper right corner shows the final thickness profile at the 8 ply region (0.01 m to 0.15m from the center)

It can be observed from the figure below that more compliant compaction curves amplifies the thinning at regions which are initially thick and thickening at regions which are initially thin. At the regions which undergo thinning (thick regions), the compaction pressure is being shared by both the fiber bed and the resin. Conversely, at regions which undergo thickening (thin regions), the compaction pressure is being shared predominantly by the resin only. It has already been established that stiffer compaction curves will reduce the hydrostatic resin pressure as more of the applied compaction pressure will be borne by the fiber bed. As such, less resin will flow out of the thick region thereby reducing thinning. Consequently, as less resin flows out of the thick region, less resin will flow into the thin region therefore reducing thickening at the thin regions.

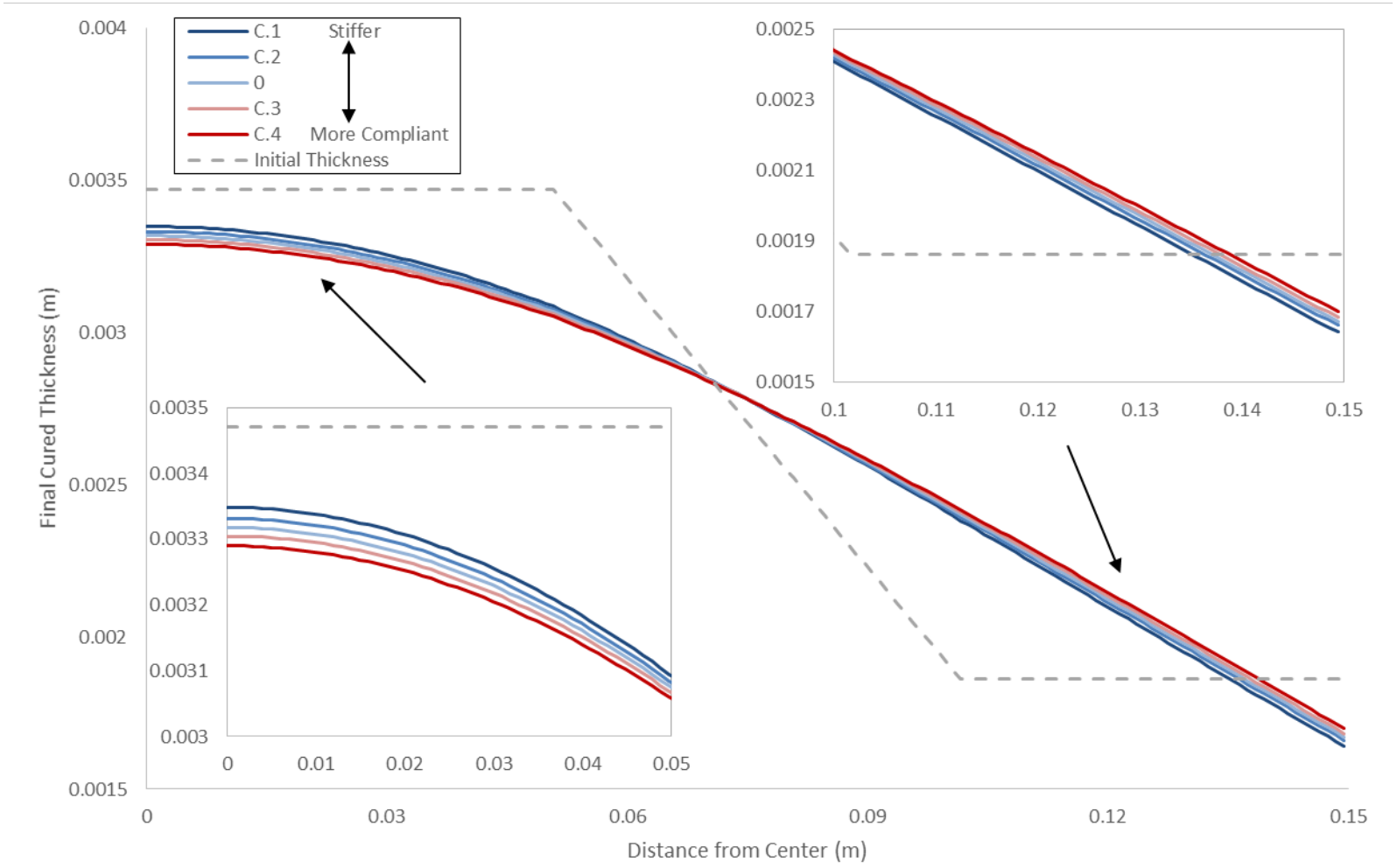

Figure 5.7 - Final thickness profile for simulations of different compaction curves (i.e. different waviness factor β). Figure only shows the thickness profile for the region of the composite section which lies beneath the caul sheet. Sub-figure for final thickness profile at 16 ply region (bottom left corner) and 8 ply region (upper right corner) also included. The data is arranged from stiffest compaction curve (blue) to most compliant compaction curve (red).

5.2.2.3 Effect of Different Viscosity and Permeability on Resin Pressure

Figure 5.8 and Figure 5.9 shows the pressure history of Nodes 3 and 5 for simulations of different viscosity and permeability respectively. The data presented in both figures below show that neither a change in viscosity nor a change in permeability have significant effect on the final resin pressure equilibrium. Although it can be seen that the V.4 and P.4 simulation did not achieve equilibrium at 25000 seconds, it can be reasonably assumed that both of these simulations would converge to the same equilibrium pressure as all of the other pressure histories, provided sufficient time were to be allotted for the simulation. Figure 5.8 and Figure 5.9 show that increasing viscosity and decreasing permeability both work to increase the amount of time required for changes in resin pressure to occur and for equilibrium to be reached. Furthermore, it can be observed that increasing the viscosity and decreasing the permeability by similar factors have an identical effects on the resin pressure history. This is due to the fact that the model used to generate these simulations utilizes Darcy's Law to compute resin flow (equation 5-1). For this reason, increasing viscosity or decreasing permeability will only work to slow down resin flow. Moreover, it can also be observed in Figure 5.8 and Figure 5.9 that decreasing the flow of resin results in higher peak pressures at the overfill region (node 3). However, this is simply due to the fact that less resin was able to flow out of this region during the application of compaction pressure. As such, less of the pressure has been absorbed by the fiber bed once the full compaction pressure is being applied to the system. Finally, it should be noted that in reality viscosity and permeability are dependent on entirely different sets of state variables. As such, the practical implications of this observation is different in the cases of both material properties. This will be discussed in greater detail in the discussion section.

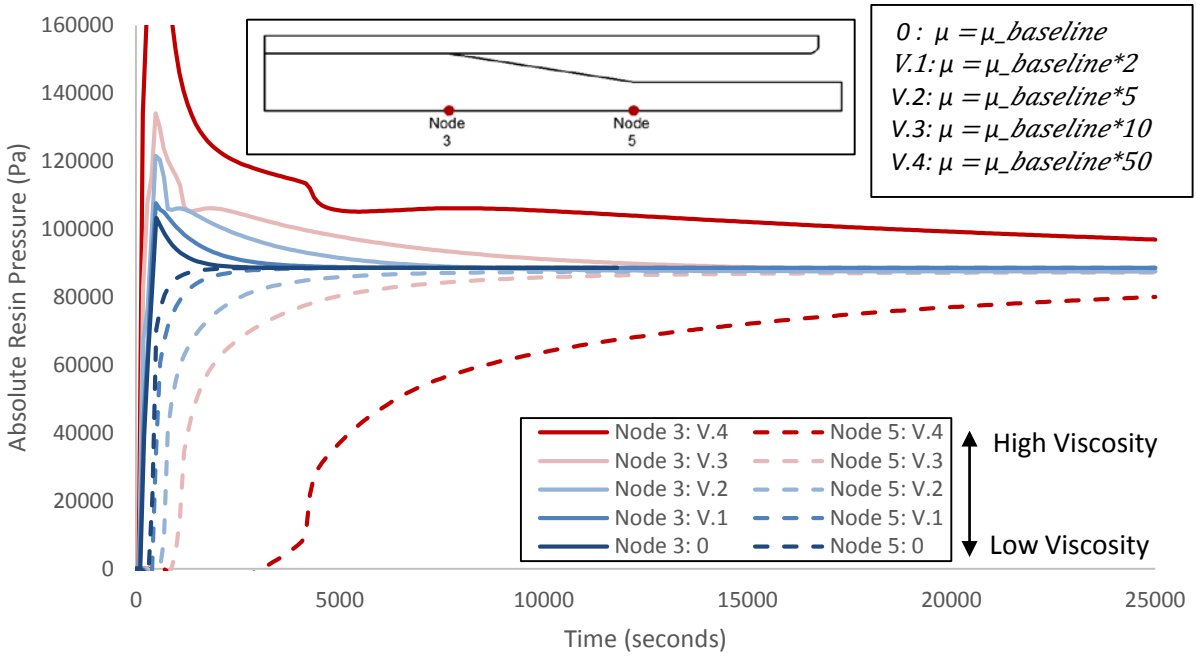

Figure 5.8 - Pressure history of node 3 (solid line) and node 5 (dashed line) for simulations of different viscosity. The data is arranged from lowest viscosity (blue) to highest viscosity (red).

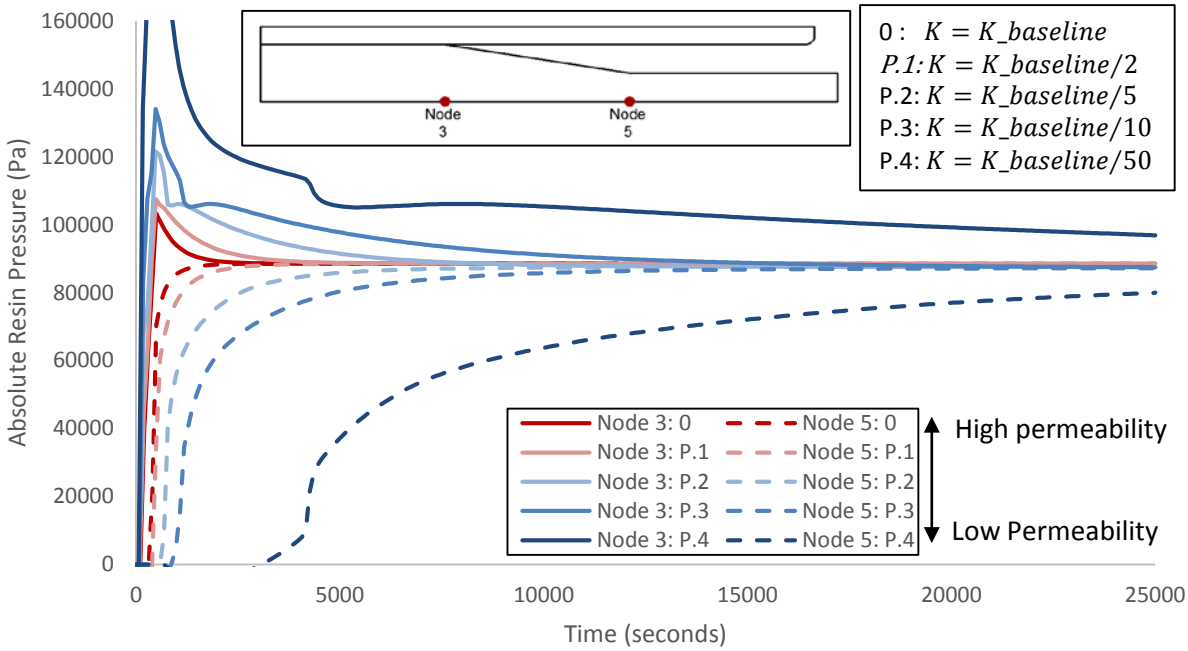

Figure 5.9 - Pressure history of node 3 (solid line) and node 5 (dashed line) for simulations of different permeability. The data is arranged from lowest permeability (blue) to highest permeability (red).

5.2.2.4 Effect of Variable Viscosity and Permeability on Final Thickness Profile

With the exception of the V.4 and P.4 simulation, it was observed that neither a change in viscosity nor a change in permeability have a significant effect on the final thickness profile of the composite section. Similar to the observations made with regards to the final equilibrium pressure, since viscosity and permeability only influence the resin flow velocity, the final thickness profile will be identical to that of the baseline simulation (simulation 0) as seen in Figure 5.7. This statement will hold true as long as the value of viscosity or permeability does not prevent the system from reaching resin pressure equilibrium within the simulation time. For the case when a resin pressure equilibrium is not reached (such is the case for the V.4 and P.4 simulations), the result is that less resin will have flown out of the overfill region (16 ply region) and into the shielded region (8 ply region). Consequently, less thinning will be incurred at the 16 ply region and less thickening will be incurred at the 8 ply region. Such a scenario is not limited to the context of this parametric study and can occur in an actual processing scenario. This will be discussed in greater detail in the discussion section.

5.3 Exercise II: Simulation of Instrumented Tool Test

The purpose of this second exercise is to determine how well a Darcy flow-compaction formulation mimics the experimental results seen in Chapter 4. In this exercise, the model will be used in an attempt to simulate the experimental pressure histories and final shape of the ply drop laminates with 4mm and 8mm caul sheets as seen in Chapter 4. From the figure below, it can be observed that the full experimental regime comprises of a debulk regime and a flow dominated regime (i.e. cure). As discussed in Chapter 4, due to the low temperatures during the debulk regime, it is much more likely that the pressure variations seen during this period of time is

caused by a stress-deformation mechanism rather than flow and compaction. Therefore a Darcy flow-compaction formulation alone cannot simulate the pressure histories during the debulk. Moreover, it should be noted that models which are formulated to simulate the debulk mechanisms were not commercially available during the time of this study. Nevertheless, in order to capture both the capabilities and limitations of the Darcy flow-compaction formulation, an attempt will be made to simulate both the full experimental regime (debulk and cure) as well as the flow dominated regime (cure only).

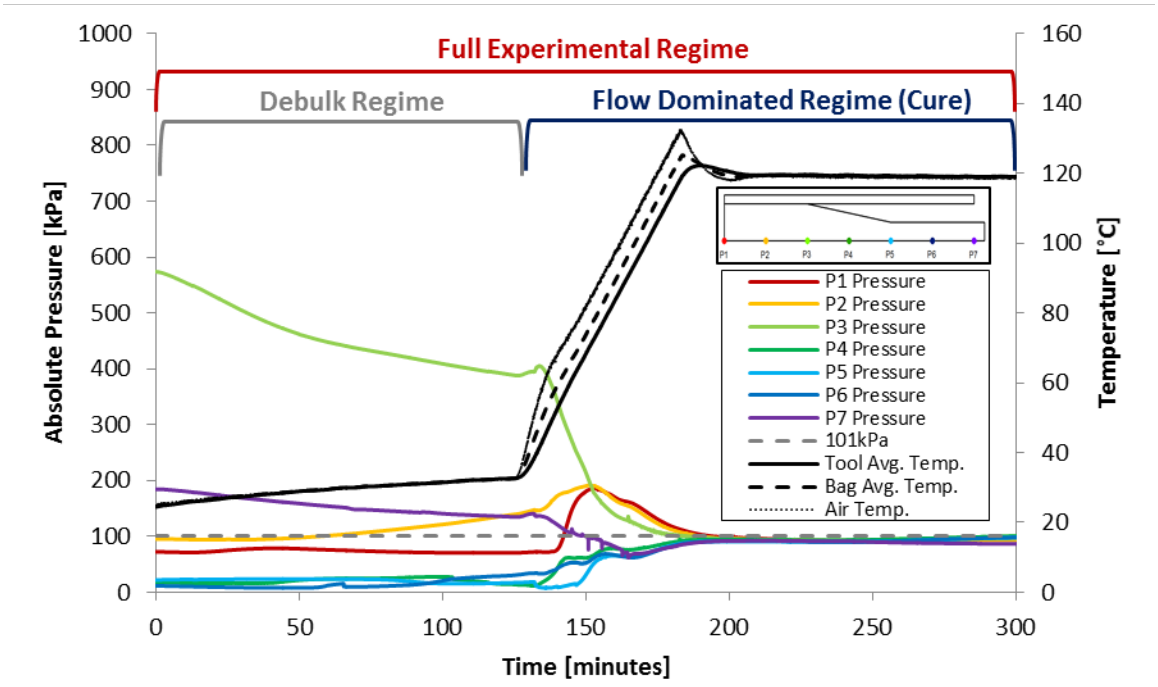

Figure 5.10 – Experimental pressure history results for the 4mm ply-drop/caul-sheet laminate annotated to illustrate the full experimental regime, debulk regime and the flow dominated regime.

5.3.1 Method and Model Parameters

5.3.1.1 Model Dimensions and Mechanical Properties

The geometry for the composite section for all simulations in this exercise was specified to match the geometries of the ply drop laminates studied in Chapter 4. Note that the ply drop configuration was identical for all experimental trials. Consequently, the dimensions and fiber bed mechanical properties of the composite section for this exercise are the same as those specified in the previous exercise (see Section 5.2.1.1).

Due to the convergence issues with regards to the contact interface (as discussed in Section 5.2.1.1), the elastic modulus of the caul section was set to 200 GPa and the thickness of the caul sheet section was specified such that its flexural rigidity (see equation 5-3) was equivalent to that of a 4mm and 8mm aluminum 6061-T6 caul sheet. The dimensions, elastic modulus (E_c) and poisons ratio (ν) for the caul sheet section are shown in Table 5.4.

In both cases, the composite section was meshed with 20-node brick elements with quadratic displacement interpolation and linear pore pressure interpolation (C3D20P) and the caul section was meshed with 20-node brick elements with quadratic displacement interpolation (C3D20). The imposed loads, boundary conditions and enforced contact behavior have been presented in Section 5.1. Table 5.4 provides a summary for the model dimensions, relevant mechanical properties and element types for the composite and caul sheet sections. Figure 5.11 illustrates the in-plane dimensions of the model sections. Note that the dimension labels shown in Figure 5.11 are in accordance to the dimensions provided in Table 5.4.

Table 5.4 - Summary of model dimensions, relevant mechanical properties and element type for simulation of instrumented tool test study (exercise II).

	[4mm] Caul Sheet	[8mm] Caul Sheet	Composite
Relevant Mechanical Properties	E_c =200 GPa* v=0.3	E_c =200 GPa* v=0.3	<u>Fiber Bed Properties</u> E_1=121 GPa E_2=11 MPa E_{3t}=11 kPa E_{3c}=*As Specified by Compaction Curve (Shown in Figure 5.16)* G_{12}=3.65 MPa $G_{12}=G_{13}=G_{23}$
Dimensions	h_c=0.0028m* l_c=0.1524m R=0.002m w=0.003m	h_c=0.0056m* l_c=0.1524m R=0.002m w=0.003m	l_t=0.15875m h_16=0.00347m l_16=0.0508m h_8=0.001862m l_8=0.05715m w=0.003m
Element (Type/Number)	C3D20/1683	C3D20/2814	C3D20P/1431
* The caul sheet elastic modulus (E_c) and thickness (h_c) are specified such that the flexural rigidity is equivalent to that of a 4mm or 8mm aluminum 6061-T6 caul sheet.			

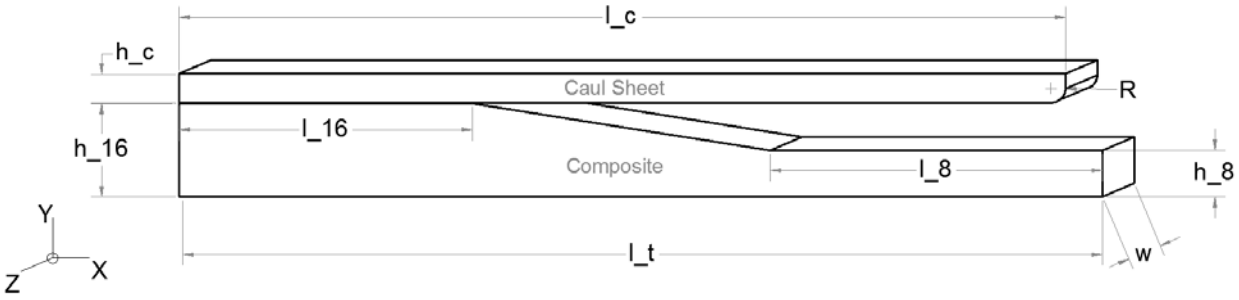

Figure 5.11 - Illustration of model dimensions for simulation of instrumented tool test study (exercise II).

5.3.1.2 Composite Material Property Inputs

The cure kinetics and the resin viscosity of the MTM45-1 resin system has been previously characterized [1]. As such, the simulation solves for increasing degree of cure as a function of time and temperature and updates the local viscosity values accordingly.

The compaction behavior of the HTS40 E13 3K plain weave fabric has not been previously characterized. As such, tests were performed to measure the compaction curve for this specific material. The compaction curve was measured directly from the MTM45-1/CF0526A prepreg as per the method outlined by Hubert et al. [71]. The tests were conducted by Mr. Alastair McKee at Convergent Manufacturing Technologies and the raw data was supplied for analysis by the author. The method and results shall be discussed later in this chapter (sections 5.3.1.5 and 5.3.2.1 respectively).

The liquid permeability of the HTS40 E13 3K fabric has not been characterized. Furthermore, the version of COMPRO that is being used for this study only incorporates permeability models which are primarily applicable to tapes. Out of all the permeability models incorporated in COMPRO V2, the Kozeny-Carmen permeability model [70] (shown in equation 5-6) is the most generic.

$$K_l = \frac{r_f^2}{4k_x}\frac{\left(1-V_f\right)^3}{V_f^2}$$
$$K_t = \frac{r_f^2}{4k_z}\frac{\left(1-V_f\right)^3}{V_f^2} \quad (5\text{-}6)$$

Where K_l and K_t are the longitudinal and transverse permeability, k_x and k_z are the longitudinal and transverse Kozeny constants respectively, r_f is the fiber radius and V_f is the fiber volume fraction.

Since permeability only dictates the resin flow velocity (as concluded in the first exercise) the Kozeny-Carman permeability model was used to scale the simulated pressure histories to the experimental results with reasonable accuracy. This was achieved simply varying the Kozeny constants such that the simulated pressure histories fit the pressure histories measured experimentally. For this study, the values of the longitudinal and transverse Kozeny constants which best fit the experimental results where .005 and .02 respectively. Figure 5.12 shows the resulting longitudinal and transverse permeability with respect to fiber volume fraction when the above Kozeny constants are used.

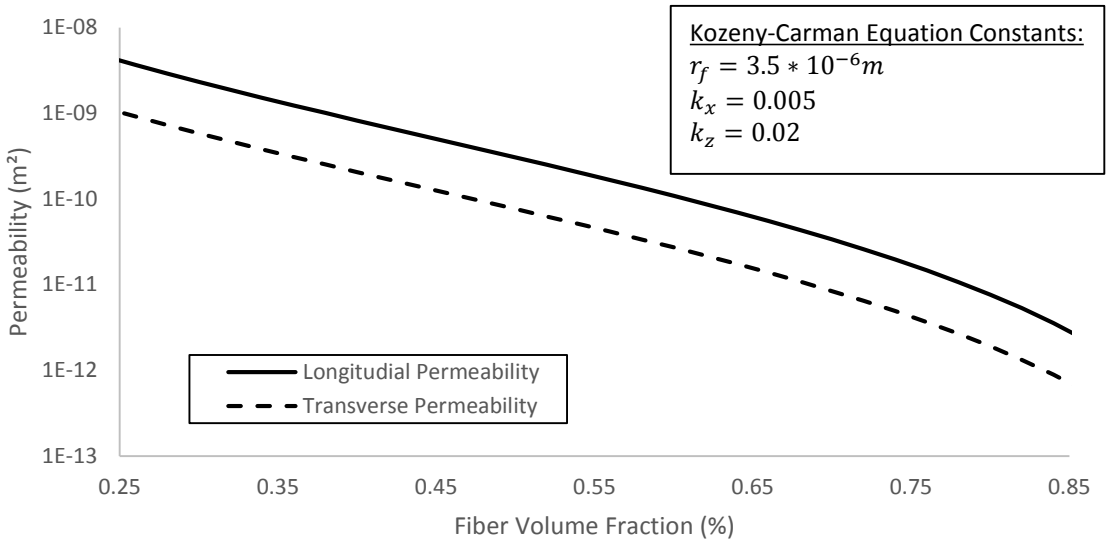

Figure 5.12 – Longitudinal and transverse permeability vs. fiber volume fraction as modeled by the Kozeny-Carman permeability model.

5.3.1.3 Temperature Histories

Two temperature histories were used to perform the simulations for the full experimental regime and flow dominated regime (see Figure 5.10). Figure 5.13 shows the imposed temperature history and boundary pressure history for the full experimental regime simulations (left) and flow dominated regime simulations (right). The histories are plotted with respect to the simulation time and the time relative to the experimental results.

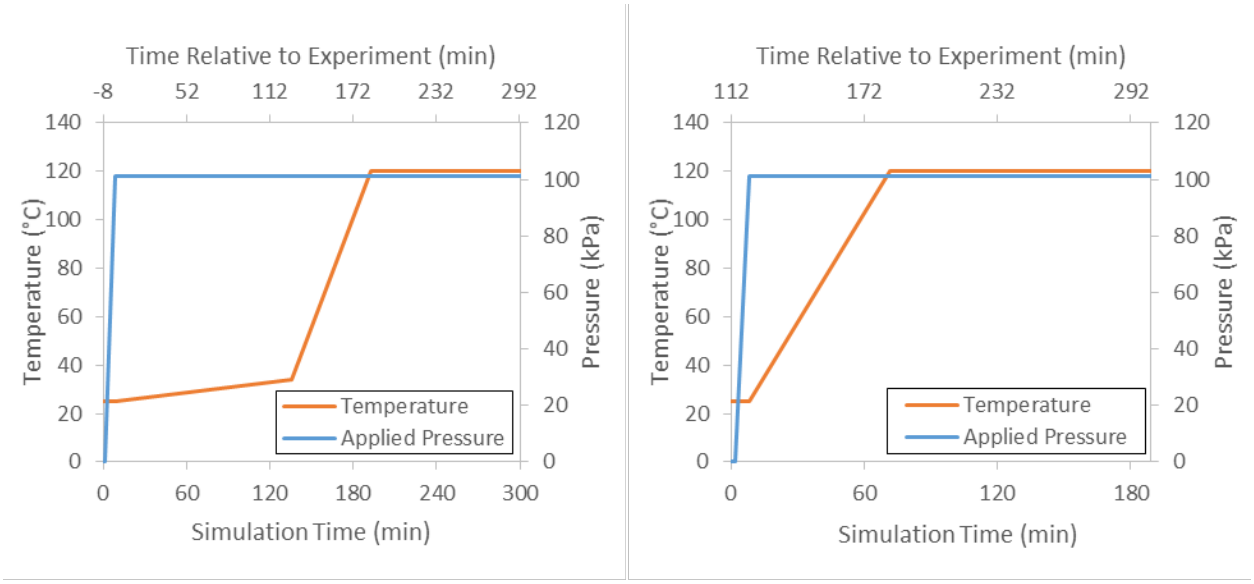

Figure 5.13 – Prescribed temperature history and boundary pressure history for full experimental regime simulations (Left) and flow dominated regime simulations (right). Histories are plotted with respect to simulation time (bottom axis) and the time relative to experimental results (top axis).

All of the simulated pressure histories presented in this second exercise will be plotted with respect to the time relative to the experimental trials (seen in Chapter 4). This has been done in order to ease comparisons between the simulated and experimental results.

5.3.1.4 Output Parameters

For this study, the output parameters of interest are the pressure history and final thickness profile of the composite section.

In this exercise, only the pressures at the locations where a sensor was positioned in the experimental trials was considered. For each sensor location, the pressure history of all nodes within the width of the senor location was averaged and reported. As such, similar to the experimental results, seven individual pressure histories where reported. In order to evaluate the performance of the model, both simulated and experimental pressure histories were plotted on the same figure for each simulation.

Similar to the parametric simulation study, the final thickness of the composite section was outputted by reporting the coordinates of all nodes on the upper surface of the composite section at the final time step. The final thickness profile of the composite section at the final time step was compared to the experimental results.

5.3.1.5 Compaction Tests

Here an overview of the compaction test method and analysis is provided. Prepreg specimens are prepared and inserted into a mould and piston assembly as seen in Figure 5.14. The layup, weight and dimensions of the prepreg samples can be found in appendix B.1. The mold is heated such that the resin is free to flow. The specimen is constrained by the mould and piston assembly such that the fiber bed can only deform along the z-axis and resin is free to flow along the x-axis.

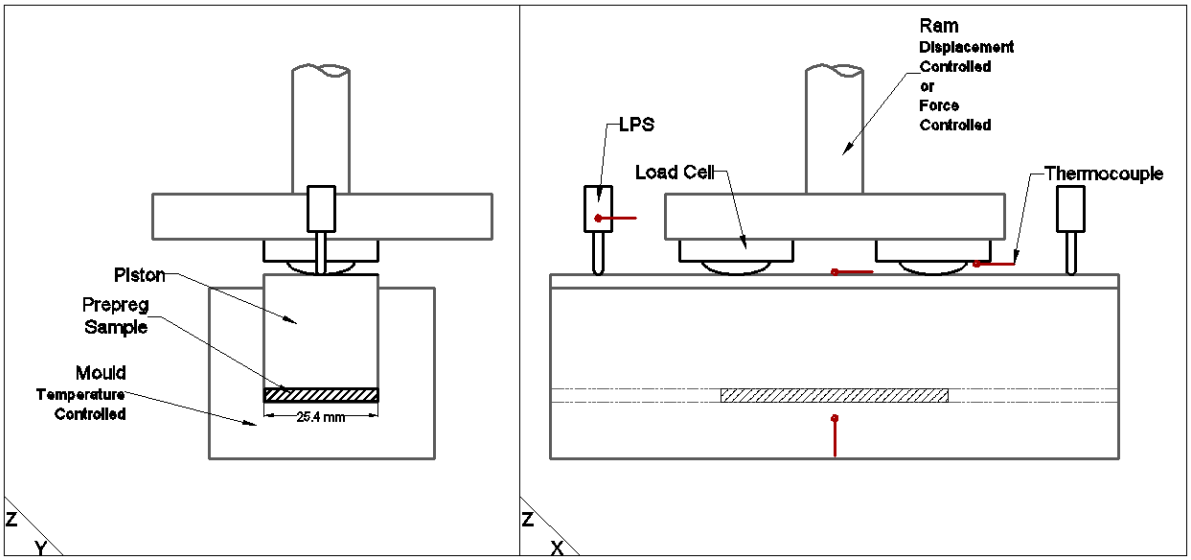

Figure 5.14 –Illustration of experimental set up for compaction test setup [1].

The position of the piston along the z-axis is controlled via a stepper motor. This mode of operation is referred to as the displacement control test. Both the displacement and the reaction force is monitored throughout the entirety of the tests via the use of linear position sensors (LPS) and load cells. In this study, the operating range of the load cells is up to 8900 N and the error is 5% of the full range (445N). The operating range of the LPS used is up to 12.7mm (1/2 inch) and the error is 1% of the full range (.127mm). The piston is displaced downwards along the z-axis by increasing increments of displacement. For each increment, the piston compresses the prepreg

sample and the imposed strain results in a reaction force which is tracked by the load cell. Initially, the reaction force is representative of the resin pressure and fiber bed effective stress (i.e. $\sigma = \bar{\sigma}_f + P_r$). While maintaining the piston position, resin is free to flow out of the fiber bed thereby leading to a decay in the measured reaction force. Once the reaction force has decayed to a stable value, referred to as the relaxed load, resin flow has stopped and the resin is unpressurized (i.e. $P_r = 0$). As such, the reaction force measured upon full relaxation should be representative of the fiber bed effective stress (i.e. $\sigma = \bar{\sigma}_f$). By repeating this process for increasing levels of displacement, the compaction curve of the fiber bed can be extracted. The load and displacement history produced by displacement controlled test is illustrated in Figure 5.15 A. For this study, three independent displacement control tests were performed.

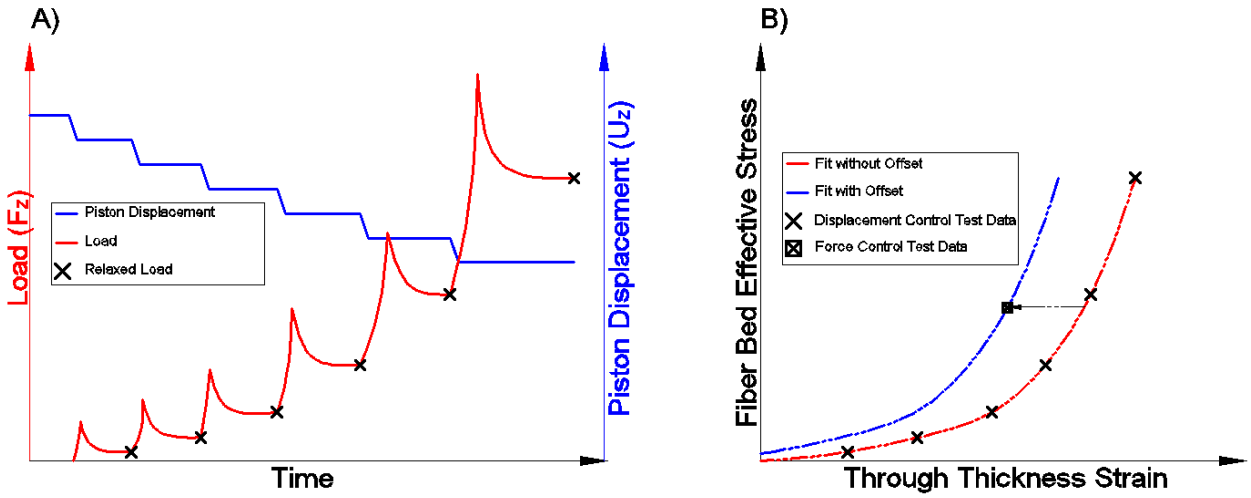

Figure 5.15 – Illustration load and displacement history for load control test (A) and compiled stress-strain compaction curve formulation (B).

The load and displacement data from the load control tests are converted to stress and strain through equations 5-7 and 5-8 respectively. Following this conversion the relaxed load points from the displacement control test are plotted on stress-strain curve (as seen in Figure 5.15 B).

$$\varepsilon_z = U_z / h_{0\ sample} \tag{5-7}$$

Where ε_z is the through thickness strain, U_z is the piston displacement along the z-axis and $h_{0\ sample}$ is the initial thickness of the prepreg sample.

$$\bar{\sigma_f} = F_z / Area_{sample} \tag{5-8}$$

Where $\bar{\sigma_f}$ is the fiber bed is effective stress, F_z is the measured load on the sample and $Area_{sample}$ is the effective area of the prepreg sample.

Once the stress-strain curve is fully populated, an exponential equation (see equation 5-9) is fitted to the stress-strain curve data. For this study, this was done using a generalized reduced gradient nonlinear solving algorithm (GRG non-linear solver) in Microsoft Excel.

$$\bar{\sigma_f} = A\epsilon_{abs}^{B} \tag{5-9}$$

Where $\bar{\sigma_f}$ is the fiber bed effective stress, ϵ_{abs} is absolute value of strain and A and B are constants used for fitting.

The final step involves shifting the stress-strain curve obtained from the displacement control tests along the strain axis (as shown in Figure 5.15 B). Essentially, the curve is forced to pass through a stress-strain point by applying an offset constant to equation 5-9. This point is obtained from an independent compaction test where the applied force of the piston is controlled rather than displacement. This mode of operation is referred to as a load control test. This shift in the strain axis is necessary because it is difficult to determine the onset of specimen loading when conducting the displacement control tests. The final stress-strain equation which defines the compaction behavior of the material is show below (equation 5-10).

$$\bar{\sigma_f} = A\epsilon_{abs}^{B} + Off \tag{5-10}$$

Where $\bar{\sigma_f}$ is the fiber bed effective stress, ϵ_{abs} is absolute value of strain, A and B are constants used for fitting and Off is the offset value calculated with the load control test data.

5.3.2 Results

5.3.2.1 Compaction Test Results

This section will only discuss the final results of the compaction tests. The individual load and displacement results from the displacement controlled tests and load controlled test can be reviewed in appendix B.2 and B.3 respectively.

Figure 5.16 shows the stress-strain data points for the HTS40 E13 3K PW fiber bed resulting from the displacement controlled tests (CTS.Disp) and load control test (CTS.Load).

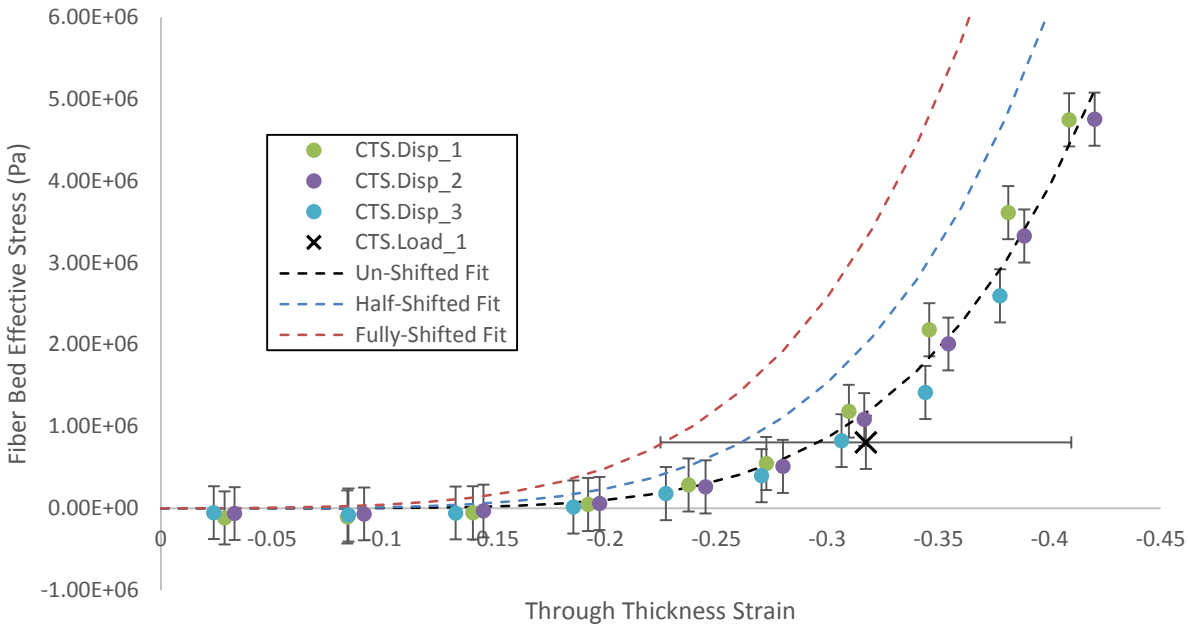

Figure 5.16 – Stress-strain data points from displacement control tests (CTS.Disp) and force control test (CTS.Load). Three exponential fits with different strain offsets are also plotted (dashed lines).

As can be seen from the figure above, there exists a great deal of uncertainty with regard to the strain value of the load controlled test (as indicated by the horizontal error bars). The cause for this ambiguity is due to the data acquisition frequency and is explained in detail in appendix B.4. Due to this uncertainty, it is not possible to determine the offset value of the exponential fit with the load control test data alone. For this reason simulations were implemented to determine the best approximation. Three compaction curves with three different strain offset values were trialed and can be seen in Figure 5.16. These are the fully-shifted fit, the half-shifted fit and the un-shifted fit. The values of constants A, B and Off (as specified in equation 5-10) for these curves are summarized in Table 5.5. Note that an offset value which would shift the curve in the negative strain direction of the un-shifted fit was not considered here. This is because such a fit

would presume that the fiber bed was preloaded prior to the initiation of the displacement controlled tests.

Table 5.5 – Summary of constant values for exponential fit equations of compaction curves.

	Constants		
	A	***B***	***Off***
Un-Shifted Fit	4.915E+08	5.268E+00	0.000E+00
Half-Shifted Fit	4.915E+08	5.268E+00	3.461E-02
Fully-Shifted Fit	4.915E+08	5.268E+00	6.921E-02
Fit Equation: $\bar{\sigma_f} = A\epsilon_{abs}^{B} + Off$			

Simulations were run to predict the final equilibrium resin pressure for each fit in the cases of the ply drop laminate with 4 mm and 8 mm caul sheet. The results of all simulations were compared to the experimental results (as seen in Chapter 4) to assess which fit best approximated the compaction curve of the material. Since the transient pressure history is not of interest in this evaluation, the viscosity, longitudinal permeability and transverse permeability where set to a constant value 10 Pa s, 8.32e-11 m² and 2.08e-11m² respectively. The time period for all simulations was such that equilibrium was achieved prior to the final time step (25000 seconds). The results for the final equilibrium resin pressure for all simulations and experimental results are shown in the table below.

Table 5.6 – Simulated final equilibrium resin pressure for compaction curve exponential fits with varying strain offset values.

	Final Equil. Resin Pressure (Pa) Caul Sheet Thickness		**Error (Pa/%)** Caul Sheet Thickness	
	4mm	8mm	4mm	8mm
Experimental	***93350***	***81646***	N/A	N/A
Un-Shifted Fit	98530	80043	5181/5.55%	-1603/-1.96%
Half-Shifted Fit	96457	66831	3107/3.33%	-14815/-18.15%
Fully-Shifted Fit	92247	50682	-1103/-1.18%	-30964/-37.93%

As shown in Table 5.6, the final equilibrium resin pressure for simulations of the 4mm caul sheet are fairly close to the equilibrium pressures seen in the experimental trial. Better results are found when the fully-shifted fit is applied to the compaction curve. However, for the case of the ply drop laminate with an 8mm caul sheet, significant discrepancies are found between the experimental results and simulations when the half-shifted fit and fully-shifted fit are applied to the compaction curve. This seems to suggest that a simple shift may not be sufficient to approximate the compaction curve of the material. Rather, the shape of the curve may need to be manipulated as well. However, since the un-shifted fit was able to predict the final equilibrium resin pressure with reasonable accuracy in both cases, this fit will be used to define the compaction curve of the material. As such, unless otherwise specified, the results presented in the following sections have been simulated by using the un-shifted fit as an approximation for the compaction curve of the material.

5.3.2.2 Pressure History Simulation for Full Experimental Regime

In this section the full experimental regime simulated pressure histories will be evaluated and compared to the experimental results. Figure 5.17 and Figure 5.18 show the simulated pressure history (dashed lines) and experimental pressure histories (solid lines) for the ply drop laminates with 4mm and 8mm caul sheets respectively. Both the experimental and simulated pressure histories utilize the same color coding scheme to identify their equivalent positions along the laminate. The prescribed temperature history (dotted black line) and boundary pressure history (dotted grey line) of the simulation has also been plotted. Note that both the simulated and experimental results are presented with respect to the time relative to the experimental results.

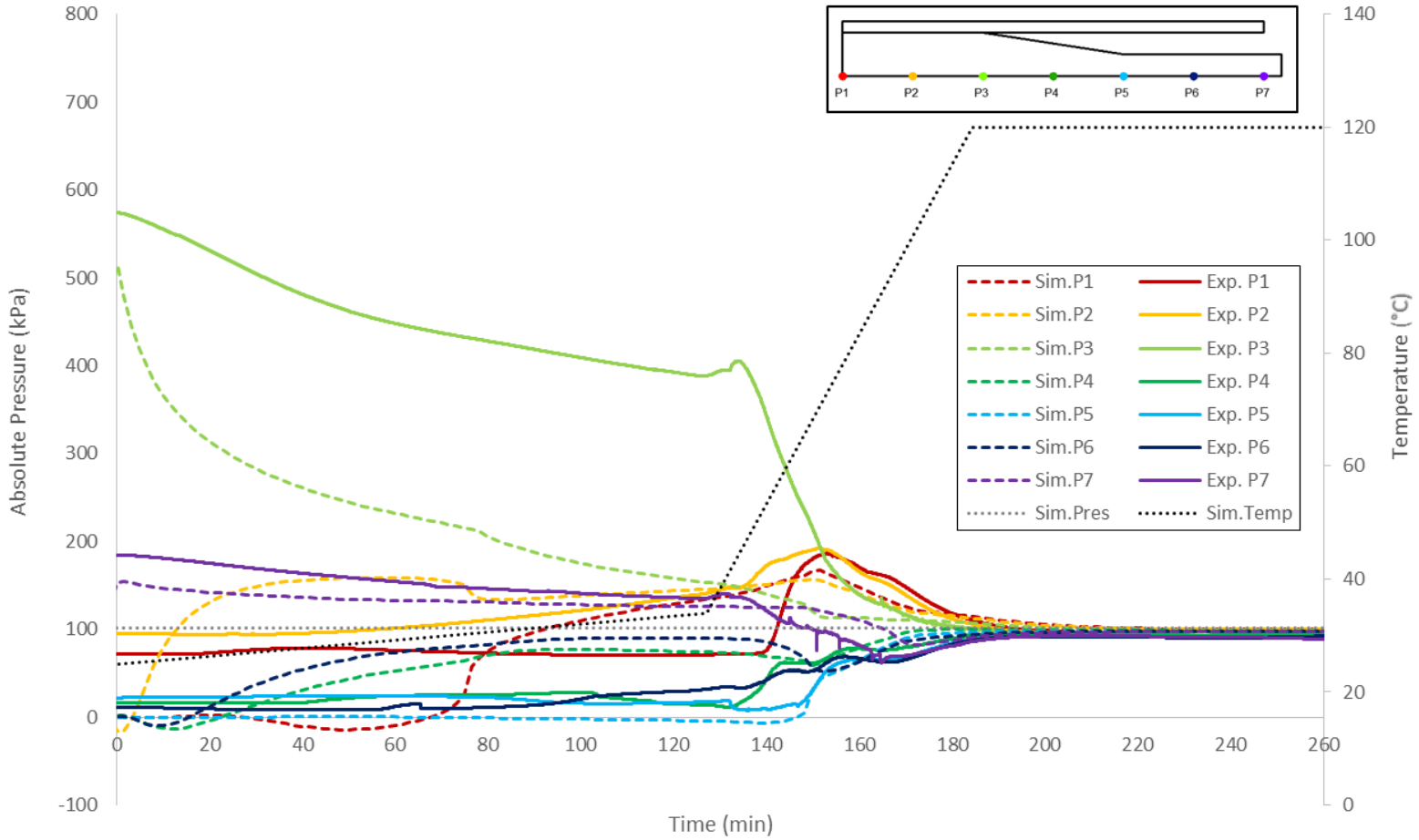

Figure 5.17 – Simulated resin pressure history (dashed lines) and experimental resin pressure histories (solid lines) for the ply drop laminate with 4mm caul sheet laminate for full experimental regime. Both the experimental and simulated pressure histories are color coded to identify the position of the pressures (see legend and sub-figure on upper right corner). For reference, the prescribed simulation temperature history (Sim.Temp) and pressure history (Sim.Pres) are also plotted.

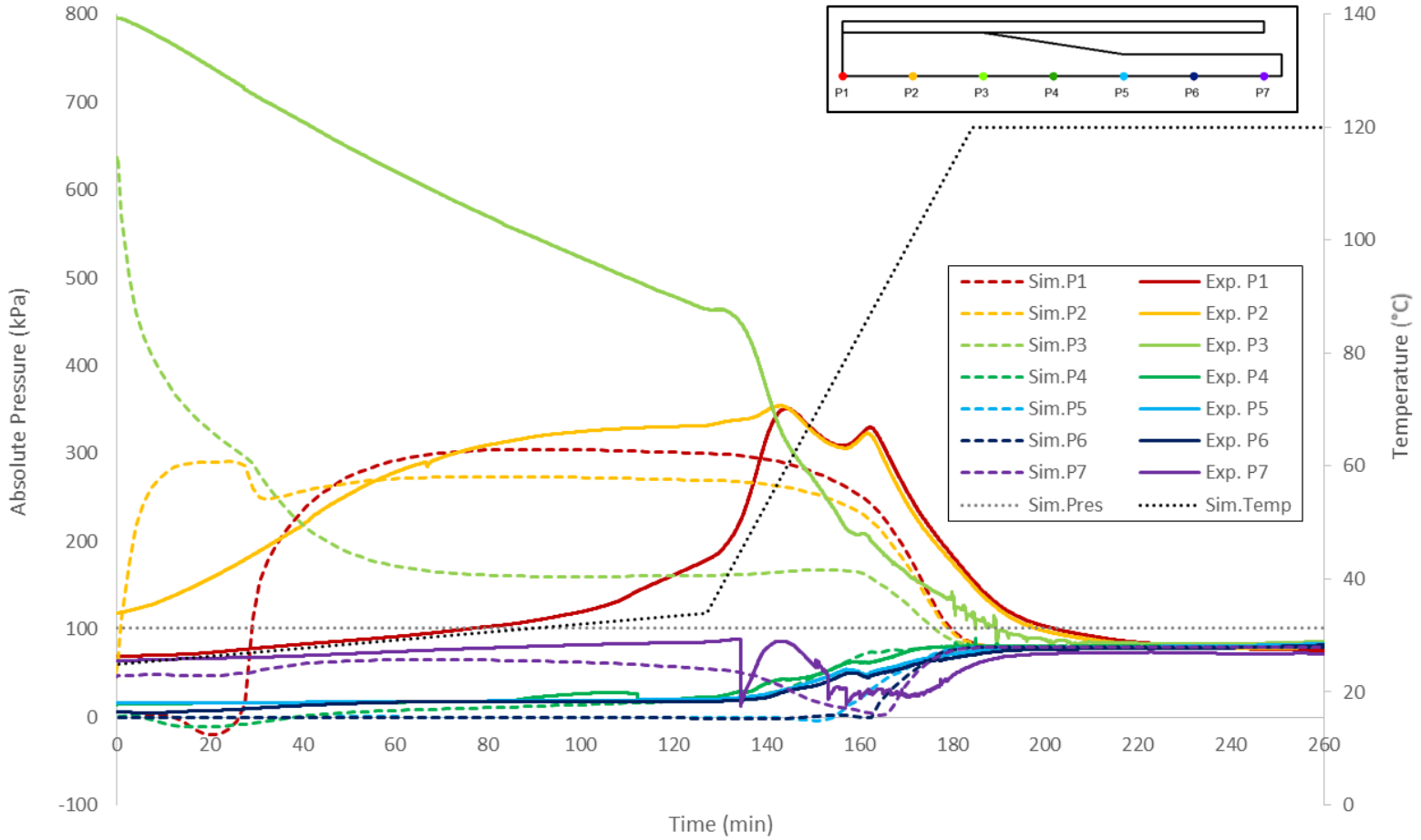

Figure 5.18 – Simulated resin pressure history (dashed lines) and experimental resin pressure histories (solid lines) for the ply drop laminate with 8mm caul sheet laminate for full experimental regime. Both the experimental and simulated pressure histories are color coded to identify the position of the pressures (see legend and sub-figure on upper right corner). For reference, the prescribed simulation temperature history (Sim.Temp) and pressure history (Sim.Pres) are also plotted.

As can be seen from the figures above, significant discrepancies exist between the simulated and experimental pressure histories during the debulk phase (i.e. between 0 to 120 minutes). With respect to the simulated pressure histories of the ply drop laminate with 4mm caul sheet (Figure 5.17), it can be seen that initially, only the P3 and P7 regions are pressurized, whereas all other regions are unpressurized. This indicates that the simulations only predict the formation of a pressure cell at the P3 and P7 initially. This is not the case in the experimental results. Furthermore, during the debulk, the P3 region undergoes a significant pressure decay which is unparalleled by the experimental results. Meanwhile, as the pressure at the P3 region decreases the adjacent region soon became pressurized. Specifically, P2 is the first unpressurized region to increase in pressure, followed by the P6, P4, P1 and finally P5 region. However, due the rapid decay at the P3 region, it can be seen that the pressure at this region drops below the P1 and P2 regions sooner in the simulation than in the experimental results.

Similar discrepancies can be identified in the case of the ply drop laminate with 8mm caul sheet (Figure 5.18). Again, at 0 minutes the simulations only predict the formation of a pressure cell at the P3 and P7 region. Note that the pressure decay at P3 region is even more rapid in this case as compared to the case of the ply drop laminate with 4mm caul sheet. As such the pressure at the P3 region will drop below the pressure at the P1 and P2 regions even earlier (40 minutes). Moreover, for the ply drop laminate with 8mm caul sheet, it seems as though the pressures at the P1, P2 and P3 regions converge to an equilibrium value during the debulk.

It is clear that the inability to simulate the debulk results in significant discrepancies between the simulated and experimental pressure histories. This is especially true for the thick regions (P1, P2 and P3) because these regions bear the brunt of the pressure overfill during the debulk period (as discussed in Chapter 4). However, in observing the pressure histories during the flow dominated regime (i.e. 120 minutes and beyond), it can be seen that the pressure variations seen in the simulations bear similarities with the variations seen in the experimental results. Although the numerical values are not exact, the changes in pressure (i.e. increasing or decreasing) and the sequence in which these changes occur in time are consistent with the experimental results. However, due the discrepancies incurred when attempting to simulate the full experimental regime, it is difficult to make these observations at first glance. As such these similarities will be discussed in greater detail in next section which evaluates simulations which have been restricted to the flow dominated regime.

5.3.2.3 Pressure History Simulation of Flow Dominated Regime

In this section the flow dominated regime simulated pressure histories will be evaluated and compared to the experimental results. Figure 5.19 and Figure 5.20 show the simulated pressure history (dashed lines) and experimental pressure histories (solid lines) for the ply drop laminates with 4mm and 8mm caul sheets respectively. Both the experimental and simulated pressure histories utilize the same color coding scheme to identify their equivalent positions along the laminate. The prescribed temperature history (dotted black line) and boundary pressure history (dotted grey line) of the simulation has also been plotted. Note that both the simulated and experimental results are presented with respect to the time relative to the experimental results.

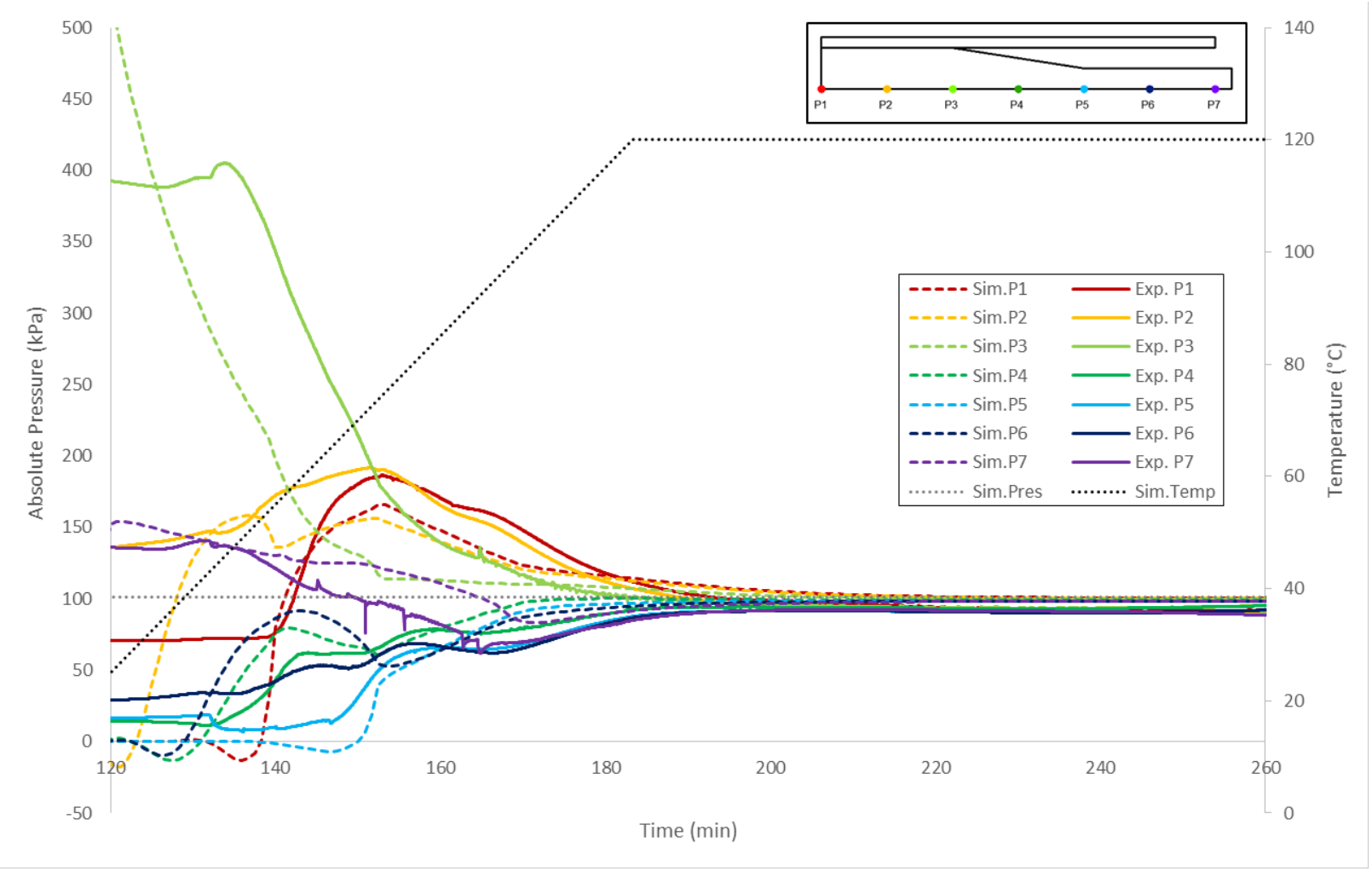

Figure 5.19– Simulated resin pressure history (dashed lines) and experimental resin pressure histories (solid lines) for the ply drop laminate with 4mm caul sheet laminate for flow dominated regime. Both the experimental and simulated pressure histories are color coded to identify the position of the pressure (see legend and sub-figure on upper right corner). For reference, the prescribed simulation temperature history (Sim.Temp) and pressure history (Sim.Pres) are also plotted.

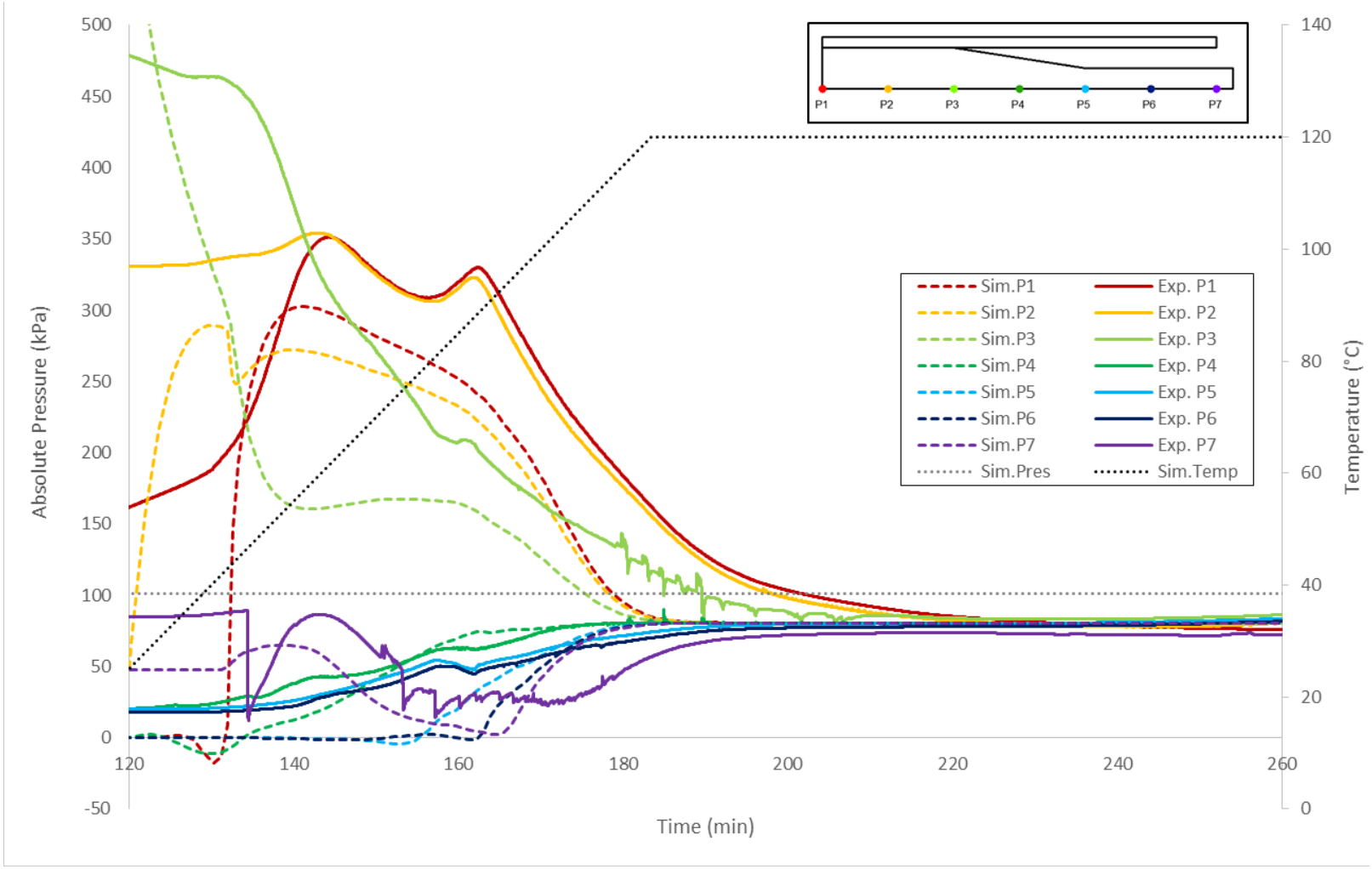

Figure 5.20– Simulated resin pressure history (dashed lines) and experimental resin pressure histories (solid lines) for the ply drop laminate with 8mm caul sheet laminate for flow dominated regime. Both the experimental and simulated pressure histories are color coded to identify the position of the pressure (see legend and sub-figure on upper right corner). For reference, the prescribed simulation temperature history (Sim.Temp) and pressure history (Sim.Pres) are also plotted.

While disregarding the initial errors (i.e. between 120 minutes and 150 minutes), which we already know to be caused by the inability to simulate the debulk, it can be seen from the figures above that the changes in pressure and the sequence in which these changes occur are consistent with the experimental results. As such, the model is able to capture the behaviors of critical importance to this complex processing scenario. The most important of these behaviors is the relationship between final resin pressure and caul sheet stiffness. For both the ply drop laminates with 4mm and 8mm caul sheets (Figure 5.19 and Figure 5.20 respectively), as the temperature increases to 120°C, the pressure at all regions change such that the values of pressure decrease in magnitude the farther away the region is from the center of the laminate (i.e. pressure decreasing as we go from P1 to P7). Past this point, all regions gradually converge to the equilibrium pressure. This behavior is consistent with the experimental pressure histories. More importantly, the simulations show that the use of stiffer caul sheets will decrease this equilibrium pressure. Specifically all regions in the case of the ply drop laminate with 4mm caul simulation converge to an equilibrium pressure of 98kPa. For the case of the ply drop laminate with 8mm caul simulation, all regions converge to an equilibrium pressure of 80kPa.

Additional evidence which demonstrates the models ability to capture this relationship can be seen by pressure variations of a more particular nature. Consider the simulated and experimental pressure histories of the ply drop laminate with 4mm caul (Figure 5.19). Note that both the simulation and experimental results show that the P5 region is the last to become pressurized (at 150 minutes). This implies that this region was the last to come into contact with the caul sheet. Additionally, note that both the experimental pressure histories and simulated pressure histories show that pressure at the P7 region is consistently lower for the case of the ply drop laminate

with 8mm caul than the case when a 4mm caul is used. This indicates that the thicker caul sheet cannot deflect as effectively as the thinner caul sheet and therefore less pressure is transferred to the P7 region. As such, the relationship between pressure distribution and caul sheet rigidity as captured by the simulations is consistent with the experimental observations during the flow dominated regime.

Finally, it can also be observed that the pressure history of the simulations shown in this section (flow dominated regime) is consistent with the pressure histories shown in the previous section (full experimental regime) past 150 minutes. To illustrate this observation more clearly, Figure 5.21 and Figure 5.22 show the pressure history of the flow dominated regime simulations superimposed onto the full experimental regime simulations for ply drop laminate with 4mm and 8mm caul sheets respectively. As can be seen, regardless if the full experimental trial is being simulated or just the flow dominated regime, both simulations will inevitably converge to the same pressures once resin flow is the dominant mechanism. As such, by simulating only the flow dominated regime rather than the full experimental regime, the error caused by the inability to simulate the debulk has not been removed but rather, compressed within a shorter period of time.

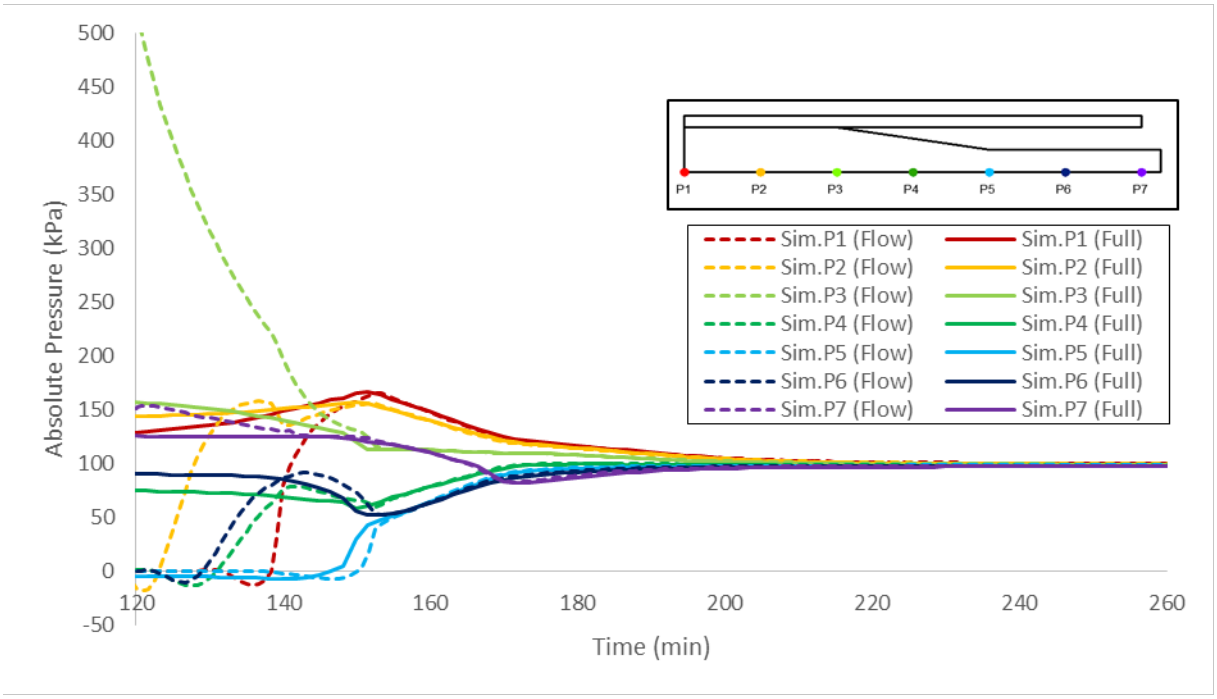

Figure 5.21 – Superposition of flow dominated regime (dashed lines) and full experimental regime simulations (solid lines) at for the ply drop laminate with 4mm caul sheet.

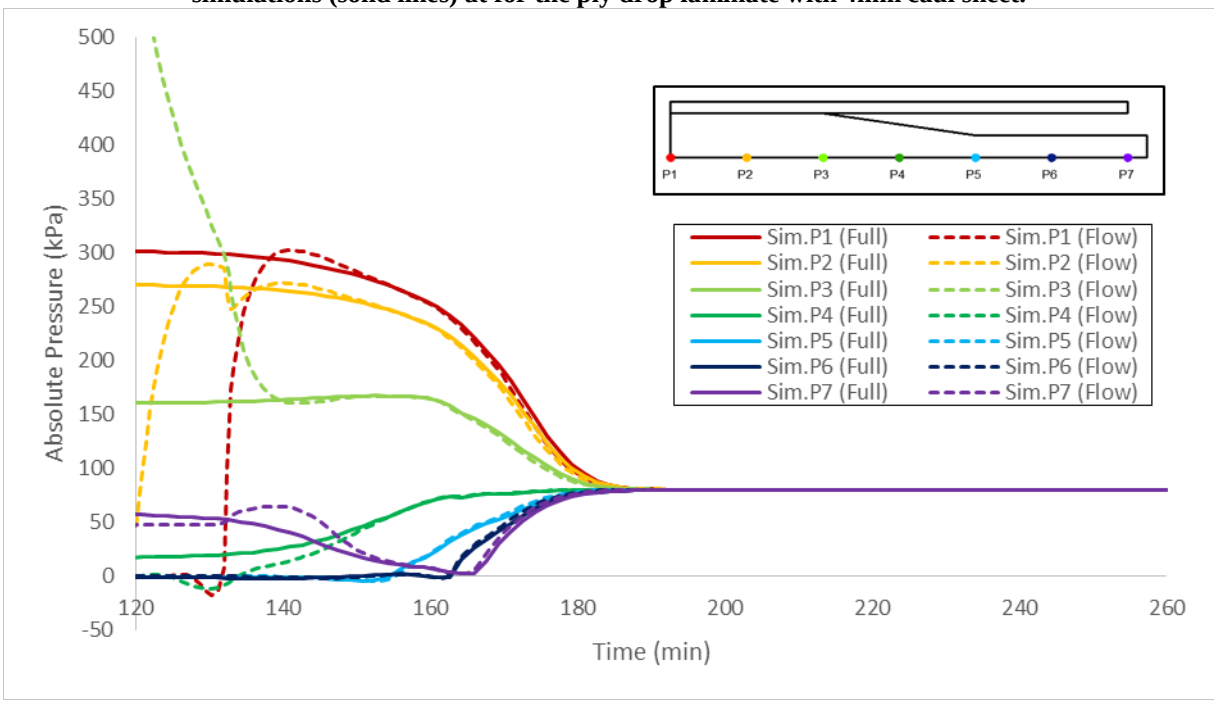

Figure 5.22 – Superposition of flow dominated regime (dashed lines) and full experimental regime simulations (solid lines) at for the ply drop laminate with 8mm caul sheet.

5.3.2.4 Predicted Final Thickness Profile

Several final thickness profiles where simulated for the ply drop laminates with 4mm and 8mm caul sheets. For each laminate, three distinct final thickness profiles where simulated by using the un-shifted fit, half-shifted fit and fully-shifted fit (as seen in section 5.3.2.1) to define the compaction behavior of the material. Figure 5.23 and Figure 5.24 shows the simulated and experimental final thickness profiles of the ply drop laminates with 4mm and 8mm caul sheets respectively. As can be seen, although discrepancies exist between the simulated and experimental results, it can be said that the model captures the relationship between the thickness profile of the laminate and the stiffness of the caul sheet. That is to say that regardless of which fit is used to define the compaction curve, the simulated final thickness profile for ply drop laminate with 4mm caul will always be more tapered than that of the ply drop laminate with 8mm caul. This behavior is consistent with the experimental results.

It can also be seen that the final thickness profile which was simulated when the compaction curve was defined by the fully-shifted fit agrees better with the experimental results. This is true for both ply drop laminates with 4mm and 8mm caul sheets. Although the stiffest compaction curve produces more accurate thickness results, recall that it performed poorly in predicting the final equilibrium pressure in the case of the ply drop laminate with 8 mm caul (section 5.3.2.1). This again suggests that a simple shift may not be a sufficient manipulation to approximate the compaction curve of the material and that the shape of the curve may need to be better defined. As such better predictions for both the pressure history and final thickness profile could be obtained provided a better approximation of the compaction curve shape where made available. This can be achieved simply by acquiring better instrumentation for the compaction test.

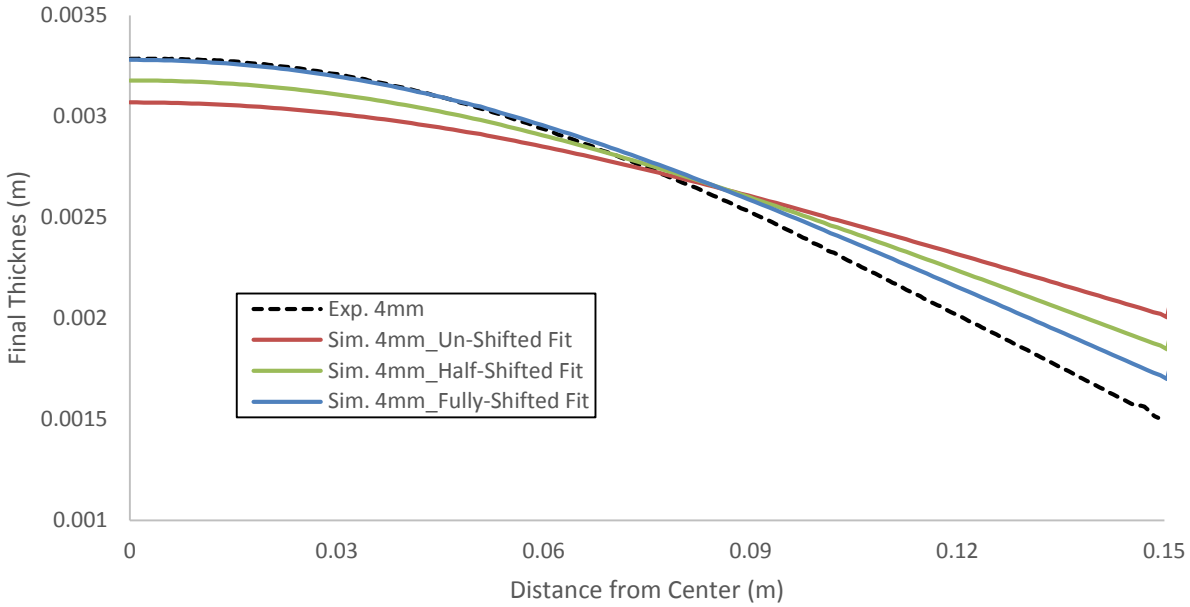

Figure 5.23 –Simulated and experimental final thickness profile for ply drop laminate with 4mm caul sheet. The simulated final thickness profiles for when the compaction curve is defined by the un-shifted fit, half-shifted fit and fully shifted fit is plotted by the red, green and blue solid lines respectively. The experimentally measured final thickness profile is plotted by the dashed black line.

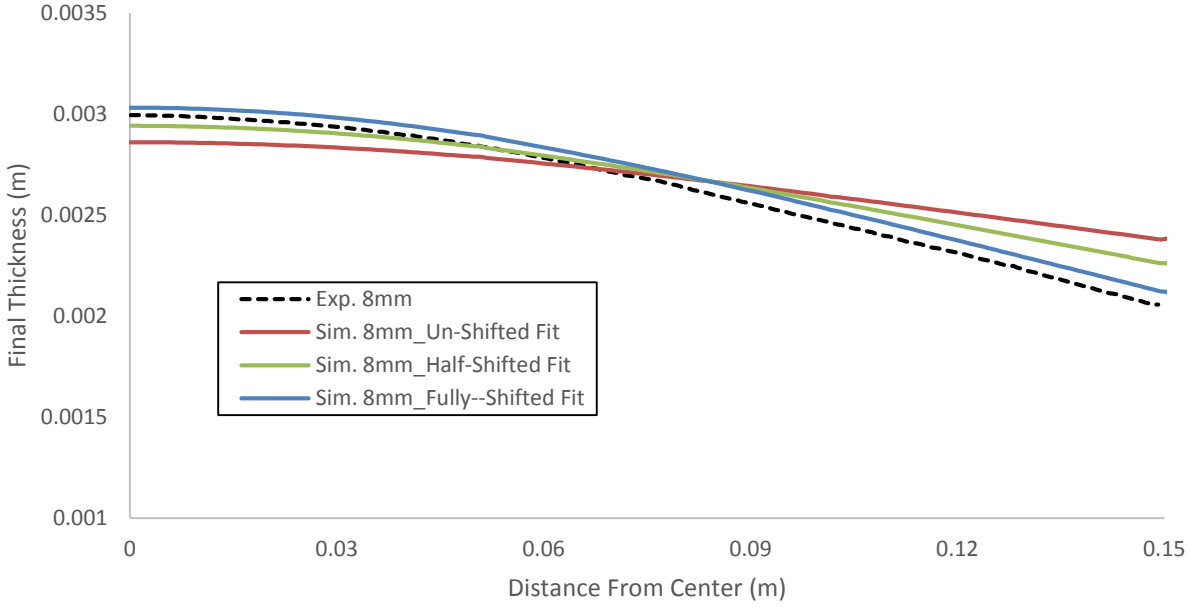

Figure 5.24 - Simulated and experimental final thickness profile for ply drop laminate with 8mm caul sheet. The simulated final thickness profiles for when the compaction curve is defined by the un-shifted fit, half-shifted fit and fully shifted fit is plotted by the red, green and blue solid lines respectively. The experimentally measured final thickness profile is plotted by the dashed black line.

5.4 Discussion

5.4.1 Parametric Simulation Study

5.4.1.1 Effect of Fiber Bed Compaction Behavior

It has been shown in section 5.2.2.1 that the compaction curve of the material dictates the amount of consolidation pressure that will be absorbed by the fiber bed. Stiffer compaction curves will cause more of the compaction pressure to be borne by the fiber bed at regions subject to resin depletion (i.e. pressure overfill regions). This will thereby reduce the hydrostatic resin pressure and present a greater risk of void growth.

From the results presented in section 5.2.2.2, it can also be noted that the effect of the material compaction behavior on resin pressure is intrinsically linked to its effect on the final thickness profile of the laminate. This is because the final thickness profile is dependent on resin migration which is driven by the hydrostatic resin pressure gradients. As such, more absorption of the applied compaction pressure by the fiber bed at the overfill regions will result in smaller pressure gradients. For the configured structures studied in this thesis, stiffer compaction curves ultimately result in more tapered final thickness profiles.

It has been shown that the time to reach hydrostatic equilibrium is increased for more compliant compaction curves. However, regardless of the state of the pressure gradients, it has also been shown that the most shielded regions of the laminate achieves higher resin pressures in shorter amounts of time when the compaction curve is more compliant. Therefore, as far as porosity is concerned, more compliant compaction behavior presents less risk of void growth.

5.4.1.2 Effect of Resin Viscosity and Fiber Bed Permeability

It has been shown that variations of viscosity or permeability do not affect the final hydrostatic equilibrium pressure to which the resin pressure at all regions converge to. Rather, viscosity and permeability simply effect the amount of time required for this convergence to occur. However, this observation only bears relevance within the context of the parametric simulation study. In reality, it is well known that there is a finite amount of time for which resin flow can occur and for the pressures at all regions to converge to the final equilibrium pressure (i.e. the time between the onset of viscous behavior and gelation). As such, although viscosity and permeability do not change the final equilibrium pressure, the implication here is that the effect of viscosity and permeability can make it so that the system runs out of time. That is to say that a pressure gradient can get locked in at gelation.

It has also been noted that increasing viscosity and decreasing permeability or vice-versa bears the exact same effect on resin flow. This is because resin flow in this model formulation obeys Darcy's law (equation 5-1). Again, this observation only bears relevance within the context of the parametric simulation study. In reality, the range of variation for the value of viscosity differs greatly from the range variation for the value of permeability because these material properties depend on extrinsic sets of state variables. Viscosity is dependent on the cure kinetics of the resin, as such its range is virtually unbounded. For example, the viscosity of MTM45-1 resin at room temperature is on the order of 25000 Pa s. Subject to a temperature ramp of 1.5°C/minute to 120°C followed by the standard four hour hold, the value of viscosity will decrease to a minimum of value of 10 Pa s and increase infinitesimally at gelation. Permeability, on the other hand, is dependent on the fiber bed architecture of the material. Although permeability deviates

in magnitude as the fiber bed architecture changes with resin flow, the range with which permeability varies is dwarfed by the range of variation to which viscosity is subject to. For example, with respect to the Kozeny-Carmen permeability model, a change in fiber volume fraction from 35% to 75% will only cause permeability to decrease by a factor of 80 regardless of the Kozeny constants. Considering how the magnitudes of variation for viscosity and permeability scale with respect to each other in an actual processing scenario, it can be stated that the permeability will generally dictate the velocity at which resin is able to flow whereas, viscosity will dictate both the resin flow velocity and the amount of time available for resin flow to occur.

5.4.2 Simulation of Experimental Results

5.4.2.1 Model Performance During Debulk

In section 5.3.2.2, it has been shown that large discrepancies exist between the pressure history of the simulations and the experimental pressure history during the debulk phase. Moreover, these discrepancies are very pronounced at the thick region (P1, P2 and P3). It was stated that these discrepancies are due to an inability to simulate the relevant physics during the debulk stage when only the Darcy flow-compaction formulation is used. To elaborate on this concept, consider Figure 5.25 shown below. Figure 5.25 shows the resin pressure distribution for the ply drop laminate with 4mm caul at the instant when the full compaction pressure is applied (i.e. 8.33 minutes for the simulation time).

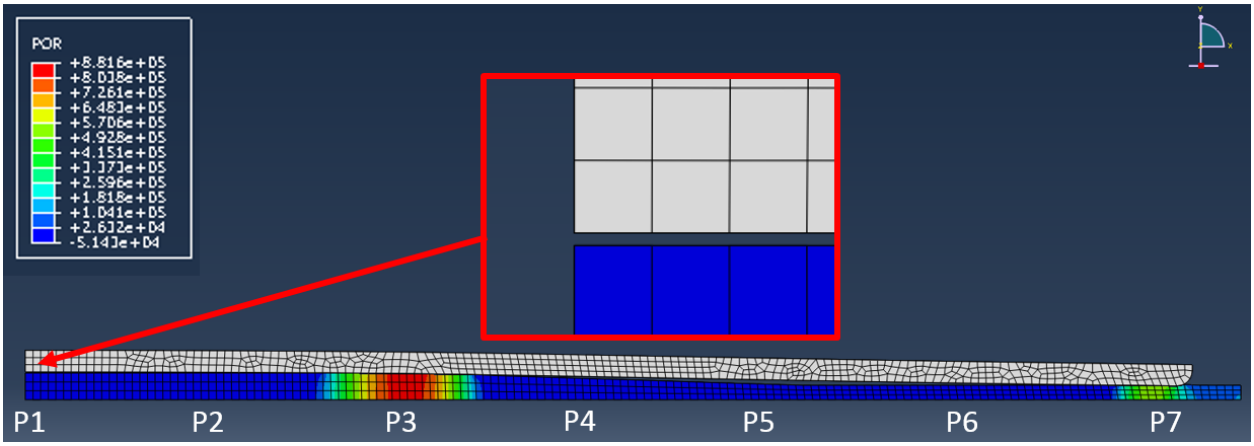

Figure 5.25 – Capture of resin pressure profile at full compaction pressure application for the ply drop laminate processed with 4mm caul sheet simulation.

It can be seen from the figure above that pressure cells have only formed at regions P3 and P7, all other regions are unpressurized. Although this is consistent with the experimental results for regions P4, P5 and P6, the experimental results also showed that regions P1 and P2 were in fact pressurized. As such, the simulations show an initial pressure distribution which is much more localized than the distribution in the experimental results. In observing Figure 5.25, it can be seen that the P1 and P2 regions are unpressurized because there exists a gap between the caul sheet and the laminate at these regions. In order for the caul sheet to come into contact at the P1 and P2 region, the P3 region must undergo compressive strain. Moreover, since the model assumes the composite material to be a solid phase (fiber bed) fully saturated by an incompressible fluid (resin), a compressive strain must elicit a loss in resin pressure due to more of the compaction pressure being born by the fiber bed. In reality, the composite is actually a three phased material comprised of the fiber, resin and air. As such, compressive strains do not necessarily elicit resin flow during the debulk phase. This thereby allows for pressure cells to form at the P1 and P2 region without resin depletion at the P3 region.

Although the pressure variations of the simulation at the flow dominated regime where similar to the pressure variations seen in the experimental trials, it is clear that in order to accurately replicate the exact pressure histories, one must be able to simulate the stress-deformation mechanisms occurring during the debulk stage.

5.4.2.2 Model Performance during Flow Dominated Regime

While disregarding the initial discrepancies of the simulations (which we know are due to an inability to simulate the debulk) it has been shown that the pressure variations during the flow dominated regime is similar to the pressure variations seen in the experimental results. One of the most important behaviours captured by the model is that of the pressure gradient evolving in such a way that resin migrates from the center of the laminate (thick region) towards the outer edge (thin region). This observation, amongst other observations of a more particular nature, demonstrate that the model is able to capture the relationship between the resin pressure of the ply drop laminates and the caul sheets stiffness. As such, the model is able to simulate the critical physics which lead to a reduction in hydrostatic resin pressure. Since resin pressure plays a key role in void evolution, this implies that the model can be used as a tool in understanding the relationship between the geometrical complexities of configured structures and the risk of void stabilization.

It can be seen that the pressure values of the simulation are not exactly consistent with pressure values seen in the experimental results. This is especially true for the P1, P2 and P3 regions because the debulk plays a much more significant role in the distribution of pressure at these regions. However, these discrepancies can be attributed to a multitude of factors which are

known to be sources of error in this exercise. Namely, the inability to simulate the debulk, the lack of accuracy in the compaction curve measurements, the use of the Kozeny-Carmen permeability model, and some other inconsistencies between the model definition and actual experimental configuration (e.g. simulation does not include resin film, the fillet at the edge of the caul is not representative of the actual caul sheet etc.). Although the exact numerical values of pressure where not replicated in this exercise, it can be stated that the proper behavior was indeed captured during the flow dominated regime. As such, the ability to simulate the general behavior can be of very practical use in making decisions in manufacturing. This is discussed in greater detail in the following section.

5.4.2.3 Utility and Limitations of Darcy Flow-Compaction Model

One obvious utility of the model is in determining the amount of compaction pressure that will be lost to the fiber bed as a result of the lack of compliance within the assembly of configured structures. Such information can allow practitioners to partially assess the risk of void growth for a given process at the conceptual level. For example, in the case of the structural configuration of interest to this thesis, one can use the model simulations to evaluate how much resin pressure is lost to the fiber bed for various caul sheet designs, layup strategies (e.g. ply pitch length) or materials. However, the final pressure lost to the fiber bed is only part of the mechanism by which void evolution can occur through lack of resin pressure. In order to better assess the risk of void growth for a given process, one also needs to account for the amount of time that shielded regions remain unpressurized and whether or not a pressure gradient gets locked in at gelation. In order to do this one needs to be able accurately simulate the resin pressure history of the laminate. Although, for reasons previously discussed, the simulated pressure histories do not

demonstrate exact equivalence with experimental values, it has been shown that the overall behavior of the pressure variations are consistent with the experimental results at the flow dominated regime. As such, it can be said that the model can be used to assess the changes in behavior in relation to variations in manufacturing specification. For example, one can use Darcy flow-compaction simulations to evaluate the change in pressure histories with respect to various cure cycle specifications. In evaluating how the pressure histories change from one cure cycle to the next, one is able to make a more informed decision with regards to the cure cycle specifications that should be implemented.

One of the most significant limitations of the model studied here lies in the inability to simulate the pressure histories during the debulk. In this study, it has been shown that the inability to simulate the debulk results in large discrepancies during the regimes where the resin pressure is not primarily influenced by resin flow and fiber bed compaction mechanisms. It should be noted that the model formulation used in this study (COMPRO V2) is a sequential flow-compaction and stress-deformation formulation[72]. In other words, the stress-deformation analysis is only performed after the flow-compaction analysis is completed. As such, to capture the effects of debulking, an integrated approach is required whereby the stress-deformation and flow-compaction mechanisms are fully-coupled and solved simultaneously. Such a model has already been proposed by Haghshenas [73] and is currently being implemented into the newer generations of COMPRO (COMPRO Integrated-Flow-Stress) [72]. Moreover, a model formulation which incorporates a gas phase within the integrated-flow-stress model formulation (resulting in a three-phase integrated-flow-stress model) is currently being researched and developed [74].

Chapter 6: Summary, Conclusions and Future Work

6.1 Summary and Conclusions

The objective of this thesis was to advance our knowledge of porosity for the processing of configured structures. The configured structures of interest studied in this thesis were ply drops and caul sheets. A series of parts made of MTM45-1/CF0526A plain weave prepreg with various combinations of ply drops and caul sheets was manufactured in order to study the effects of ply drops and caul sheets on porosity parametrically. The final porosity content and thickness profile of these parts were measured through the use of optical microscopy and thickness measurements. From this parametric study, it was concluded that the lack of compliance between the ply drop laminates and caul sheets bares adverse effects on the resin pressure of the material during processing which in turn can lead to void stabilization and growth. In order to demonstrate these mechanisms, the resin pressure distribution of ply drop laminates processed with and without caul sheets of various thickness was tracked in-situ through the use of instrumented tooling. Moreover, these experimental results were simulated with the use of a Darcy flow-compaction model so as to further advance our understanding of the dominate mechanisms. Based on the findings presented in this thesis, the following conclusions can be made:

1) **The risk of void generation increases with greater lack of compliance.**

   In this thesis, the lack of compliance between the ply-drop laminates and the caul sheet was controlled and adjusted simply by using caul sheets of various bending stiffness (i.e. the stiffer the caul sheet the greater the lack of compliance). In doing so, the relationship between lack of compliance and the risk of voids was demonstrated systematically. In a small scale parametric study, it was shown that a greater lack in compliance between the ply drop

laminates and caul sheets always leads to a greater risk of void generation regardless of the alterations made to the processing conditions. The implication here is of great engineering value to current practices because it states that regardless of the structural configurations involved, assessing the producibility of a part can in large be reduced to a simple problem of basic mechanics. Specifically, practitioners can give some estimate as to whether or not a manufacturing specifications is at risk of resulting in voids simply by answering the following question: Does the tooling conform to the part? If the answer to this question is no, then one must take into account the consequential downstream effects or reconsider the manufacturing specifications such that better compliance is achieved.

2) **Lack of compliance between the caul sheet and the ply-drop laminate shields the resin from the applied compaction pressure which increases the risk of void stabilization.**

The use of caul sheets in the processing of ply drop laminates alters the load paths such that the regions of the laminate which are not in contact with the caul sheet are shielded from the compaction pressure and the regions which are in contact with the caul sheet carry the residual pressure being applied to the system. In this thesis, these regions have been dubbed as the pressure shielded regions and pressure overfill regions respectively. In the absence of configured tooling, the flexibility of the consumable bagging arrangements make it so that the applied compaction pressure is distributed evenly at all regions of the laminate. If configured tooling is to be used, regardless of the type (i.e. matched die tooling, caul sheets etc.) if the tooling's stiffness and geometry makes it so that there exists a lack of compliance between the tooling and the part being manufactured, the result is a pressure shielded region.

The resin at these regions will remain unpressurized until such a point where contact between the tooling and the part can be achieved through resin migration. However, during this period of time, the absence of resin pressure at these regions make it so that the gas pressure within the preexisting void spaces of the material can stabilize the void structure or even cause it to grow in size.

3) **Lack of compliance between the caul sheet and the ply-drop laminate de-homogenizes the laminates resin pressure and results in resin migration. Resin migration causes the applied compaction pressure to be absorbed by the fiber bed which in turn reduces the hydrostatic pressure and increases the risk of void stabilization.**

In addition to pressure shielding, the imbalance of forces caused by lack of compliance will cause resin migration within the laminate during the flow dominated regime of the cure. This mechanism of resin migration can also work to reduce the hydrostatic resin pressure of the laminate. As the laminate is subject to a cure cycle, the increasing temperatures will decrease the viscosity of the resin which will in turn allow resin to flow. Driven by an imbalance of hydrostatic pressure, resin will flow from the pressure overfill regions to the pressure shielded regions. As flow continues, the pressure overfill regions are depleted of resin content and thus the applied compaction pressure is partially borne by the fiber bed. Since the resin flowing into the shielded regions is driven by the resin pressure at the overfill regions, this means that the fiber bed will not only hijack the resin pressure at the resin depleted regions, but it will also hijack the pressure at the regions where the fiber bed is not baring any of the applied compaction pressure. Resin migration will continue until such a point

when the resin everywhere has equilibrated to a common pressure or until gelation occurs and resin can no longer flow. As such the mechanism of resin migration is not only preordained by the interaction between the tooling and the laminate, but also by the composites material properties. To wit, the compaction behavior of the fiber bed will dictate how much of the applied compaction pressure will be lost to the fiber bed. The liquid permeability of the resin will generally dictate the achievable resin flow velocity. Finally, the resin viscosity will influence both the resin flow velocity and the time available for resin flow to occur.

4) **A Darcy flow-compaction model can be used to simulate the resin pressure history of the part in the processing of configured structures.**

In this thesis, it has been shown that a Darcy flow-compaction model can be used to mimic the transient pressure histories of the structurally configured laminates of interest to this thesis during the flow dominated regime. As such, the Darcy flow-compaction model can be used as a tool to enhance our understanding of the relationship between the composite material properties, resin pressure and the part and tooling geometries. Such a tool can enable practitioners to make more informed decisions in the manufacturing of structurally configured parts. It should also be noted that the ability to replicate the experimental results through existing simulation software also gives some insight as to the state of our current understanding in composite processing. Note that no amendments to the current knowledge base has been proposed in this thesis. That is to say that no novel physical laws, mechanics or models have been introduced. Rather, this thesis has simply addressed the relationship

between two pre-existing themes of knowledge; that of porosity and that of flow and compaction mechanics in composite processing.

With respect to the simulation results outside of the flow dominated regime, it has been shown that a Darcy flow-compaction model alone cannot capture the pressure histories during the debulk. This is because the model formulation used for this study (COMPRO V2 [2]) implements the stress-deformation analysis following the flow-compaction analysis. As such, the limitation of this sequential approach is that the bulk behavior of the resin cannot be captured throughout the cure. In order to capture the effects of the debulk, the model must be reformulated such that the stress-deformations and flow-compaction mechanisms are accounted for simultaneously [72]. Nevertheless, the fact that such formulations have already been proposed [73] and are progressively being implemented into newer versions of COMPRO [72] is reassurance that the direction of the ongoing research in the field of composite processing is in accordance with the current industrial needs.

6.2 Future Work

Based on the findings obtained in this study, the following recommendations are made for future work.

Effect of debulking on pressure distribution and resin flow behavior

In the instrumented tool tests, it was observed that significant pressure variations were seen to occur during the debulk period. Specifically, regions which were initially seen to carry the majority of the applied compaction pressure decreased in pressure while adjacent regions

demonstrated an increase in pressure. Although a slight temperature increase was seen to occur during the debulk period (from 25°C to 34°C) it was concluded that the value of resin viscosity within this temperature range was not enough to explain the pressure variations as resin flow. As such, it was concluded that better contact between the laminate and the caul sheet could be achieved during the debulk through a stress-deformation mechanism prior to the initiation of resin flow. However, questions still remain as to how much the pressure distribution prior to the initiation of resin flow influence pressure histories during the flow dominated regime of the cure. Can a change in pressure distribution during the debulk alter the final pressure distribution at gelation or do these variations simply get washed out by the mechanisms of resin flow? How much of a roll does the temperature at the debulk play in achieving better compliance between the laminate and the caul sheet? Furthermore, can heated debulks be utilized to minimize the risk of void growth in the processing of configured structures? Investigations which look to answer these questions could advance our understanding of the transition between the stress-deformation and the flow-compaction mechanism during cure and could also lead to better manufacturing practices.

Simulation of small scale parametric study results

In this thesis, a Darcy flow-compaction model was used to simulate the pressure histories observed in the instrumented tool test study. However, the final porosity for the laminates processed in the instrumented tool tests was not measured. As such, in addition to the simulations presented in Chapter 5, it would also be beneficial to simulate the pressure histories for the laminates manufactured in small scale parametric study (Chapter 3) since the final porosity content of these laminates where quantitatively measured. In doing so, a better

understanding of the relationship between resin pressure and porosity could be established. Such an investigation would not only provide quantitative understanding as to what values of resin pressure presents a higher risk of void growth but could also give some understanding as to the time dependent features of void evolution (i.e. the amount of time needed at a specified resin pressure for void stabilization to occur).

Effect of ply drops on resin pressure and gas extraction

In the instrumented tool test, pressure variations where seen to occur at the ply drop region of the laminate processed without the use of a caul sheet. Specifically, it was found that the pressure at the ply drop region was below the pressures at all other regions during the debulk and surpassed the pressure at all other regions for a period of 50 minutes when the cure cycle reached the 120°C dwell temperature. Although the pressure variations seen in this study where not significant in comparison to the ply drop laminates which were cured with a caul sheet, one must consider the scale of the parts manufactured in this study in contrast to the scale of parts commonly manufactured in industry.

As of yet, the reasons for these pressure variations cannot be stated with certainty. However, it is believed by the author that these variations are in some way linked to the additional void spaces inherent in the ply drop region. Regardless, further experimentation is required to evaluate the effect that ply drops have on resin pressure and gas transport and how these relationships could potentially work to influence void evolution.

Bibliography

[1] "Convergent Manufacturing Technologies," *Convergent Manufacturing Technologies*. [Online]. Available: http://www.convergent.ca/.

[2] "COMPRO," *Convergent Manufacturing Technologies*. [Online]. Available: http://www.convergent.ca/products/compro-simulation-software.

[3] "ABAQUS 6.14," *Dassault Systemes*. [Online]. Available: http://www.3ds.com/products-services/simulia/products/abaqus/latest-release/.

[4] Mazumdar, "Chapter 1 Introduction," in in *Composites Manufacturing*, CRC press, 2002.

[5] M. LeGault, "2011 High-Performance Resins Highlights," *Composites World*, 2011. [Online]. Available: http://www.compositesworld.com/articles/2011-high-performance-resins-highlights.

[6] Mazumdar, "Chapter 6 Manufacturing Techniques," in in *Composites Manufacturing*, CRC press, 2002.

[7] A. K. Kaw, *Mechanics of composite materials*. CRC press, 2010, pp. 29–30.

[8] F. Campbell, "Chapter 6 Curing : It ' s a Matter of Time (f)," in in *Manufacturing Processes for Advanced Composites*, Elsevier Ltd, 2004, pp. 180–220.

[9] B. Harper, G. Staab, and R. Chen, "A note on the effects of voids upon the hygral and mechanical properties of AS4/3502 graphite/epoxy," *Journal of composite materials*, no. March 1987, pp. 280–289, 1987.

[10] Z. Guo, L. Liu, B. Zhang, and S. Du, "Critical Void Content for Thermoset Composite Laminates," *Journal of Composite Materials*, vol. 43, no. 17, pp. 1775–1790, May 2006.

[11] L. Liu, B.-M. Zhang, D.-F. Wang, and Z.-J. Wu, "Effects of cure cycles on void content and mechanical properties of composite laminates," *Composite Structures*, vol. 73, no. 3, pp. 303–309, Jun. 2006.

[12] L. Farhang, "Void evolution during processing of out-of-autoclave prepreg laminates," the University of British Columbia, 2014.

[13] F. Campbell, A. Mallow, and C. Browning, "Porosity in carbon fiber composites an overview of causes," *Journal of advanced materials*, 1995.

[14] C. Ridgard, "Out of autoclave composite technology for aerospace, defense and space structures," *SMAPE 2009 Proceedings*, 2009.

[15] T. Centea, L. K. Grunenfelder, and S. Nutt, “A review of out-of-autoclave prepregs–Material properties, process phenomena, and manufacturing considerations,” *Composites Part A: Applied Science and Manufacturing*, 2014.

[16] F. Campbell, “Chapter 2 Fibers and Reinforcements : The String That Provides the Strength,” in in *Manufacturing Processes for Advanced Composites*, Elsevier Ltd, 2004, pp. 39–62.

[17] A. Arafath, “Gas transport in prepregs: model and permeability experiments,” in *Proceedings of the ICCM -17*, 2009.

[18] K. Hsiao, J. Kay, and G. Fernlund, “Gas transport and water evaporation in out-of-autoclave prepregs,” in *Proceedings of the CANCOM*, 2011.

[19] J. Kay and G. Fernlund, “Processing conditions and voids in out of autoclave prepregs,” in *Proceedings of the SAMPE 2012 conference of the …*, 2012.

[20] B. Louis, “Gas transport in out-of-autoclave prepreg laminates,” the University of British Columbia, 2010.

[21] “Raven,” *Convergent Manufacturing Technologies Inc.* [Online]. Available: http://www.convergent.ca/products/raven-simulation-software.

[22] Umeco, “ACG MTM®45-1 MATRIX RESIN Product Description,” no. 924425. Umeco.

[23] M. Lane, A. Poursartip, G. Fernlund, K. Willden, and K. Nelson, “Robust Processing of Composite Structures,” in *Proceedings of the SAMPE 2010*, 2010.

[24] T. G. Gutowski, *Advanced Composites Manufacturing*. New York: John Wiley & Sons, 1997.

[25] M. Thompson, “How vacuum bags really work: the myth of volatiles and breathers,” *International SAMPE technical conference*, 1998.

[26] T. Centea and P. Hubert, “Out-of-autoclave prepreg consolidation under deficient pressure conditions,” *Journal of Composite Materials*, no. July 2013, Jul. 2013.

[27] J. Kay and L. Farhang, “Effect of process conditions on porosity in out-of-autoclave prepreg laminates,” in *Proceedings of the ICCM-18*, 2011, pp. 1–5.

[28] T. Centea and P. Hubert, “Measuring the impregnation of an out-of-autoclave prepreg by micro-CT,” *Composites Science and Technology*, vol. 71, no. 5, pp. 593–599, Mar. 2011.

[29] S. Thomas and S. R. Nutt, “Temperature Dependence of Resin Flow in a Resin Film Infusion (RFI) Process by Ultrasound Imaging,” *Applied Composite Materials*, vol. 16, no. 3, pp. 183–196, May 2009.

[30] T. A. Cender, P. Simacek, and S. G. Advani, “Resin film impregnation in fabric prepregs with dual length scale permeability,” *Composites Part A: Applied Science and Manufacturing*, vol. 53, pp. 118–128, Oct. 2013.

[31] J. Gangloff, C. Daniel, and S. Advani, “A model of two-phase resin and void flow during composites processing,” *International Journal of Multiphase Flow*, 2014.

[32] J. Gangloff, W. R. Hwang, and S. G. Advani, “Characterization of bubble mobility in channel flow with fibrous porous media walls,” *International Journal of Multiphase Flow*, vol. 60, pp. 76–86, Apr. 2014.

[33] B. Louis, K. Hsiao, and G. Fernlund, “Gas permeability measurements of out of autoclave prepreg MTM45-1/CF2426A,” in … *Proceedings: New Materials and Processes for a …*, 2010.

[34] S. S. Tavares, V. Michaud, and J. -a. E. Månson, “Through thickness air permeability of prepregs during cure,” *Composites Part A: Applied Science and Manufacturing*, vol. 40, no. 10, pp. 1587–1596, Oct. 2009.

[35] J. Kratz and P. Hubert, “Anisotropic air permeability in out-of-autoclave prepregs: Effect on honeycomb panel evacuation prior to cure,” *Composites Part A: Applied Science and Manufacturing*, vol. 49, pp. 179–191, Jun. 2013.

[36] C. Xin, M. Li, Y. Gu, Y. Li, and Z. Zhang, “Measurement and analysis on in-plane and through-thickness air permeation of fiber/resin prepreg,” *Journal of Reinforced Plastics and Composites*, vol. 30, no. 17, pp. 1467–1479, Sep. 2011.

[37] L. K. Grunenfelder and S. R. Nutt, “Void formation in composite prepregs – Effect of dissolved moisture,” *Composites Science and Technology*, vol. 70, no. 16, pp. 2304–2309, Dec. 2010.

[38] J. Kardos, M. Duduković, and R. Dave, “Void growth and resin transport during processing of thermosetting—matrix composites,” *Epoxy Resins and Composites IV*, 1986.

[39] L. K. Grunenfelder and S. Nutt, “Out time effects on VBO prepreg and laminate properties,” *2011 SAMPE Spring Technical Conference and …*, 2011.

[40] T. Centea and P. Hubert, “Modelling the effect of material properties and process parameters on tow impregnation in out-of-autoclave prepregs,” *Composites Part A: Applied Science and Manufacturing*, vol. 43, no. 9, pp. 1505–1513, Sep. 2012.

[41] L. K. Grunenfelder, T. Centea, P. Hubert, and S. R. Nutt, “Effect of room-temperature out-time on tow impregnation in an out-of-autoclave prepreg,” *Composites Part A: Applied Science and Manufacturing*, vol. 45, pp. 119–126, Feb. 2013.

[42] P. Hubert, “Aspects of Flow and Compaction of Laminated Composite Shapes During Cure,” 1996.

[43] G. Fernlund, J. Griffith, R. Courdji, and A. Poursartip, “Experimental and numerical study of the effect of caul-sheets on corner thinning of composite laminates,” *Composites Part A: Applied …*, vol. 33, 2002.

[44] Y. Li, M. Li, Y. Gu, and Z. Zhang, “Numerical and Experimental Study of the Bleeder Flow in Autoclave Process,” *Applied Composite Materials*, vol. 18, no. 4, pp. 327–336, Sep. 2010.

[45] C. Xin, M. Li, Y. Gu, J. Luo, and Z. Zhang, “Study on the resin flow and fiber compaction of tapered composite laminates during autoclave processing,” *Journal of Reinforced Plastics and Composites*, vol. 30, no. 16, pp. 1399–1411, Oct. 2011.

[46] C. Xin, Y. Gu, M. Li, Y. Li, and Z. Zhang, “Online Monitoring and Analysis of Resin Pressure Inside Composite Laminate During Zero-Bleeding Autoclave Process,” 2011.

[47] Y. Gu, C. Xin, M. Li, Y. Cheng, and Z. Zhang, “Resin pressure and resin flow inside tapered laminates during zero-bleeding and bleeding processes,” *Journal of Reinforced Plastics and Composites*, vol. 31, no. 4, pp. 205–214, Jan. 2012.

[48] L. Repecka and J. Boyd, “Vacuum-bag-only-curable prepregs that produce void-free parts,” *47 th International SAMPE Symposium and Exhibition …*, 2002.

[49] Hexcel, “HexTow® AS4 Carbon Fiber Product Data,” vol. 000. 2014.

[50] I. Toho Tenax America, “Tanax® HTS40 Carbon Fiber Product Data.” 2010.

[51] J. M. Curry, E. R. OHNSON, and J. H. TARNES, “Effect of dropped plies on the strength of graphite-epoxy laminates,” *AIAA journal*, vol. 30, no. 2, pp. 449–456, 1992.

[52] A. D. Botting, A. J. Vizzini, and S. W. Lee, “Effect of ply-drop configuration on delamination strength of tapered composite structures,” *AIAA journal*, vol. 34, no. 8, pp. 1650–1656, 1996.

[53] a Mukherjee and B. Varughese, “Design guidelines for ply drop-off in laminated composite structures,” *Composites Part B: Engineering*, vol. 32, no. 2, pp. 153–164, Jan. 2001.

[54] M. Brillant, “Out-of-Autoclave Manufacturing of Complex Shape Composite Laminates,” McGill, 2010.

[55] J. Cauberghs, “Out-of-Autoclave Manufacturing of Aerospace Representative Parts,” 2011.

[56] L. K. Grunenfelder, C. Fisher, C. Cabble, S. Thomas, and S. R. Nutt, “DEFECT CONTROL IN OUT-OF-AUTOCLAVE MANUFACTURING OF STRUCTURAL ELEMENTS,” in *proceedings of the SAMPE*, 2012.

[57] S. M. Hughes and P. Hubert, “OUT-OF-AUTOCLAVE PREPREG PROCESSING : EFFECT OF INTEGRATED GEOMETRIC FEATURES ON PART QUALITY,” in *SAMPE 2013*, 2013, pp. 42–56.

[58] G. G. Bond and J. Luner, “Design of experiments evaluation of processing parameters for non-autoclave composite prepreg,” *SMAPE 2009 Proceedings*, 2009.

[59] K. R. Bernetich, “Evaluation of detail part fabrication using out-of-autoclave prepreg,” in *Proceedings of the SAMPE 2010*, 2010.

[60] C. J. Wade and J. R. Savage, “THE DEVELOPMENT AND APPLICATION OF AN OUT-OF- AUTOCLAVE PREPREG SOLUTION FOR AIRBUS A350XWB WING FIXED TRAILING EDGE,” *Proceedings of the SAMPE 2011 conference of the …*, 2011.

[61] M. Lane, A. Poursartip, G. Fernlund, K. Willden, and K. Nelson, “Robust Processing of Composite Structures,” in *Proceedings of the SAMPE 2010*, 2010.

[62] C. Ridgard, “Aerospace out of autoclave prepreg technology,” in *Proc. of SAMPE Europe 2011*, 2011.

[63] P. Hubert and A. Poursartip, “A review of flow and compaction modelling relevant to thermoset matrix laminate processing,” *Journal of Reinforced Plastics and …*, 1998.

[64] “Aluminum 6061-T6; 6061T651,” *ASM Aerospace Specification Metals Inc.* [Online]. Available: http://asm.matweb.com/search/SpecificMaterial.asp?bassnum=MA6061t6.

[65] “Viscosity Reference Chart,” *Research Equipment (London) Limited*. [Online]. Available: http://www.research-equipment.com/viscosity chart.html.

[66] M. Lane, “Private Communicaiton.” 2015.

[67] “Climate - Government of Canada,” 2015. [Online]. Available: http://climate.weather.gc.ca/.

[68] P. Hubert, R. Vaziri, and A. Poursartip, “A two-dimensional flow model for the process simulation of complex shape composite laminates,” *International Journal for …*, no. JANUARY 1999, 1999.

[69] “Abaqus Analysis User’s Manual,” *Dassault Systemes*. [Online]. Available: http://ubccmps-cffor24:2080/v6.12/books/usb/default.htm.

[70] T. Gutowski, Z. Cai, and S. Bauer, “Consolidation experiments for laminate composites,” *Journal of …*, no. July 1987, pp. 650–669, 1987.

[71] P. Hubert and A. Poursartip, “A method for the direct measurement of the fibre bed compaction curve of composite prepregs,” *Composites part A: applied science and …*, vol. 32, pp. 179–187, 2001.

[72] A. Forghani, “Private Communication.” 2015.

[73] S. Haghshenas, “Integrating resin flow and stress development in process modeling of thermoset composites,” 2012.

[74] S. Amini Niaki, “Private Communication.” 2015.

Appendices

Appendix A Complete Pressure History of Simulations for the Parametric Simulation Study

Figure A.1 to Figure A.13 below show the complete pressure histories (i.e. pressure history for all nodes of interest) of all simulations for the parametric simulation study.

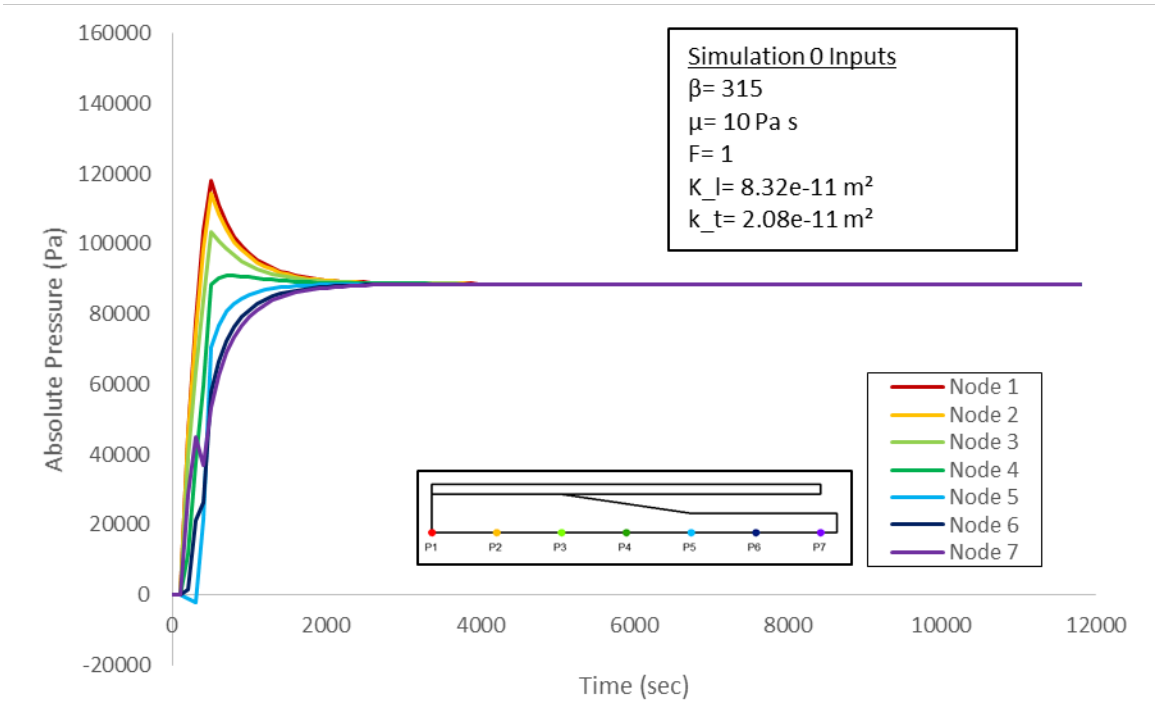

Figure A.1 – Resin pressure history for baseline simulation (simulation 0).

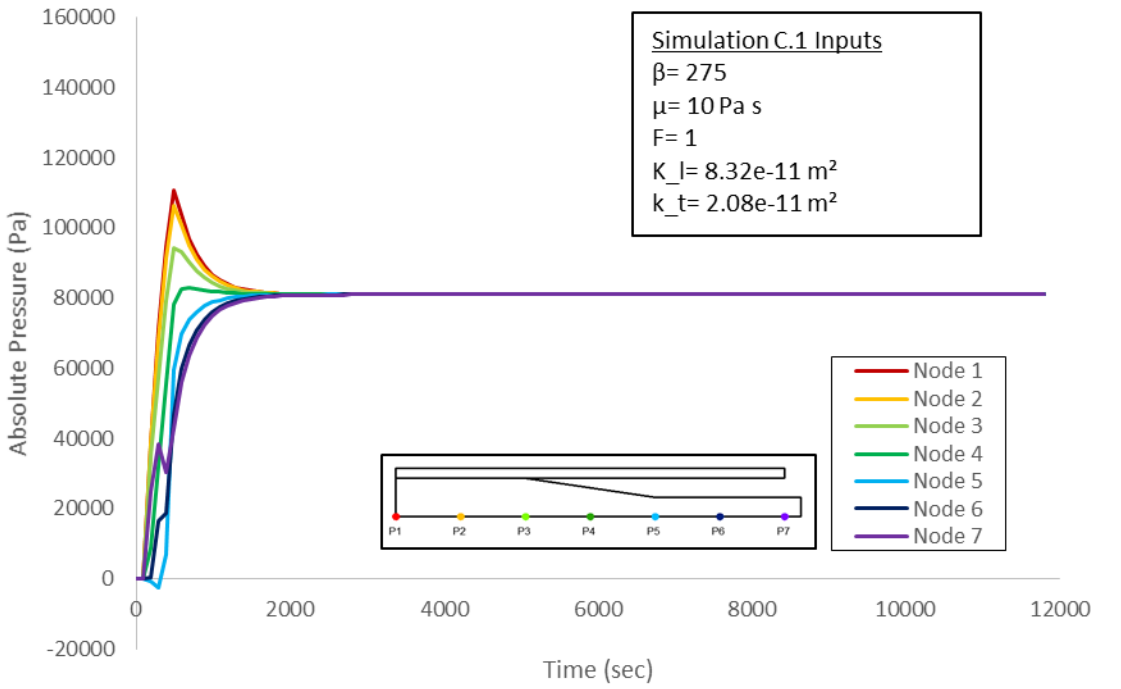

Figure A.2 - Resin pressure history for simulation with compaction curve of highest increase in stiffness from baseline (simulation C.1)

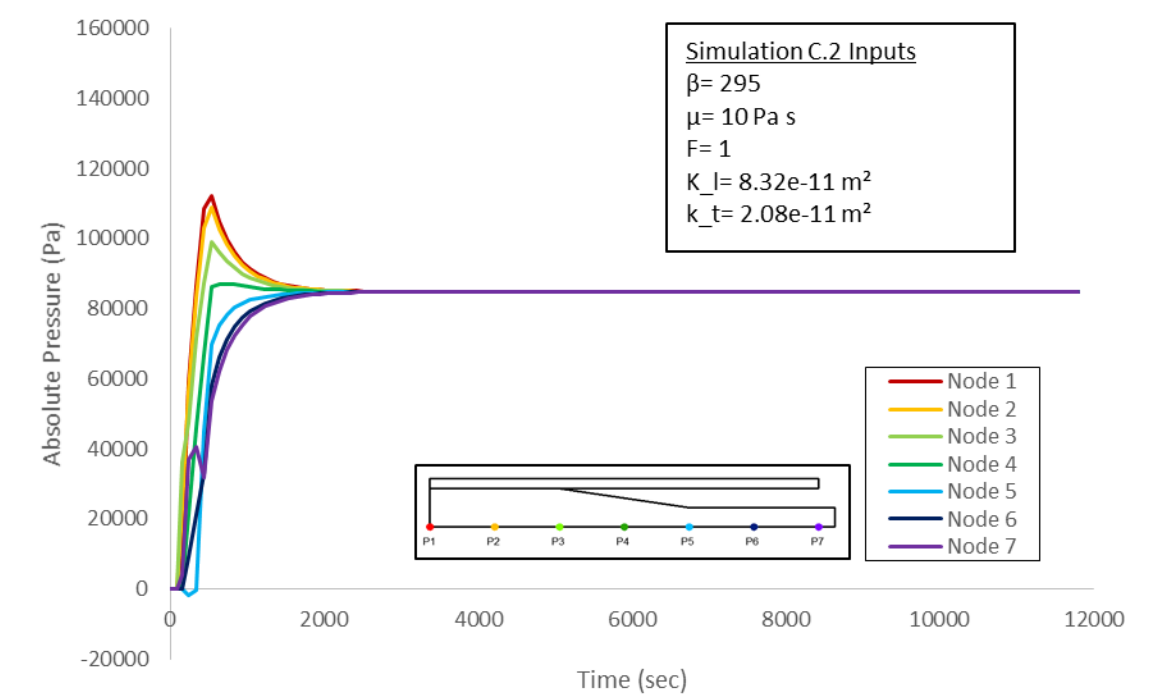

Figure A.3 - Resin pressure history for simulation with compaction curve of intermediate increase in stiffness from baseline (simulation C.2)

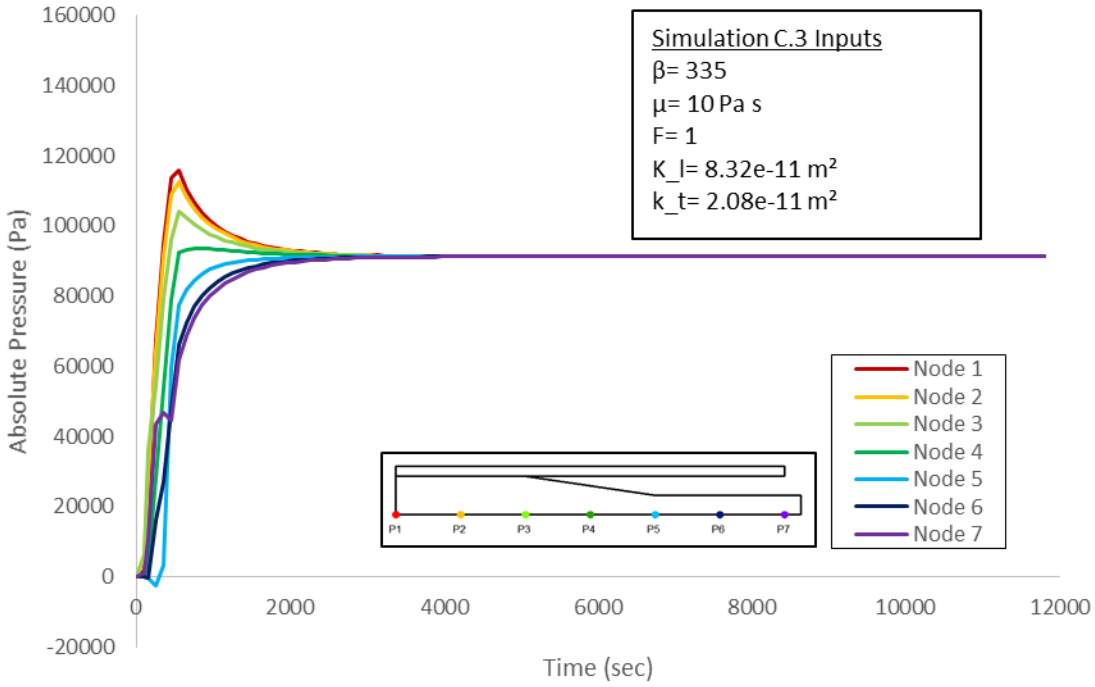

Figure A.4 - Resin pressure history for simulation with compaction curve of intermediate increase in compliance from baseline (simulation C.3)

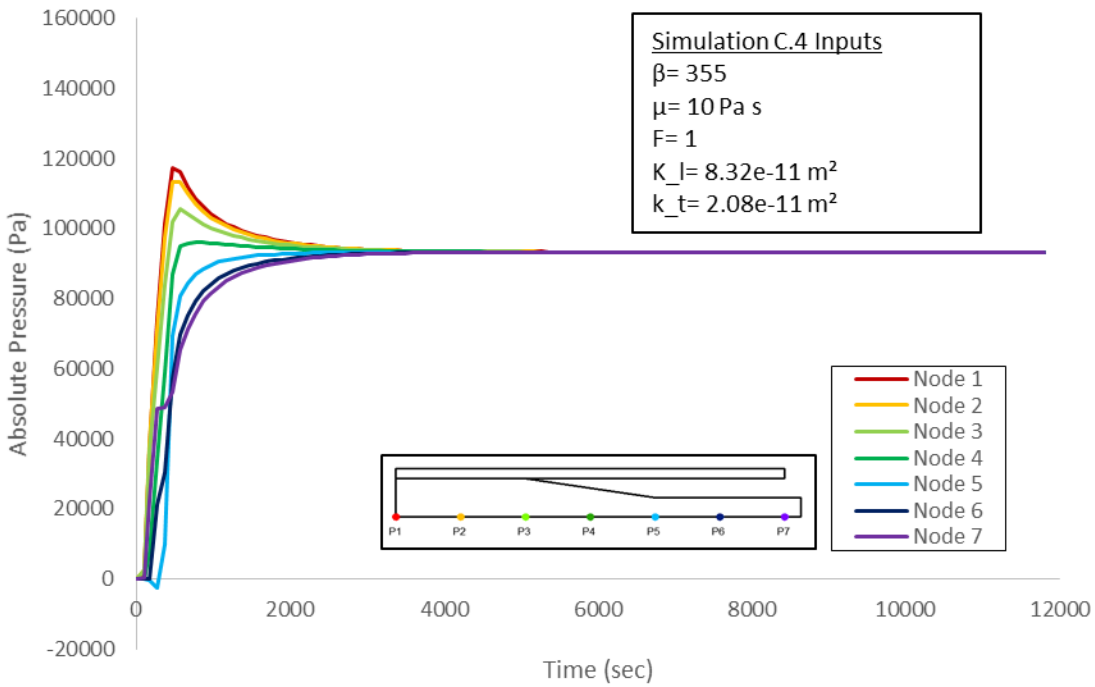

Figure A.5 - Resin pressure history for simulation with compaction curve of highest increase in compliance from baseline (Simulation C.4)

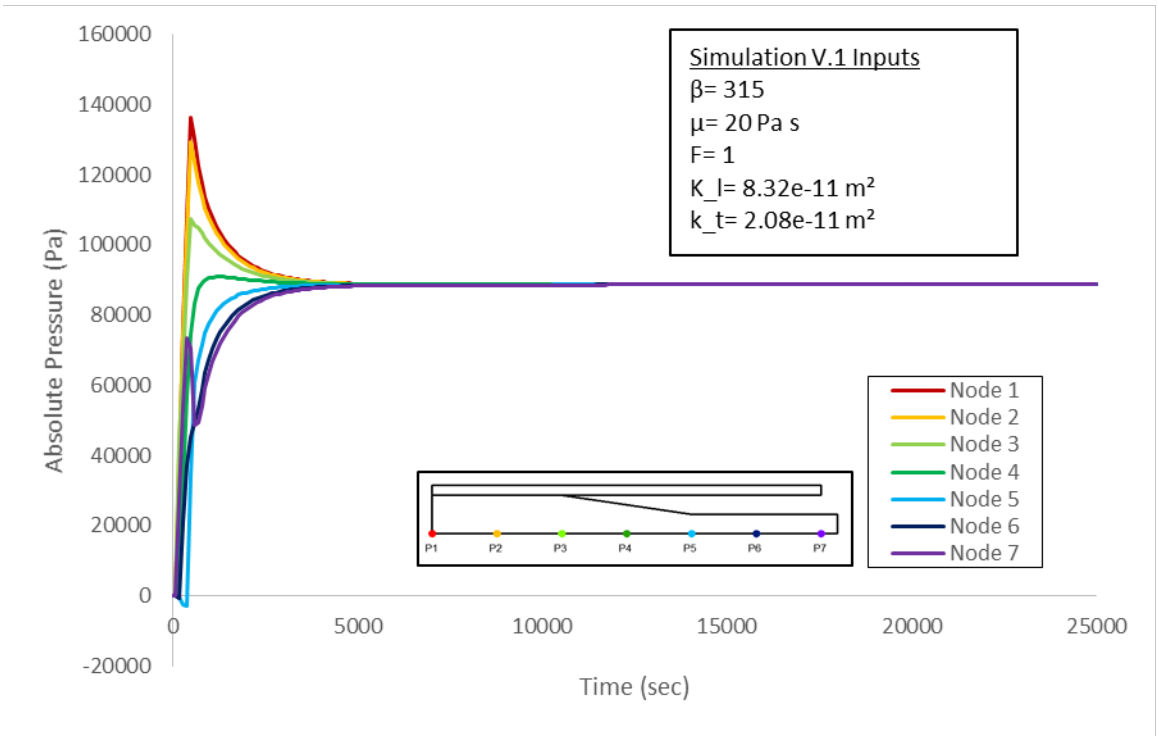

Figure A.6 - Resin pressure history for simulation with viscosity increased by a factor of 2 from baseline viscosity (simulation V.1)

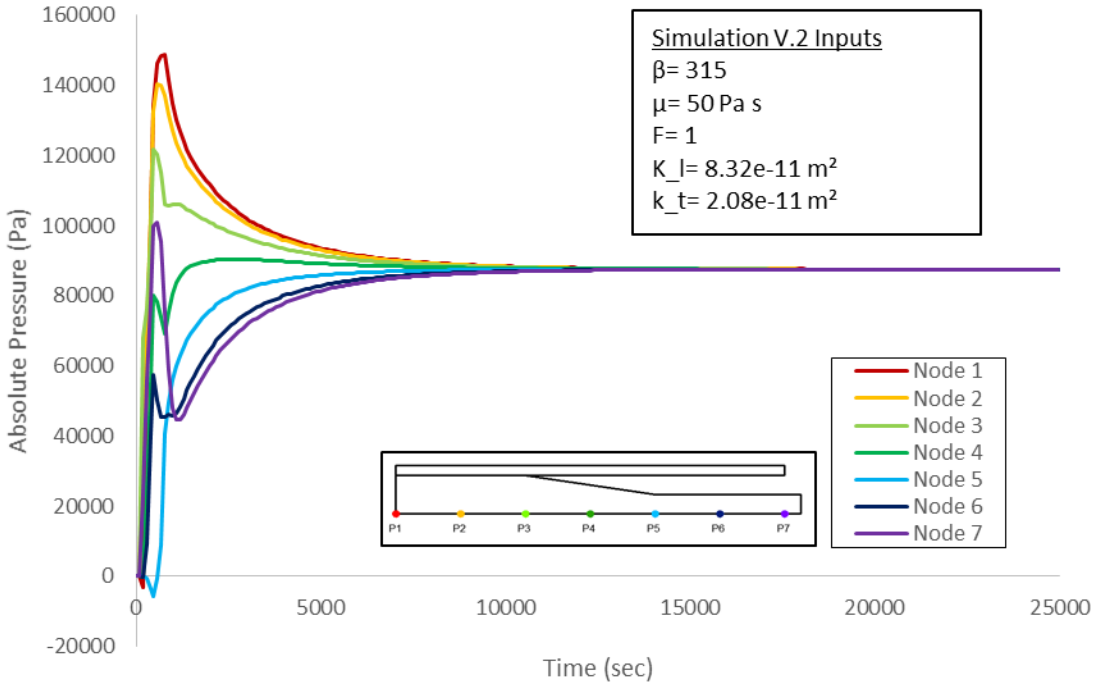

Figure A.7 - Resin pressure history for simulation with viscosity increased by a factor of 5 from baseline viscosity (simulation V.2)

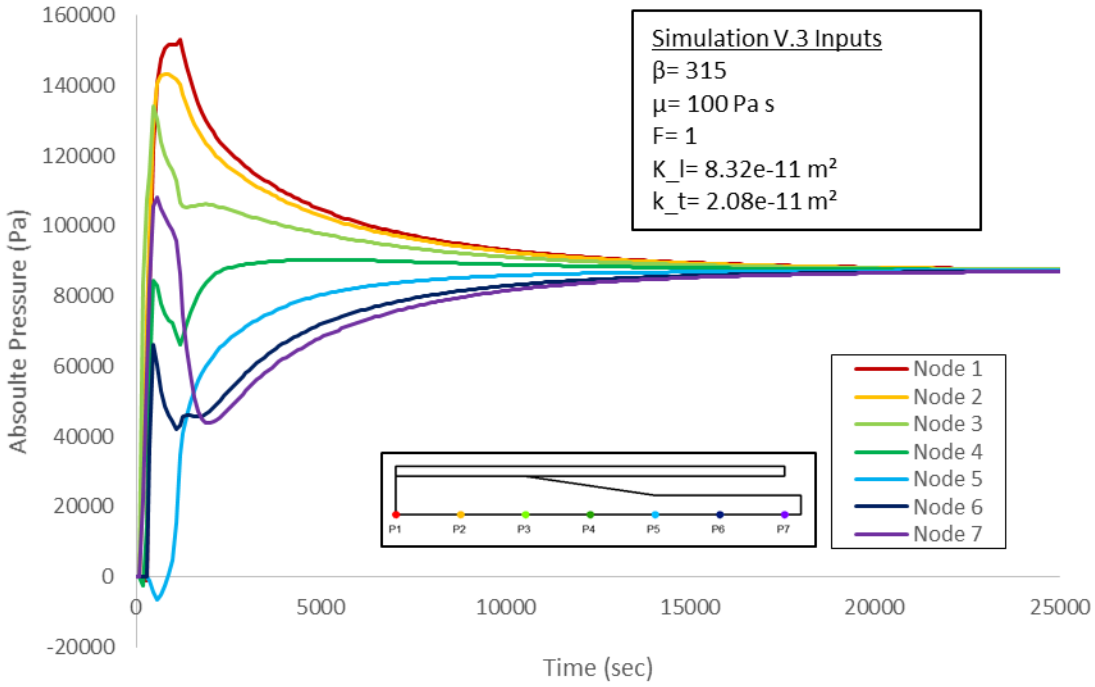

Figure A.8 - Resin pressure history for simulation with viscosity increased by a factor of 10 from baseline viscosity (simulation V.3)

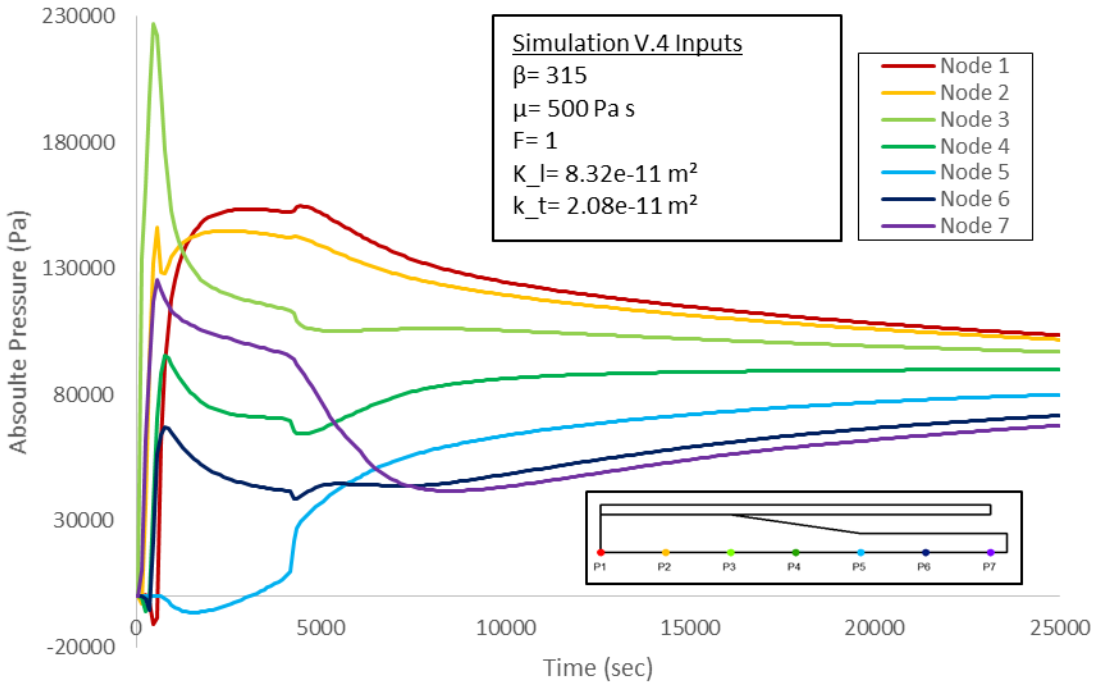

Figure A.9 - Resin pressure history for simulation with viscosity increased by a factor of 50 from baseline viscosity (simulation V.4)

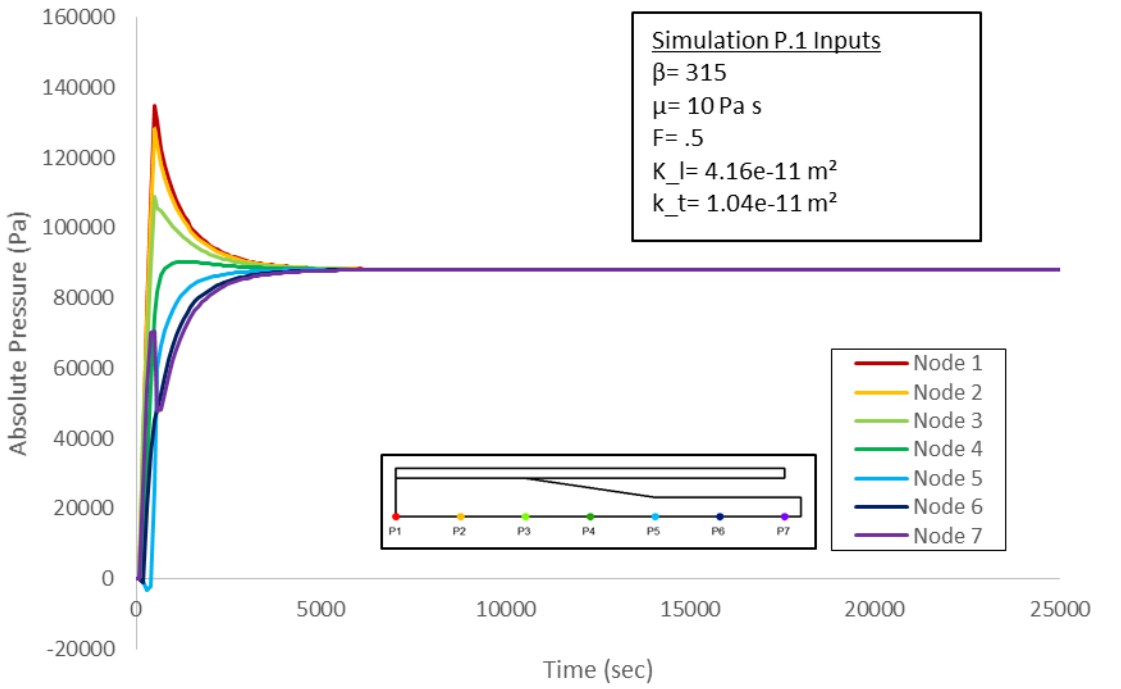

Figure A.10 - Resin pressure history for simulation with permeability decreased by a factor of 2 from baseline viscosity (Simulation P.1)

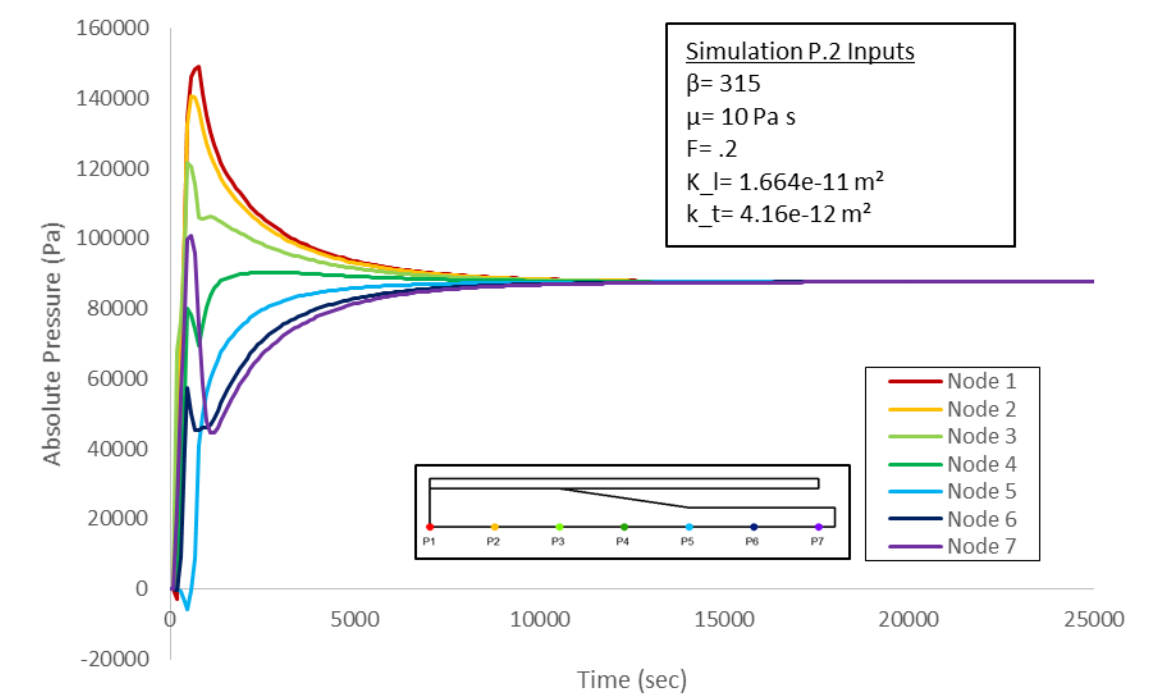

Figure A.11 - Resin pressure history for simulation with permeability decreased by a factor of 5 from baseline viscosity (Simulation P.2)

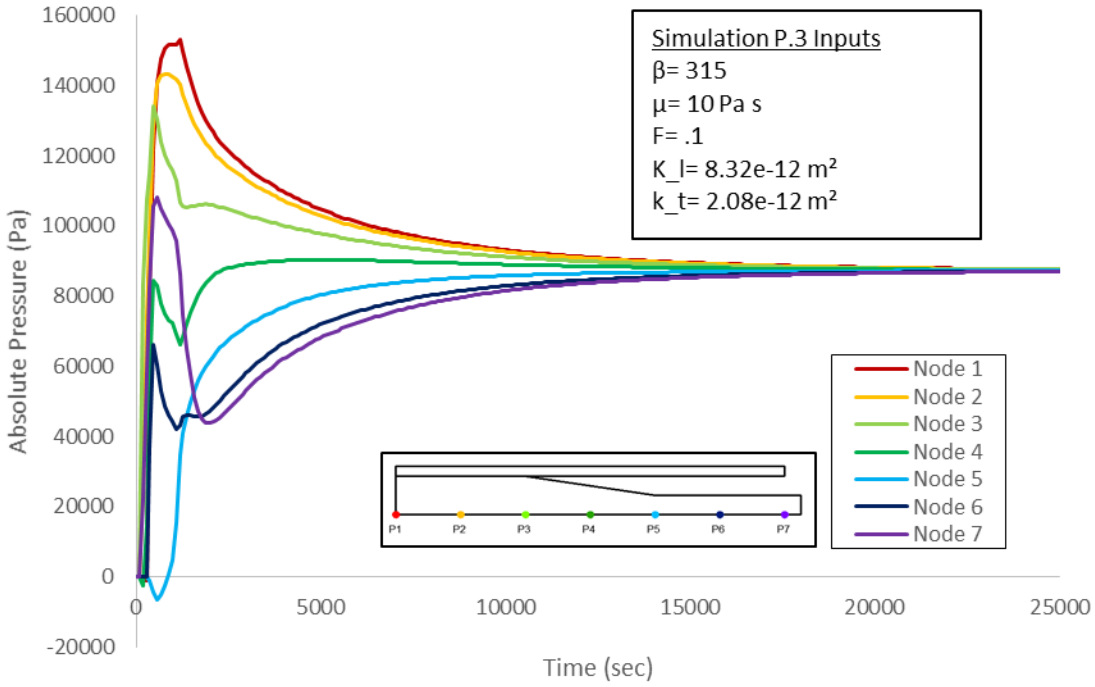

Figure A.12 - Resin pressure history for simulation with permeability decreased by a factor of 10 from baseline viscosity (Simulation P.3)

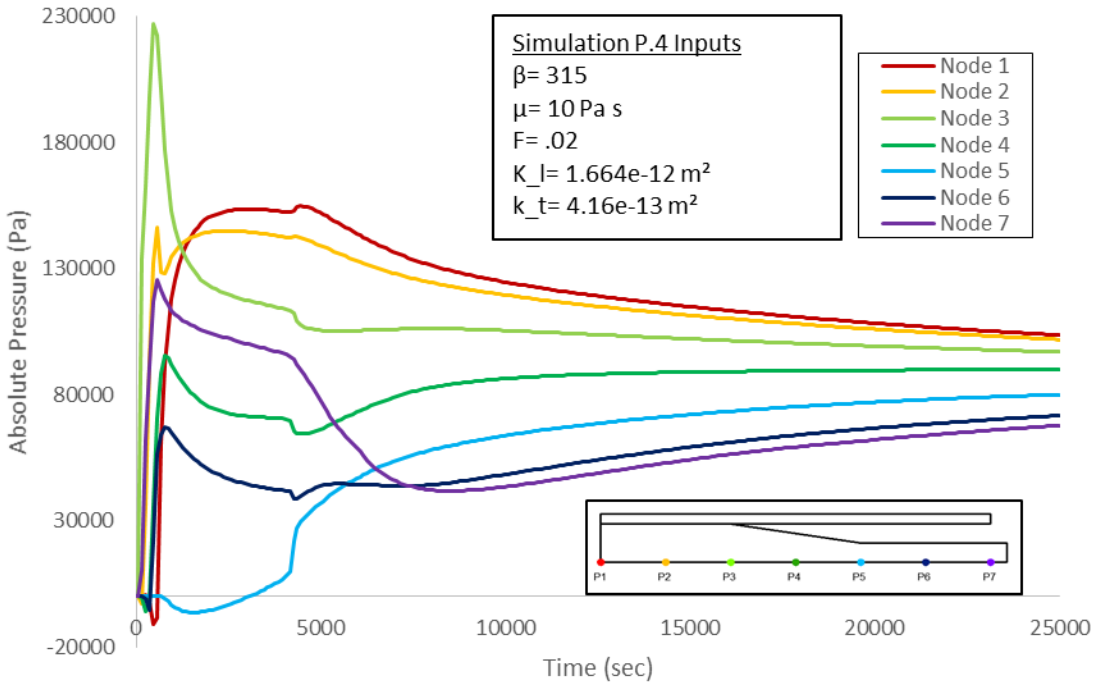

Figure A.13 - Resin pressure history for simulation with permeability decreased by a factor of 50 from baseline viscosity (Simulation P.4)

Appendix B Compaction Tests

The current section provides additional details with respect to the compaction tests discussed in chapter 5. These tests were performed to obtain the compaction curve (i.e. stress-strain curve) of HTS40 E13 3K PW fiber bed. The tests were performed by Mr. Alastair McKee of Convergent Manufacturing Technologies and the raw data was analyzed by the author. The fiber bed compaction curve was measured directly from the composite prepreg (MTM45-1/CF0526A) as per the method outlined by Hubert et al. [71].

B.1 Detailed Description of Compaction Test Method

The layup, weight and dimensions of the prepreg samples prepared for the displacement controlled test (CTS.Disp) and the load controlled test (CTS.Load) are shown in Table B.1 below. All samples where wrapped in with release film and flash tape in such so that the resin would not adhere to the mould of the compaction test set up. The samples were wrapped in such a way that the resin was free to flow out of the fiber bed. Figure B.1 shows a capture of the wrapped displacement controlled test samples.

Table B.1 – Summary of layup, dimensions and weight for prepreg samples used for displacement controlled test and load controlled tests.

Sample ID	Layup	Weight [g]	Dimensions [mm]		
			Length	Width	Thickness
CTS.Disp_1	[0˚]10	3.989	51.747	26.693	2.380
CTS.Disp_2	[0˚]10	4.130	52.287	26.870	2.407
CTS.Disp_3	[0˚]10	4.050	52.083	26.733	2.433
CTS.Load_1	[0˚]10	7.788	102.150	26.333	2.387

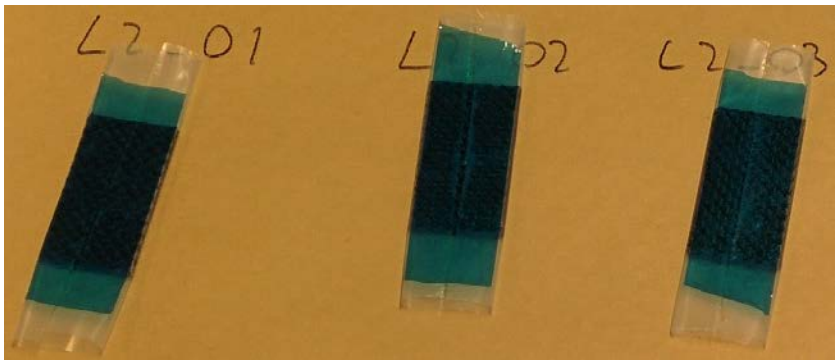

Figure B.1 – Capture of prepreg samples for load control tests wrapped in release film and flash tape.

B.2 Displacement Control Tests (CTS.Disp) Results

Figure B.2 to Figure B.4 below show the load and displacement histories for the force controlled tests. Note, due to noise, the load data shown here was smoothed by a computing the moving average for each time interval. The moving average subset domain for all load profiles shown here was 5 seconds. The relaxed load data points selected to compile the compaction curve of the fiber bed are indicted by hollow square markers.

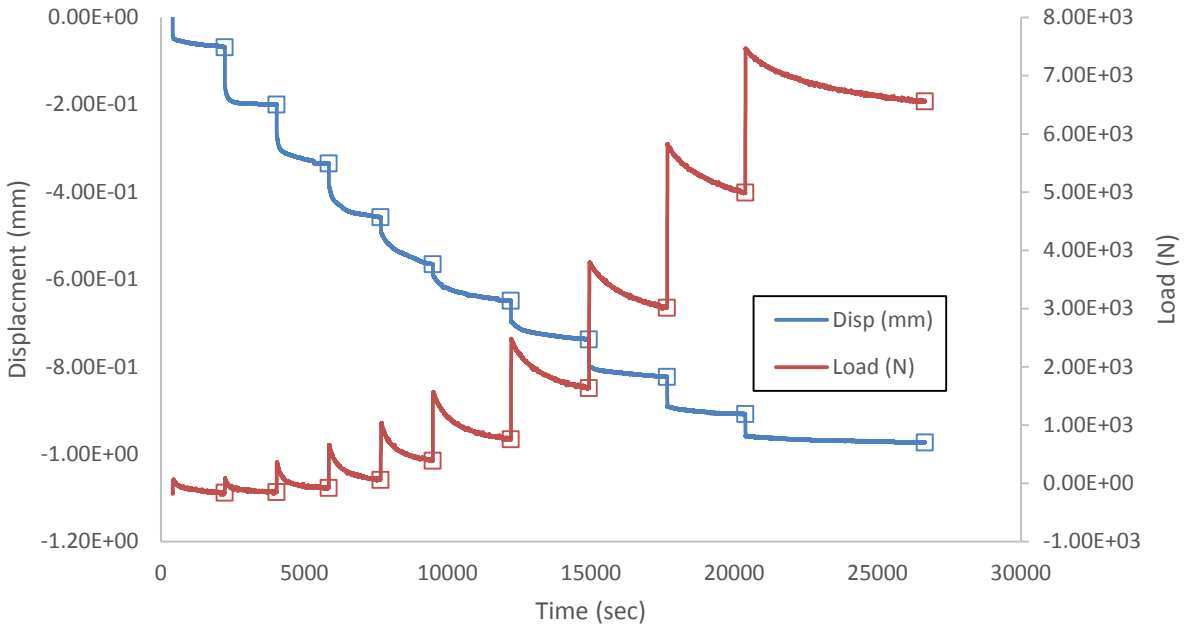

Figure B.2 – Displacement (blue) and load (red) results with respect to time for displacement controlled test results of sample CTS.Disp_1. Load and displacement at relaxed loads are indicated by the hollow square markers (see Table B.1).

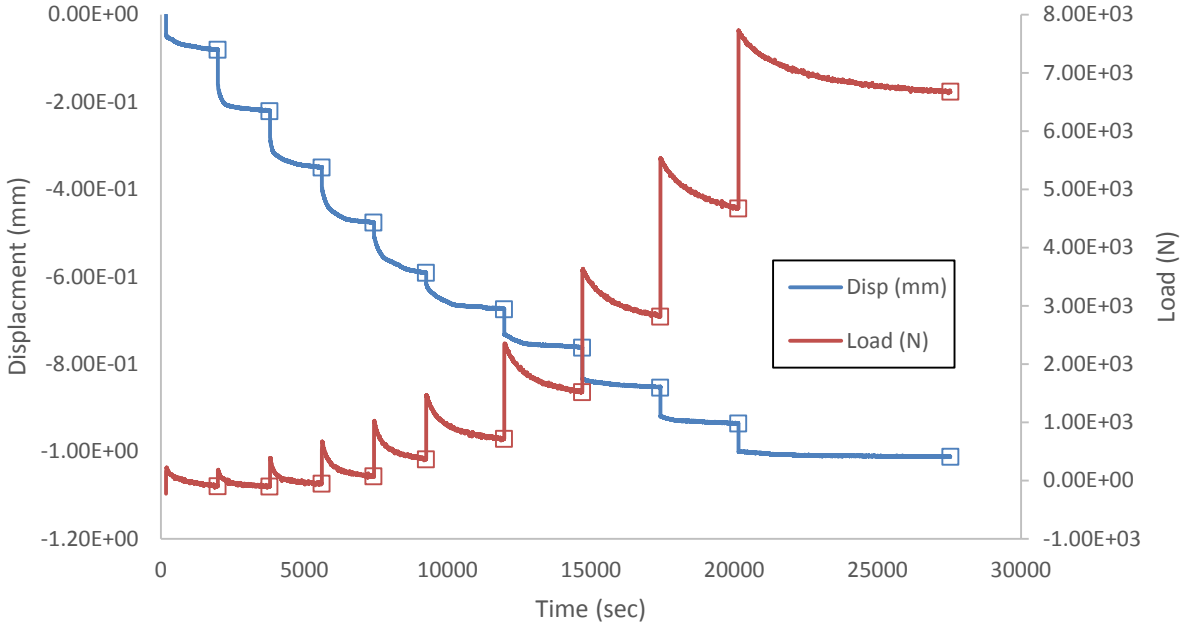

Figure B.3– Displacement (blue) and load (red) results with respect to time for displacement controlled test results of sample CTS.Disp_2. Load and displacement at relaxed loads are indicated by the hollow square markers (see Table B.1).

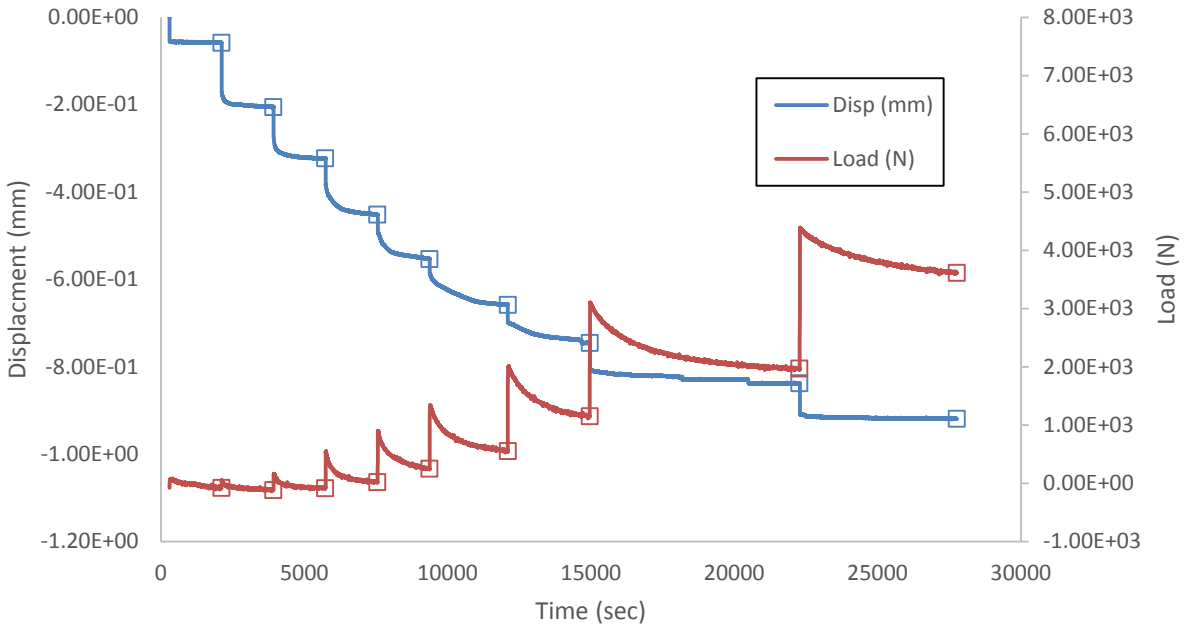

Figure B.4 – Displacement (blue) and load (red) results with respect to time for displacement controlled test results of sample CTS.Disp_3. Load and displacement at relaxed loads are indicated by the hollow square markers (see Table B.1).

Table B.2 provides a summary of the time, stress and strain values for the relaxed load points used to compile the compaction curve of the HTS40 E13 3K PW fiber bed. These data points where highlighted by hallow square marker in the previous figures (Figure B.2 to Figure B.4). The load and displacement data as seen in the previous figure was converted to stress and strain values as per the equations discussed in chapter 5. The samples initial thickness and surface area values which were used to compute the strain from the displacement data and fiber bed effective stress from the load data are also included in Table B.2.

Table B.2 – Summary of time, strain and fiber bed effective stress values for relaxed load displacement controlled test data points used to compile the compaction curve of the HTS40 E13 3K PW fiber bed.

Pressure Decay End Results								
CTS.Disp_1			CTS.Disp_2			CTS.Disp_3		
Initial Thickness (mm) =		2.38	Initial Thickness =		2.4067	Initial Thickness =		2.4333
Surface Area (mm²) =		1381.29	Surface Area =		1404.94	Surface Area =		1392.36
Time (seconds)	Strain	Eff. Stress (Pa)	Time (seconds)	Strain	Eff. Stress (Pa)	Time (seconds)	Strain	Eff. Stress (Pa)
2218	-2.86E-02	-1.18E+05	1975	-3.31E-02	-6.45E+04	2103	-2.38E-02	-5.36E+04
4027	-8.39E-02	-1.06E+05	3779	-9.14E-02	-6.93E+04	3914	-8.44E-02	-8.13E+04
5844	-1.40E-01	-5.58E+04	5602	-1.45E-01	-3.35E+04	5725	-1.33E-01	-5.75E+04
7657	-1.92E-01	4.53E+04	7413	-1.97E-01	5.74E+04	7548	-1.86E-01	1.59E+04
9473	-2.38E-01	2.84E+05	9239	-2.45E-01	2.62E+05	9363	-2.27E-01	1.81E+05
12194	-2.72E-01	5.48E+05	11964	-2.80E-01	5.13E+05	12095	-2.70E-01	4.00E+05
14923	-3.10E-01	1.19E+06	14689	-3.17E-01	1.09E+06	14953	-3.06E-01	8.27E+05
17650	-3.46E-01	2.18E+06	17411	-3.54E-01	2.01E+06	22271	-3.44E-01	1.41E+06
20379	-3.81E-01	3.61E+06	20139	-3.89E-01	3.33E+06	27757	-3.78E-01	2.60E+06
26646	-4.09E-01	4.75E+06	27536	-4.20E-01	4.76E+06			

B.3 Load Control Tests (CTS.Load) Results

Figure B.5 shows the position and load data for the load controlled test (CTS.Load_1). Note that the value of the initial position is between 4.18 mm and 3.73 mm. Due to the data acquisition frequency (1 Hz) used for this test, it was not possible to determine a more precise value for initial position. This is discussed in greater detail in section **Error! Reference source not found.**. The figure below assumes that initial position is at the middle of this range (i.e. 3.955mm).

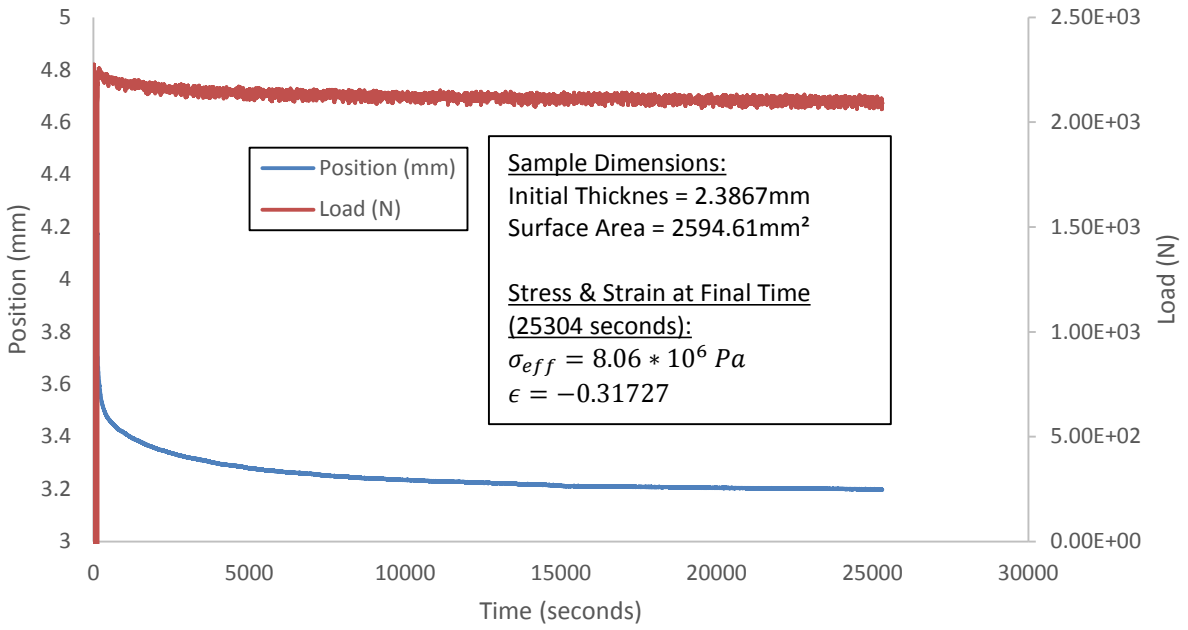

Figure B.5 – Position and load results with respect to time for load controlled test (CTS.Load_1).

B.4 Sources of Error for Load Control Test (CTS.Load)

In this section, the sources of error for the load control test (CTS.Load) as discussed in the previous section is explained. Figure B**.6** shows the position and load data for the load controlled test between 120 seconds and 140 seconds. The individual data points are indicated by the solid square markers. From this figure, one can see that load undergoes a seemingly instantaneous increases between the 129-130 second interval. This indicates that the unset of loading occurred somewhere within this interval of time. Simultaneously, it can also be seen that position data also undergoes a seemingly instantaneous decrease from a value of 4.18 mm to a value of 3.73 mm. As such, due to the data acquisition frequency (1 Hz) used for this test, it is difficult to conclude the actual the onset of specimen loading (i.e. when displacement=0 mm). For this reason, as discussed in section B.3, the onset of specimen loading was assumed to be at the middle value of the range seen at the 129 to 130 second time interval (i.e. 3.955mm). With this assumption, it

was possible to compute the final strain for the force controlled test. This was done by assuming three different offset values for the compaction curve fit and using simulation to determine the best fit as discussed in chapter 5.

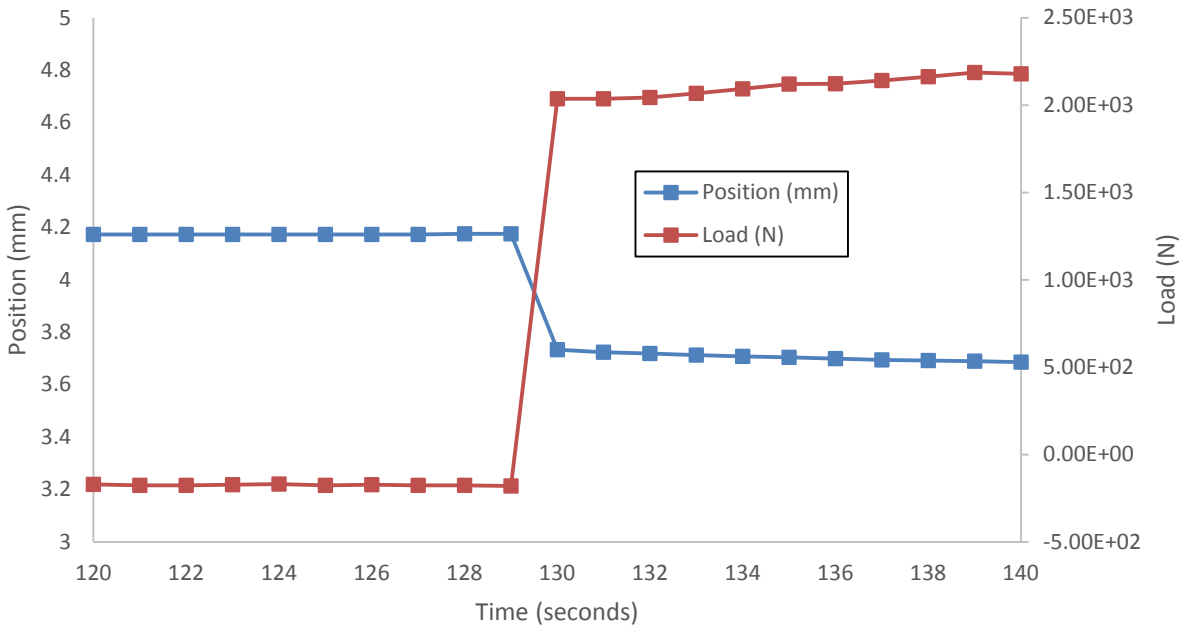

Figure B.6 – Position and load results with respect to time for load controlled test (CTS.Load_1) between 120 seconds and 140 seconds. The individual data points are indicated by the solid square markers.